The Development of Colorimetric pH Sensors and Optical-Based Detection for Monitoring Spoilage Volatiles from Packaged Seafood

by

Liam Byrne B.Sc.

Thesis submitted for the Degree of Doctor of Philosophy

Supervisor: Prof. Dermot Diamond

Dublin City University **March 2003**

Declaration

I hereby certify that this material, which I now submit for assessment on the programme of study leading to the award of Doctor of Philosophy is entirely my own work and has not been taken from the work of others save and to the extent that such work has been cited and acknowledged within the text of my work.

Signed: Liam Byrne

Liam Byrne

ID No.: 95034153

Date: 6/03/03

For Jacinta

"I have my own fish to fry"

- Don Quixote

Miguel de Cervantes
(1547-1616)

Acknowledgments

Very many people have contributed in some shape or form to the development of this thesis and to my time in DCU. I find it hard to know what to say to them and to remember everybody who has helped me, but I will make my best effort! Thanks to Dermot, who was always supportive throughout the three or so years that this work took, especially for the opportunities to travel and visit conferences. I would like to say thanks to the past and present members of the DD research group, you were very helpful, especially Kim, who was always able to answer my constant (and irritating!) questions. A big nod goes out to all the science postgrads in DCU, in particular the analytical groups whose coffee, lunch and bar breaks always helped! Thanks to the NCSR staff and the technical staff in Chemistry, who were always obliging and willing to help. On a professional note, thanks to John Joyce and the Marine Institute of Ireland for funding, BIM, Robert Lawson of City Biologic for his help with the microbial study, Shirley Hislip, Jeremy Lerner and Steve Edwards, Stephanie McIntyre and Derek Law for their input. Thanks also to Shane and Philip O'Neill for supplying Ireland's finest cod, Gwenelle for helping with handling of the fish and Conor Burke for his assistance with the profilometer and for supplying me with some ammonia gas.

On a more personal note, thanks go to my parents and family, who helped not only during the preparation of my thesis, but aided my education on a whole through constant encouragement. To all my friends who have had to listen to me carry on about working in DCU, I apologise and say thanks! Thanks to Kathrin in Bochum, who reminded me why I was doing what I was doing in the first place. David, thanks for your help with fixing all the bad things that kept happening to my PC. And last, but certainly not least, thanks to Ja for helping me every day. Without your continued support, this work would never have happened.

List of Publications and Presentations

Publications

Byrne, L., Barker, J., Pennarun-Thomas, G., Edwards, S. and Diamond, D. *Trends in Analytical Chemistry,* **19,** 517-522, 2000.
Title: "Digital Imaging as a Detector for Generic Analytical Measurements".

Byrne, L., Lau, K.T., Edwards, S. and Diamond, D. *Proceedings of SPIE*, **4205**, 267-277, 2000.
Title: "Digital Imaging as a Detector for Quantitative Colorimetric Analysis".

Byrne, L., Lau, K.T. and Diamond, D. *The Analyst*, **127**, 1338-1341, 2002.
Title: "Monitoring of Headspace Total Volatile Basic Nitrogen from Selected Fish Species using Reflectance Spectroscopic Measurements of pH Sensitive Films".

Byrne, L., Lau, K.T. and Diamond, D. *Sensors and Actuators B (chem.)*, Accepted for publication, 2002.
Title: "Development of pH Indicator Based Colorimetric Sensors for On-Package Monitoring of Headspace Volatiles during Fish Spoilage".

Byrne, L., Lau, K.T. and Diamond, D. *Irish Journal of Agricultural and Food Research*, Accepted for publication, 2002.
Title: "Development of pH Sensitive Films for Monitoring Spoilage Volatiles released into Packaged Fish Headspace".

Conferences Attended

52nd Annual Irish Chemistry Colloquium

University College Cork, Ireland, May 10-12, 2000.

53rd Annual Irish Chemistry Colloquium

University College Dublin, Ireland, June 20-22, 2001.

2nd Annual Analytical Research Forum Incorporating Research and Development Topics

Kingston University, UK, July 15-17, 2002.

Poster Presentations

Europt(r)ode V – Opt(r)ode

Lyon-Villeurbanne, France, April 16-19, 2000.

Title: "Digital Imaging as a Detector for Generic Analytical Measurements".

15th Annual Divisional Engineering Conference of Analog Devices

University of Limerick, Ireland, September 12-14, 2000.

Title: "Digital Imaging as a Detector for Generic Analytical Measurements".

1st Annual Analytical Research Forum Incorporating Research and Development Topics

University of East Anglia, UK, July 16-18, 2001.

Title: "Assessment of Chromogenic Dyes as Indicators for Fish Spoilage".

2nd Annual Conference on Analytical Sciences in Ireland

Institute of Technology, Tallaght, Ireland, April 4-5, 2002.

Title: "Development of pH Sensitive Films for Monitoring of Packaged Fish Headspace".

2nd Annual Conference on Analytical Sciences in Ireland

Institute of Technology, Tallaght, Ireland, April 4-5, 2002.

Title: "Development of Solid State Sensors for Ammonia Detection in Wastewater".

54th Annual Irish Chemistry Colloquium 2002

Queen's University, Northern Ireland, April 10-12, 2002.

Title: "Development of a Gas Phase Solid State Ammonia Sensor for Wastewater Analysis".

32nd Annual WEFTA meeting

Galway Bay Hotel, Ireland, May 13-15, 2002.

Title: "Monitoring of Packaged Fish Headspace using pH Sensitive Films".

Eurosensors XVI

Czech Technical University, Czech Republic, September 15-18, 2002.

Title: " Development of pH Sensitive Films for Monitoring of Packaged Fish Headspace".

Oral Presentations

Photonics East 2000

Boston, USA, November 5-8, 2000.

Title: "Digital Imaging as a Detector for Quantitative Colorimetric Analysis".

Seminar Series 2001-2002

Dublin City University, School of Chemical Sciences, October 10th 2001.

Title: "The Application of Colorimetric Sensors to pH Measurements".

Table of Contents

		Page Number
Title Page		**I**
Declaration		**II**
Dedication		**III**
Acknowledgements		**V**
List of Publications and Presentations		**VI**
Table of Contents		**IX**
Abstract		**XIV**
Abbreviations		**XV**
Prologue		**XVII**
Chapter 1	**Theory and Background**	**1**
1.1	Chemical sensors	2
	1.1.1 Modes of transduction	4
	1.1.2 Optical sensors	4
1.2	Principles of spectroscopy	7
	1.2.1 Electromagnetic radiation	7
	1.2.2 UV-Vis spectroscopy	9
	1.2.2.1 Beer-Lambert Law	9
1.3	pH	11
	1.3.1 Determination of pH	12
	1.3.2 pH indicators	12
	1.3.2.1 Theory of chromophores	13
	1.3.2.2 Relationship to spectral features	15
	1.3.2.3 Factors affecting the colour changes of pH indicators	16
1.4	Applications of pH indicator dyes	19
	1.4.1 Selection of pH indicator dye	19
	1.4.2 Immobilisation methods	20
	1.4.3 Fibre-optic based pH sensors	21
	1.4.4 Sol-gel based pH sensors	24

1.4.5 pH sensors based on cellulose binders 26
1.4.5.1 Plasticisers 27
1.4.5.2 Applications of cellulose based pH sensors 28
1.5 Seafood spoilage monitoring 32
1.5.1 Sensory evaluation 32
1.5.1.1 Quality Index Method 33
1.5.2 Spoilage microorganisms 33
1.5.2.1 The growth curve 34
1.5.2.2 Microbial populations during spoilage 36
1.5.3 Spoilage volatiles 38
1.5.4 Determination of TVB-N 39
1.5.4.1 Monitoring TVB-N using chromogenic dyes 42

Chapter 2 Sensor Preparation and Optimisation 49

2.1 Introduction 50
2.2 Instrumentation 52
2.2.1 Imaging Spectrograph 52
2.2.1.1 Spectral Imaging 53
2.2.1.2 Spectral imaging with the PARISS system 54
2.2.1.3 Spectral classification 55
2.3 Dye selection 57
2.4 Experimental 58
2.4.1 Materials 58
2.4.2 Sensor preparation 59
2.4.2.1 Sensor dot production 60
2.4.3 Analysis of prepared sensor dots 61
2.4.3.1 Rapid screening of sensor dots 61
2.4.3.2 Analysis of sensor dots with PARISS 64
2.4.4 Effect of dye loading on sensor formulation 65
2.4.5 Determination of the pK_a of cresol red 66
2.4.5.1 Study of dye in free solution 66
2.4.5.2 Study of dye in polymer binder 67
2.4.6 Study of the effect of temperature on pK_a 68

2.4.7 Sensor calibration 68

2.5 Results and discussion 70

2.5.1 Rapid screening of sensor dots 70

2.5.1.1 RGB analysis of E_3 sensors 70

2.5.1.2 RGB analysis of E_5 sensors 72

2.5.2 Analysis of sensors using PARISS 77

2.5.2.1 E_1 sensors (dried in air) 77

2.5.2.2 E_4 sensors (dried at 4 °C) 79

2.5.2.3 E_5 sensors (dried in sealed environment) 80

2.5.3 Effect of dye loading on the sensor formulation 81

2.5.4 Comparison study of the pK_a of the dye in free solution and polymer binder 84

2.5.4.1 Free solution study 84

2.5.4.2 Polymer binder study 87

2.5.4.3 Comparison of data 87

2.5.5 Study of the effect of temperature on pK_a 88

2.5.6 Calibration of sensors to headspace NH_3 90

2.6 Conclusion 95

Chapter 3 Monitoring of Headspace Spoilage Volatiles released from Packaged Fish using a Colorimetric Chemical Sensor 97

3.1 Introduction 98

3.2 Experimental 99

3.2.1 Materials 99

3.2.2 Equipment 99

3.2.3 Sensor fabrication 99

3.2.4 Experimental setup 100

3.2.4.1 Whiting samples 100

3.2.4.2 Orange roughy (whole) and black scabbard 102

3.2.4.3 Cod and orange roughy (fillets) 103

3.2.5 Spectral monitoring of sensors 106

3.3 Results and discussion 108

3.3.1 General trends identified 108

3.3.2 Sensors monitoring TVB-N of whiting 108
3.3.3 Sensors monitoring TVB-N of orange roughy (whole) and black scabbard 111
3.3.4 Sensors monitoring TVB-N of cod and orange roughy (fillets) 115
3.3.4.1 Subtraction of reference spectra 117
3.3.4.2 Results from cod samples 120
3.3.4.3 Results from orange roughy samples 122
3.3.4.4 History of samples 124
3.4 Conclusion 126

Chapter 4 Correlation of Chemical Sensor Response with Microbial Populations and Headspace Volatiles during Fish Spoilage 127

4.1 Introduction 128
4.2 Experimental 129
4.2.1 Materials and equipment 129
4.2.2 History of fish samples 129
4.2.3 Experimental setup 131
4.2.4 Determination of headspace TVB-N levels 132
4.2.5 Enumeration of microbial populations 133
4.3 Results and discussion 134
4.3.1 General trends identified 134
4.3.2 Sensors monitoring TVB-N of cod (a) and plaice 134
4.3.3 Sensors monitoring TVB-N of cod (b) 136
4.3.3.1 Reproducibility of sensor fabrication and response 137
4.3.4 Determination of headspace TVB-N levels 138
4.3.4.1 Comparison of TVB-N levels and sensor response 142
4.3.5 Microbial populations 143
4.3.5.1 TVC of cod (a) and plaice 143
4.3.5.2 TVC of cod (b) 144
4.3.5.3 Pseudomonas populations of cod (b) 146
4.3.6 Summary of results 149
4.3.7 Fish spoilage prediction 153
4.4 Conclusions 157

Chapter 5 Development of a Portable Handheld Colour Scanner for Analysis of Fish Spoilage Sensors **158**

5.1 Introduction 159
5.2 Instrumentation 161
5.3 Experimental 167
5.3.1 Materials 167
5.3.2 Characterisation of scanner 167
5.3.2.1 Characterisation of LED emission spectrum 167
5.3.2.2 Calibration using cresol red standards 167
5.3.2.3 Effect of sensor thickness on reflected light intensity 167
5.3.3 Calibration of sensor dots with scanner 169
5.3.4 Testing sensors and scanner with real fish samples 170
5.4 Results and discussion 172
5.4.1 Characterisation of scanner 172
5.4.1.1 Characterisation of yellow LED 172
5.4.1.2 Calibration using cresol red standards 173
5.4.1.3 Effect of thickness on the reflected light intensity 176
5.4.2 Calibration of sensors with scanner device 181
5.4.3 Relationship of scanner to threshold of spoilage 183
5.4.4 Testing sensors and scanner with real fish samples 185
5.4.4.1 First batch of samples tested 186
5.4.4.2 Second batch of samples tested 189
5.5 Conclusions 193

Chapter 6 Overview, Trends and Future Work **195**

References **201**

Abstract

"The Development of Colorimetric pH Sensors and Optical-Based Detection for Monitoring Spoilage Volatiles from Packaged Seafood."

Liam Byrne

My PhD programme of research at the National Centre for Sensor Research has focussed on the development of colorimetric sensors based on pH indicator dye chemistry. Part of the research programme was funded by the Marine Institute of Ireland and Bord Iascaigh Mhara (the Irish Sea Fisheries Board). This was specifically to develop a colorimetric headspace gas sensor to monitor the release of volatile spoilage compounds from fish samples. In our approach, the sensors reacted with target spoilage compounds to produce a measurable change in colour. Novel spectral and colour processing techniques were used to quantitatively monitor changes in the sensor response.

The sensor formulation developed was optimised and the sensor response was characterised and calibrated to headspace ammonia. An experimental setup was devised for the routine screening of different fish species in parallel. The microbial populations of fish samples during spoilage were determined, and the working sensor correlated to microbial populations of fish samples tested and to the concentration of headspace spoilage compounds released during the course of a spoilage experiment. In the final section of work, a novel handheld colour scanner device was developed to enable routine measurements of colour changes to be made "on-package". The device uses 2 LEDs for illumination and a photodiode for detection, and is a low cost, portable device that can be battery-operated. The combination of scanner and sensor was tested with real fish samples, and the results obtained show that the system is operating satisfactorily.

Abbreviations

au	Absorbance Units
CCD	Charge Couple Device
CFU	Colony Forming Units
CTABr	Cetyltrimethylammonium Bromide
DBP	Dibutyl Phthalate
DMA	Dimethylamine
DOS	Dioctyl Sebacate
EM	Electromagnetic
FOCS	Fibre-Optic Chemical Sensors
GC	Gas Chromatography
HOMO	Highest Occupied Molecular Orbital
ISE	Ion-Selective Electrode
LOD	Limit of Detection
LUMO	Lowest Unoccupied Molecular Orbital
MCC	Minimum Correlation Coefficient
MS	Master Spectrum
NH_3	Ammonia
NPOE	2-Nitrophenyl Octyl Ether
PARISS	Prism and Reflector Imaging Spectrometer System
PET	Polyethylene Teraphthalate
Protein-N	Nitrogenous Protein
PVC	Polyvinyl Chloride
QIM	Quality Index Method
RAM	Random Access Memory
RGB	Red, Green and Blue
ROI	Region of Interest
RSD	Relative Standard Deviation
S/N	Signal to Noise
SSO	Specific Spoilage Organisms
SSR	Sum of Squared Residuals
TEOS	Tetraethoxysilane
T_g	Glass Transition Temperature

TMA	Trimethylamine
TMAO	Trimethylamine Oxide
TMOS	Tetramethoxysilane
Total-N	Total Nitrogenous
TVB-N	Total Volatile Basic Nitrogen
TVC	Total Viable Count
UV-Vis	Ultraviolet-Visible

Prologue

It was the aim of this project to produce sensors that could be incorporated into fish packaging to give an indication, visual or otherwise, of the point of spoilage of a sample. Chapter 2 describes the development of an on-package sensor to monitor the levels of TVB-N of spoiling fish samples. Different components in the sensor formulation were routinely tested to determine which produced the most homogeneous sensors. This included a study of different plasticisers in the matrix, altering the printing and drying conditions of the sensors, varying the amount of polymer binder and studying different ratios of binder to plasticiser. Two analysis methods were used to determine the homogeneity of the sensors. A rapid screening method based on digital imaging techniques was developed, and more in-depth analysis of those sensors of interest was performed using an imaging spectrograph system. These techniques facilitated the development of a homogeneous sensor dot based on cresol red physically entrapped in plasticised cellulose acetate. A study of the shift in pK_a of the dye in the matrix compared to in free solution was performed, and an investigation of the effect of dye loading on the sensor allowed an optimised dye concentration to be determined. A study of the effect of temperature on the pK_a of the dye was carried out, and the depth profiles of the sensor dots were determined. The sensors were calibrated against ammonia in headspace, to demonstrate the feasibility of the sensors for monitoring TVB-N levels.

Chapter 3 describes the development of an experimental design that facilitated the routing screening of up to 24 real fish samples in parallel, using the sensor developed in Chapter 2. The real fish samples tested were whiting, cod, orange roughy and black scabbard. All the samples tested caused significant changes in the sensor colour. Reflectance UV-Vis measurements allowed the colour changes to be quantified, and results from this chapter clearly demonstrate that the sensors are ideal for monitoring TVB-N levels in headspace.

Chapter 4 is a key chapter in all of the results presented. A focus was placed on the cod species, and reflectance measurements of the sensors were taken for different fish to quantify the reproducibility of the sensors, some of which were produced in different batches. Samples were removed from the fish at fixed intervals, and the

microbial populations of the samples were quantified, for both the total viable counts and the pseudomonas species. The headspace TVB-N levels released during spoilage were also quantified at fixed time intervals. The correlation of the sensor data to the microbial populations and to the headspace TVB-N levels was determined, and this allowed the sensor response at the critical threshold of spoilage to be determined.

Chapter 5 focuses on the characterisation of a newly developed portable handheld colour scanning device for on-package analysis of the sensor response. The device was calibrated against the cresol red sensors and was compared to data from a benchtop colour reference measurement system. A number of real fish samples that were "use-by" date stamped from a local supermarket were tested with the combination of sensor/scanner, and the correlation between the colour threshold at the point of spoilage and the dates on the package was determined. Finally in chapter 6, the conclusions of the thesis and future work sections that could be performed to extend this project are outlined, and a brief attempt is made to place the work in this thesis into a wider context.

1 Theory and Background

1.1 Chemical sensors

A chemical sensor is a device that provides information to a user about the chemical nature of its environment [1]. It typically consists of a physical transducer and a chemically selective layer. The chemically selective layer interacts with the environment to produce a measurable signal via transduction (Figure 1.1).

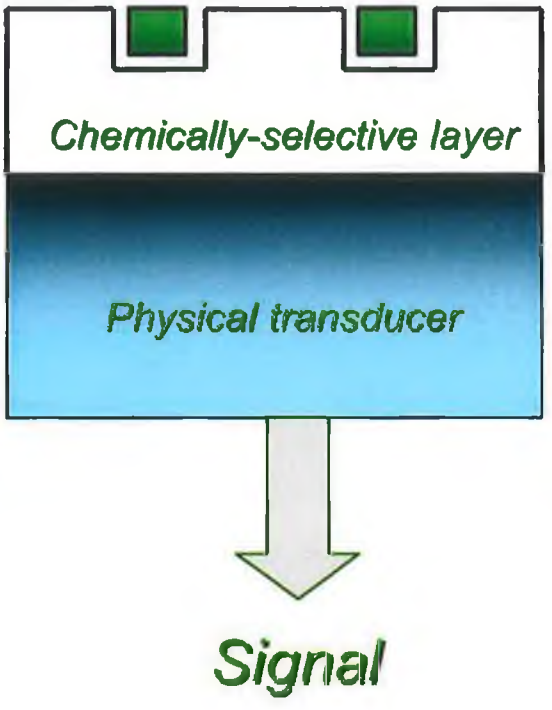

Figure 1.1: Schematic of operation of a typical chemical sensor. The analyte of interest interacts with the chemically selective layer, to produce a measurable signal via a transduction event.

The chemically selective layer is the "heart" of the sensing device. It controls factors such as the selectivity of the device (its ability to interact primarily with the analyte of interest), the sensitivity (the signal generated per unit concentration of the analyte), the lifetime, and the response time of the device [1]. Its composition is crucial to the developed sensor, as it governs all of the aforementioned properties. In Figure 1.1, the analyte of interest (shown as squares) is recognised by the chemically selective layer, causing some result (e.g. a binding event) that is detected by the physical transducer, to generate a measurable signal. An ideal sensor should have a high signal-to-noise (S/N) ratio and a fast response that is both selective and

sensitive, with no hysteresis of the signal. Ideally, no sampling, reagent addition or dilution step should be required, and the data should be available in real-time [2].

The interaction of a chemical species (X) with a typical reversible chemical sensor (S) can be described by the following equilibrium [3]:

$$X+S \underset{k_r}{\overset{k_f}{\rightleftharpoons}} XS \qquad \textbf{Equation 1.1}$$

where k_f, k_r = rate constants for forward and reverse reactions.

The ratio of the rate constants describes the equilibrium constant, *K*:

$$K = \frac{k_f}{k_r} = \frac{a_{XS}}{a_X a_S} \qquad \textbf{Equation 1.2}$$

where *a*= activity of a species, defined as:

$$a = fC \qquad \textbf{Equation 1.3}$$

where *f*= activity coefficient

C = concentration of analyte of interest.

The response time of a sensor is hence heavily influenced by the value of the rate constants, together with the mass-transport parameters of the analyte of interest involved in the transduction mechanism of the sensing scheme (Figure 1.1).

1.1.1 Modes of transduction

Transduction plays a vital role in any sensor and many different transducers are commonly used in modern sensing technology. There are four principal modes of transduction, namely methods involving thermal, mass, electrochemical or optical transduction. Thermal sensors involve the use of a thermal probe to measure the heat involved in a chemical reaction, taking place in a chemically selective layer coated onto the probe [4]. Catalytic sensors that can detect low concentrations of flammable gases in air for safety reasons in mining operations are a typical example. Mass sensors measure changes in mass on a chemically selective layer due to specific interactions between the sensor and target molecules [5]. One common example of mass sensing is the use of piezoelectric crystals in quartz crystal microbalance devices that are used typically in the so-called "electronic nose".

Electrochemical sensors represent the most well-established and oldest group of chemical sensors [6]. Techniques such as potentiometry, voltammetry and amperometry have all grown out of the field of electrochemistry to become widely used techniques [7]. Analytical potentiometry involves measuring the electromotive force (emf) in a cell where a spontaneous chemical reaction is occurring [7]. The most common example of an ion-selective electrode (ISE) is the glass-membrane electrode that is used worldwide for pH measurements, due to its very high selectivity for H_3O^+ ions and its chemical ruggedness.

1.1.2 Optical sensors

Optical sensors, according to Wolfbeis, "have always played the dominant role in various fields of analytical sciences" [8]. Optical sensors involve the reaction of a chemically selective layer with a species of interest to produce changes in the optical properties of the sensor. This may be a change in absorbance or fluorescence intensity, and is typically detected colorimetrically or spectrally. Optical sensors are extremely well established, dating back to the ca. 1930s when pH indicator paper

was developed, by immobilising pH indicator dyes on cellulose strips [8]. Fibre-optic chemical sensors are another example of a huge field that rely on optical transduction to detect analytes of interest. Optical sensors have a number of advantages over other sensing methods [9], such as:

- No separate reference signal is required, unlike electrochemical sensors.
- Transmission of signals over very large distances has been made possible by developments in fibre-optics from the telecommunications industry.
- No electrical interference from surrounding sources occurs.
- Coupling of sensors to create arrays or bundles of sensors is much simpler than for electrochemical sensor arrays. There is direct physical contact between the signal pathway and sensing membrane, which facilitates simultaneous monitoring of many analytes of interest without crosstalk between sensors.
- Optical sensing is typically a non-destructive method, a key issue when only small amounts of sample are available.
- The simple design of most optical sensors make them more suitable for mass production than their electrochemical counterparts.

There are of course disadvantages of optical sensing over other sensing methods, namely:

- Interference from ambient light. This only affects visible sensors and requires strict control over the surrounding environment where a measurement is taken. Conversely, this is not an issue in optical fluorescent sensing.
- The response time for analytes with small diffusion coefficients is typically poor, as mass transfer is necessary before a steady-state equilibrium is reached.
- Sensors with immobilised indicators are prone to leaching when placed in solution. This is also an issue for electrochemical sensors.
- For pH sensors, the dynamic range is much less than that available from the common pH glass electrode.

Thus optical sensors are widely used for sensing in many common and extensively funded areas of research, such as environmental sensing, diagnostics and clinical testing.

1.2 Principles of spectroscopy

Spectroscopy can be defined as the study of the interaction of electromagnetic (EM) radiation with matter, and it occurs over a broad range of frequencies [10]. Typically, a sample (be it gas, liquid or solid) is irradiated with monochromatic (i.e. single wavelength) light, and the interaction between the two is measured by comparison to the original wavelength source. Different frequencies of EM radiation give inherently different information about a sample, and Table 1.1 gives a summary of the range of molecular spectroscopies available to optical sensors [10].

Region	Wavelength / μm	Transitions studied	Information obtained	Energy of transition /kJ mol^{-1}
Far-IR	10-1000	Rotations	Interactions	0.42
IR-Raman	1-10	Vibrations	Functional groups	4.2
UV-Vis	0.1-1	Electronic shell	Ionisation energy	42-420
X-ray	0.01-0.1	Electronic core	Bond dissociation	420-4200

Table 1.1: Summary of molecular spectroscopies and their applications.

1.2.1 Electromagnetic radiation

EM radiation itself is made up of two sinusoidally oscillating electric and magnetic fields, in phase, that are perpendicular to each other (Figure 1.2).

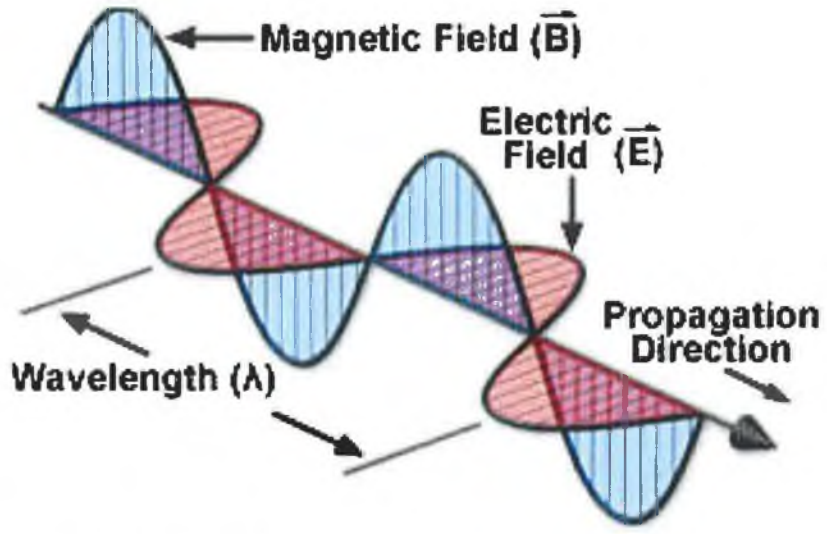

Figure 1.2: Schematic of an electromagnetic wave [11].

The wave travels through space with a velocity (c) of ca. 3 x 10^8 m s^{-1}. The frequency (ν), wavelength (λ) and velocity are related by [10]:

$$\lambda \upsilon = c \qquad \textbf{Equation 1.4}$$

Light energy may be considered to be quantised, meaning that it does not exist at all energies, but at definable energy levels known as quanta. Each quantum of energy (ΔE) is called a photon, and is defined by the classical Bohr model [10]:

$$\Delta E = \frac{hc}{\lambda} \qquad \textbf{Equation 1.5}$$

where h= Planck's constant, 6.63 x 10^{-34} J s.

Hence, energy is seen to increase with frequency (Table 1.1). Wavenumbers are sometimes used instead of frequency, and are the inverse of wavelength (cm^{-1}) [12]. Wavenumbers thus also increase with energy.

1.2.2 UV-Vis spectroscopy

Optical sensors operate primarily in the ultraviolet (UV) and visible (Vis) regions of the EM spectrum [10]. Hence, the interactions are limited to electronic transitions that occur when a beam of radiation (intensity I_o) is absorbed by a sample (Figure 1.3), leading to a decrease in the intensity of the beam (intensity I). Absorption is the inverse of transmission, e.g. a sample that absorbs no energy will hence transmit 100 % of the light intensity, i.e. $I_o = I$.

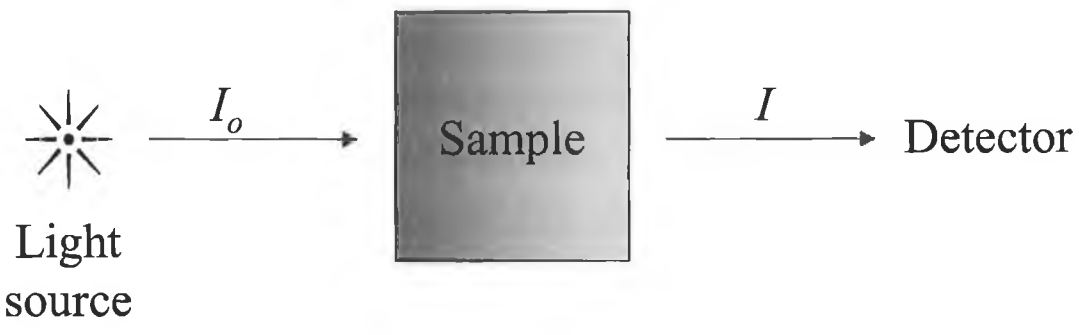

Figure 1.3: A sample of interest in irradiated with intensity I_o, transmitting a beam of intensity I, following absorption of some of the incident radiation.

Typically, the frequency of the irradiating beam is scanned, and the degree of absorption of the interacting light varies, to produce an absorption spectrum. When a molecule absorbs a photon of light of the correct energy (Equation 1.5), it is excited from its electronic ground state to its first excited state. Each electronic state has a set of vibrational sub-energy levels, in which the energy separating the states is much lower than the energy between electronic states. The excited molecule can then lose its energy by relatively weak rapid collisions, or radiatively, i.e. fluorescence.

1.2.2.1 Beer-Lambert Law

The absorbance (A) of a species of concentration C is characterised by the Beer-Lambert law (often shortened to Beer's law) [13]:

$$I = I_0 10^{-\varepsilon c L}$$ **Equation 1.6**

where ε = molar absorbtivity / L mol^{-1} cm^{-1}, a measure of the degree of probability of an electronic transition from ground to an excited state,

L = light path length /cm.

This is often rearranged to the more common form shown:

$$A = \log_{10}\left(\frac{I_o}{I}\right) = \varepsilon C L$$ **Equation 1.7**

On a practical level, this main outcome of this equation is principally when I_o and I are known, the absorbance can be calculated, and is directly proportional to the concentration of an absorbing species. This is often used to generate linear calibration curves, to relate an unknown concentration of a species to its absorbance. Additionally, deviations from Beer's Law are commonly seen when monochromatic light is not used, or in samples that are highly absorbing or highly scattering [13].

1.3 pH

pH is defined as a measure of the amount of hydrogen ions in solution [14]. For an acid HA, the following dissociation produces hydrogen ions (sometimes called protons, H^+, or more correctly H_3O^+):

$$HA + H_2O \rightleftharpoons H_3O^+ + A^- \qquad \textbf{Equation 1.8}$$

This is based on the Brønsted-Lowry definition of acids and bases from 1923, which defines an acid as a proton donor, and a base as a proton acceptor [15]. Sørensen *et al.* did much work on the field of pH, and in 1909 proposed a definition of the hydrogen ion activity [16]:

$$pH = -\log a_{H_3O^+} \qquad \textbf{Equation 1.9}$$

where a_x implies activity of species x [a].

Hence, a stronger acid drives Equation 1.8 to the right hand side, which produces more hydrogen ions, which by definition has a lower pH value. This is the standard definition of pH. The relative strengths of acids and bases are described by their dissociation constants (K_a), defined as the ratio of dissociated species to undissociated [17]:

$$K_a = \frac{[H_3O^+][A^-]}{[HA]} \qquad \textbf{Equation 1.10}$$

---

a In solutions of low activity and ionic strength, the activity coefficient approximates unity and concentration terms are typically used in place of activity. [x] implies the concentration of x.

From which the following expression is derived, the Henderson-Hasselbalch equation [17]:

$$pH = pK_a + \log_{10} \frac{[A^-]}{[HA]} \qquad \textbf{Equation 1.11}$$

where the pK_a is defined as the negative logarithm of the dissociation constant. A stronger acid will have a lower pK_a, whilst a weaker acid will have a higher pK_a.

1.3.1 Determination of pH

Two commonly used methods are typically used to determine pH. The electrochemical method of pH measurement is used in laboratories worldwide and it is the gold standard for pH measurements in solution. The pH function of the glass electrode was first discovered at the start of the last century in 1906 [18]. A pH meter is essentially a high impendence millivolt meter that measures the changes in cell potential arising from ion-exchange processes occurring at the electrode membrane in contact with the sample solution. pH meters are convenient to use, require little maintenance, can measure in a variety of environments often without strong interferences and are relatively inexpensive. However, they require calibration at two pH values before measurements are taken if the slope of the measurement is required.

1.3.2 pH indicators

pH indicator dyes are typically weak organic acids that change colour as a function of the acidity of the surrounding environment, which is usually aqueous [19]. pH indicators may be characterised formally on the basis of their pK_as [17], and hundreds are available that range across virtually all pH values [20]. For a particular application, the pK_a of a dye should be close to the pH range that the user requires.

An approximate definition is that the working range of an indicator in solution is ± 1 pH unit of the pK_a [17].

1.3.2.1 Theory of chromophores

pH indicators are based on molecular groups that are characteristically coloured, and Witt in 1876 found a relationship between the colour of an indicator in solution and chemical groups of the compound, which he termed chromophores [17]. Typical chromophores are shown in Table 1.2. Note that the common chemical feature is the presence of double bonds, i.e. conjugation.

Group	Formula	Group	Formula
Nitro	$-NO_2$	Nitroso	-N=O
Azo	-N=N-	Ene	>C=C<
Carbonyl	-C=O	Azoxy	-N=N-O-
Thiocarbonyl	-C=S	Azoamine	-N=N-NH-

Table 1.2: Typical chromophores and their chemical compositions.

In order to fully understand why chromophores are coloured, it is necessary to explain more fully the electronic transitions that occur at a molecular level. There are a number of electronic energy levels in a molecule [21]. Each of these in ascending order of energy are:

Bonding σ (σ) - *least energetic*
Bonding π (π)
Non-bonded (η)
Antibonding π (π^*)
Antibonding σ (σ^*) - *most energetic*

Pairs of electrons occupy each of the electronic energy levels. In some cases, a lone electron in an orbital may be able to undergo an energy transition, provided that the

transition is allowed and favourable. The energy gap of this transition must match exactly to the energy of an incoming photon, since the energy levels are quantised. Excitation of an electron occurs between the highest occupied molecular orbital (HOMO) and the lowest unoccupied molecular orbital (LUMO) [19]. The transitions of most importance in pH indicator dyes are π to π^* transitions (Figure 1.4).

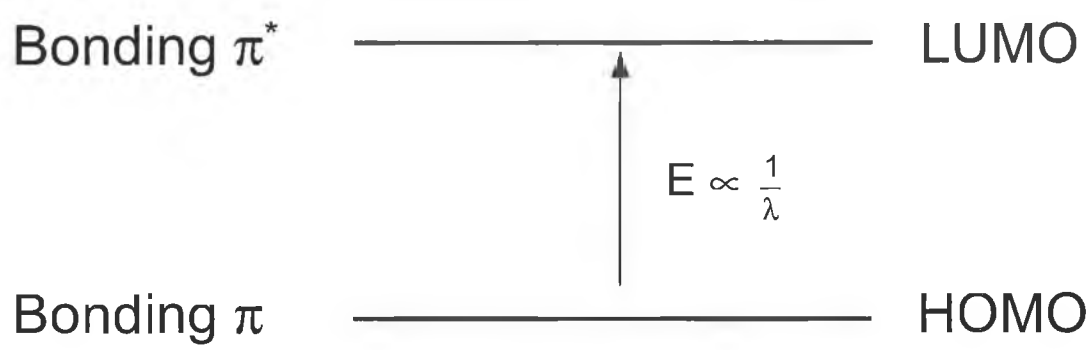

Figure 1.4: Electronic transition of most importance in indicator dyes.

One or more non-bonding orbitals (η) can be present between the π and the π^* orbitals. These contain electrons that do not contribute to the bonding in the molecule, e.g. lone pairs of electrons from nitrogen bonding. η to π^* transitions are also possible, but contribute less to the colour of a dye. Calculations have shown that the presence of chromophores in a molecule decreases the energy gap between the HOMO and LUMO, by raising the HOMO energy and lowering the LUMO energy (Figure 1.4), i.e. shifting the emitted radiation to longer wavelengths [19]. Hence, molecules that contain extended conjugation are typically coloured and this gives rise to a visible absorption band. Generally, an increased amount of conjugation increases the light absorption, and shifts the λ_{max} to longer wavelengths (lower energy).

Ring substituents also play a vital role in altering the energy gap between the HOMO and LUMO, and hence the λ_{max} of the absorption spectrum. These groups have an important affect on the colour of a compound, but are not by themselves coloured. For this reason, they were termed auxochromes by Witt [17]. Electron donating groups such as methyl groups have the effect of stabilising a molecule by feeding

electron density into a delocalised π system. This decreases the HOMO energy level (more stable), hence making the energy required for a π to π^* transition larger. This shifts the wavelength maximum of a dye to lower wavelengths. Conversely, electron withdrawing groups such as nitro or halogen groups reduce the stability of a molecule by pulling electron density out of a delocalised π system. This raises the HOMO energy level (less stable), leading to a lower energy requirement for a π to π^* electronic transition. This has the effect of shifting the wavelength to a higher value.

1.3.2.2 Relationship to spectral features

When a pH indicator dye is placed in solution of pH greater than the pK_a of the dye, a proton is removed, since the dye itself is a weak acid. This displacement causes a change in the electronic distribution within the molecule, which is expressed as a change in the colour of the dye. Bromophenol blue, for example, has a pK_a of 3.8 and is a commonly used pH indicator dye [20]. Chemically, it consists of many of the chromophores shown in Table 1.2 (Figure 1.5). The removal of the acidic proton causes a distinct change in the spectra of the dye, and Figure 1.6 shows the spectra of the protonated and deprotonated forms of bromophenol blue.

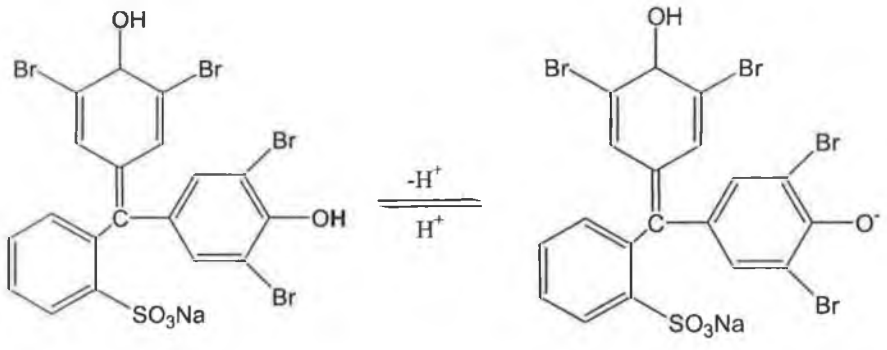

Figure 1.5: Removal of the acidic proton of bromophenol blue. The labile proton is highlighted in bold.

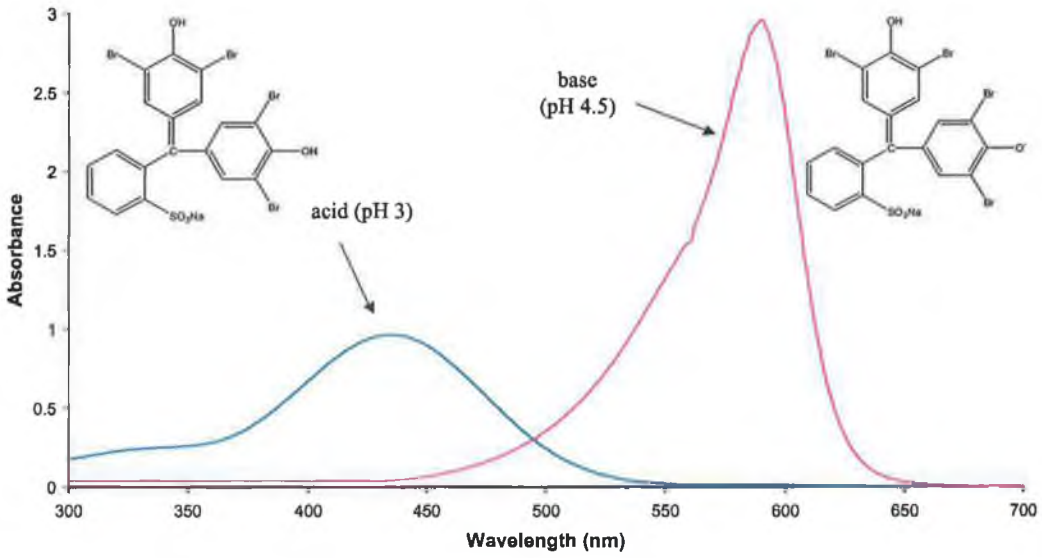

Figure 1.6: Removal of the acidic proton causes a distinct shift in the λ_{max} of bromophenol blue, from 438 nm (yellow) to 580 nm (purple).

This example clearly highlights how large spectral changes can result from small changes in pH of the surrounding environment. It also shows the narrow working range of a pH indicator dye.

1.3.2.3 Factors affecting the colour changes of pH indicators

Indicator concentration

High amounts of indicator dye reduce the limit of perceptibility of a visual transition interval. Generally, the colour change occurs over a broader wavelength range at higher indicator concentrations [17]. This occurs if the absorption peaks of the two forms of the dye are overlapping each other, which greatly reduces the sensitivity of the colour change. It also requires more sample to generate the colour change.

Dissolved CO_2

Carbon dioxide is greatly soluble in alkaline conditions. For this reason, dyes with high pK_a values are all significantly sensitive to the presence of CO_2 in the surrounding environment of the solutions in which they are prepared. Removal of CO_2 by boiling is typically performed prior to addition to the measurement solution [17].

Solvent effects

The ion product of water (K_w) [22] is defined as:

$$K_w = [H_3O^+][OH^-] = 10^{-14} \qquad \textbf{Equation 1.12}$$

Hence, using the Henderson-Hasselbalch relationship (Equation 1.11), the pK_a is defined as:

$$pK_a = 14 + \log_{10}\frac{[A^-]}{[HA]} - \log[OH^-] \qquad \textbf{Equation 1.13}$$

However, $\log_{10}$ of K_w is only -14 in pure aqueous solutions, and the addition of organic solvents can have a major effect on the pK_a of the dye. This is most noticeable in alcoholic solvents [17]. Hence, when a pK_a value of an indicator dye is quoted, the solvent conditions must also be reported.

Temperature

At elevated temperatures, the colour of acid-sensitive indicators is typically shifted more towards the acidic direction, and the colour of alkali-sensitive indicators is typically shifted more towards the alkali direction. This effect is not completely understood. The most common (and simple) explanation is that the ion product of

water varies greatly with temperature, shifting from 14 at room temperature to 12.2 at 100 °C [17]. This affects the pK_a as shown in Equation 1.13.

Salt effects

The presence of foreign neutral salts will shift the transition interval of an indicator acid more towards lower pH values, i.e. higher proton concentrations, and shift an indicator base more towards the higher pH values, i.e. lower proton concentrations. This can be explained by the theory of Debye and Hückel, which describes the relationship between the apparent pK_a (pK_a`) and the ionic strength (μ) of a solution. For each of the three charge types of indicators, the pK_a alters as:

$$HA^+ \rightleftharpoons H^+ + A$$
$$\Rightarrow pK_a` = pK_a + 0.5\sqrt{\mu}$$

$$HA \rightleftharpoons H^+ + A^-$$
$$\Rightarrow pK_a` = pK_a - 0.5\sqrt{\mu}$$

$$HA^- \rightleftharpoons H^+ + A^{2-}$$
$$\Rightarrow pK_a` = pK_a - 1.5\sqrt{\mu}$$

The error introduced for an indicator dye with two negative charges is thus large. It is clearly important to regulate all of the experimental conditions mentioned that can have substantial effects on the pK_a of the indicator dyes.

1.4 Applications of pH indicator dyes

Immobilisation of pH indicator dyes is a key issue in the design of optical pH sensors. Three main classes of optical sensors are typically produced by immobilisation of indicator dyes onto a substrate, and these will be covered in detail in the coming sections. Each of these methods produces sensors that have inherently different properties, and hence are suitable for different applications. In all optical based sensing, the general principle is that the reaction of an immobilised dye with a target analyte causes a change in the optical property of the sensor (Figure 1.7).

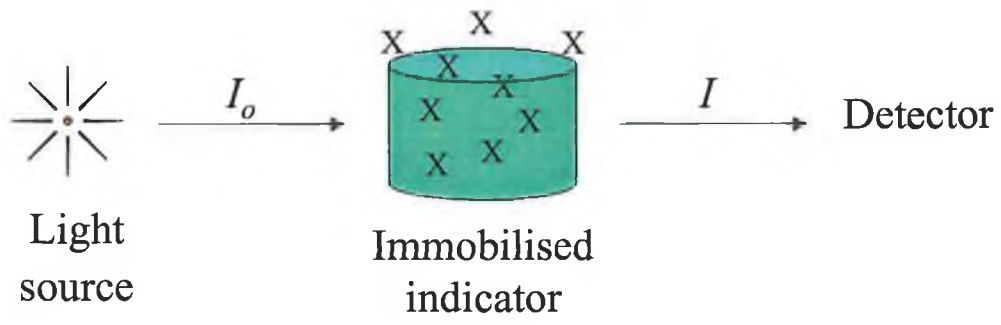

Figure 1.7: General schematic of optical sensing. The indicator is immobilised on a surface, and interaction with the target analyte (X) causes a change in the optical properties of the sensor.

1.4.1 Selection of pH indicator dye

There are a number of requirements to be met when choosing a pH indicator dye for an application, and these include [23]:

- A pK_a close to the pH range of interest.
- Large separation between the two absorption peaks, to improve the sensitivity of the response, as overlap can be a problem.
- Strong absorption in the visible region (ca. 400 nm – 700 nm), to allow inexpensive optics to be used to measure the optical properties. Strong absorption is expressed through a high extinction coefficient, ε.

- Chemical stability and photostability. This relates to the sensor before exposure to the analyte (e.g. to infer a long shelf-life), and to the stability of the changes in optical properties, so that these can be measured easily.
- The availability of chemical functional groups for immobilisation purposes. This is most relevant in the case of covalent immobilisation of indicator dyes.

The selected pH indicator dye is typically immobilised onto a surface, and the interaction of the immobilised dye and the target analyte is monitored via optical detection. A review of the literature reveals that there are a number of novel substrates that are used for optical pH sensing, and each of these are covered in the following sections.

1.4.2 Immobilisation methods

Immobilisation is thus a key feature of sensor design. The following points must be taken into consideration when choosing a method for immobilisation [24]:

- Compatibility of the reagent with the immobilisation method.
- Tolerance towards leaching; leaching can in some instances be tolerated but, in other applications such as in the food or medical industries, leaching can be a major concern. In general, it is better that it does not happen.
- The reproducibility of the immobilisation method.
- The complexity of the immobilisation method.
- The influence of the immobilisation method on the chemically selective layer, e.g. changes in sensing properties.
- Physical and chemical properties that are required of the support matrix, e.g. gas sensors must have high permeability for target analytes in order to have fast sensor response times.
- The ease by which the immobilisation procedure can be transferred to mass production. This point is of key importance in any commercial applications of the sensor.

An excellent recent review by Lin [25] covers applications of each main method of immobilisation in much more detail than is possible here. Dyes are typically either covalently bound, or physically entrapped into a polymer matrix. In covalent binding, the indicator dye is covalently linked onto a solid substrate. The main advantage of forming a covalent bond is that the dye is strongly linked into the polymer and cannot leach from the matrix when the sensor is placed in solution. However, this approach is typically highly complex and time-consuming, and should only be used if necessary. Another approach is to entrap the indicator in a porous polymer substrate, which has the advantage of being quick and simple. Leaching may occur if the sensor is placed in solution, so the working environment and tolerance to leaching must be considered when designing an immobilised dye sensor.

1.4.3 Fibre-optic based pH sensors

Fibre-optic based chemical sensors (FOCS) are a relatively recent field that grew out of advances in the telecommunications industry [8]. FOCS can be classified as those that are direct spectroscopic sensors, in which the fibre operates as a lightguide, or reagent-mediated sensors, often termed optrodes (from optical-electrode) [26]. The latter is most relevant here, and this review is limited to this group of sensors.

Reagent-mediated FOCS involve immobilising an indicator onto a fibre tip (Figure 1.8), which can be a single fibre, or a bunch of fibres. Light propagates through the fibre-optic by the phenomenon of total internal reflection, since the cladding of the fibres has a higher refractive index than the inner core. Light can be passed over long distances, and FOCS can offer the advantage of imaging, as well as chemical sensing.

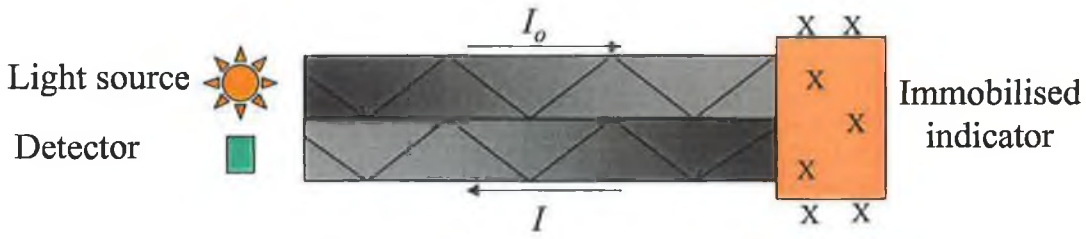

Figure 1.8: Schematic of reagent-mediated FOCS (optrodes). The analyte (X) reacts with the immobilised indicator, and the changes in optical properties are measured. The fibre-optic is surrounded by cladding of a higher refractive index (not shown).

This approach has a number of attractive properties, namely [26]:

- The optical techniques used are already well established.
- Remote in-situ monitoring of analytes in hazardous or difficult locations is possible, e.g. groundwater monitoring.
- Devices based on fibres are relatively simple to miniaturise, due to geometric flexibility and advances in the telecommunications industry, from which the development of fibre-optics has been huge.

A recent biennial review by Wolfbeis on FOCS and biosensors [27] reveals that this is a flourishing area of research, with ca. 140 papers published on this topic in the past two years. The main areas of interest are identified as time-resolved and spatially-resolved spectroscopy, surface plasmon resonance and multi-dimensional data acquisition.

A limited number of papers are present in the literature that describe the use of pH indicator dyes immobilised onto FOCS for pH monitoring. One paper describes immobilising phenol red (pK_a 7.5) by adsorption onto a thin coating of resin mounted on the surface of an optical fibre [28]. This was developed for monitoring the pH of seawater, which is a special environment due to the variable temperature of the water and its high salinity, which can introduce a large salt error. A single fibre-optic tip was used to monitor the changes in absorption at the λ_{max} of the dye as a function of pH, and a study of the effect of temperature and salinity on the readings was

performed. The device was found to have a working range of ca. 2 pH units, which is typical of such sensors. A linear dependence on salinity and temperature response was reported within the ranges most typically encountered, although the chemistry behaves erratically at the extremes of both. The data obtained was comparable to data from a glass electrode within the range of linearity [28].

One advantage of FOCS is the small sizes that can be prepared to produce so-called submicron optochemical sensors. Wolfbeis *et al.* recently described sensors for pH monitoring on fibre-optic tips that ranged from 50 to 300 nm in diameter [29]. The pH indicator dye bromothymol blue was used in a donor-acceptor complex as the acceptor from a luminescent donor. The indicator complex was immobilised onto polymeric membranes based on hydrogels that were spin-coated onto fibre-optic tips, and the change in decay time as a function of pH was measured. Excellent results between pH 6 and 8 were achieved, and the sensor is hence suitable for measurements in typical physiological fluids.

Walt at Tufts University, Massachusetts, has published several papers on the use of arrays of sensors on fibres for pH sensing, amongst other examples. The challenge of monitoring pH in whole blood was targeted by the use of many sensing sites photopolymerised onto the ends of fibres [30]. Three individual pH-sensing areas are presented on a single sensor, and the degree of fluorescence of the active sites are measured and spatially discriminated by the use of a charge-couple device (CCD) based video camera.

This approach was taken further by immobilising Nile Red on fibre-optic tips and measuring the changing response patterns obtained upon exposure to different organic vapours [31]. This approach is essentially mimicking the olfactory system. By immobilising the dye in polymer matrices of varying polarity, hydrophobicity, pore size, flexibility and tendency to swell, sensing sites that respond differently when exposed to different vapours were prepared. 14 different polymers were used in this study [32]. The mode of coating was also varied from photopolymerisation to solvent evaporation dip-coating, to create arrays of different sensors. A CCD array

was again used to discriminate between the sensing sites. The developed methodology has been refined to create sensing arrays with hundreds of sites on a single fibre-optic tip [33]. The signals from each of the different fluorescent sites based on phenol red are powerful enough to allow 6 different analytes to be discriminated. 3 simple odours (toluene, acetone and 1,3-dinitrotolune) and 3 complex odours (coffee beans) were successfully discriminated. The main difficulty with these sensing arrays is that a reduction in size typically equates to a reduction in signal. By using many sensing sites on the one tip, Walt has developed a novel approach around this.

1.4.4 Sol-gel based pH sensors

Sol-gels are silica based (glass) films that have found much application in the entrapment of indicators for pH sensing [34]. They are produced from silicon alkoxide precursors that undergo various reactions to produce films of different densities. The most common precursors are tetramethoxysilane (TMOS) and tetraethoxysilane (TEOS). A nanoporous nondensified glass matrix can be produced if the cocktail of water, ethanol and precursor in hydrochloric acid (catalyst) are correct, and if the temperature-curing program used is less than 200 °C. The sol-gel acts as a support matrix for analyte-sensitive indicator dyes, which are added to the precursor cocktail prior to coating onto a substrate. Dip-coating onto planar surfaces is typically performed, followed by drying at 70 °C for 18 h [34]. Careful selection of the dopant indicator molecule in general ensures that leaching is not an issue.

Lin and Liu recently described a sol-gel based optical pH sensor with a linear response over a broad pH range [35]. Four pH indicator dyes were used in this study, namely bromocresol green, bromocresol purple, phenol red and thymol blue. These four similar sulphonephthalein indicators were selected on a basis of their pKa values, which ranged from ca. 4 to 8. Additionally, the base forms of the four indicators all have similar spectral features. A linear pH response over 4 pH units was obtained for the dyes in free solution. Three of the indicators were co-entrapped

into a TMOS sol-gel glass film, and a linear response over 3.5 pH units was obtained. A linear response over a large pH range is not possible with a single indicator dye and the approach taken here is favourable since it lends itself to a simple calibration procedure. Furthermore, the sensors had constant sensitivity over the working pH range, which was achieved by matching the concentration of individual dopant indicators, and choosing those dyes that had a ΔpK_a of approximately 1.5 (this value was derived empirically by testing different ratios of all four indicators). The authors propose that this method could be extended to developing sensors with an even wider pH range.

Sol-gel chemistry was combined with recent advances in pin-printing technology to produce chemical sensor arrays for simultaneous monitoring of pH and O_2 [36]. The use of smart pin-printing techniques allowed sensors 100 μm in diameter and ca. 2 μm thick to be produced, at a rate of < 1 s per sensor, per pin used. The pH sensing indicator used was fluroescein-labelled dextran, which was mixed into a sol-gel cocktail of TEOS and TMOS. The arrays were exposed to pH buffers in solution, and the response was measured by excitation with an argon laser, and detected with a CCD array. The response is linear in the range of pH 5-7. Clearly this approach lends itself well to multi-analyte arrays, or to creating pH sensors with a broad range, by printing selected indicators that cover the entire pH range of interest.

Bromothymol blue has been entrapped into sol-gel matrices that each included a luminescent europium complex [37]. A single sensor layer based on TMOS was used to generate results over the very broad pH range of 5-9. The sensors showed optical and chemical stability over 1 year. The response time of the sensors is slow however, in the order of > 10 min. This slow response is unlikely to be due to the response of the dye; it is apparently an issue of mass transport into the matrix. However, another paper that used a different sol-gel matrix has shown much faster response times [38]. Both bromocresol green and cresol red were doped into TEOS sol-gel films to produce sensors of excellent stability and uniformity, with response times as fast as < 60 sec. The authors note that this is a significant improvement over other papers that show response times as long as 20-100 min. All films show a linear pH response

over ca. 2-3 pH units, and interestingly, the pK_a values of both dyes shift by ca. 2-3 pH units, which is attributed to hydrophobic interactions between the indicators and the silicate film. As with other sol-gel based methods, no significant dye leaching in solution is reported.

1.4.5 pH sensors based on cellulose binders

Cellulose and its derivatives are widely used for the entrapment of indicator dyes to create optical pH sensors. Cellulose is an ideal support for pH indicator dyes as it has high permeability for water and ions, and is stable for use equally in the acidic and basic pH ranges [25]. It is very widely available, since it is the main component of the cell walls of plants [39]. Chemically, it is a basic carbohydrate with the molecular formula $(C_6H_{10}O_5)_n$, where n can be thousands, creating a large linear polymer matrix. The OH groups of the monomer units interact with each other, to create a large, hydrophobic macromolecule that is water-insoluble. Acetylation of cellulose creates a material that is the basis for X-ray and cine film, cellulose acetate (Figure 1.9).

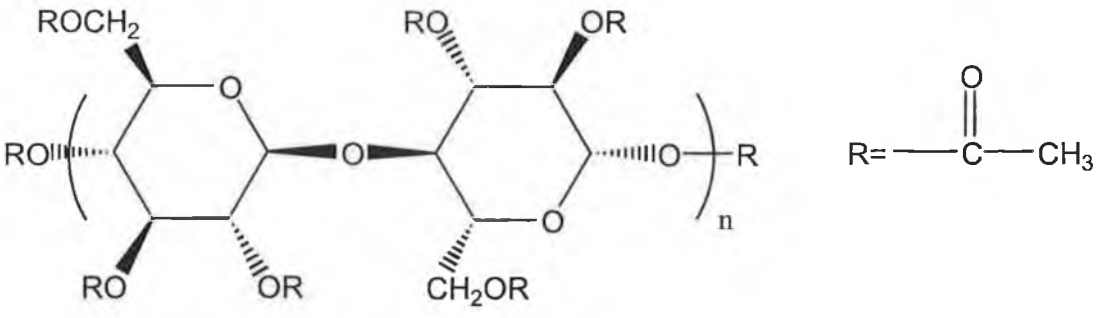

Figure 1.9: Cellulose acetate. The R groups are acetate groups; in naturally occurring cellulose, the R groups are hydrogens.

Cellulose acetate has found much use in the field of pH sensing. A 1997 paper by Dybko *et al.* described the polymer as having high water permeability and excellent dye-retaining capacity [40], due to the disruption in hydrogen bonding by the

acetylation of cellulose. Cellulose acetate films are brittle and are not generally suitable for durable, rugged support matrices. At room temperature, the molecular rotation around single bonds is energetically difficult. This is explained by a thermal property of linear polymers known as the glass transition temperature, T_g [41]. This is a temperature where the molecular rotation around single bonds becomes easier; there is hence a significant change in the rate of change of volume versus temperature.

1.4.5.1 Plasticisers

The presence of plasticisers is known to lower the T_g of a polymer [41]. Plasticisers are typically liquids with molecular masses much lower than the polymer to which they are added. They can be thought of as non-volatile solvents, albeit with higher molecular masses than typical organic solvents. The presence of a plasticiser in a polymer matrix creates homogeneous materials that are more flexible and softer than the polymer alone. Plasticisers act as spacers at a molecular level, essentially fitting into a polymer matrix at available sites [41]. Less energy is thus required to allow C-C bond rotation, which results in a reduction of the glass transition temperature, creating a softer, more flexible support matrix. In the case of cellulose acetate, this is advantageous for sensor design, as it may make the sensor less brittle, and hence more rugged.

One of the most common examples of the effects of a plasticiser is the addition of di-iso-octyl phthalate to polyvinyl chloride (PVC). PVC is typically a rigid solid at room temperature; the incorporation of 70 parts phthalate into PVC converts the polymer into a rubbery material used commonly in personal protective clothing. The T_g of PVC is reduced from a value higher than room temperature (without plasticiser) to a value that is below room temperature (with plasticiser). This is not the only role that a plasticiser can play in a solid support matrix however. By making the polymer support solvated [41], there may be a reduced mass-transport time for an analyte of interest to diffuse into the bulk of the polymer matrix. Thus the response

time of a sensor can potentially be reduced by the addition of a plasticiser. Hence plasticisers are often used in ISE membranes and gas sensors.

1.4.5.2 Applications of cellulose based pH sensors

Typically, various pH indicator dyes can be either covalently bound to the support matrix, or physically entrapped in it [25]. Each of these methods are described in this section.

Covalent binding approach

In this approach, the cellulose is subjected to exhaustive base hydrolysis, followed by soaking in the chosen indicator solution. Using this approach, any number of suitable pH indicator dyes can be entrapped into cellulose via dye/cellulose covalent bonding between sulphonyl (SO_3-OH) groups of the indicator dye and OH groups of the cellulose. Jones and Porter prepared porous cellulose acetate based films with congo red forming covalent bonds within the polymer matrix [42]. Using this approach, they reported a rapid response time (< 1.3 s) and a large dynamic range (ca. 4 pH units). The support matrix was shown to be stable from pH 0-13.

Kostov *et al.* performed an investigation into the characteristics of sensors produced by covalently immobilising neutral red and congo red into cellulose acetate films that were previously hydrolysed [43]. They found that the sensors have excellent durability, and that they continue to operate over more than 9 months. The response time to reach 95 % of the full-scale response was less than 30 s. The shift in the pK_a values of both dyes in the polymer matrix was determined. The average shift was ca. 1.4 pH units in the acidic direction. The authors do not make clear the reason for this shift, but they suggest that it may be due to the influence of the covalent binding procedure, which potentially removes a proton from the amino groups (which are auxochromes) during linkage, likely causing a change in the electronic distribution of the dyes. The authors neglect to describe the basis of the covalent binding, but

suggest that it is possibly formed between the OH groups of the deesterified cellulose acetate and NH_2 groups on the dyes.

Mohr and Wolfbeis have covalently linked novel azo dyes into cellulose acetate via ethylsulphonyl (SO_2-CH_2-CH_2-OH) groups, after base-hydrolysis [44]. They describe the advantages of cellulose acetate pH sensors over glass-immobilised materials such as sol-gels, as they are more easily manufactured and handled. The covalent approach presented allows the production of sensors with tailor-made optical properties and pK_a values, to produce sensors that cover the whole pH range of interest. The spectral properties of the dyes are excellent, with little overlap between the absorption maxima of both forms of the dye. A study of the shift in pK_a of the dye in free solution compared to covalently linked into the matrix was performed. There is a shift in the values obtained from those in free solution, by ca. 1 pH unit for all dyes tested (in both the acidic and basic direction). Additionally, no dye leaching was evident from the sensors.

The efficiency of this procedure for the preparation of so-called ion-sensitive optomembranes was investigated by Dybko *et al.*, who entrapped congo red and neutral red into cellulose acetate films [40]. The authors describe cellulose acetate as ideal for pH sensing in solution or gas phase, since it has a large active surface for immobilisation and is porous, making it highly permeable to ions and gases. The developed sensors were prepared by base-hydrolysis of the cellulose acetate, and no leaching of dye from the prepared films was noted over 30 days soaked in water. The response time was less than 30 s for each sensor to reach a steady state response.

An optical pH sensor for the high alkaline pH range was reported by covalently linking thiazole yellow (pK_a 12.8) into base-hydrolysed cellulose acetate [45]. This is a pH range that is traditionally difficult to measure with a glass electrode, since at this range there tends to be a large alkaline error, where the electrode responds to alkali metal cations in solution, and records a pH lower than the real value. The pK_a of the dye shifted ca. 0.5 pH units in the acidic direction, and responded well to changes in pH. The sensors are reported to have a rapid equilibration time, high

reproducibility of response and manufacture, good long-term stability and high sensitivity in the pH range of interest.

Physical entrapment approach

The use of physical entrapment of indicator dyes into cellulose acetate has also found much application, particularly in the field of FOCS. Wróblewski *et al.* described a complex formulation of congo red entrapped in cellulose acetate that has a hydrophobic plasticiser added [46]. A wetting agent, ethylene glycol, was added to the formulation to enhance hydrophobicity and therefore reduce the tendency of the dye to leach from the matrix. Different plasticisers were tested to see which best suited the formulation. Since plasticisers affect a bulk property of the polymer, this was done on a trial-and-error basis for a number of commonly available plasticisers, as it is virtually impossible to predict which plasticiser works best. The widest dynamic range was observed for the most hydrophobic plasticiser, dibutyl phthalate. The sensor operated over a wide dynamic range of pH 2.5 to 5.5, and steady state responses were obtained in less than 30 s, depending on the thickness of the prepared coatings. Similar sensors were prepared for the acidic pH range with bromothymol blue and thymol blue. Although the authors neglected to characterise the shift in pK_a for each of the immobilised dyes, the working linear range of each sensor is presented.

Cardwell *et al.* present a similar set of results for a number of azo dyes entrapped in a plasticised cellulose acetate matrix [47]. Although similar, these results are significant because of the extremely fast response time of less than 1 s per sensor. Some straightforward applications of one of the dyes (pK_a 3.8) are presented, from a titration indicator coated onto a magnetic stirrer bar, to static and dynamic pH measurements in a flow-through cell. The authors have also presented very similar results for other pH indicator dyes in the same experimental setup in another publication [48].

In summary, if the issue of dye leaching is not of major concern, indicator dyes can readily be entrapped into cellulose acetate, with no prior treatment necessary. Sensors prepared in this manner exhibit a fast response, a large dynamic range, chemical and photo stability and excellent permeability for gases and ions. More complex matrices can be prepared by hydrolysing the polymer prior to covalently linking an indicator dye, although this approach is best used in situations where tight control over dye leaching is necessary.

1.5 Seafood spoilage monitoring

In the fisheries industry, there is a large amount of interest in developing rapid methods to evaluate the quality of seafood using general quality indicators. One concept is that of a smart package sensor that gives an indication of the condition of seafood samples at various points along the distribution chain, from "harvest-to-home". Under EU directive 79/112/EEC, seafood, similar to other foodstuffs and pre-packed foods, must display either a "date of minimum durability" or, when considered highly perishable, a "use by date" [49]. A recent review of freshness, quality and safety in seafood has stated that microbial, chemical, biochemical or other instrumental methods are all appropriate methods for determination of fish freshness [50]. The emphasis is that the analyses must be convenient, fast and inexpensive to perform.

1.5.1 Sensory evaluation

The simplest and most well established method for evaluation of freshness and quality is the use of sensory methods, which rely heavily on trained assessors [51]. This is usually performed by specialist and trained personnel at fish auctions and is based on particular EU schemes relating to fish hygiene [52]. A general appraisal of whole and gutted fish is performed, including for example, investigation of skin odour, general appearance, eyes, outer slime, gills and belly cavity. It is recognised, however, that the remaining shelf life of seafood cannot be determined from freshness grades [50] and that the methods require much training for the assessors. Additionally, there is a clear lack of standardisation using this approach, due partly to differences in personal judgement. Despite this, sensory methods remain the most widely used approach for fish freshness appraisal and determination of spoilage.

1.5.1.1 Quality Index Method

It has been suggested that a quality index method (QIM) be used to further refine the sensory methodology described previously [53]. A large number of parameters relating to fish quality are measured by trained assessors, based on defined QIM schemes [54]. Points are totalled to generate QIM index points (demerit points) and there is a direct linear relationship between QIM index points and storage time at 0 °C, which allows the remaining shelf life of fresh fish to be evaluated. QIM schemes are species specific, however and need to be evaluated on a species-to-species basis. Furthermore, they are only valid at defined temperatures, normally 0 °C, and some seafood such as filleted fish or lightly preserved seafood appear to be unsuitable for characterisation under QIM schemes. The limitations of subjective sensory methods (either those using QIM schemes or not) are many, highlighting the need for objective sensory methods, which are essential for grading of fish, quality control and accurate shelf-life predictions. More carefully controlled methods should be used to supplement (and complement) sensory methods evaluation in order to obtain the most accurate freshness determination of a fish catch, and to accurately define the point of spoilage.

1.5.2 Spoilage microorganisms

Microbiological methods have been applied extensively to monitoring fish quality and predicting spoilage times [55]. There is some debate in the literature as to whether or not fish muscle tissue is normally sterile in whole, unfilleted fish [56]. The microorganisms known to cause fish spoilage are shown in Table 1.3 [57]. The bacteria most frequently found on whole fish allowed to spoil aerobically are from the genera pseudomonas or shewanella. They are both gram-negative, rod-shaped bacteria that dominate the microflora of temperate water fish such as cod. It has been found that the pseudomonas species are able to grow at temperatures lower than 0 °C, albeit at slow rates. Studies on the flora present on the outer skin of 4 different fish

revealed that the pseudomonas species are present at levels between 32-60 % of the total microbial count [58].

Genus	Gram reaction	Genus	Gram reaction
Acinetobacter	-	Flavobacterium	-
Aeromoas	-	Lactobacillus	+
Alcaligenes	-	Listeria	+
Bacillus	+	Moraxella	-
Corynebacterium	+	**Pseudomonas**	-
Enterobacter	-	Psychrobacter	-
Enterococcus	+	**Shewanella**	-
Escherichia	-	Vibrio	-

Table 1.3: Genera of bacteria most frequently found on seafood [57]. The groups of bacteria that occur most frequently are highlighted in bold.

1.5.2.1 The growth curve

Growth is defined as an increase in cellular constituents [59]. Due to the size of individual microorganisms and the huge numbers in which they grow, it is not possible to study the growth and reproduction of single microbes. Instead, changes in total population are followed, plotted as the logarithm of cell number as a function of time, and is known as the microbial growth curve [59]. This curve is shown in Figure 1.10 and is made up of four distinct phases.

In the lag phase, there is no immediate increase in cell numbers. For example, this could be the population of microorganisms on a fresh food sample. During this stage, the cells are synthesising new components to aid the division that will follow [59]. The lag phase varies in length with the nature of the sample and the age and condition of the microorganisms. The lag phase may be absent if a young growing culture is transferred to a fresh sample of the same composition from the one it was taken from.

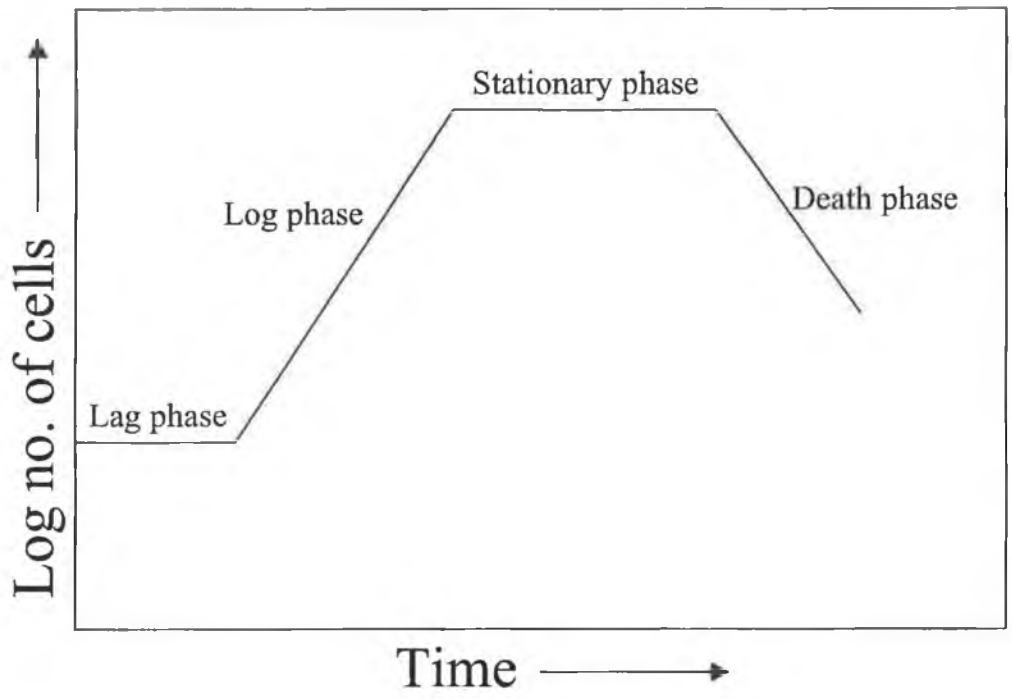

Figure 1.10: Microbial growth curve in a closed system.

In the log phase, sometimes known as the exponential phase, the cells are growing and dividing at the maximum rate possible. Factors that affect this rate include the nature of the sample, the genetic potential of the microorganisms and the conditions in which they are growing. The rate of growth is constant; the cells are doubling in numbers at a fixed interval.

During the stationary phase, the population growth stops and the growth curve therefore has reached a plateau. The cell count at this stage varies from 10^6-10^9 cells per ml or g of sample [59]. During this phase, the total number of viable microorganisms (living – dead) remains constant. A balance is typically reached during this stage between cell division and cell death. This balance doesn't last, however, and the cells enter the final phase, known as the death phase. This phase is typically entered when nutrients have been depleted, or there is a build-up of toxic waste products, and no new medium is available upon which to grow. The death phase is also logarithmic, where a fixed number of cells die in a fixed interval.

1.5.2.2 Microbial populations during spoilage

Total viable counts (TVCs) have been described in the legislation in the USA, Japan and some European countries as a method to determine seafood standards. TVC assays calculate the total amount of microorganisms present in a sample of known mass, typically 25 g or larger. There are various guidelines that can be followed, and most of them suggest that levels higher than or equal to 10^5 CFU (colony forming units) /g of seafood are indicative of a fully spoiled sample [60, 61]. There is some debate about these guidelines and it is understood that some seafood can have higher TVC levels and still be perfectly acceptable. The correlation between TVCs and remaining shelf life is poor, as spoilage is typically caused by only a small fraction of microorganisms present in fresh seafood, known as specific spoilage organisms (SSOs) [50]. One of the most common SSOs in whole, unfilleted fish is the pseudomonas species (Table 1.3). The limited information available to relate pseudomonas counts to seafood spoilage suggests that levels higher than 10^2 CFU /g of seafood may result in off flavours, off odours and some visual defects [62].

During spoilage, the rate of SSO growth is significantly faster than fish microflora growth, and SSOs are responsible for off-flavours and off-odours, thus resulting in an undesirable product. SSOs are used as indicators of the condition of a fish sample and the remaining shelf life of a product may be predicted from SSO populations [63]. Whenever microbial measurements are being taken to determine the quality of a sample or predicted remaining shelf life, it is recommended that numbers of SSOs be measured instead of the more traditional TVCs (Figure 1.11) [50]. The figure shown, taken from a recent study on fish spoilage by bacteria, clearly illustrates the relationship between TVC and SSO growth with time.

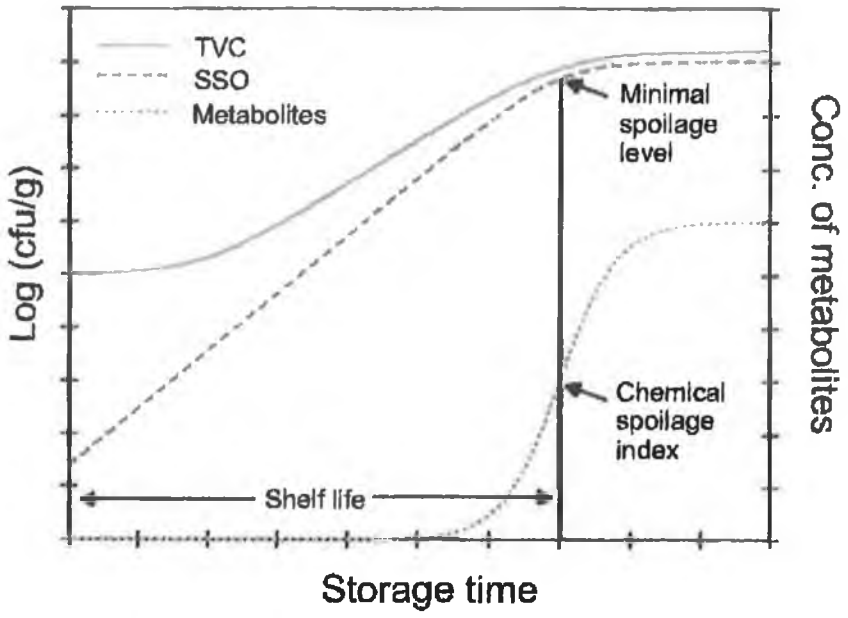

Figure 1.11: Results from a recent study show the relationship between TVCs, SSOs and the concentration of spoilage metabolites with time [50]. A number of different fish species were examined at 0 °C. The correlation between remaining shelf life and TVC levels is poor; SSO counts are recommended to be taken in order to determine the quality of a sample or the remaining shelf life.

Figure 1.11 shows that TVC values are naturally much higher than their SSO counterparts at the beginning of storage. The changes in TVC values with time are gradual and are represented by a sigmoid-shaped function. The figure also shows that there is a poor correlation between remaining shelf life and TVC numbers. In contrast, the SSO counts rise over a longer period of time and correlate much better to remaining shelf life. The SSO values allow a minimal spoilage level to be determined, and the concentration of spoilage metabolites at this point has been termed the chemical spoilage index. The metabolites are only produced in significant quantities after some time. The data shown suggests that a chemical sensor that follows the levels of spoilage metabolites cannot be used to predict remaining shelf life of an unspoiled product. Furthermore, a working metabolite sensor would, in principle, correlate much better to SSO numbers than to TVCs.

1.5.3 Spoilage volatiles

Saltwater and freshwater fish both contain high amounts of proteins and other nitrogenous constituents [58]. The nature of the nitrogenous compounds is of particular importance as not all nitrogenous compounds in fish are in the form of proteins. Table 1.4 shows the relative percentages of total nitrogenous (total-N) compounds and protein nitrogenous (protein-N) compounds from the flesh of 5 different common species [58]. The non-protein nitrogenous compounds include, for example, the free amino acids and volatile nitrogenous bases.

Species	Total N (%)	Protein N (%)	Ratio of Protein N / Total N
Cod (Atlantic)	2.83	2.47	0.87
Herring (Atlantic)	2.90	2.53	0.87
Sardine	3.46	2.97	0.86
Haddock	2.85	2.48	0.87
Lobster	2.72	2.04	0.75

Table 1.4: Relative distribution of nitrogen in fish and shellfish flesh.

The outer slime is composed of mucopolysaccharide components, free amino acids, trimethylamine oxide (TMAO) and other related compounds. Also likely present are fish spoilage bacteria [a]. According to studies performed [58], TMAO levels decrease during fish spoilage with the production of volatile compounds such as trimethylamine (TMA), ammonia (NH_3) and dimethylamine (DMA). These compounds are hence indicator compounds of fish spoilage, and are collectively known as total volatile basic nitrogen compounds (TVB-N).

The ratios of amines comprising TVB-N are species dependant and appear not to relate to the type of microorganisms that cause spoilage [64]. Ammonia is produced by bacterial degradation of proteins, peptides and amino acids; TMA is produced

---

a There is some debate on this in the literature. If the bacteria do not arise on the outer slime, they most certainly arise in the digestive system of the seafood [56].

from the bacterial degradation of TMAO, and DMA is produced by enzymatic degradation of TMAO by TMAO dimethylase (TMAO-ase), which releases equimolar amounts of DMA and formaldehyde [64]. TMA is produced in the highest quantity, although the vast majority of testing that is performed determines the levels of the collective bases, TVB-N. By taking this approach, it is not necessary to know the ratio of the amines present.

1.5.4 Determination of TVB-N

TVB-N levels have been recognised as useful indicators of seafood spoilage; under EU directive 95/149/EEC, the European Commission has specified that TVB-N levels be used if sensory methods raise doubts about the freshness of seafood species [65]. Critical limits have been set for groups of seafood species, quoted as mg TVB-N per 100 g of seafood tissue, e.g. 30 mg TVB-N per 100 g of tissue for the cod species. The EU directive refers to unpackaged fish only and it recommends that levels be determined by steam distillation and subsequent titration, a straightforward but timely procedure. The volatile amines are extracted from a sample by a solution of perchloric acid. This extract undergoes steam distillation, where the amines are absorbed by an acid receiver. This is subsequently titrated with standard hydrochloric acid to determine the TVB-N concentration of a tissue sample. Based on EU guidelines, this procedure will confirm if a sample has spoiled or not.

A limited number of novel methods have appeared in the literature in the past decade for monitoring of TVB-N levels. They each take a different approach to the determination of spoilage indicator compounds. One recent two-part paper described a novel short column gas chromatography (GC) method to determine the concentration of total amines [66, 67]. The amines were adsorbed onto a commercially available solid phase micro extraction fibre, by placing the fibre into the headspace of selected fish samples for ca. 2 min. Classical chromatographic separation of the components was not performed; instead, the method allowed the rapid and quantitative determination of the TVB-N levels. This was achieved by

desorbing the amines onto a very short non-separating column, which were subsequently detected by a standard flame ionisation detector. The peak heights and areas were calculated, to allow the TVB-N levels in a sample to be determined. Results were obtained for both salmon and whiting, and the uncertainty of a measurement increased with sample age. The initial levels of amines in whiting were higher than in salmon, as was the increase of amines during storage. This is an excellent method that rapidly determines the level of spoilage of a fish sample. However, it does require some sample preparation, albeit a short step.

Another approach is to use the establishing method of the electronic nose to determine volatile amines in real-time released into the sample headspace. This approach suffers from a practical viewpoint, in that two chambers are required (one for the fish sample and the second for the sensors), and that the poor signal-to-noise ratio of most electronic nose devices requires multiple injections with a gas-tight syringe, which is not an easy task to perform reproducibly by hand. A recent paper took the approach to prepare a portable, low-cost electronic nose made from commercially available sensors [68]. The simplicity is attractive to the operator, as an intermediately trained technician could perform the analysis. A fish sample of known mass was placed in the chamber of the device, and the changes in voltage signals from polycrystalline tin dioxide sensors were measured, as a function of the release of volatile amines. Using principal component analysis, the authors show that it is simple to distinguish between fresh and spoiled samples. This approach was used on Argentinean Hake, and further distinctions were drawn on the basis of sample mass, storage condition, sample age and variability between samples.

Zhao *et al.* recently published details of a reversible TMA probe based on a sensitive membrane coated onto a piezoelectric crystal [69]. The probe can detect TMA in the range of 5-200 ppm, and on this basis is presented as a fish freshness assay. The effects of interference of other basic gases, e.g. DMA and NH_3 were determined to be very high, but this is a point that is of little relevance if applied to TVB-N determination. Data from the probe upon exposure to TMA vapours correlated well with results from the standard EU-defined TVB-N method described previously and

from GC analysis. The basic principle behind the paper is flawed, however, since TMA levels are an indicator of *spoilage*, not of freshness. Additionally, no real fish samples were tested with the system.

A thin-film gas microsensor has been used for monitoring fish spoilage via TMA emissions [70]. Manganese phthalocyanine is an organometallic substance whose electrical conductivity is very sensitive to adsorbed amines, and it was used to monitor TMA levels from two Indian fish, katla and pomfret. The data demonstrates that volatiles from fish samples can be monitored rapidly and sensitively by the microsensor. Most recently, Hammond *et al.* demonstrated the use of a semiconducting metal-oxide array to monitor spoilage volatiles. The electrical conductivity of the gas sensor changes as a function of exposure to amines from spoiling fish. The data from analysis of Atlantic salmon, haddock and Atlantic cod correlated well with sensory evaluation by a trained panel over 2 months, a colorimetric method for TMA analysis, pH tests with a glass electrode and TVC microbial populations.

Most of these approaches, however, require trained operators at central locations to perform the analysis. Some of the methods are prone to interferences and have reproducibility issues, and in some cases, the equipment is relatively expensive, e.g. GC. They are generally not suitable for use as distributed "point-of-need" techniques. Hence these methods, while useful in providing accurate reference measurements, will not meet the rapidly growing interest in "on-package" sensing of food quality.

1.5.4.1 Monitoring TVB-N using chromogenic dyes

Very few examples exist in the literature for monitoring TVB-N levels from fish samples by pH-sensitive sensors. Instead, most applications focus on the detection of basic gases. According to a recent review by Wolfbeis [27], practically all sensors for ammonia and amines are based on the their effect on pH-sensitive polymers. A limited number of pH-indicator dyes have been used for this application, in both aqueous and gas phase. Thus, Werner *et al.* have demonstrated the use of an aqueous based ammonia sensor based on an indicator dye prepared in a silicone polymer layer [71]. The indicator dyes tested were bromophenol blue and bromocresol green, pK_as 4.0 and 4.8 respectively. Lipophilised versions of the dyes were prepared by reaction with cetyltrimethylammonium bromide (CTABr), via the following reaction:

$$\text{Indicator-}SO_3^-Na^+ + CTA^+Br^- \rightarrow \text{Indicator-}SO_3^-CTA^+ + NaBr$$

This lipophilisation ensures that the dye will not leach from the silicone polymer when placed in solution. The dye reacts with ammonia in solution, causing a measurable colour change:

$$\text{Indicator-O}\mathbf{H}\text{ (yellow)} + NH_3 \rightleftharpoons \text{Indicator-}O^-\text{ (blue)} + NH_4^+$$

The study performed demonstrated that sensors based on bromophenol blue show a higher sensitivity to ammonia than sensors based on bromocresol green, due to having a lower pK_a. A limit of detection of ca. 15 ppb for sensors based on bromophenol blue was established. A more thorough study was performed one year later when an investigation of membrane composition and thickness was undertaken [72]. The fastest response time was obtained when the film thickness was ca. 10 μm. The instrumentation was improved with a flow-through cell that used an LED for excitation at the λ_{max} of the dye, and a photodiode for detection of output signal intensity.

Attention is now focussed on those sensors for monitoring gaseous ammonia and amines. Bromothymol blue was immobilised on a hydrophobic polymer matrix based on Amberlite polymer beads, and used in a fibre-optic configuration to monitor ammonia vapours [73]. Very few results were shown, but the authors clearly demonstrate the reaction of ammonia vapour with the indicator dye to be:

$$NH_{3\,(g)} + H_2O \rightleftharpoons NH_4^+ + OH^-$$

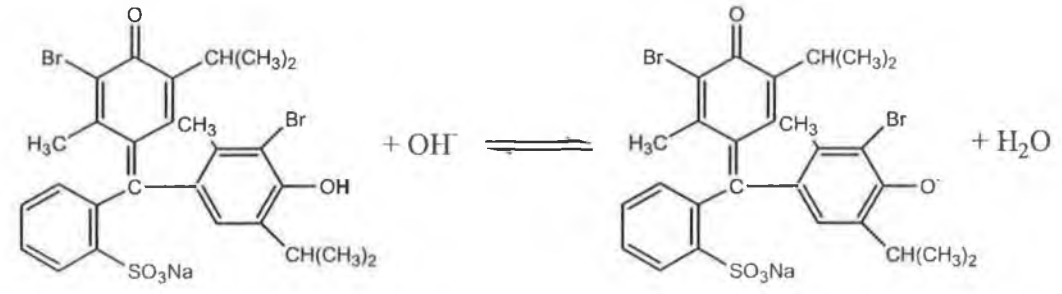

In the first step, the ammonia vapour gains a proton from water present in the atmosphere. In the second step, the OH^- formed from step one facilitates the deprotonation of the indicator dye, causing the characteristic change in colour. This explanation shows how the ammonia vapour is not depleted with time, how the reactions are in equilibrium, and that water vapour is necessary for the reactions to occur.

Bromocresol purple has been immobilised into sol-gel glass films based on TEOS and TMOS [74]. Absorption spectra on optical fibres were measured as a function of exposure to gaseous ammonia. There was an issue with elongated response times, e.g. ca. 250 min for 50 ppm ammonia. The authors attribute this to slow diffusion by ammonia into the matrix, due to the polarity of the glass film. Sol-gel films have not been used for TVB-N monitoring, since there exists health and safety issues about the close proximity of a glass-like film to real fish samples.

Zhao *et al.* coated bromocresol purple into a polymer matrix and attached this to the ends of a fibre-optic configuration [75]. Photo-initiated polymerisation of methyl

methacrylate was used to entrap the dye on the fibre tip. This matrix has reportedly good optical and chemical stability. The sensor produced has good sensitivity to ammonia vapours, due to its excellent gas permeability. Furthermore, Potyrailo et al., published two papers in the same year on the immobilisation of bromocresol purple into polymethylphenylsiloxane for ammonia gas monitoring [76, 77]. This matrix was selected because of its high gas permeability and inherent hydrophobic and sensor film-creating possibilities. The effect of temperature from 20-40 ^{o}C and relative humidity from 50-85 % on the sensor performance was investigated, and the change in the pK_a of the dye entrapped in the polymer matrix was ascertained. An LED and photodiode setup was used to measure the response of the sensor to gaseous ammonia. The equilibration time of the sensor was ca. 120 s to achieve 90 % of a full-scale response and hence the authors propose this system as a portable photometric ammonia gas analyser for use under field operating conditions.

Of the limited number of papers that use pH-indicator dyes for fish spoilage determination, Sadok *et al.* used bromothymol blue to determine levels of TMA by flow injection analysis [78]. The TMA was extracted from samples of pollack and cod by perchloric acid, and an inexpensive flow injection/ gas-diffusion system was used to monitor levels of the spoilage compound, by measuring the changes in absorbance of the dye. The limited results show that it is possible to monitor TMA levels from spoiling fish using this dye-based approach. However, the sampling methodology is destructive and some training and expertise are required to generate results from samples.

A chromogenic calixarene based on an azophenol structure has found some use in the field of monitoring TVB-N from spoiling fish samples. McCarrick *et al.* originally developed the complex for the determination of alkali metal ions [79]. Calixarenes consist of repeating phenolic units that are connected in a macrocycle via methylene bridges (Figure 1.12). Calixarenes with 3-20 repeating units are known, although the tetramer (and to a lesser extent the hexamer) has found most use analytically, i.e. calix[4]arene.

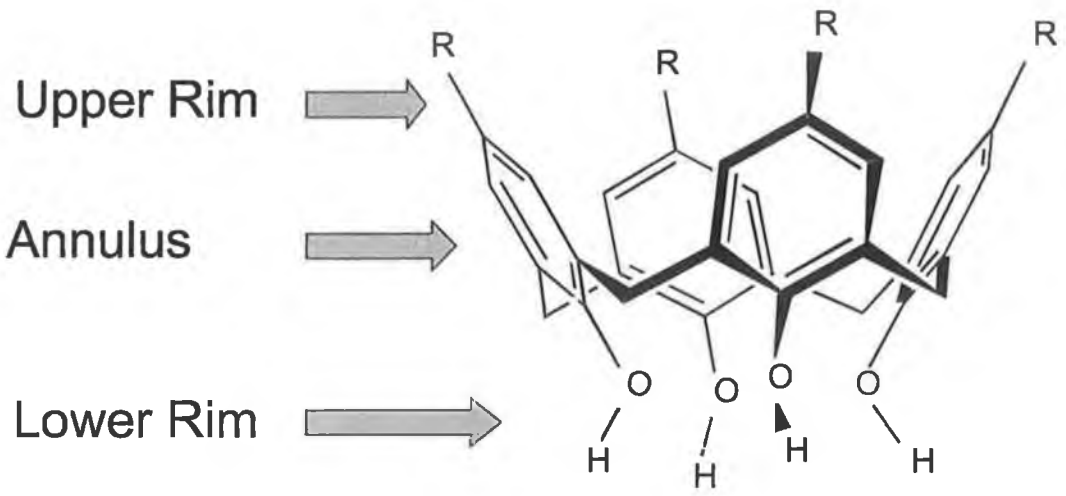

Figure 1.12: Calix[4]arene (tetramer) structure.

Calixarene chemistry is a huge area of interest that includes applications in optical sensing, cation-selective electrodes and chiral recognition [80]. The authors used a nitrophenylazophenol ligand shown in Figure 1.13, and a p-*tert*-butyl calix[4]arene tetraacetic acid structure shown in Figure 1.14 to create a tetra-substituted nitrophenylazophenol calix[4]arene, shown in Figure 1.15.

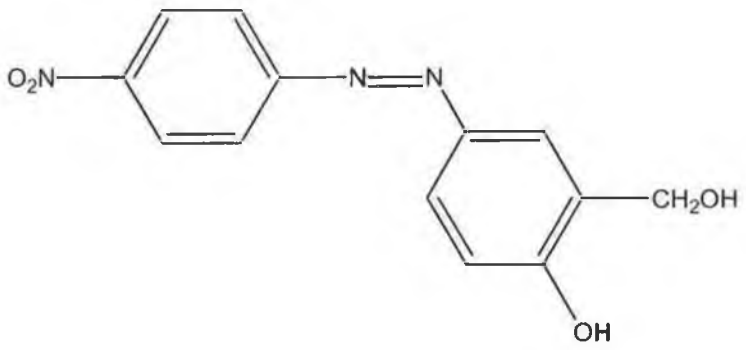

Figure 1.13: Nitrophenolazophenol dye structure. The labile proton is shown in bold.

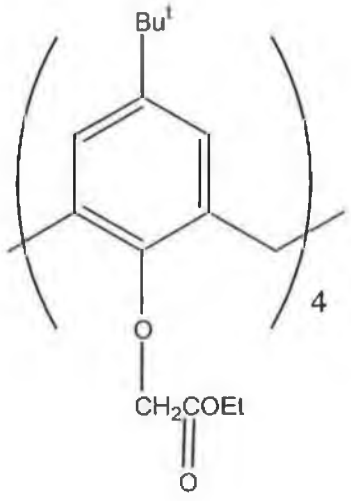

Figure 1.14: p-*tert*-butyl calix[4]arene tetraacetic acid.

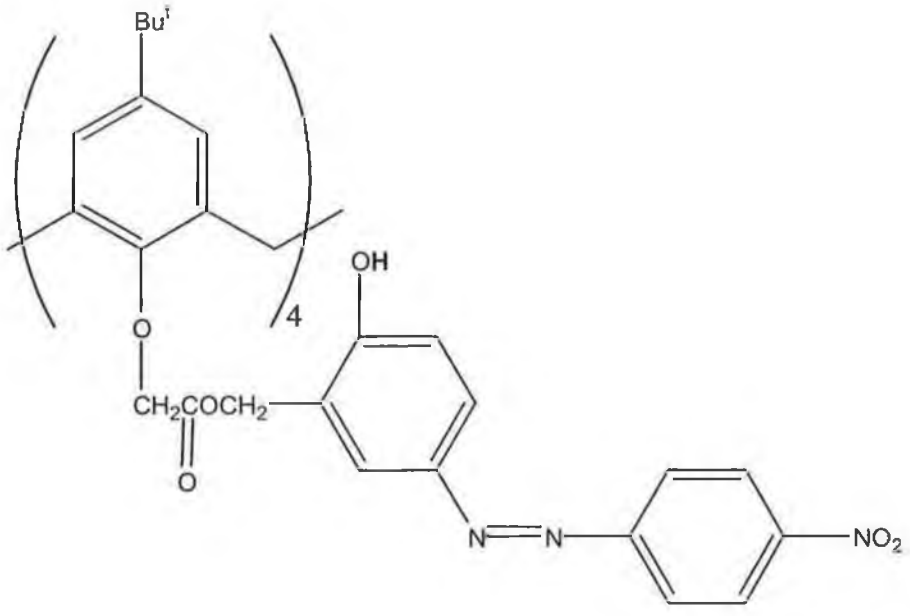

Figure 1.15: Structure of the nitrophenylazophenol calix[4]arene. The labile proton is shown in bold.

A rapid and concentration-dependant colour change was observed from yellow to red (380-520 nm) upon the addition of lithium perchlorate in the presence of amines such as ammonia. No colour change was observed in the absence of base. It is believed that the metal-ion complex has a more acidic nature than the free ligand, creating a more sensitive indicator dye. Thus this complex was used by Grady *et al.* to create an optical sensor for gaseous ammonia [81]. The sensor was prepared by immobilising

the calixarene-based dye into a PVC-based film in a fibre-optic configuration, and the sensor response was monitored as a function of ammonia vapour concentration. The sensitivity of the response was tuneable, as it was dependant on whether or not the free ligand or the ligand doped with lithium was used. The sensitivity of the response was fine-tuned by altering the mole ratios of lithium to calixarene, and ammonia vapour in the range 5-50 ppm was readily detectable. The response time took several minutes to reach steady state, but this approach is powerful for TVB-N monitoring, since the sensitivity of the complex can readily be altered, which may be required, since different fish species release different levels of TVB-N, of different composition. This approach could hence be tailored for use in a fish spoilage sensor.

Loughran and Diamond used this approach in one of the few papers in the literature to use pH-sensitive sensors for fish spoilage determinations [82]. The calixarene-based dye was impregnated onto filter paper discs that were exposed to the sample headspace of cod and whiting samples that were allowed to spoil. The absorbance of the dye on the filter paper discs was monitored by UV-Vis reflectance spectroscopy, as a function of the release of TVB-N. The sensitivity of the response was tuned by varying the mole ratio of lithium to dye complex [81]. The results demonstrate that it is feasible to monitor the release of spoilage compounds measured through the colour changes of an acidochromic dye. The authors show that the release of TVB-N from whiting samples is much faster than from other species tested, a trend that was confirmed in another study mentioned previously of TVB-N levels of whiting and salmon, measured by GC analysis [67]. A study of the release of TVB-N as a function of storage conditions was also performed, for samples stored on ice or at room temperature, and the complex operated well in all conditions tested.

A limited search of the patent literature also shows some interesting research in on-package determination of food spoilage. This introduces the concept of intelligent packaging, central to the theme of this thesis. Miller *et al.* have proposed a concept relating to volatile amines reacting with a pH indicator dye to indicate the freshness of a seafood sample [83]. This concept is patented under the title of "Food Quality Indicator Device", patent number WO9904256. The authors describe a generalised

approach of using an indicator compound that is a pH-sensitive dye, entrapped in a polymeric matrix and coated onto the food packaging. The dye reacts with spoilage indicator compounds and causes a visual change in colour. This concept has been marketed by COX recorders, under the trade name of Freshtag^{tm} [84]. Additionally, Horan has patented the concept of using a chemical indicator to monitor the levels of harmful microorganisms in food packaging [85]. The indicator responds over time as the level of bacteria increases in a food package, giving a warning of a spoiled product.

2 Sensor Preparation and Optimisation

2.1 Introduction

This chapter presents results that follow the development of a working chemical sensor for measuring changes in TVB-N levels released by gradually spoiling seafood samples. As described in Section 1.5.3, determination of TVB-N levels gives information about the degree of spoilage of a seafood sample. Section 1.5.4.1 showed that it is possible to monitor the changes in TVB-N levels by measuring the degree of interaction of volatilised bases with a colorimetric indicator dye that is sensitive to changes in pH. Selection of a suitable indicator dye and an appropriate method of immobilising the dye to produce a working sensor were crucial in sensor design and development. The mode of immobilisation chosen was to physically entrap the dye into cellulose acetate, since sensors based on this matrix were shown in Section 1.4.5 to have a rapid response time, high gas-permeability, excellent stability in acidic and alkaline conditions, and a lengthy shelf life.

In this chapter, results are presented showing how the sensor production process was optimised by systematically altering different components in the sensor formulation. This included investigating the use of different plasticisers, solvents, drying conditions, and the relative amounts of each chemical component used. A simple screening method was devised, based on digital imaging techniques and colour analysis using in-house developed LabVIEW software, to determine the homogeneity of each batch of sensors prepared. Selected sensors were further analysed using a state-of-the-art imaging spectrograph system, which gives spatially distributed spectral information about each sensor tested. This facilitated the development of an optimised sensor formulation.

Sensors based on this optimised formulation were further studied and characterised. The effect of dye loading on the sensor formulation was investigated. A comparison study was performed of the pK_a of the dye in the polymer matrix, compared to the value obtained in free solution. Calibration of the sensors against ammonia in headspace was performed. This allowed classification of important analytical

parameters, such as the upper and lower limits of linearity of the sensor response, the lower limit of detection to ammonia, and the reproducibility of the sensor response. Some of the results in this chapter were recently accepted for publication in the Irish Journal of Agricultural and Food Research [86].

2.2 Instrumentation

2.2.1 Imaging Spectrograph

A PARISS imaging spectrograph (Lightform Incorporated, New Jersey, USA) is available for research purposes in our laboratories. PARISS is an acronym for **P**rism and **R**eflector **I**maging **S**pectrometer **S**ystem. The PARISS system can be fitted to any standard microscope with a video port via a C-mount adaptor; in our system, it is fitted to a Nikon Eclipse series E-800 microscope (Micron Optical, Wexford, Ireland). Fitted onto the microscope is a Prior Proscan motorised stage, an x-y joystick controlled stage with a step-size of 0.01 microns (Figure 2.1).

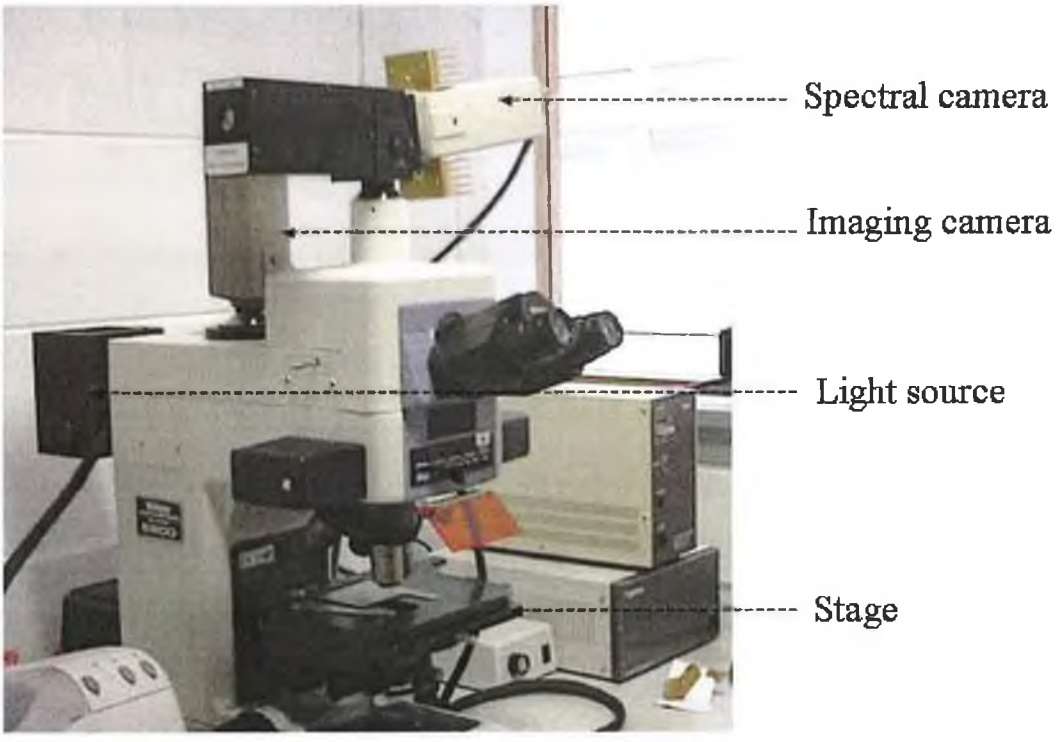

Figure 2.1: PARISS Imaging Spectrograph system on Nikon E-800 microscope. The spectral camera is mounted to the front of the microscope and the imaging camera to the rear.

2.2.1.1 Spectral Imaging

Spectral imaging differs from traditional spectroscopic methods, in that the complete spectrum is obtained in one acquisition. Scans can then be performed across an area to create two dimensional, spatially distributed images. Spectral imaging provides a significant additional dimension that enables each object to be defined by multiple, even hundreds, of wavelengths, often making it possible to differentiate between objects that are otherwise visually identical. The majority of spectral imaging systems operate by using many wavelength filters that sequentially overlay images taken at incremental wavelengths [87]. The main disadvantage of this is that it only generates pseudo-spectral images. Additionally, any data processing that is required must be performed post-acquisition, adding to the time required for analysis.

The PARISS system differs by using a technique that acquires complete spectra simultaneously and forms images incrementally [87]. This method, unlike the filter method, generates true spectral images. The so-called "push-broom" technique can be achieved by using either a diffraction grating or a prism in order to disperse all wavelengths simultaneously. Generic push-broom advantages include:

- Fast, low-memory 180-kilobyte acquisitions, compared to over 20-megabyte file sizes for filter-based acquisitions [87].
- Reduced photo-bleaching of sample, as only small "slices" of a sample are irradiated and interrogated in one acquisition.
- Data analysis is carried out during an acquisition, making it only as fast as the exposure time set for an acquisition (in the region of less than 250 milliseconds for the PARISS system).

Hence, the PARISS system offers a non-destructive method that can collect reflectance, absorption, transmission and fluorescence spectra of samples (when fitted with the appropriate light source). It is one of the most powerful types of instrumentation available for spectral classification and analysis.

2.2.1.2 Spectral imaging with the PARISS system

The PARISS system generates true spectral images by taking simultaneous spectral and grey-scale images through the two cameras mounted above the microscope (Figure 2.1). There is absolute pixel-to-pixel correlation between these two images. The spectra of up to 240 objects are acquired simultaneously, with each object being characterised by up to 640 wavelength points between ca. 390 and ca. 810 nm. This provides enough information to enable robust proprietary spectral comparison algorithms, which allows spectral classification routines to be successfully performed.

A slice of the image projected by the microscope is focused onto the entrance slit of the spectrometer and strikes the first curved surface of a prism, is refracted, strikes the second surface and exits to strike a spherical mirror. The wavelength dispersed light then returns through the prism to be focused onto the CCD array. A schematic of the operation of the spectrometer is shown in Figure 2.2.

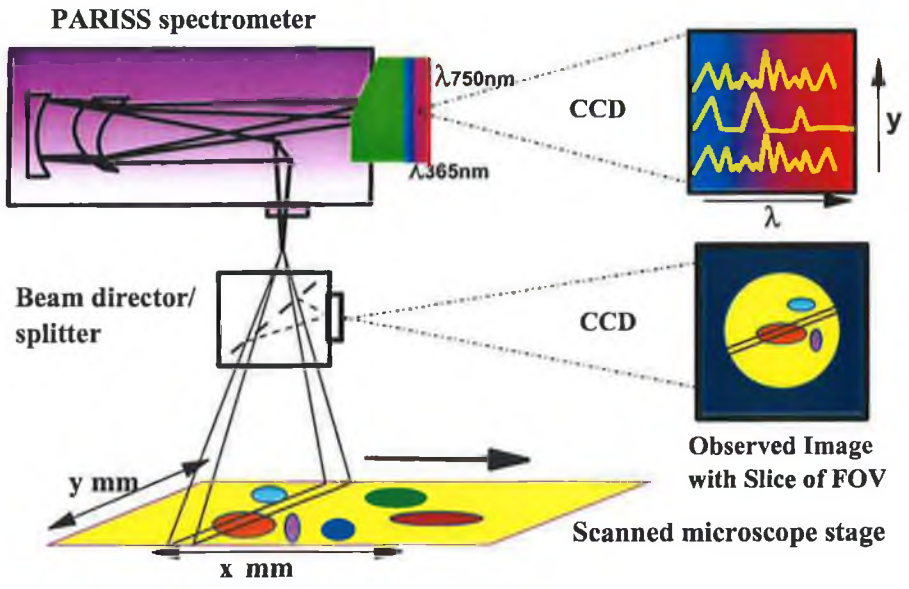

Figure 2.2: Schematic showing the dispersion of light within the prism-based PARISS system (Image from Lightform Incorporated, New Jersey, USA [88]).

2.2.1.3 Spectral classification

Each slice from an image contains 240 spectra with 640 wavelength points. Spectra are sorted by the software algorithms into classes based on spectral features such as shape and area under the spectral curve. A user-selected threshold sets the degree of sensitivity of the classification process. Spectral classes are assigned a colour code and can then be inserted into a Master Spectrum (MS) library. The user can then edit the MS library to add or remove spectra as necessary. An example of 4 similar but significantly different spectra classified into a MS library is shown in Figure 2.3.

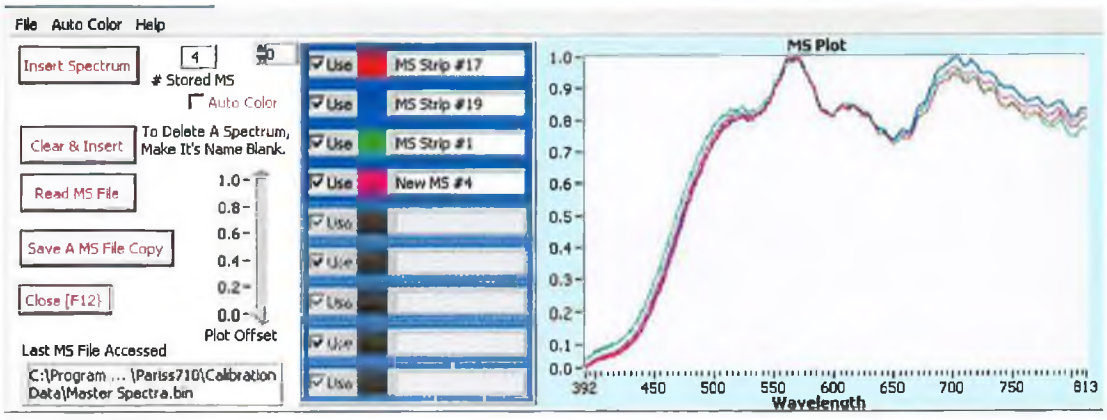

Figure 2.3: Each of 4 different spectra in the MS library is classified as different on the basis of proprietary algorithms.

New acquisitions that are obtained are then correlated against the MS library. The degree of correlation is set by the user as any value less than or equal to unity. All spectra that match a spectral signature contained within the MS library are assigned a pseudo-colour code that matches the colour code of the library. Areas that are unclassified by the software remain black. By scanning across a Region of Interest (ROI) and acquiring new spectra, which are classified according to "goodness-of-fit", a spectral topographical map is generated. A sample map of a cross-section of stained human skin, taken from the Lightform Inc. web site, is shown in Figure 2.4.

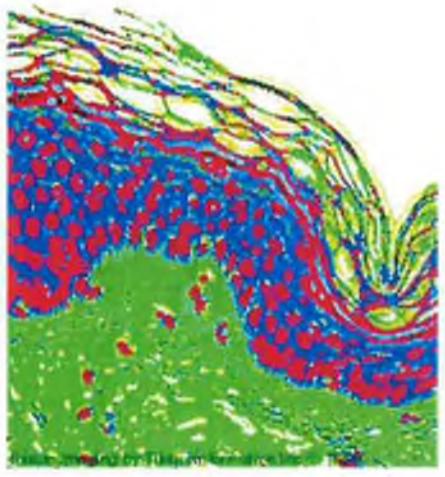

Figure 2.4: Human skin that has been classified in terms of its colour spectral signatures. The different sections of the tissue have all been clearly delineated. (Image copyright Tissueinformatics Inc, Pittsburgh, USA [89])

The spectral classification techniques used by the PARISS system are based on complex algorithms, of which there are few details available [87]. These functions collect and sort spectra into classes of similar (but unique) spectral signatures. The routines then correlate newly acquired spectra against those stored in the MS library, based on a threshold value set by the user. Broadly speaking, the proprietary correlation recognition algorithms used in the PARISS software are based on the following parameters:

- Position in the spectral range.
- Shape of the spectral area (also called the spectral "envelope").
- Classification values that are compared to library spectra - hence, it is better to have complete representative spectra in the MS library.

All spectra are normalized to unity; therefore, recognition is a binary condition that is either "recognized" or "not recognized" within a user selected Minimum Correlation Coefficient (MCC). Put simply, the higher the MCC value that is selected, the more stringent the algorithms used to compare two or more spectra. A low MCC value is likely to show little difference between similar spectra, and will hence classify them as the same.

2.3 Dye selection

Several dyes were candidates in the development of a working sensor [20]. In order to produce a sensor that changes colour around the point of spoilage, careful selection of the pK_a was considered. The main components of the TVB-N, i.e. TMA, ammonia and DMA, each have pK_as of 9.80, 9.25 and 10.70 respectively [90]. If a dye with a pK_a of ca. < 6 was selected, for example, then the sensor would readily be deprotonated by the TVB-N released during spoilage, and would thus not respond at the critical threshold of interest, where the levels of TVB-N released are relatively high [64]. It was necessary to select a dye that has a pK_a of ca. 1-2 pH units less than the pK_as of the principal amine components of TVB-N.

Cresol red (o-cresolsulphonphthalein) was selected as the candidate dye to develop a working sensor. It has a pK_a of 8.3, and has a λ_{max} (base form) of 573 nm [20]. In addition, there is a large separation between the acidic and basic forms of the dye, from yellow (451 nm) to purple (573 nm). The dye is readily commercially available, although there is limited research in the literature that uses the compound. Figure 2.5 shows the structure and deprotonation equilibrium of cresol red [20].

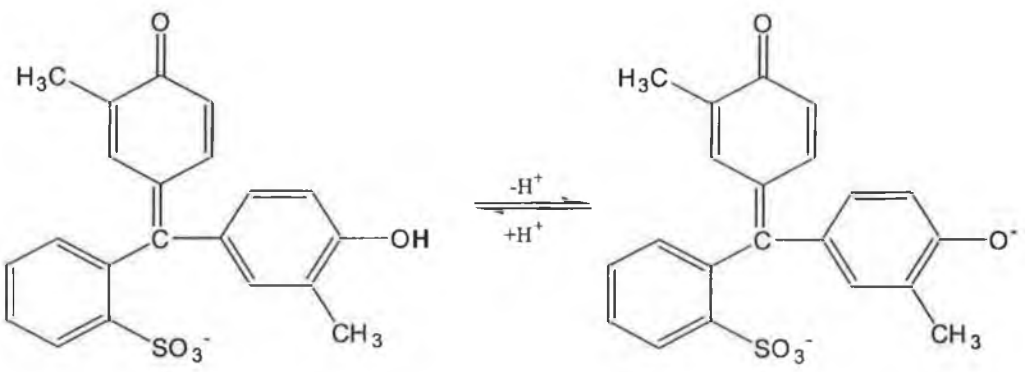

Figure 2.5: Deprotonation of cresol red shifts the dye from its yellow form (451 nm) to its purple form (573 nm).

2.4 Experimental

2.4.1 Materials

Cresol red (sodium salt), dioctyl sebacate (DOS), 94%, cyclohexanone (analar grade), potassium hydrogen phosphate and cellulose acetate (mw approximately 30,000 g/mol) were obtained from Sigma-Aldrich (Dublin, Ireland). Dibutyl phthalate (DBP), 98%, boric acid and 2-Nitrophenyl octyl ether (NPOE) were obtained from Fluka Chemicals (Dublin, Ireland). Optically clear polyethylene teraphthalate (PET) sheets were obtained from Oxley plc (Cumbria, UK). Polypropylene caps were supplied by Sarscedt (Wexford, Ireland). Fast cure epoxy was obtained from Permabond (Eastleigh, UK). The chemical structures of the three plasticisers tested are shown in Figure 2.6. These were selected since they are commonly used plasticisers, with significantly different chemical structures.

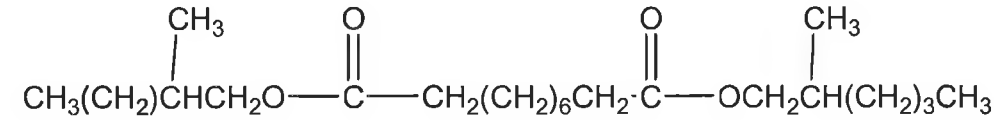

A

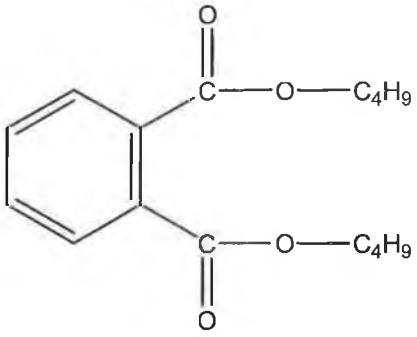

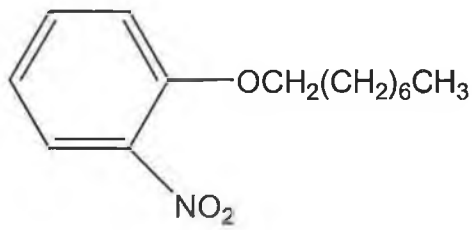

B C

Figure 2.6: Structures of the three plasticisers used; A was dioctyl sebacate (DOS), B was dibutyl phthalate (DBP) and C was 2-nitrophenyl octyl ether (NPOE).

2.4.2 Sensor preparation

Sensor preparation was divided into two sections. Firstly, the sensor formulation was prepared. This involved testing five chemically different formulations. Secondly, each of the formulations was printed onto PET substrate, to produce sensors dots. Analysis of these dots was performed as described in Section 2.4.3, and the analysed data guided the chemical composition of subsequent formulations. Additional parameters were tested for the final formulation used, such as the solvent used, the ratio of binder to plasticiser, and the drying conditions of the sensor dots. Each formulation prepared (and hence each batch of sensor dots) was labelled from "A" to "E". Initially, the ratio of binder to plasticiser was set at 1:1, and the concentration of each was 5 % w/v. This produced the first batch of sensor dots, labelled "A". The chemical composition of each of the sensor formulations "A" to "E" is shown in Table 2.1.

Formulation	% w/v binder	Plasticiser	Solvent used
A	5	5 % v/v DOS	Acetone
B	3	3 % v/v NPOE	Acetone
C	3	3 % v/v DBP	Acetone
D	3	3 % v/v DBP	Cyclohexanone
E	3	3 % v/v DBP	1:1 acetone/cyclohexanone

Table 2.1: Five formulations were prepared that varied the concentration of binder used, the concentration of a chosen plasticiser used and the solvent used.

For example, sensor formulation "A" was prepared by producing 10 ml of 5 % w/v cellulose acetate in acetone. The cellulose acetate was slowly mixed with the solvent in order to reduce aggregation of the polymer. The use of a sonicator was required in order to fully dissolve the polymer. 0.5 ml stock DOS solution was added to the cellulose acetate solution, such that the final concentration of DOS was 5% v/v. 20 mg cresol red (sodium salt) was added to the mixture, such that the concentration of dye was 0.2% w/v. A few drops of reagent grade methanol were required to aid solubility of the dye. Solutions were prepared in 20 ml disposable polypropylene

vials and were sealed immediately and wrapped in parafilm, to minimise solvent evaporation effects. All other solutions "B" to "E" were prepared similarly according to the chemical compositions shown in Table 2.1.

Some further variations were made to the E formulation to further optimise the sensors being produced. The ratio of plasticiser to binder was varied and the optimum drying condition of the sensors was determined, as shown in Table 2.2.

Formulation	% w/v binder	Plasticiser	Drying conditions
E_1	3	3 % w/v DBP	Room temp
E_2	3	2 % w/v DBP	Room temp
E_3	3	5 % w/v DBP	Room temp
E_4	3	3 % w/v DBP	4 °C (Fridge)
E_5	3	3 % w/v DBP	Sealed

Table 2.2: A number of variations were made on the E formulation. This varied the ratio of plasticiser to binder and the drying conditions used for sensor production. All formulations described used a 1:1 mixture of acetone to cyclohexanone as solvent.

Room temperature was measured at approximately 20-21 °C. "Sealed" means that sensors were dried in a sealed environment that was saturated with acetone vapour. This was achieved by using a dessicator with the dessicant removed and a 10 ml vial filled with acetone. This created more control over the rate of evaporation of the solvents, which took approximately 3 hours. All formulations described in Table 2.2 used a 1:1 mixture of acetone to cyclohexanone as solvent.

2.4.2.1 Sensor dot production

PET substrate was cut with scissors into strips of approximately 3 x 10 cm. The strips were washed with deionised water and were air-dried. The thickness of the substrate was approximately 100 μm. The material is flexible and can be easily rolled for storage. 3 μl of the each formulation from Table 2.1 and Table 2.2 was printed

onto PET substrate, from a fixed height of 5 mm using a 20 µl Brand® transferpipette. Approximately 50 sensors were produced from each formulation prepared. A different micropipette tip was used for each sensor formulation, in order to avoid any cross-contamination between formulations.

2.4.3 Analysis of prepared sensor dots

The analysis of prepared sensor dots was split into two sections. Initially, sensors were rapidly screened by a simple colour analysis method to give an indication of the homogeneity of a sensor dot (i.e. the evenness of colour), a key issue in sensor design. Selected sensors were then further examined using the spectral imaging technique outlined in Section 2.2.1.2, to investigate the prepared sensor dots that warranted further study.

2.4.3.1 Rapid screening of sensor dots

This screening method quickly and easily returns parameters to the user about the evenness of colour. Images were captured using a colour digital camera and were analysed using in-house developed LabVIEW based software. The digital camera used was a Mini DV Digital Video Camcorder (Model: MV1, Canon Incorporated, Japan). Images were acquired with the camera at 90° to the sample (Figure 2.7), which was found in previous work to be the optimum setup for images to be captured [91]. Two macro lenses, of + 2 and + 4 magnification, were placed over the camera lens to allow a full sensor dot to be acquired in one image. The lighting setup used was a Polytec DCR II continuous cold ringlight source (Lambda Photometrics Limited, Hertfordshire, UK). This offers better control over the temperature and evenness of the light than the ringlight used in previous work [91]. The light intensity was set to the highest value for all image acquisitions. Additionally, a cardboard housing was constructed to place sensors inside when acquiring images. This was lined with black paper, in order to reduce the issue of reflected (and hence stray) light.

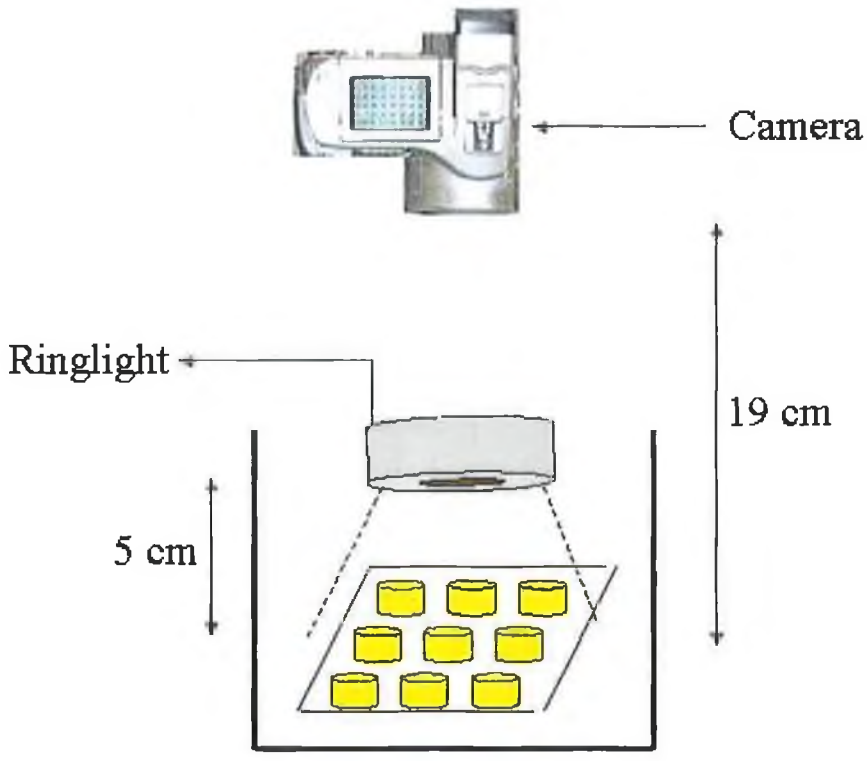

Figure 2.7: Image acquisition setup used for rapid analysis of sensors produced. The entire setup was placed inside a darkened cardboard housing to reduce stray light effects.

Once images were captured, they were transferred to a PC where the images were analysed using in-house developed LabVIEW based software [91]. This outputs a series of numerical values in bit numbers that represent a particular colour at a particular location within the image. This colour is broken down into red, green and blue (RGB) values within a user-selected area, each of which has an 8-bit resolution. The procedure for image analysis was:

- The image file was saved in bitmap format.
- This image was opened in the LabVIEW software by selecting which directory the file had been saved under.
- The region of interest (ROI) was selected as an area 15 pixels high and across the approximate centre of the dot (Figure 2.8). The same sized ROI was selected for each analysis; 250 pixels wide by 15 pixels high.

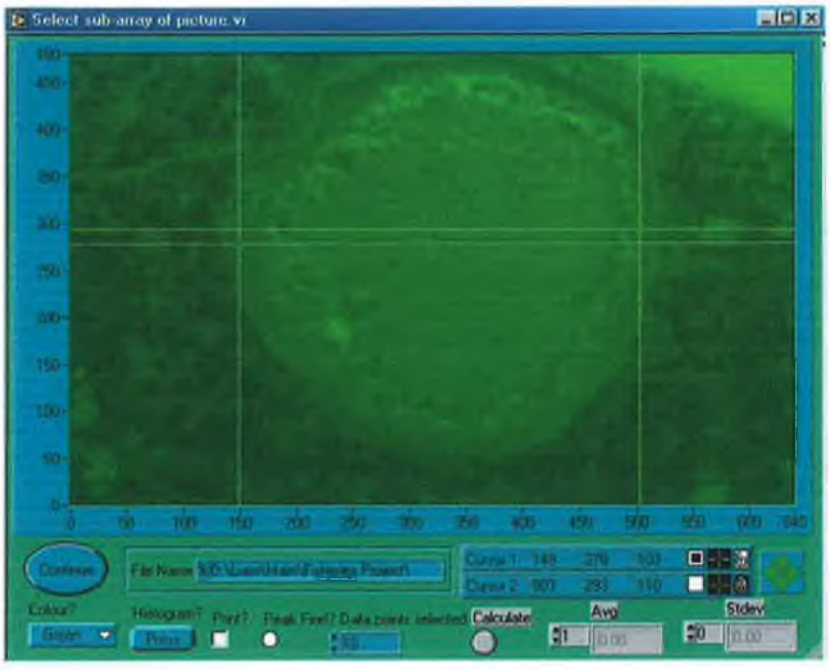

Figure 2.8: An area 15 pixels high by 250 pixels wide across the centre of a spot was selected for analysis. The false colour filter of green was assigned in software to the image.

- A histogram was generated in the software that shows the average values for the 250 pixels selected along the horizontal axis of the ROI. This file was saved as a data (.dat) file.

A simple Microsoft Excel macro was used to process the data in the .dat file. This formats the 250 data points and plots the colour intensity for each of the three colour channels against the position in the spot, from left to right. The macro also calculates the average and % relative standard deviation (% RSD) for each of the three colour channels.

In this way, the user rapidly obtains three single values (% RSD in each RGB channel) describing the amount of variation across a spot, which is a direct representation of the evenness of colour in the spot. An even-coloured spot would return low % RSD values to the user; a spot with poor homogeneity would return higher % RSD values. Three typical sensors dots from each batch produced (Table 2.1 and Table 2.2) were analysed. The results from this section were used as a screening mechanism to select sensors for further analysis.

2.4.3.2 Analysis of sensor dots with PARISS

Certain dots were selected for further analysis after the initial screening procedure described in Section 2.4.3.1. The PARISS imaging spectrograph system (Section 2.2.1.1) was used to scan across a ROI to determine the variation in spectral features across the region. This gives much more data than is possible with the screening method devised. 5 sensor dots from each formulation batch were examined and for simplicity, only one typical scan from each formulation batch is presented here.

Spectra from the centre of a sensor spot were classified and added to the MS library, as described in Section 2.2.1.2. An autoscan of a region of interest was then performed across the central region of an entire spot at 100x magnification. Data was collected for the field of view that falls onto the spectrometer slit, one slice at a time. A total of 1500 individual acquisitions were obtained, at an average speed of 2 acquisitions per second; hence it took approximately 750 seconds to build up a complete spectral topographical profile with this setup. The spectrometer slit is 25 μm wide by 100 μm high; an area of only 2500 μm^2 is collected in any one acquisition. 240 spectra were collected in any single acquisition. To reduce the dataset to a more manageable level, every ten spectra were averaged to one, resulting in all 240 spectra being averaged to 24. A full profile obtained still contains 36000 distinct spectral features, even after averaging. A schematic of the autoscan procedure across the surface of a single sensor dot is shown in Figure 2.9.

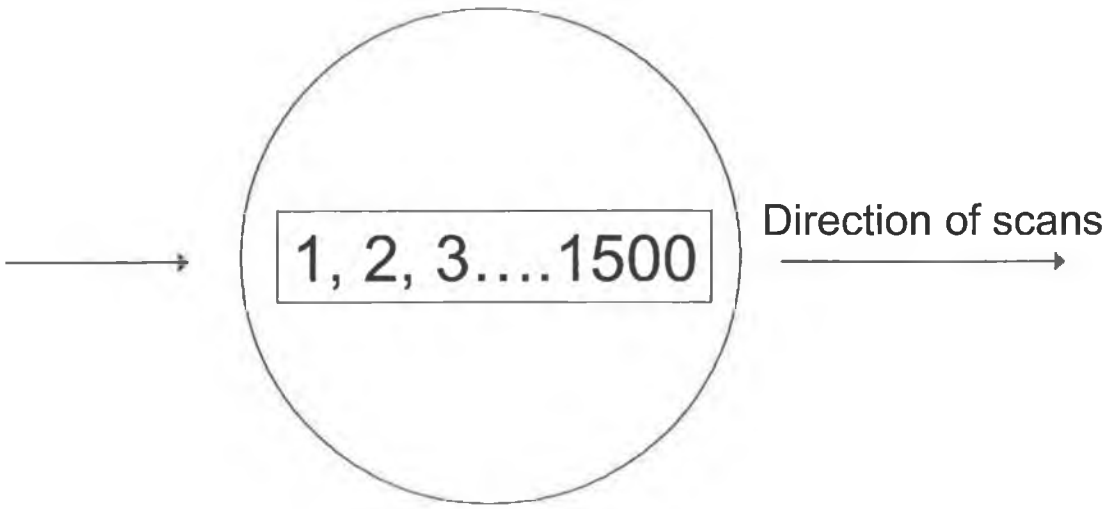

Figure 2.9: Schematic showing how 1500 scans are collected across the surface of an entire spot, at 100x magnification. Each of the numbers represents a spectral "slice".

The MCC was set in the software as 0.9990. The PARISS software produces a histogram that shows the overall % of each different spectral signature detected in a classified image of a sensor dot.

2.4.4 Effect of dye loading on sensor formulation

All sensor dots described thus far (Section 2.4.2) had a concentration of 0.2 % w/v cresol red dye. The concentration of dye present in a sensor could affect the sensitivity of the sensor response, the homogeneity of the coating and the detection of colour changes when exposed to basic gases. Batches of the E_5 formulation were prepared with half the dye concentration (0.1 % w/v) and twice the dye concentration (0.4 % w/v), with no changes to all other formulation components. Spectral scans at each concentration were obtained with the PARISS system as described in Section 2.2.1.2, to investigate the effect of dye loading on the homogeneity of the sensor dots. These scans allowed an optimised dye loading to be determined.

2.4.5 Determination of the pK_a of cresol red

A series of phosphate and boric acid buffers ranging from pH 6.3 to pH 10.3 were prepared [92]. Details of the buffers used are provided in Appendix A. These buffers were used in a study of the pK_a of cresol red in free solution, compared to values obtained when bound in the polymer matrix, as described in the following sections.

2.4.5.1 Study of dye in free solution

10 mg of cresol red (sodium salt) was added to a 20 ml sample of each buffer prepared, such that the dye concentration in each sample prepared was 0.05 % w/v. 16 buffers solutions were used, with the majority of buffers prepared close to the literature value of the pK_a of the dye [20]. A UV-Vis spectrum of the dye in pH buffer 10 was collected to determine the wavelength maximum (λ_{max}) of the basic form of the dye. To facilitate rapid data collection, 200 µl of each sample containing dye in buffer was pipetted into a 96-well plate, and data were acquired on a plate-well reader (Model µ-Quant, supplied by Medical Supply Company, Dublin, Ireland). The absorbance at the λ_{max} was then measured as a function of increasing pH; it took approximately 60 sec to read the entire plate. The absorbance of a blank (buffer with no dye) was collected and was subtracted from all sample absorbance readings taken. All dye in buffer solutions were prepared in triplicate.

Best-fit logistic-sigmoid curves were fitted to the data obtained using the Solver function in Microsoft Excel [93]. This was achieved by extracting the data describing the change in the dye response against pH and then using Solver to model the best-fit curve. The equation used was:

$$Abs(573nm) = \left[\frac{a}{(1+\exp[b(pH-c)])^{e}}\right] + d \qquad \textbf{Equation 2.1}$$

where a = peak height at 573 nm / au (absorbance units)

b = slope coefficient

c = pH from beginning of the peak to the inflection on the rise (i.e. the pK_a)

d = baseline offset /au

e = symmetry parameter for the sigmoid

Abs (573nm) = Dye in buffer absorbance at a particular pH /au

The formula was entered into Microsoft Excel to model the fit of the data obtained. The residuals, the residuals squared and the sum of the squared residuals (SSR) were all computed [93]. Solver was set to minimise the SSR value by changing the values of *a, b, c* and *d*. The value of *e* was set equal to 1 and a best-fit model was obtained. The parameters of the best-fit were used to compute extrapolated values between the data points, e.g. every 0.05 pH units, to produce best-fit curves to the data collected. This facilitated the determination of the pK_a of the dye.

2.4.5.2 Study of dye in polymer binder

The optimised sensor formulation was prepared as previously described (Section 2.4.2). 6.3 mm diameter discs were cut out from cleaned, uncoated PET with a hole-puncher, and single discs were placed on the base of individual wells in a 96-well plate. Sensor discs were prepared in each well of the plate by pipetting 4 µl of the optimised formulation into each well, and allowing the discs to dry in an acetone-saturated environment for ca. 3 hours. In this manner, the plastic base of the multi-well plate remained optically clear and undamaged by the solvents used. 100 µl of buffer was then added to each well, and the absorbance values at λ_{max} were collected using the plate-well reader. During this short timeframe (< 3 min), there was no discernible leaching of dye from the polymer matrix. The response of a blank (coated PET disc with no dye, and buffer sample) was collected and all readings were taken in triplicate. The absorbance data collected allowed the pK_a of the dye in the polymer binder to be calculated, and hence compared to the value obtained in free solution.

2.4.6 Study of the effect of temperature on pK_a

The pK_a of cresol red was determined at room temperature in free solution in Section 2.4.5.1. It is important to know the effect of temperature on the chemistry of the dye, since the application will likely require the sensor to function at 4 °C, where fish are typically stored. The same setup as prepared in Section 2.4.5.1 was used in this study, after storage overnight in a fridge at 4 °C. The absorbance at λ_{max} was measured as a function of pH, in triplicate. The rapid scan time of the plate well reader (ca. 60 sec) ensured that all solutions were analysed with no significant increase in temperature.

2.4.7 Sensor calibration

50 ml of 100 ppm NH_3 gas was obtained by mixing 1 % v/v NH_3 in N_2 with pure N_2 gas, at a flow rate of 500 ml/min (set via a mass-flow controller) into a 50 ml gas-tight sampling barrel for ca. 6 sec. A single sensor dot was placed face-down on a filter paper disc of 10 mm diameter, on top of a 16 mm diameter, 20 mm height polypropylene cap, with a 6mm hole drilled in it. The surface of the cap was covered with a small section of sticky tape sealed with fast-cure epoxy glue, sufficient to form a seal. This cap fitted tightly into a 2-necked 50 ml round-bottom flask (B14 size). A small stirrer bar was placed inside the setup to aid circulation of air, and a rubber seal was used to cover the second neck of the flask (Figure 2.10). A sequential series of 0.5 ml NH_3 gas samples per analysis were injected through the rubber seal with a gas-tight syringe, and were allowed to equilibrate with the sensor by stirring for 5 min. All injections were repeated in triplicate.

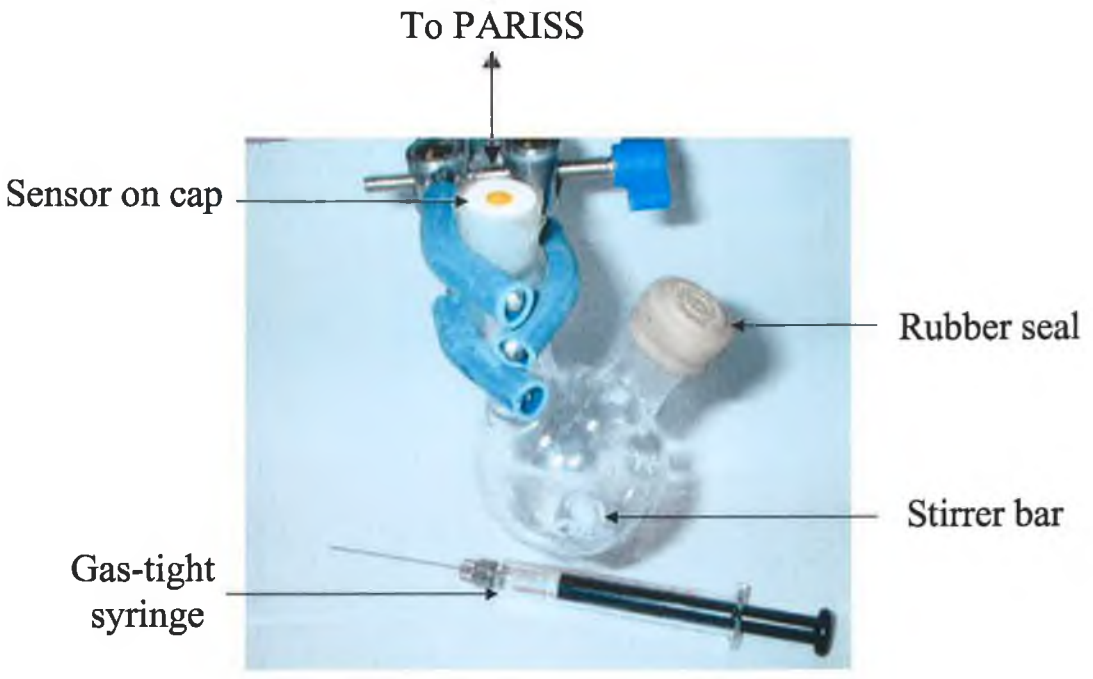

Figure 2.10: 2-necked flask setup that was used to calibrate sensor (in cap) against injected headspace ammonia samples.

The PARISS system was used to monitor the spectral changes in the sensor with increasing NH_3 concentration. Spectra were acquired at 10x magnification in the central portion of each sensor. All 240 spectra were averaged to 1 in the PARISS software. A blank spectrum was acquired of a certified reflectance white standard and subsequently, the acquired spectra from sensor acquisitions were ratioed to the average of the white spectrum in the software. The difference in the ratios is a measure of the decrease in light intensity due to absorbance of light by the sample. It is essentially absorbance measured in reflectance-mode. The absorbance spectral data were exported to Microsoft Excel and were baseline corrected between 650-800 nm. A best-fit sigmoid function was modelled to the data by using Solver in Excel, to return relevant analytical calibration data.

2.5 Results and discussion

The first set of results obtained describes the process of optimisation of a chemical formulation that produces homogeneous cresol red sensor dots entrapped in cellulose acetate. This was done using a rapid screening process and a more in-depth spectral reference measurement system. The effect of altering the dye loading on this optimised formulation was investigated. The pK_a of the dye was determined in free solution and was compared to the value obtained for the dye entrapped in the polymer binder, to investigate any potential effects of polymer entrapment. A study of the effect of temperature on the pK_a of the dye was performed. Finally, a calibration of the optimised sensor dots to ammonia in headspace was performed to characterise analytical parameters of the sensor.

2.5.1 Rapid screening of sensor dots

The data obtained by rapidly analysing the RGB values across a ROI of the sensor formulations in Table 2.1 and Table 2.2 is described in this section. Three sensor dots from each formulation were analysed, and for simplicity, only two of these formulations are described in detail below; all other RGB sensor dot data is summarised in Table 2.3 and Table 2.4

2.5.1.1 RGB analysis of E_3 sensors

These sensors have 3 % w/v binder to 5 % w/v DBP (Table 2.2). It was plainly seen by eye that each of the sensor dots has a poor distribution of colour (Figure 2.11). They have a doughnut-type shape, with a dark spot in the centre, where the formulation has not coated well.

Figure 2.11: The evenness of the colour in this E_3 sensor is shown to be poor. Note the poor spread of colour in the centre of the spot, diameter approximately 4000 μm. The photo was taken on a black background.

The results from the analysis of this spot show large variations in the RGB values across the spot (Figure 2.12). The % RSD values for each of the RGB channels for this E_3 sensor were 31.79%, 28.38% and 23.45% respectively. The ratio of plasticiser to binder creates poor coatings. Higher plasticiser concentrations create a more oily coating, likely due to saturation of the polymer matrix by the plasticiser. This oversaturation of the polymer prevents the sensor formulation from producing an even spot; therefore, there is too much plasticiser present in these sensor spots.

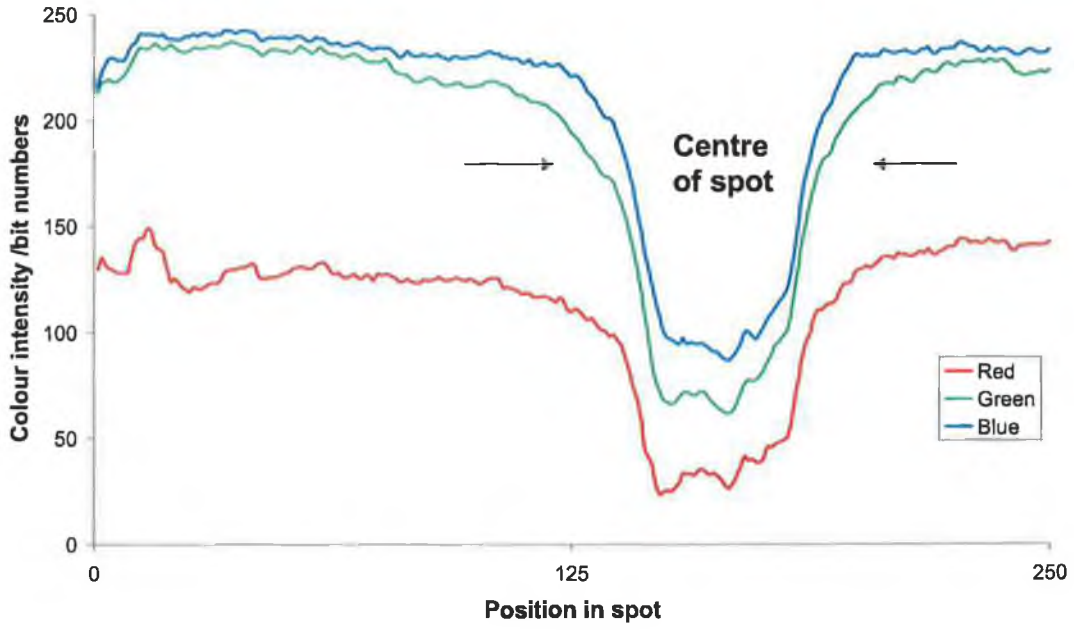

Figure 2.12: The variations in the RGB values correspond to the poor colour intensity across the E_3 sensor dots.

2.5.1.2 RGB analysis of E_5 sensors

These sensors have 3 % w/v binder to 3 % w/v DBP; they were dried in a sealed acetone-saturated environment (Table 2.2). Each of the sensors has excellent homogeneity (Figure 2.13). The E_5 sensors are more opaque than the E_3 sensors previously shown. The RGB data obtained from LabVIEW analysis clearly shows the evenness of the colour distribution across the centre of the spot (Figure 2.14). The corresponding RSD values for the RGB colour channels are 5.85 %, 3.21 % and 2.33 % respectively.

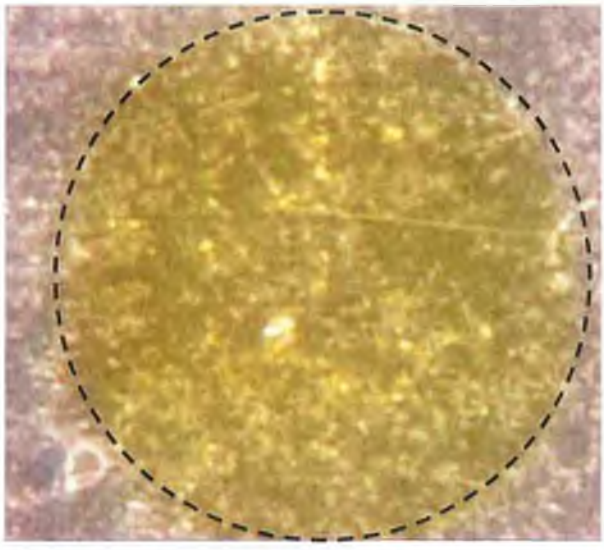

Figure 2.13: The evenness of the E_5 sensor dot is much better than the E_3 sensor dot shown in Figure 2.11. The diameter of the dot is approximately 4000 μm. A black border was added to the image for visual aid only.

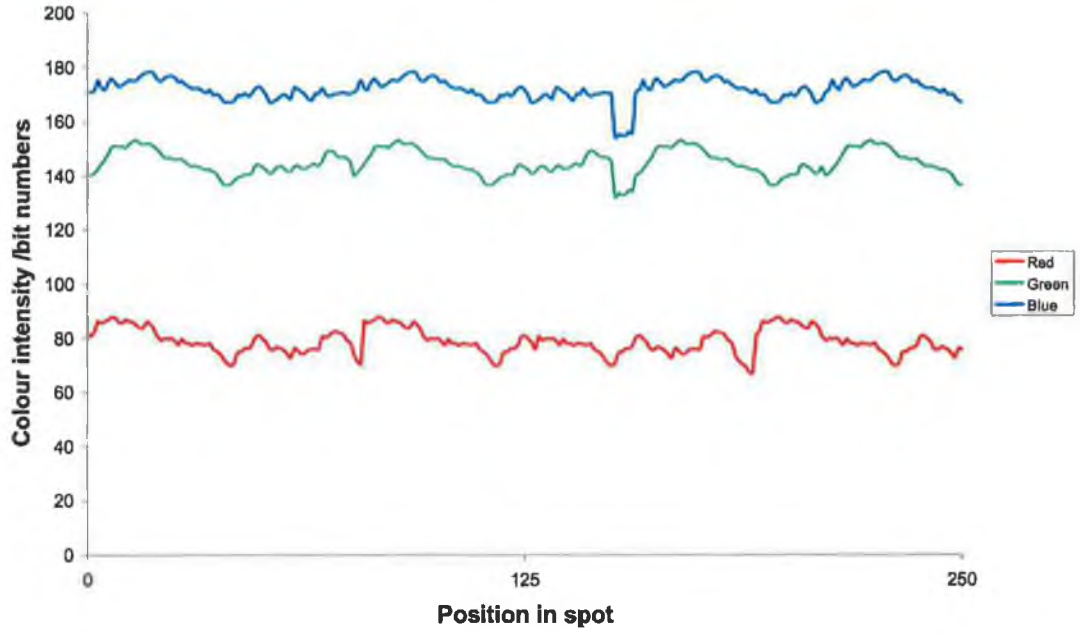

Figure 2.14: The evenness of the colour distribution across the spot can be clearly seen in the evenness of the red, green and blue values across the sensor dot.

In order to comment on the level of variation in RGB colour values, the noise of the system was evaluated. Three images of the black background were taken as described in Section 2.4.3.1. Each image was analysed and the results are a direct indication of the amount of noise inherent in any measurement of colour variation

(Figure 2.15). It was assumed that the colour of the black background was the same in the small area analysed; a valid assumption, since it was created from an inkjet printer.

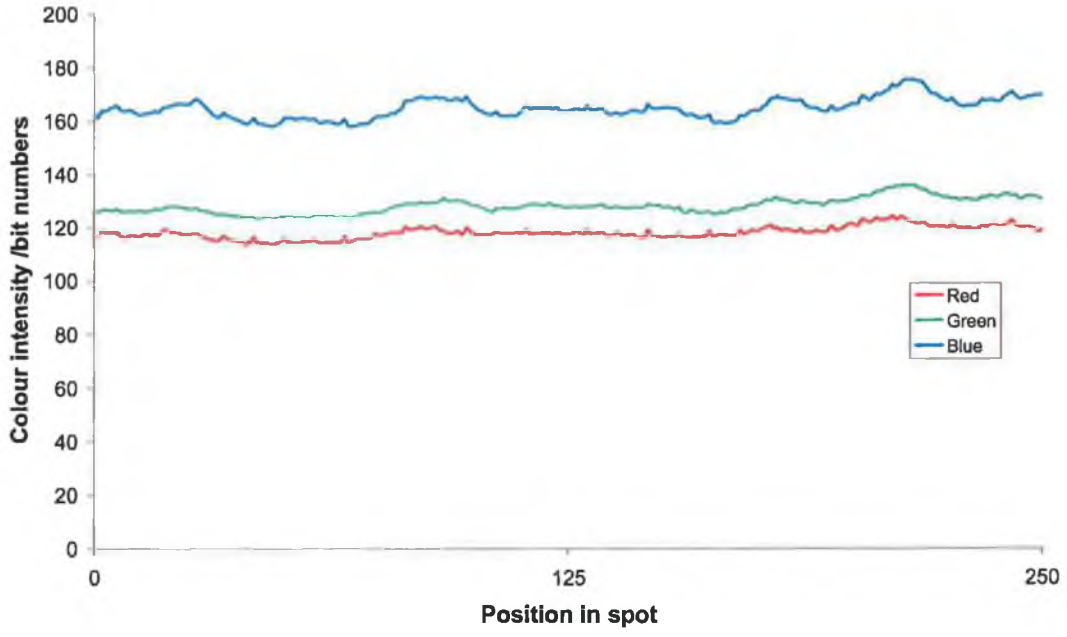

Figure 2.15: The variation in RGB channels across the background gives a direct indication of the amount of noise in the system.

The average RSD values for each of the RGB channels for the three images taken were 2.22 %, 2.35 % and 2.20 %. This implies that for every measurement taken using this imaging acquisition setup, there is at least a 2 % error per colour channel due to the noise of the measurement. Most of this noise likely comes from the CCD array of the camera; the lighting is too well controlled within such a small space to contribute so greatly to noise. Hence this type of system is better suited to screening dots rapidly; it is less suited to in-depth colour reference measurements. In summary, the average % RSD values for each of the three replicate sensors for each formulation "A" through "E" was calculated, and the results are shown in Table 2.3.

Formulation	% RSD (n=3)		
	Red	Green	Blue
A	9.34	5.28	4.36
B	8.42	5.54	5.50
C	9.12	3.71	3.76
D	9.49	9.78	7.43
E	6.95	5.73	5.49

Table 2.3: The % RSD in all colour channels, for each formulation "A" through "E", gives a rapid and clear indication of the approximate evenness of colour.

Examination of these results clearly shows large amounts of variation in sensors "A" through "D". Sensor formulations containing DOS and NPOE plasticisers are poor. Inspection by eye shows that the sensor dots prepared from these formulations are not homogeneous or reproducible. They are not useful in this application and are hence unsuitable for further study. Conversely, the formulation containing DBP creates coatings that are much more even. At a chemical level, this is difficult to interpret; it is likely that DBP simply distributes itself more evenly than either of the other two plasticisers tested. Section 1.4.5.1 describes how the plasticiser affects the *bulk* property of the polymer matrix [41], and was hence selected on a trial-and-error basis, rather than predicting the effectiveness of a particular formulation.

By examining the sensors produced by eye, in conjunction with the rapid screening of RGB colour evenness described, it was clear that the E-type formulation was producing the best sensors. For most sensors, the % RSD of the red channel is usually higher than for green or blue. This is likely to be explained by the auto-compensation of the digital camera. The amount of variation in each of the three colour channels is not necessarily the same. The camera compensates in a different manner for each colour channel, depending upon the lighting conditions that are used. This is done using highly convoluted proprietary compensation algorithms, designed for the home-user market to create even illumination in most lighting

conditions. A higher specification camera may remove this problem; the cost of such a camera escalates rapidly, however [94].

A number of different variations in the E-type formulation were examined in order to further optimise the chemistry and the sensor production process. Analysis of E_1 through to E_5 sensor dots was again performed as per Section 2.4.3.1 (Table 2.4).

Formulation	% RSD (n=3)		
	Red	Green	Blue
E_1	6.95	5.73	5.49
E_2	10.02	6.81	5.82
E_3	17.04	17.46	13.32
E_4	5.96	5.24	5.13
E_5	5.08	4.69	4.18

Table 2.4: The variation in red, green and blue colour intensities for a number of different sensor formulations and production methods.

These results show a consistent evenness of colour for each of the RGB colour channels for sensors E_1, E_4 and E_5. There is an unacceptable amount of colour variation seen for the E_2 and E_3 sensors. The ratio of binder to plasticiser is clearly a key issue in the chemistry of the formulation to produce an evenly coated sensor dot. Too little or too much plasticiser produces uneven coatings.

At this stage of analysis, it is not possible to tell which sensor formulation and production method is working the best. The purpose of the screening methodology was to remove those sensors that were not worthy of further analysis; these have been selected as the A through D sensors and the E_2 and E_3 sensors. The remaining sensors, namely E_1, E_4 and E_5 sensors, were selected for further analysis with a more in-depth colour and spectral referencing system.

2.5.2 Analysis of sensors using PARISS

Further analysis was performed for sensor formulations E_1, E_4 and E_5, as described in Section 2.4.3.2. Autoscans were generated for these groups of sensor dots to give an indication of the evenness of the coating, and this produced data with a higher resolution than is possible with the simple 8-bit imaging system described in Section 2.4.3.1.

2.5.2.1 E_1 sensors (dried in air)

A spectral topographical profile for one of the E_1 sensor dots is shown in Figure 2.16. This cross-section shows that much of the spot is returning the same spectral signature, which has been classified in red. The edges of the spot, coloured as yellow, were classified as different than the red regions. The black regions of the profile are areas where the formulation did not coat or dry well. Although localised, a photo captured by the PARISS image camera (Figure 2.17) shows that surface of the spot is covered in many tiny pinholes. The edges of the sensor spot have clearly dried differently than the rest of the spot.

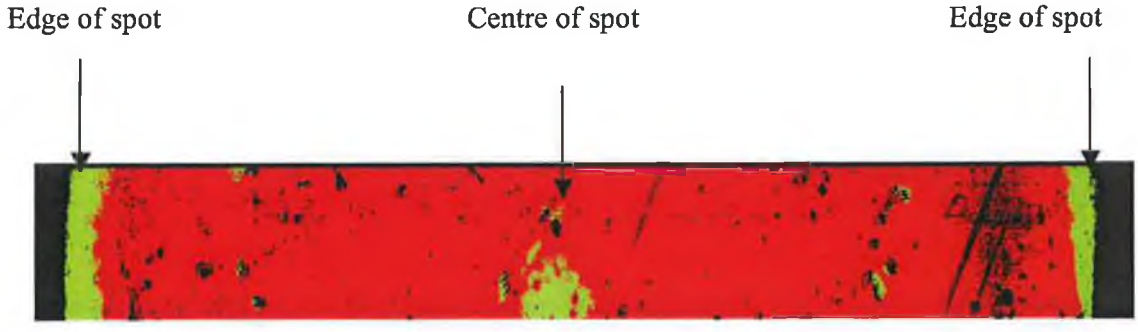

Figure 2.16: Spectral topographical profile for an E_1 sensor dried in air. Scans were performed at 100x magnification to generate the cross-section shown.

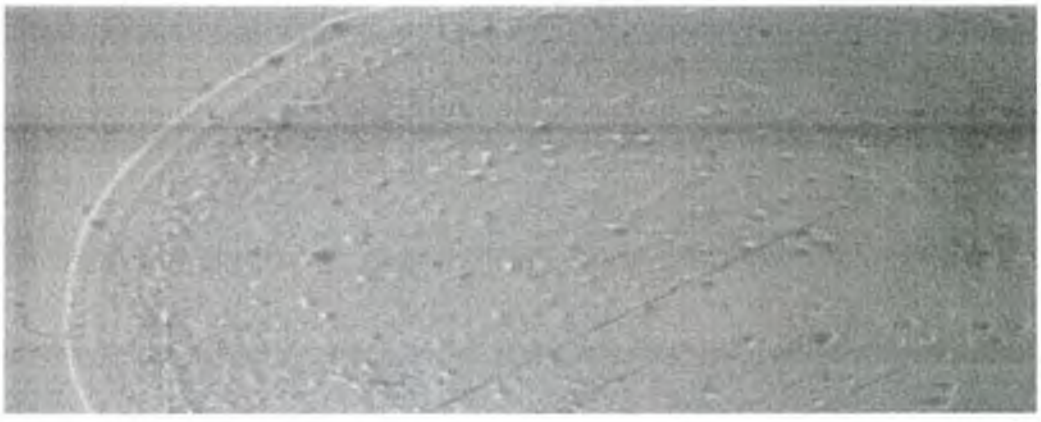

Figure 2.17: An image of an E_1 sensor captured with the PARISS system image camera at 100x magnification shows small "pinhole" regions where the formulation has not evenly dried. This may be due to the rate of solvent evaporation from the surface. The difference between the centre and edges of the spot is clearly shown.

Analysis of the % composition of the classified image shows that over 90 % of the overall spectral signature is comprised of the spectrum classified in red (Figure 2.18), with approximately 8 % of the spot classified as different, in yellow.

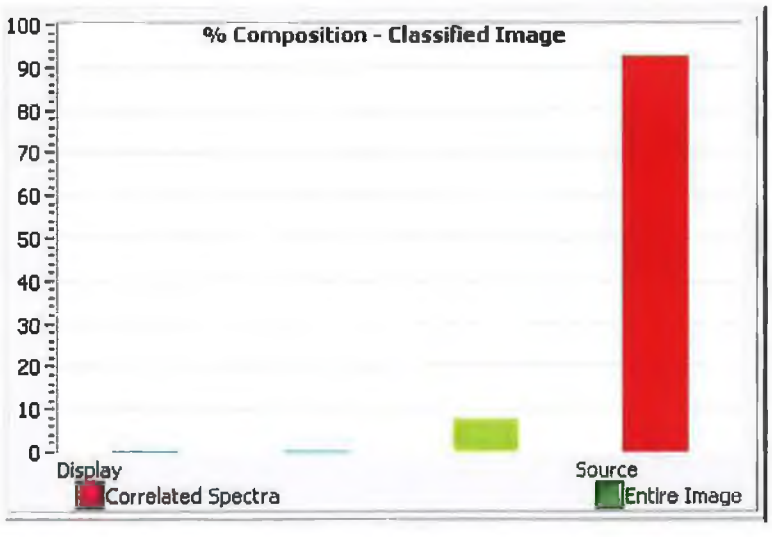

Figure 2.18: The % composition of the classified image shows that over 90 % of the correlated spectra are comprised of the same spectral signature, with the MCC set to 0.9990.

This is a very positive result. The majority of the spot is comprised of the same spectral signature, even with a high MCC during spectral classification. This is significant, since it implies that a spectral reading taken from over 90% of the spot would return the same reading. There are some minor concerns about the distribution

of the formulation however. There are many "pinholes" in the spot that can be seen under high magnification. Even though this batch of sensor dots appears to be very evenly coated, there are small regions where the formulation has not dried well, and this was a typical artefact for all of the E_1 sensor dots examined. It is difficult to explain this easily, but it may be due to the rate of evaporation of solvents from the surface, since there is a lack of control over the drying conditions during the sensor production process. To see what affect the drying conditions had on the evenness of a sensor coating, sensor dots were prepared at 4 °C (E_4) and in a sealed acetone-saturated environment (E_5).

2.5.2.2 E_4 sensors (dried at 4 °C)

An autoscan obtained for one of the E_4 sensor dots (Figure 2.19) shows an uneven spectral topography.

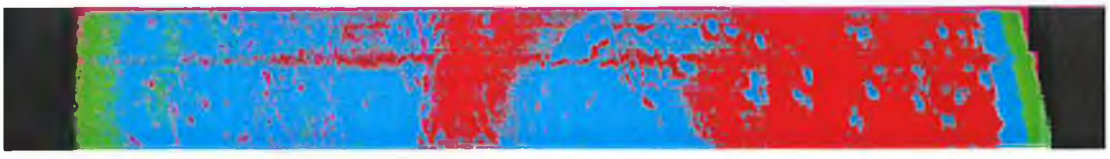

Figure 2.19: Spectral topographical information for an E_4 sensor dried in air. Scans were performed at 100x magnification. The uneven spectral distribution is clearly seen. The black regions are the edges of the spot.

There are two main spectral signatures that were classified by the PARISS software, one coloured blue and one coloured red. The relative amounts of each of these spectral signatures are almost equal, and the overall % of each of these regions is shown in Figure 2.20.

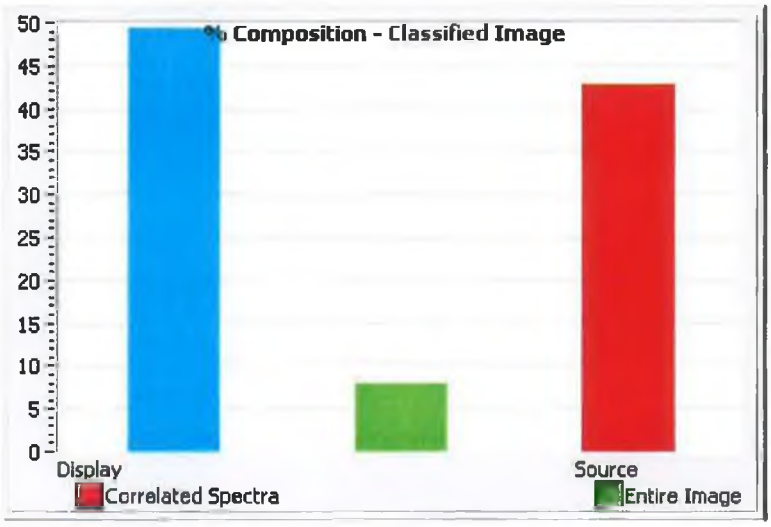

Figure 2.20: The % composition histogram of the classified image reveals that the E_4 sensor is comprised of two main spectral signatures, shown as blue and red. Scans were obtained with a MCC of 0.9990.

The uneven spectral topography clearly shows that the sensor formulation did not coat well. The apparent difference between the red and blue classified spectral signatures was not detectable by eye. One explanation for the poor sensor dot formation is the rate of drying. A low temperature means that the spot dries very slowly and, apparently, unevenly. This suggests that more control is needed over the rate of drying of the spot.

2.5.2.3 E_5 sensors (dried in sealed environment)

An autoscan of an E_5 sensor (Figure 2.21) reveals a consistent spectral topography across the cross-section of the sensor dot.

Figure 2.21: The spectral topography of an E_5 sensor dried in a sealed, acetone-saturated environment demonstrates that the majority of the spot is comprised of the same spectral signature. The MCC was set at 0.9990. The black regions are the edges of the spot.

Clearly this is very satisfactory result, with the vast majority of the spot comprised of the same spectral signature, classified as red. The % composition histogram (Figure 2.22) confirms the same result.

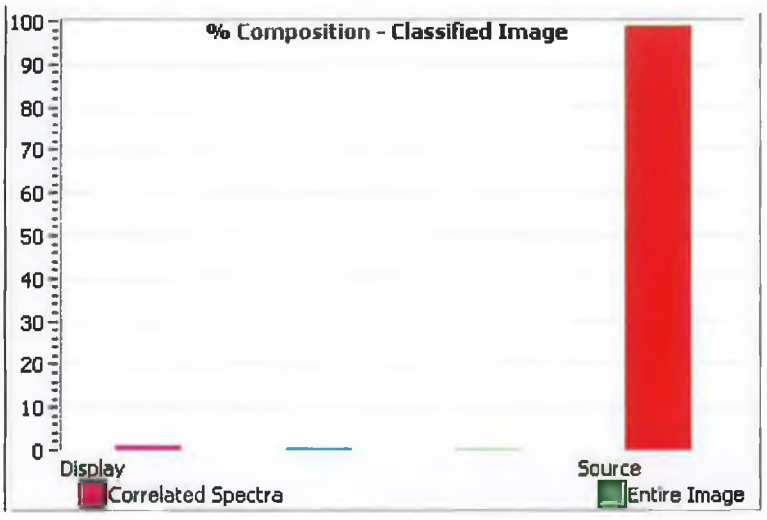

Figure 2.22: The % composition histogram clearly shows the majority of the spot is comprised of the same spectral signature, classified as red.

Sensors prepared from the E_5 formulation were typically similar and this is an excellent result. It implies that a spectral or colour measurement can be taken from practically anywhere in the spot, to return the same numerical value. Regardless of what technology is used to interrogate the sensor dot (digital camera, by eye, or spectrally), the coatings prepared are consistently even. This chemical formulation was hence selected for further study for monitoring amines released from spoiling fish samples. The following sections in this chapter describe work that was performed to further characterise the optimised sensor dots produced.

2.5.3 Effect of dye loading on the sensor formulation

The spectral data obtained for sensor dots containing 0.2 % w/v cresol red (Section 2.5.2.3) clearly shows a homogeneous sensor has been produced. Figure 2.23 shows a typical spectral topographical profile that was obtained for sensor dots containing half the amount of dye (0.1 % w/v) compared to the E_5 formulation.

Figure 2.23: A typical spectral topographical profile obtained when the dye loading was half of that previously tested (0.1 % w/v), with a MCC of 0.9990. The black regions are the edges of the spot.

It can be clearly seen that although most of the spot is comprised of one spectral signature (light green), there are three other spectral features that were classified as different (dark green, pink and red). The relative % composition of the classified image in Figure 2.23 is shown in Figure 2.24.

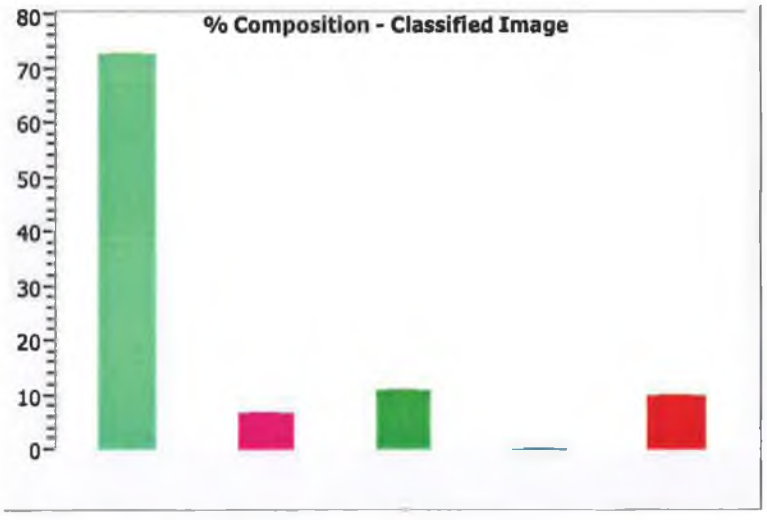

Figure 2.24: The % composition histogram of the classified image shows clearly that over 25 % of the image is classified as different to the main spectral signature (light green).

Reducing the dye loading by two has clearly had an adverse effect on the homogeneity of the sensor dots produced. The dye no longer distributes itself evenly within the coated sensors, and this is unacceptable. Figure 2.25 shows a typical spectral topographical profile that was obtained for sensor dots containing twice the amount of dye (0.4 % w/v) as the E_5 formulation.

Figure 2.25: A typical spectral topographical profile obtained when the dye loading was twice that previously tested (0.4 % w/v), with a MCC of 0.9990. The black regions are the edges of the spot.

The spectral features seen in this typical sensor dot are similar to those when the dye loading was 0.1 % w/v (Figure 2.23). The % composition histogram of the classified image confirms the different spectral features (Figure 2.26).

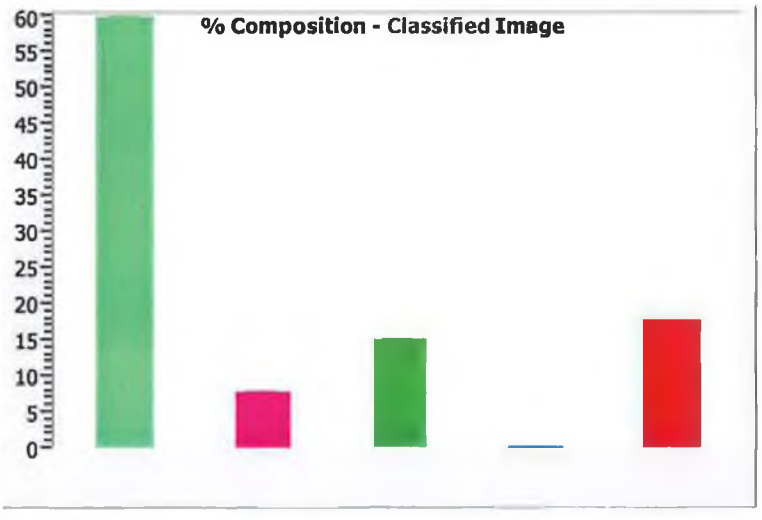

Figure 2.26: The % composition histogram of the classified image shows clearly that over 40 % of the image is classified as different to the main spectral signature (light green).

Although there is 60 % of the sensor dot composed of the same spectral signature (light green), there are other spectral features that manifest themselves at the edges of the sensor dots. It is difficult to predict why this is happening, but perhaps it is an artefact that is introduced during the drying of the sensor dot during the sensor production process. It is possible that the sensor dot dried differently when the concentrations of the chemical components were altered. Apparently too much or too little dye causes uneven sensor dots to be produced with the current chemical cocktail. The balance between the components in the formulation would have to be altered if the dye loading is changed.

Changing the dye loading will have a marked effect on the sensitivity of the response of the sensor. A reduction in the amount of dye present will reduce the upper limit of detection of the sensor to basic compounds, as the sensor will become saturated at lower exposure limits. The lower limit of detection may be improved however. Conversely, increasing the dye loading will widen the working range of the sensor, since it will take more basic compounds to saturate the dye. The sensitivity at the lower range of detection will be raised however. In general, there is a trade-off between the working range and lower limit of detection of the sensor, which can be tuned by altering the dye loading. At present, the optimised dye concentration is 0.2 % w/v, in view of the fact that this produces the most homogeneous sensor dots. This is therefore the dye concentration that was used for all further studies.

2.5.4 Comparison study of the pK_a of the dye in free solution and polymer binder

2.5.4.1 Free solution study

A UV-Vis scan obtained of the cresol red dye in pH 10 buffer is shown in Figure 2.27. The λ_{max} was determined from this spectrum to be 573 nm. This is very close to the literature value of 570 nm [20].

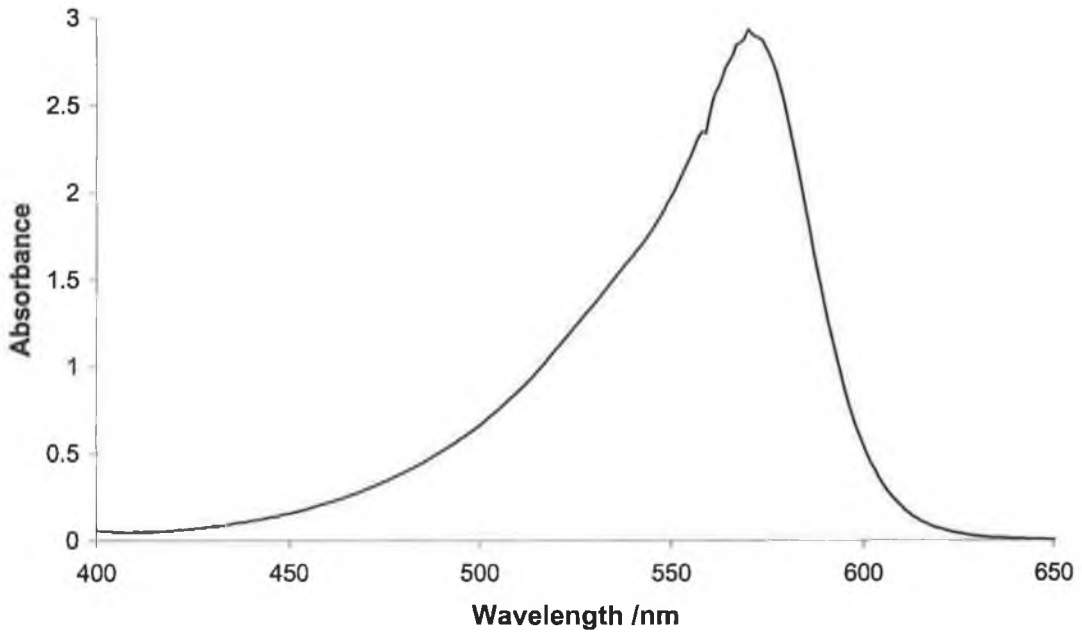

Figure 2.27: UV-Vis spectrum of cresol red in pH 10 buffer, taken to determine the λ_{max} of the dye in free solution.

The colours of each of the dye samples in buffer varied from yellow to purple, and are shown in Figure 2.28. The absorbance at 573 nm was measured for each of the dyes in buffer solutions, in triplicate, and a best-fit sigmoid model was fitted to the data using Solver (Figure 2.29). The parameters of the best-fit model aided the determination of the pK_a of the dye in free solution.

Figure 2.28: The cresol red dye in buffer samples varies in colour from yellow (protonated form) to purple (deprotonated form).

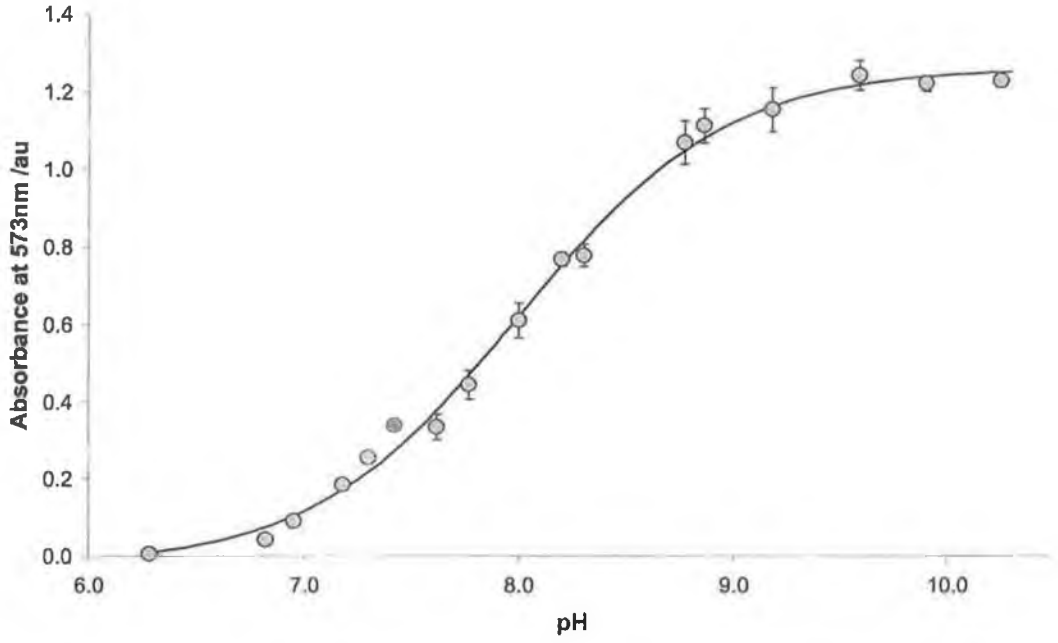

Figure 2.29: The absorbance of the dye at 573 nm as a function of pH for the dye in free solution. The error bars are ± standard deviation, where n=3. The sum of squared residuals for the best-fit curve is 0.0330.

The value of the pK_a obtained (the "C" parameter) was 8.01 ± 0.017 (0.22 % RSD, n=3). There is some deviation between this and the literature value of 8.30 [20]; this may be in part due to differences in batch-to-batch purity of the dye, which is only 95% pure. Hence, the same batch of cresol red dye was used for all the studies that were carried out in this thesis.

2.5.4.2 Polymer binder study

The work shown in Section 2.5.4.1 was repeated for cresol red entrapped in the cellulose polymer matrix. A UV-Vis scan at pH 10 (not shown) was collected to show that the λ_{max} of the dye doesn't shift in the polymer matrix. A best-fit sigmoid function was modelled to the absorbance data at 573 nm (Figure 2.30), to allow the pK_a of the entrapped dye to be determined. The value of the pK_a was calculated as 7.98 ± 0.020 (0.25 % RSD, n=3).

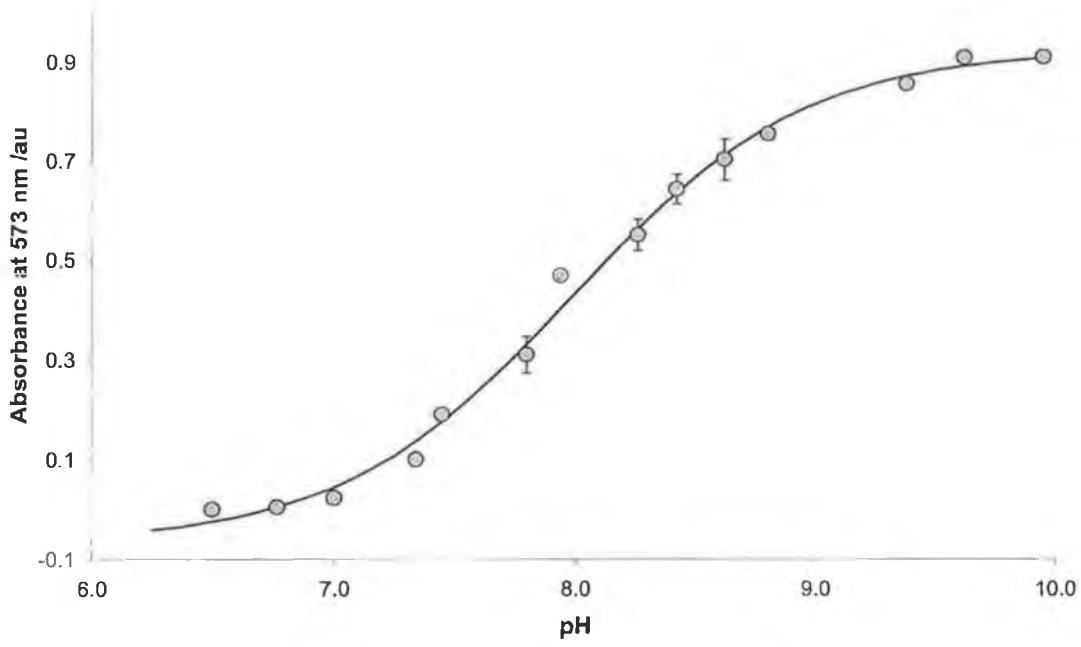

Figure 2.30: The absorbance of the dye at 573 nm as a function of pH for the dye entrapped in the cellulose polymer matrix. The error bars are ± standard deviation, where n=3. The sum of squared residuals for the best-fit curve is 0.0114.

2.5.4.3 Comparison of data

The data comparing values obtained in free solution to those entrapped in the polymer binder are shown in Table 2.5. Section 1.4.5.2 reviewed literature that noted results similar to those described in this section.

Format of dye	pK_a
In free solution	8.01 ± 0.017
In polymer matrix	7.98 ± 0.020

Table 2.5: Summary of shifts in pK_a of the dye in free solution and entrapped in the cellulose polymer matrix. n=3 for all replicate measurements performed.

These are very positive results. The pK_a does not significantly shift when trapped in the cellulose polymer binder; hence the sensitivity of the dye in the sensor spot will not be affected when interacting with basic gas compounds.

2.5.5 Study of the effect of temperature on pK_a

The pK_a at room temperature (21 °C) was determined to be 8.01 ± 0.017. The same solutions were analysed at 4 °C, and a best-fit sigmoid function was modelled to the absorbance data at 573 nm (Figure 2.31), to allow the pK_a at 4 °C to be determined. The pK_a from Figure 2.31 was calculated as 7.97 ± 0.019. Thus a change in temperature of almost 20 °C introduced no major effect on the chemistry of the dye.

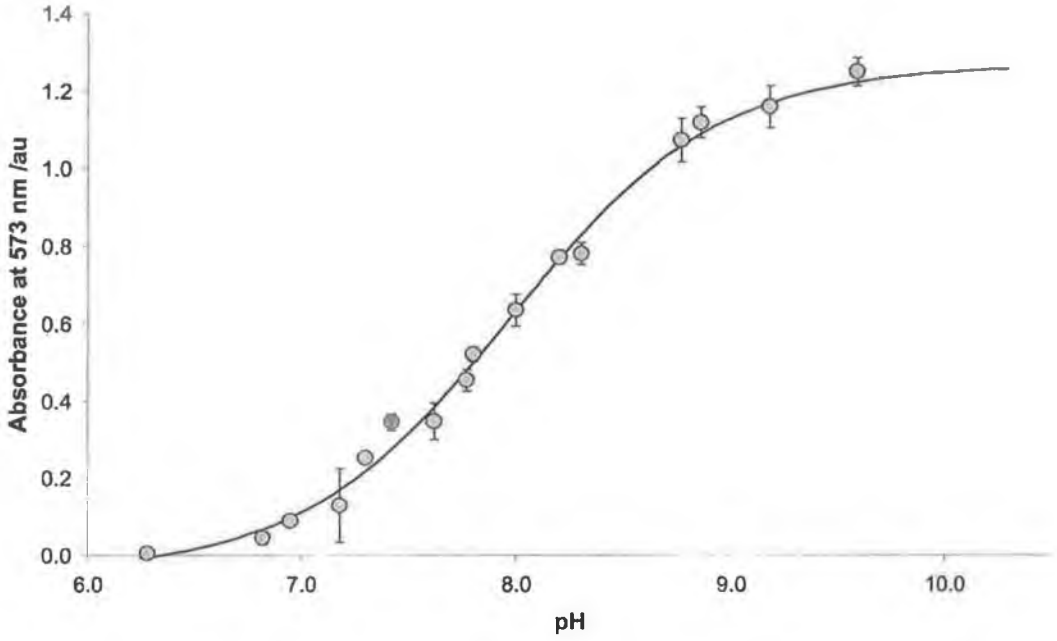

Figure 2.31: The absorbance of the dye at 573 nm as a function of pH for the dye in free solution at 4 °C. The error bars are ± standard deviation, where n=3. The sum of squared residuals for the best-fit curve is 0.0014.

An overlay of both best-fit sigmoid functions obtained, shown in Figure 2.32, clearly proves that the chemistry of the dye is not affected by this temperature shift. This is an excellent result that demonstrates the suitability of the sensor dots to be placed at 4 °C on fish packaging. The sensor dots are suitable for any conditions between refrigerated and room temperature, and the temperature of the system (provided it is between these two values) does not need to be taken into consideration when a sensor dot reading is taken.

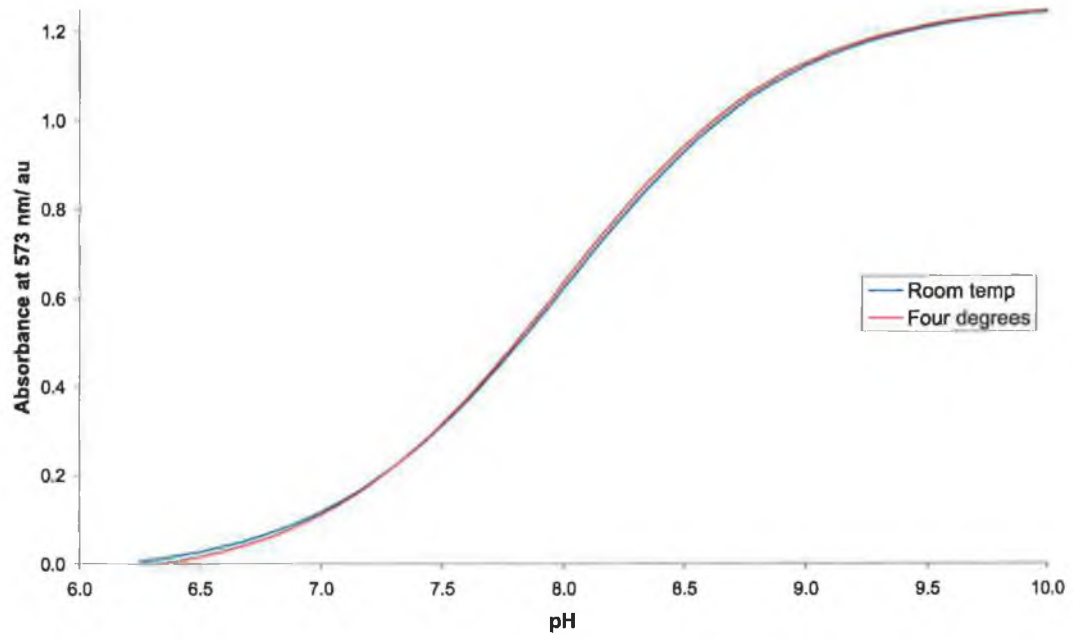

Figure 2.32: An overlay of both best-fit sigmoid functions obtained at room temperature and 4 °C. The data at both temperatures is very similar. Thus the temperature of the system (once between these limits) does not need to be taken into consideration when a sensor reading is taken.

2.5.6 Calibration of sensors to headspace NH_3

Spectra were acquired with the PARISS system to monitor the changes of the sensor with increasing NH_3 concentration. Each spectrum acquired was ratioed to the spectrum of a white reflectance standard, and software-converted into absorbance values. The sensor colour changed rapidly (ca. < 30 s, observed by eye) from yellow to purple with each sequential injection of NH_3. This response time is comparable to values from the literature (Section 1.4.5.2). After ca. 30 s, no further colour changes were observed by eye, i.e. the sensor has reached equilibrium with the ammonia. Figure 2.33 shows the sensor colour changes that were observed for 5 sample injections for the same sensor.

Figure 2.33: The colour changes that were seen (after 5 min) from 0 ppm NH_3 (left) to 8.62 ppm NH_3 (right). Each of the photos were taken with a generic digital camera and are presented for visual aid only.

The headspace NH_3 concentration was calculated using the following equation:

$$C_{NH_3} = \frac{V_{inj}}{V_h} \times 100 \text{ ppm} \qquad \textbf{Equation 2.2}$$

where C_{NH3} = concentration of NH_3 in headspace /ppm

V_{inj} = volume of NH_3 gas injected into flask

V_h = Headspace volume of flask = 50 ml + volume of sensor cap (2.198 ml, determined gravimetrically by filling with water).

The values obtained were multiplied by 100, as this was the concentration of the stock NH_3 sample. Figure 2.34 shows 7 example spectra that were obtained for 7 different injections of ammonia. The rising response of the sensors at λ_{max} is clearly evident. A best-fit sigmoid function was modelled to the absorbance data at 573 nm collected in reflectance-mode, and is shown in Figure 2.35.

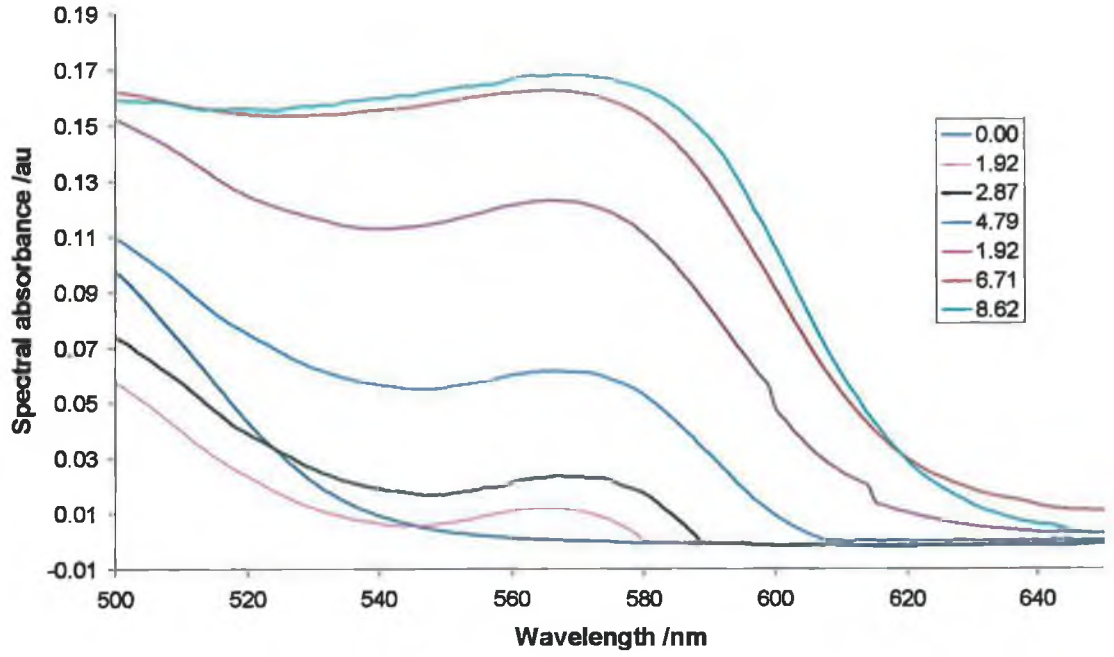

Figure 2.34: 7 full sensor spectra are shown for increasing NH_3 concentration in headspace (given in the legend in ppm). The absorbances were measured in reflectance-mode, 5 min after an injection was made. The rise at the λ_{max} (573 nm) is clear.

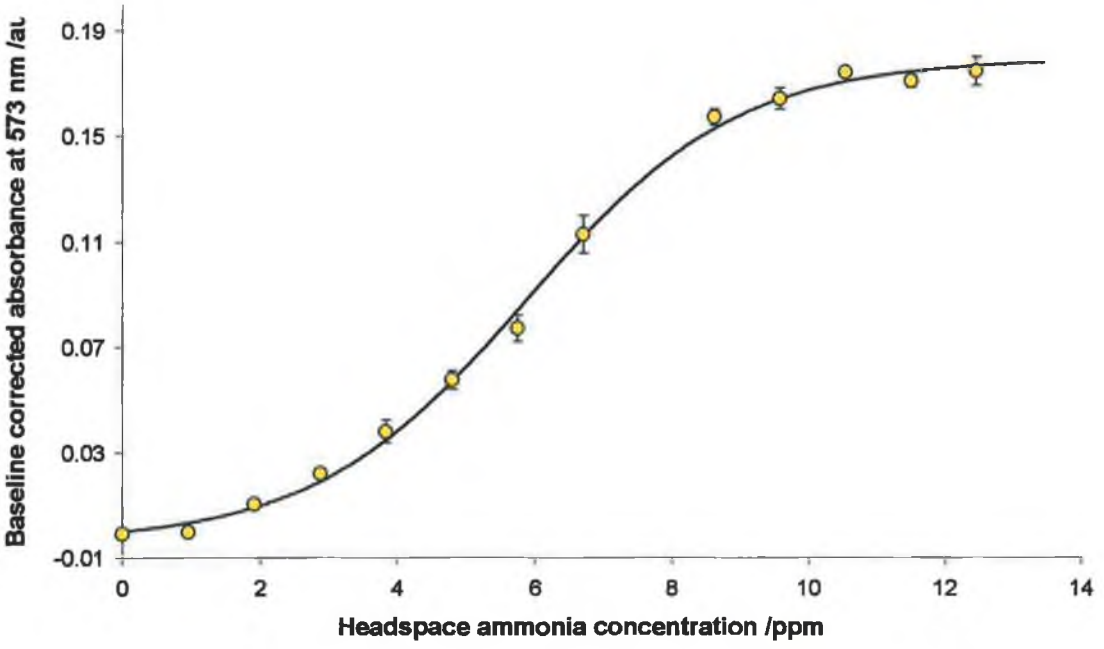

Figure 2.35: The spectral absorbance of the sensor dot at 573 nm as a function of increasing NH_3 headspace concentration. The absorbances were measured in reflectance-mode. The error bars are ± standard deviation, where n=3. The sum of squared residuals for the best-fit curve is 0.0001.

Figure 2.34 shows that the position of the λ_{max} does not shift with increasing sensor response. The excellent fit to the data in Figure 2.35 is seen in the SSR value for the best-fit model. The standard deviation (6.35 % RSD) is also acceptable for three sets of injections that were performed. The mid-point of the sigmoid function was at 5.86 ppm NH_3 headspace concentration for the best-fit curve shown. The pK_a of cresol red entrapped in the polymer binder was already shown to be 7.98 ± 0.020. Hence, it is valid to assume that the headspace pH was ca. 8 when the headspace NH_3 concentration was ca. 5.9 ppm.

The linear portion of the data collected gave an equation of the line (y = 0.0255x - 0.0632) that was used to filter out those data that were outside a 5 % tolerance of deviation from the best-fit sigmoid function (Figure 2.36). The lower limit of detection (LOD) of the sensor response was calculated as three times the standard deviation of the baseline response (LOD = 3σ).

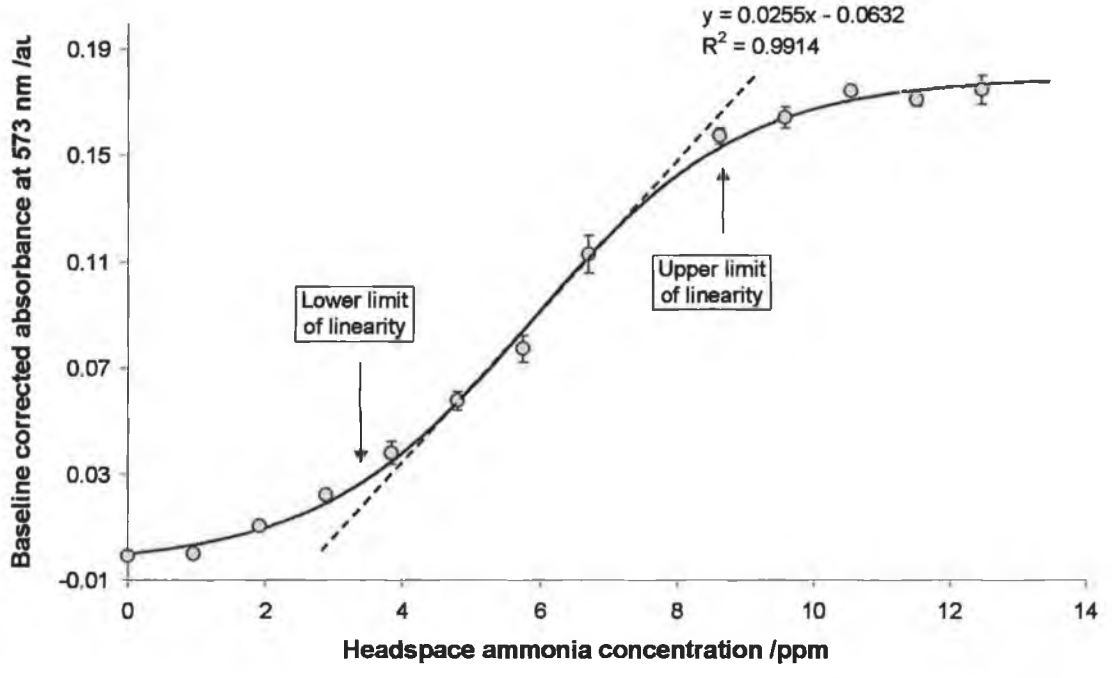

Figure 2.36: The linear portion of the spectral absorbance measured in reflectance-mode of the sensor dot at 573 nm was used to filter out those data that were outside a 5 % tolerance from the best-fit sigmoid function, to determine the upper and lower limits of linearity of the sensor response to NH_3. The error bars are ± standard deviation, where n=3.

From Figure 2.36, the lower and upper limits of linearity were 3.65 ppm ± 0.235 ppm and 8.95 ppm ± 0.577 ppm respectively (n=3). The standard deviation of the baseline was 0.00033 au, used to calculate the lower LOD as 0.35 ppm. Put simply, the sensor can detect NH_3 in headspace from 0.35 ppm, but only responds in a linear fashion from 3.65 – 8.95 ppm. Above 8.95 ppm, the sensor response is saturated, and is purple in colour (Figure 2.33). This is quite a narrow working range, attributed to the chemistry of the dye that becomes saturated at concentrations of NH_3 > 10 ppm. There are potential ways to increase the upper limit of detection of the sensor, and these are discussed in Chapter 6.

2.6 Conclusion

The first part of this chapter was concerned with optimising the sensor formulation and sensor production process to prepare homogeneous sensor dots. Different batches of sensors were produced, which included testing three different plasticisers in different ratios to the polymer binder, in different solvents. A simple screening process was developed, using a digital imaging setup and RGB analysis, that allowed those sensors not worthy of further study to be removed. Selected sensors of interest were studied in more detail with the imaging spectrograph (PARISS) system, which itself is described in detail in the instrumentation section. Spatially resolved spectral topographical profiles were generated, with % histograms that describe the relative proportions of individual spectral signatures in a sensor dot. This data, coupled with a study of the drying conditions of the sensors, allowed an optimised formulation to be developed. This consisted of 3 % w/v cellulose acetate, 3 % v/v dibutyl phthalate and 0.2 % w/v cresol red dye (sodium salt) in 1:1 acetone to cyclohexanone, dried in sealed, acetone-saturated environment. A study of the effect of dye loading was also performed, with twice and half the dye concentration tested. Too much or too little dye causes the sensor dots to form non-homogeneous coatings with the current chemical cocktail used.

The effect on the pK_a of the dye entrapped in the polymer binder compared to in free solution was studied. Best-fit sigmoid functions were modelled to the datasets to return values of interest. The pK_a of the dye in the polymer binder does not shift significantly from in free solution. A study of the effect of temperature on the dye in free solution was performed and it was determined that the pK_a of the dye does not shift noticeably from room to refrigerated temperature. The depth profiles of the sensor dots were measured to characterise the average width and height of the sensors produced. It was determined that, as expected, the manual sensor production process does have its limitations.

A headspace calibration against ammonia was performed to determine the upper and lower limits of linearity, and the lower LOD of the sensor dots. The sensor can detect between 3.65-8.95 ppm headspace NH_3 in a linear fashion, and has a lower LOD of 0.35 ppm. The sensor response has an RSD of 6.35 % (n=3). On the basis of the results presented in this chapter, the developed sensor appears highly suitable for the chosen application.

The outcome of these results is that a working sensor has been produced that can monitor the changes in headspace TVB-N levels released from gradually spoiling fish samples. The sensor dots produced are homogeneous and a reading taken from practically any region of the same sensor will return the same spectral intensity value. The first major direction to go from here is to determine the sensor response to real fish samples. This should include calibrating the sensor against different species, and ideally, an experimental setup should be designed to facilitate the rapid analysis of many samples. It is important to relate the sensor response to headspace TVB-N levels, since the sensor has only been calibrated against NH_3 thus far. The headspace TVB-N levels released from a spoiling fish sample should be quantified and compared to the sensor response to obtain a full set of calibration data for the sensor.

One other major direction is to study the relationship between the sensor response and the microbial populations of a fish sample. The increase in microbial population of a spoiling fish sample directly causes an increase in headspace TVB-N levels. There should exist a strong correlation between the sensor response, the headspace TVB-N levels and the microbial populations of a sample. This correlation needs to be determined if the sensor response at the critical spoilage region is to be identified. Furthermore, if this correlation were identified, there would exist for the first time, a chemical sensor that can be used to infer microbial populations of a sample, through a reading of the colour intensity of the sensor.

3 Monitoring of Headspace Spoilage Volatiles released from Packaged Fish using a Colorimetric Chemical Sensor

3.1 Introduction

This chapter presents the first set of results obtained for monitoring the release of headspace spoilage volatiles from real fish samples, using the cresol red based sensor developed in Chapter 2. A simple experimental setup was devised that allowed many fish samples to be analysed in parallel. The imaging spectrograph (PARISS) system was used to monitor the spectral changes in the sensor during a spoilage experiment, and results are presented as the change in absorbance at 573 nm (the λ_{max} of the basic form of cresol red) as a function of time, as the samples spoil. Preliminary results were obtained with 3 different species; market-bought whiting, with no knowledge of the sample history, and orange roughy and black scabbard, deepwater fish that were supplied by the Irish Sea Fisheries Board (BIM), with known sample histories. A study of the temperature dependence of the storage conditions was investigated. The experimental setup was modified, and further results were obtained from market-bought fillets of cod and orange roughy. The results shown indicate that the sensors are performing well for the developed task, and can readily monitor the changes in headspace volatiles released by the gradual spoilage of a number of different fish species. Some of the results in this chapter were recently accepted for publication in the Irish Journal of Agricultural and Food Research [86]; the remained of the results from this chapter formed the basis of a 2002 publication in The Analyst [95].

3.2 Experimental

3.2.1 Materials

Cresol red (sodium salt), cellulose acetate (mw approximately 30,000 g/mol), 2-butanone (99 % spectrophotometric grade) and cyclohexanone (analar grade) were obtained from Sigma-Aldrich (Dublin, Ireland). Dibutyl phthalate was obtained from Fluka Chemicals (Dublin, Ireland). Optically clear polyethylene teraphthalate sheets were obtained from Oxley plc (Cumbria, UK). Fast cure epoxy was obtained from Permabond (Eastleigh, UK). Polypropylene caps and 24 multi-well plates were supplied by Sarscedt (Wexford, Ireland). A certified reflectance white standard was obtained from Foss (Dublin, Ireland).

3.2.2 Equipment

Visible spectra were collected in reflectance mode with the PARISS imaging spectrograph system as detailed in Section 2.2.1. PARISS spectral imaging software version 5.1 was used for data collection and post-run data analysis was performed using Microsoft Excel. A Sorvali Omni-Mixer blender (Dupont Instruments, Stevenage, UK) was used to homogenise selected samples.

3.2.3 Sensor fabrication

Batches of the optimised sensor formulation were prepared as previously described (Section 2.4.2). Thus PET substrate was cut with scissors into strips of approximately 3 x 10 cm. The strips were washed with deionised water and were air-dried. 0.6 g of cellulose acetate was prepared in 20 ml of 1:1 acetone:cyclohexanone (Ar grade). After full dissolution by sonication, 0.62 g of dibutyl phthalate was added. 40 mg of cresol red (sodium salt) was then added to the mixture, with a few drops of methanol

to aid solubility. A series of spots were produced by dispensing 3 µl of this solution with a micropipette, from a fixed height of 5 mm, onto the pre-cleaned PET. The sensors were placed in a sealed acetone-saturated environment until dry (approximately 3 hours).

3.2.4 Experimental setup

Preliminary results were obtained by monitoring the levels of headspace spoilage volatiles released from whiting, orange roughy (whole) and black scabbard. The latter two samples are deepwater fish, which are slowly being introduced into domestic markets. There is interest in alternative fish for the consumer market since Irish Sea Fisheries Policy and Development have placed very heavy quotas on common fish such as cod and whiting [96] (in fact, a quota is being introduced for orange roughy in 2003, since so much interest has been expressed in it as an alternative to the more common fish typically used [97]). A modified experimental setup was developed to monitor the levels of headspace spoilage volatiles from cod and orange roughy (fillet) samples. Unless otherwise specified, samples were stored at room temperature, which was measured at 19-21°C. The sampling procedure used for each fish was standardised, as any deviations from this could have a crucial effect on the quality of a sample, and hence on the amount of amines released into the headspace. For each sample tested, aseptic techniques were used to avoid bacterial contamination of fish. This involved swabbing the area with 70 % ethanol (to clean) and using a gas flame from a bunsen burner to clean all utensils and to prevent bacterial contamination of samples.

3.2.4.1 Whiting samples

Whiting, stored on ice, was obtained at a local market (Figure 3.1) and was washed, bled and gutted within one hour of purchase, where it was divided into three sections of head, body and tail (Figure 3.2). Each of these sections were homogenised using a blender/mixer. PET strips were cut into individual sensors with scissors. Single

sensors were placed face-down on a filter paper disc (made using a standard hole-puncher) on top of a 16 mm diameter, 20 mm height polypropylene cap, with a 6mm hole drilled in it. The surface of the cap was covered with a small section of sticky tape, sufficient to form a seal. Sensor caps were prepared in batches of approximately 100. Four replicate whiting samples of 500 mg each were placed in a 24 multi-well plate and sealed with a polypropylene cap modified with a sensor (Figure 3.3). The sensor caps formed a tight seal inside the wells in the multi-well plate. The edges of each sensor cap were sealed with fast cure epoxy to inhibit the release of amines into the environment. The plate was stored at room temperature for the duration of the experiment.

Figure 3.1: Whole whiting obtained at a local market.

Figure 3.2: Whiting, after gutting, was divided into 3 sections of head, body and tail.

Figure 3.3: 24-well plate fitted with polypropylene caps, each modified with a sensor. A blank cap (no sensor) is positioned at the top-right.

3.2.4.2 Orange roughy (whole) and black scabbard

Polypropylene caps, modified with sensors, were prepared as described in the previous section. Orange roughy and black scabbard whole fish samples were caught during a four-day sea excursion. The full history of catches was known, unlike the market-bought whiting samples. Samples were stored on ice from the moment of catch and were obtained whole and unfilleted (Figure 3.4). The fish were labelled as per the day of their catch, from days 1-4. The fish were washed, bled and gutted and samples were removed from the central portion of each fish. Aseptic techniques were used throughout. The samples were not homogenised in any way, since this best represents how fish are naturally stored.

Figure 3.4: Orange roughy (top) and black scabbard. Both samples were obtained whole and were stored on ice from the moment of catch.

Three whole fish were obtained per species (six fish in total). 500 mg duplicate tissue sub-samples were taken from each of the fish species and were added to a 24-well plate and sealed with sensor caps (Figure 3.5). A total of 12 samples per multi-well plate were thus removed for sensor analysis. Two multi-well plates were prepared in parallel; one was stored at room temperature and the other was stored on ice in a fridge at 4°C.

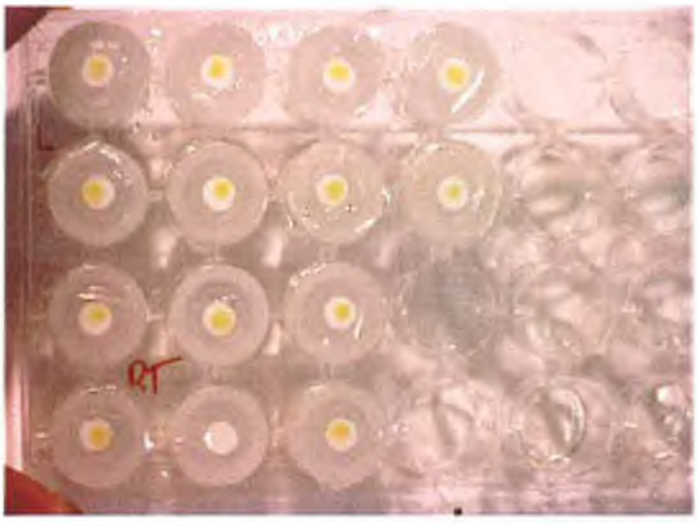

Figure 3.5: 24-well plate fitted with polypropylene caps, each modified with a sensor. The photo was taken at time zero for the plate stored at room temperature. All 12 samples for analysis, plus a reference sensor and blank, were included on the plate.

3.2.4.3 Cod and orange roughy (fillets)

Sensors were prepared as described previously, except that butanone was used instead of cyclohexanone. Butanone serves the same purpose as cyclohexanone, but is easier to handle in the laboratory, e.g. less pungent. The method of fitting the polypropylene caps to the 24-well plate was modified. PET sensor strips were cut into individual sensors of approximately 1 cm^2 and were placed face-up on the base of the wells in the plate. A filter paper disc, 15 mm in diameter, was placed over the sensor to give a white background for spectral imaging and to hold the sensor in place at the bottom of the well. The plate was then inverted, so that the sensors were

facing down and the back of the sensors were facing up for imaging. A schematic of the experimental setup is shown in Figure 3.6.

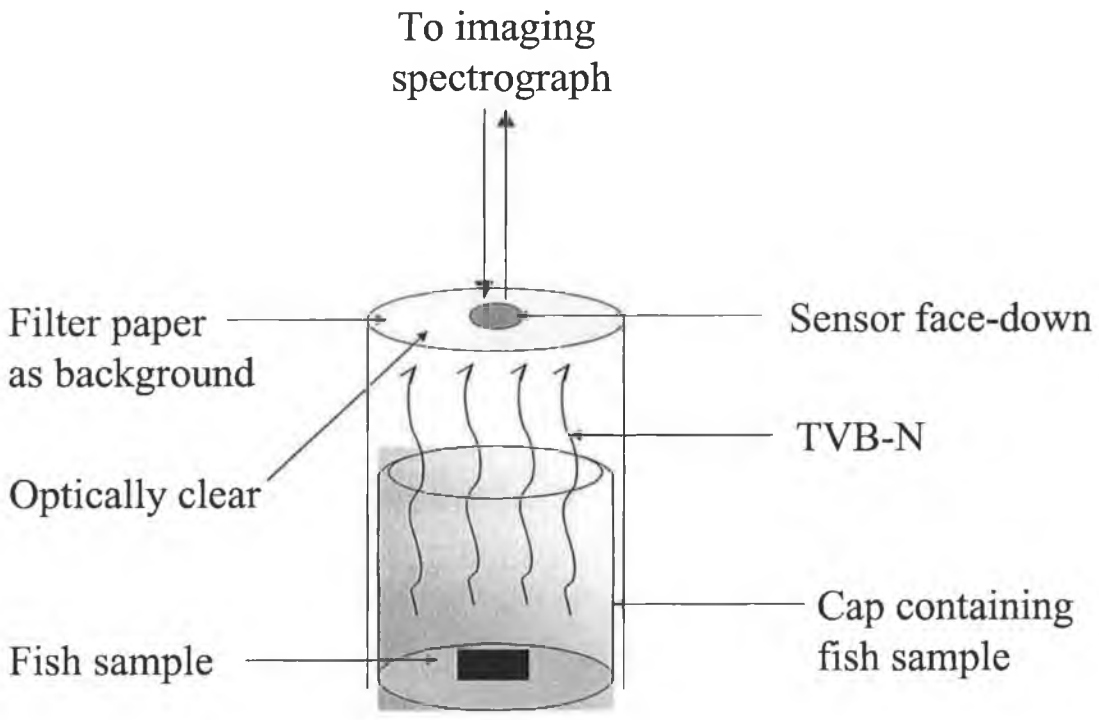

Figure 3.6: Schematic showing how the caps and sensors were placed into the 24-well plate with test fish samples.

Three fillets of cod (Figure 3.7) and three fillets of orange roughy (Figure 3.8) were obtained at a local market on ice. It is believed that they were all approximately between 1-3 days old when purchased. They were stored at –18 °C for approximately 72 hours, whereby they were thawed slowly overnight at 4 °C, followed by final thawing at room temperature for approximately 1 hour.

Figure 3.7: Cod fillets that were used for analysis, after thawing to room temperature.

Figure 3.8: Orange roughy fillets that were used for analysis, after thawing to room temperature.

The fish were washed with tap water and three replicate tissue samples of ca. 500 mg were removed from the centre of each of the three fish, per species, using aseptic techniques. A total of 18 samples were thus removed for sensor analysis, i.e. 9 cod samples and 9 orange roughy samples. Fish samples were placed inside the polypropylene caps and were fitted inside single wells of the 24-well plate incorporated with the sensor (Figure 3.9). The edges of each sensor cap were sealed with fast cure epoxy to create a permanent gas-tight seal.

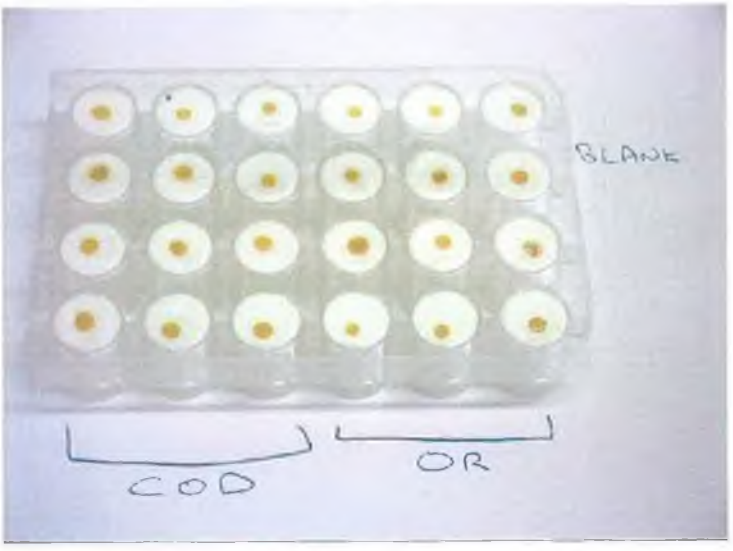

Figure 3.9: 18 samples of cod and orange roughy were used for analysis. The photo shown is the plate at time zero, which includes a row of 6 reference sensors (wells with no sample present) across the top of the plate.

3.2.5 Spectral monitoring of sensors

The PARISS imaging spectrograph system was used to collect spectra of the sensors monitoring the fish samples, to record the change in spectral response from a gradually spoiling fish sample. The PARISS imaging spectrograph returns 240 spectra in the range of 390-810 nm, for the entire area that falls on the spectrometer slit for one acquisition. Spectra were acquired at 10x magnification in the central portion of each sensor. All 240 spectra were averaged to 1 in the PARISS software. A blank spectrum was acquired of a certified reflectance white standard and subsequently, the acquired spectra from sensor acquisitions were ratioed to the average of the white spectrum, to return an absorption spectrum per sensor. Essentially, the difference in the ratios of the spectra is a measure of the decrease in light intensity due to absorbance of light by the sample. The spectral data were exported to Excel and were baseline corrected between 650-800 nm. The height of the deprotonated dye peak (λ_{max}, 573 nm) was measured as a function of time. This procedure was repeated for each sensor in the multi-well plate. The time taken to analyse an entire plate of 24 samples was approximately 10 minutes and the plate

was monitored over the entire time of spoilage, with acquisition of spectra at specific intervals. The timeframe of the spoilage experiment varied with different samples tested, and depended upon the storage regime (room temperature or on ice).

Best-fit logistic-sigmoid curves were fitted to the data obtained using the Solver function in Microsoft Excel [93]. This was achieved as described in Section 2.4.5.1 using Equation 2.1. The formula was entered into Microsoft Excel to model the fit of the data. The residuals, the residuals squared and the sum of the squared residuals were all computed. Solver was set to minimise the SSR value by changing the values of *a, b, c* and *d*. The value of *e* was set equal to 1 and a best-fit model was obtained. The parameters of the best-fit were used to compute extrapolated values between the data points, e.g. every 0.5 hours, from time zero, to produce best-fit curves to the spoilage data collected.

3.3 Results and discussion

3.3.1 General trends identified

A similar trend was seen for all of the samples that were tested. The sensors do not respond for an initial period, the length of which is related to storage temperature and the apparent condition of the samples at time zero. After this period, the sensors begin to change colour, which can be clearly seen by eye and is hence detected spectrally. The sensors continue to change colour as the samples spoil further, until the readings stabilise and the sensor has reached an apparent saturation. The data obtained follows a sigmoidal best-fit. There were some issues that were resolved for the sensors monitoring the whiting, orange roughy (whole) and black scabbard species. As a result, the experimental procedure was modified, and the results for the sensors monitoring the cod and orange roughy (fillets) show that the sensors are working well.

3.3.2 Sensors monitoring TVB-N of whiting

A visual colour change was seen for some sensors after ca. 24 hours at room temperature to a pale orange colour, which continued to a deeper purple colour, seen up to the end of the experimental timeframe (Figure 3.10). Spectral reflectance measurements of the sensor dots were taken at regular time intervals from time zero to 54 hours, and the change in absorbance at 573 nm (λ_{max}) was monitored as a function of time (Figure 3.11). The sensor response remains unchanged from time zero until time 18-24 hours. There is a clear increase in TVB-N levels at time 24-36 hours, for each of the three portions of whiting examined. A visual colour change from yellow to purple coincided with the spectral shifts measured.

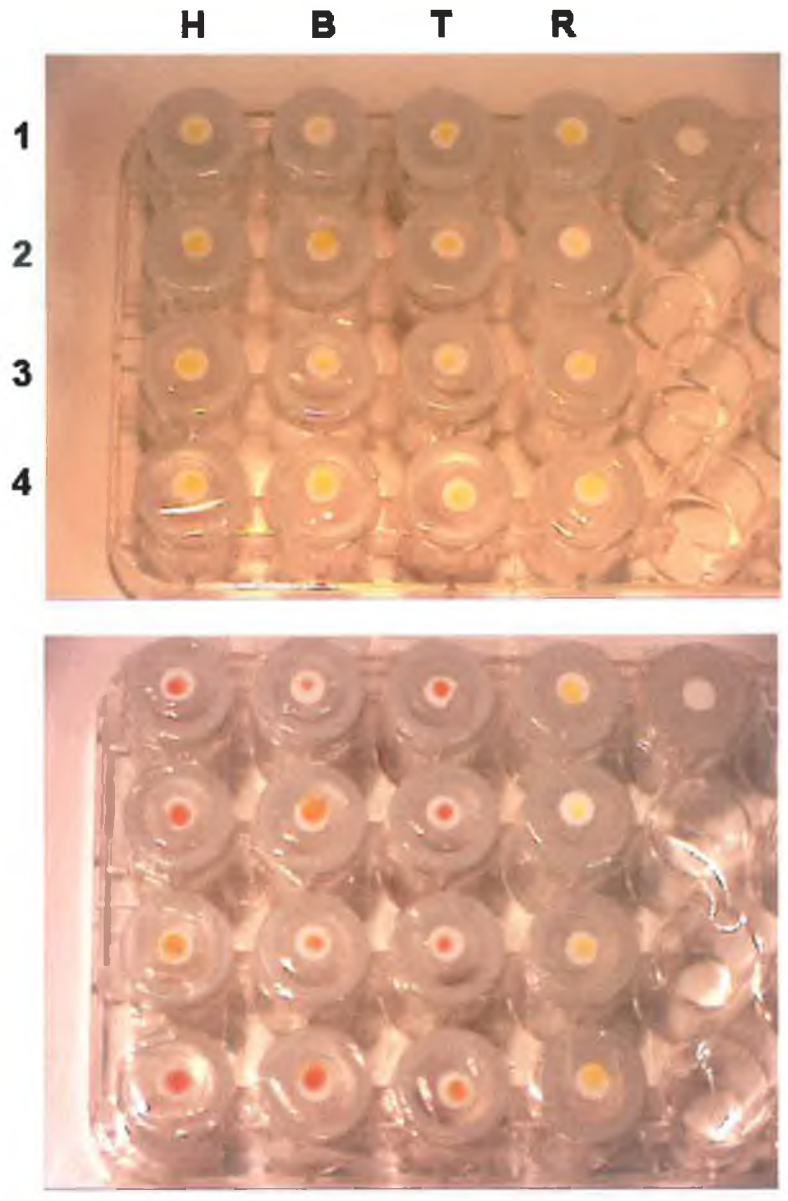

Figure 3.10: Photos of plate at time zero (top) and time 54 hours. The first three columns are replicates of head (H), body (B) and tail (T) portions. The last column is a set of reference sensors (R), i.e. no fish samples included.

There was a discernable smell of amines during the experimental timeframe. Examining Figure 3.10, it is clear that only some sensors responded during the experimental timeframe. The sticky tape seal that was used was not strong enough to prevent the amines escaping into the surrounding environment. As the concentration of amines released into the headspace increases, the pressure put on the seal also increases, causing it in some cases to rupture. This can be seen clearly for body

samples B_1-B_4. The sensors monitoring two of the samples, B_1 and B_4 gave a strong colour change at the end of the experimental timeframe, whereas the sensors monitoring samples B_2 and B_3 ruptured at some stage, due to the gradual increase in pressure against the seal. This can be more closely seen in Figure 3.12, which shows the changing levels of amines over the 54 hour timeframe for the body portions of whiting.

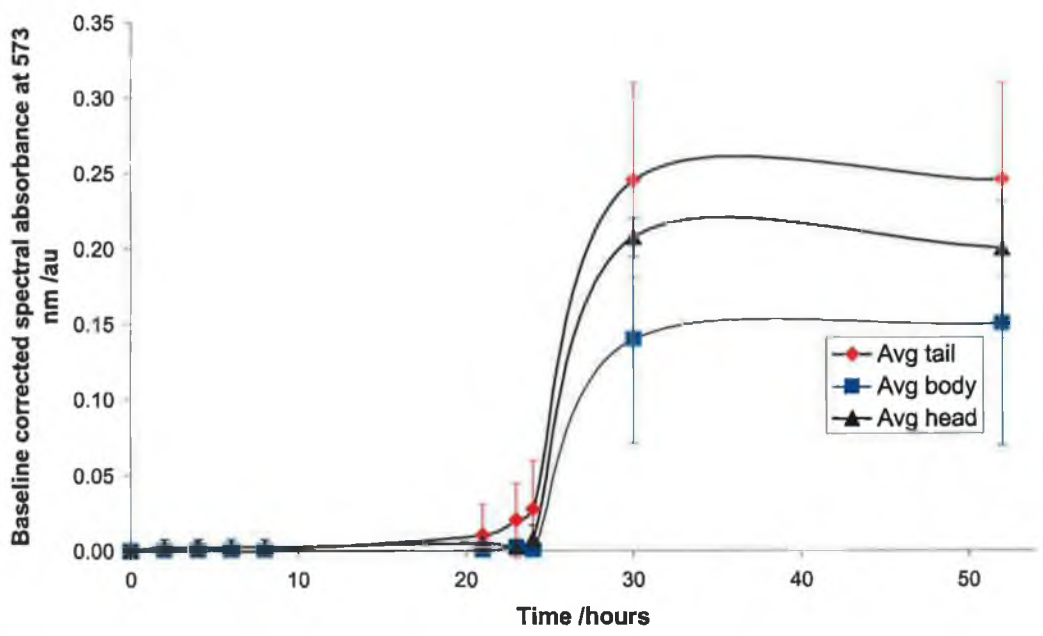

Figure 3.11: The response of the sensors to three portions of whiting. The sensor response remains unchanged from time 0-24 hours, whereby the response increases at time 24-36 hours, due to an increase in the TVB-N levels released from the spoiling fish. The lines are drawn for visual aid only and the error bars are the standard deviation between readings, where n=4.

The response of the sensors monitoring the body tissue portions of whiting clearly shows the abnormal responses seen (Figure 3.12). However, a general dynamic trend of increasing sensor response is seen over the experimental timeframe.

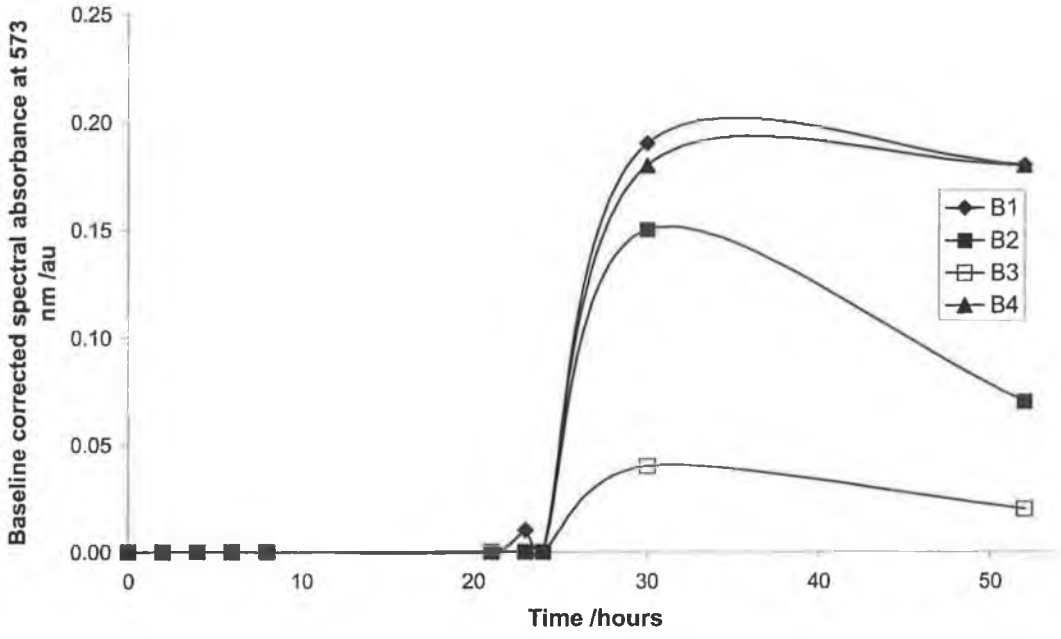

Figure 3.12: The response of the sensors to the 4 body tissue portions of whiting. The rising and falling trends support the case that the amines are leaking into the surrounding environment.

In summary, it is clear that the sensor caps were not gastight, and as such, the variation between replicate measurements is too large to be acceptable. On a more positive note, the majority of the sensors are clearly changing colour from yellow to purple during the spoilage experiments, as they are responding to changes in the levels of volatile amines released into the package headspace. More data needs to be collected in order to determine how well the sensors are performing.

3.3.3 Sensors monitoring TVB-N of orange roughy (whole) and black scabbard

A similar colour change was seen for the sensors in these experiments as those described in the previous section. At time 30-45 hours, there is a clear increase in TVB-N levels of orange roughy, for each catch examined (Figure 3.13). Similarly, the TVB-N levels of black scabbard increase at approximately the same time interval (Figure 3.14). The same general trend is seen for each sample examined; the sensor

response remains unchanged for ca. 30 hours, until the sensor begins to respond to the output of TVB-N of the fish samples, where the sensors form a plateau at ca. 45 hours.

However, there was still a smell of amines during the experimental timeframe, which clearly indicates that the sensor caps needed some modifications in order to reduce the error introduced by this, as this has implications on the results obtained. Almost every sensor seal was ruptured by the increasing amounts of amines released into the confined headspace during the experimental timeframe. The sensor response behaved erratically, and results are only shown for a small number of sensors. Furthermore, the sensor response at the end of the experimental timeframe is greatly diminished, with values of ca. 0.01-0.04 au. The responses of those sensors to samples that leaked amines into the surrounding environment are not shown. The issue of leaking amines clearly needs to be addressed, and is seen additionally in the large and unacceptable variations between readings. A trend identified shows the changing dynamics of the sensor response to orange roughy (whole) samples (Figure 3.13) and black scabbard samples (Figure 3.14) during the experimental timeframe.

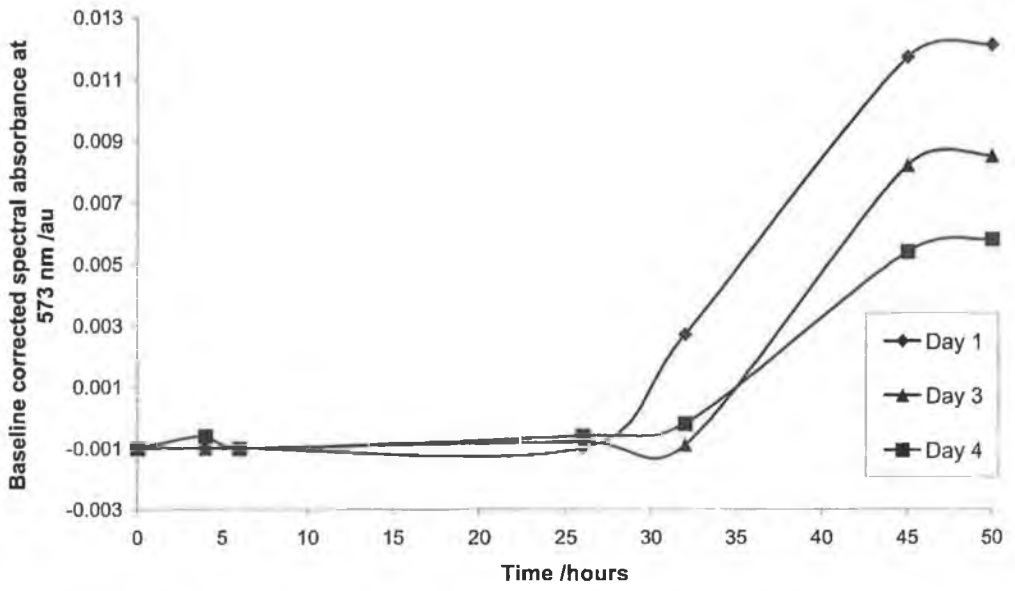

Figure 3.13: The response of the sensors to three different samples of orange roughy. The sensor response remains unchanged from time ca. 0-30 hours, where the sensor response increases at time ca. 30 hours, due to an increase in the TVB-N levels released by the fish. The lines are drawn for visual aid only.

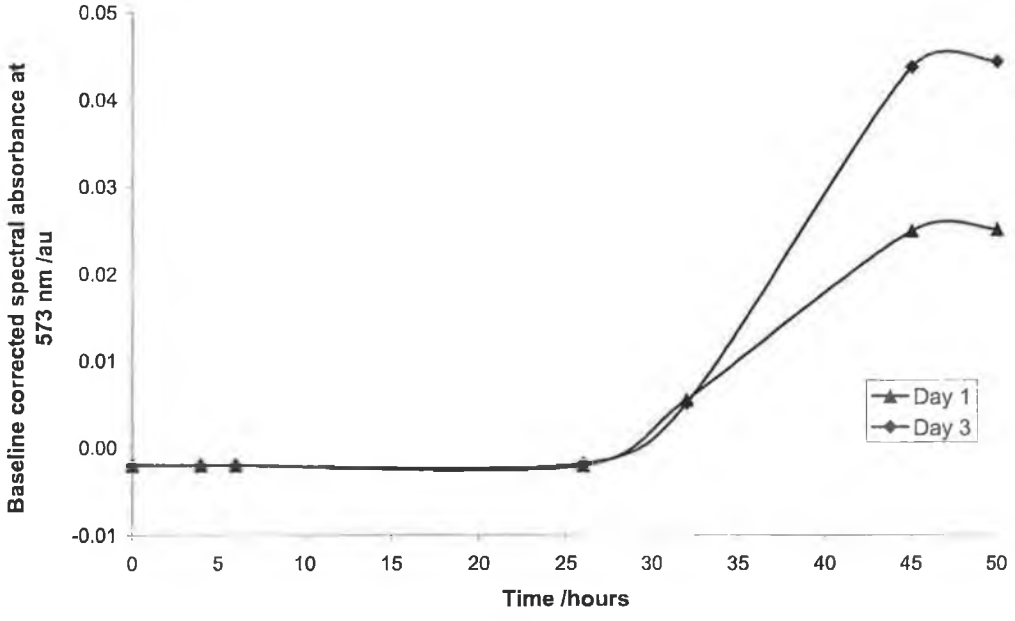

Figure 3.14: A very similar response to orange roughy is seen for black scabbard. The sensor response for the two samples tested increases at time ca. 30-45 hours, due to an increase in TVB-N levels after an unchanging phase. Results from the third sample are not shown since the sensor did not respond at all. The lines are drawn for visual aid only.

Orange roughy samples kept on ice took approximately 160-200 hours to achieve a similar level of TVB-N release (Figure 3.15). The responses of those sensors to samples that leaked amines into the surrounding environment are not shown. Storage at a lower temperature would imply that it takes longer for the spoilage organisms to reach similar levels of growth. Hence, it takes longer for similar levels of TVB-N to be released into the same size headspace.

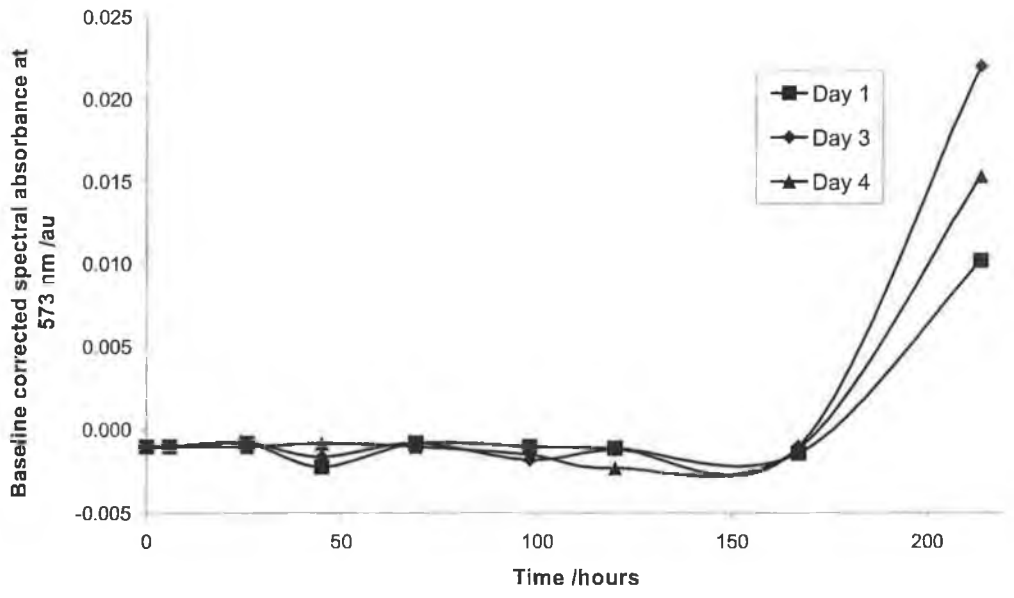

Figure 3.15: Orange roughy samples that were kept on ice show no response from time 0-160 hours (6.67 days). A definite change in the sensor response is seen at time ca. 160-200 hours, as the TVB-N levels are increasing. The lines are drawn for visual aid only; these are the only sensors that responded to orange roughy at 4 °C.

There are clearly not enough data points collected during the experimental timeframe, particularly at the time of spoilage. When the sensor begins to respond, it is essential that the maximum number of data points be collected in this region. The key point, however, is that for all 3 fish species and 2 storage regimes tested, the sensors respond to the changing levels of TVB-N released into the sample headspace. In order to further study the sensor response over time, two important points were addressed:

- The experimental setup was modified, to reduce the possibility of amines escaping into the surrounding environment. This allows more reliable data to be collected.
- More data points over the experimental timeframe were collected. This facilitated a better sigmoidal fit to the data and is shown in subsequent sections.

This new methodology was applied to two fish species, *viz.* cod and orange roughy (fillets).

3.3.4 Sensors monitoring TVB-N of cod and orange roughy (fillets)

By the end of the study period (48 hours), a clear sensor colour change from yellow to purple was seen for each sample tested (Figure 3.16). The wells of each plate have been labelled to show the position of samples. Samples labelled "C" are cod samples, and samples labelled "OR" are orange roughy samples. The bottom row samples, labelled "B" for blank, are empty wells that have no fish samples. Using these as reference sensors for comparison, a clear colour change can be seen over the 48 hour time period. There was no smell of amines during the entire experimental timeframe, which suggests that the modified experimental setup has corrected this important issue.

Spectra were collected at regular intervals, except for the overnight period. An overlay of spectra over the experimental timeframe obtained from a typical orange roughy sample, $OR_{1,4}$ are shown in Figure 3.17. The spectral features shown are broad, and are typical of the spectra collected. A clear rise in the peak height at 573 nm is shown, and the wavelength of this absorption maximum does not shift with increasing time, i.e. exposure to increasing levels of TVB-N released by the gradually spoiling fish samples.

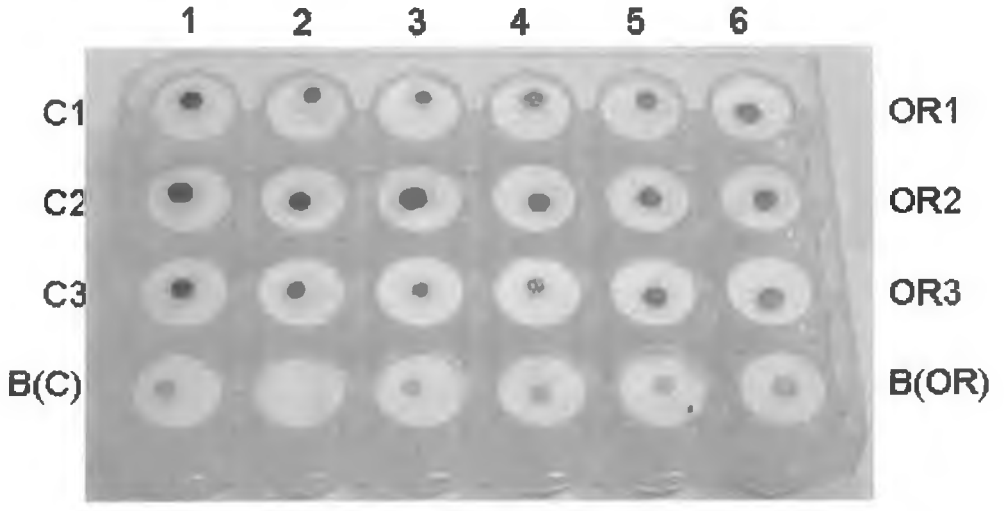

Figure 3.16: A clear sensor colour change can be seen over the 48 hour time period for each of the samples tested.

From Figure 3.16, it is seen that the sensors monitoring the cod samples are a darker colour after the experimental timeframe than the orange roughy samples, which indicates that they have released more TVB-N into the headspace than the orange roughy samples. The bottom row is a row of blank sensors, i.e. sensors that are not exposed to any fish sample. They can be used as a visual comparison to show the degree of colour change of a sensor during the experimental timeframe.

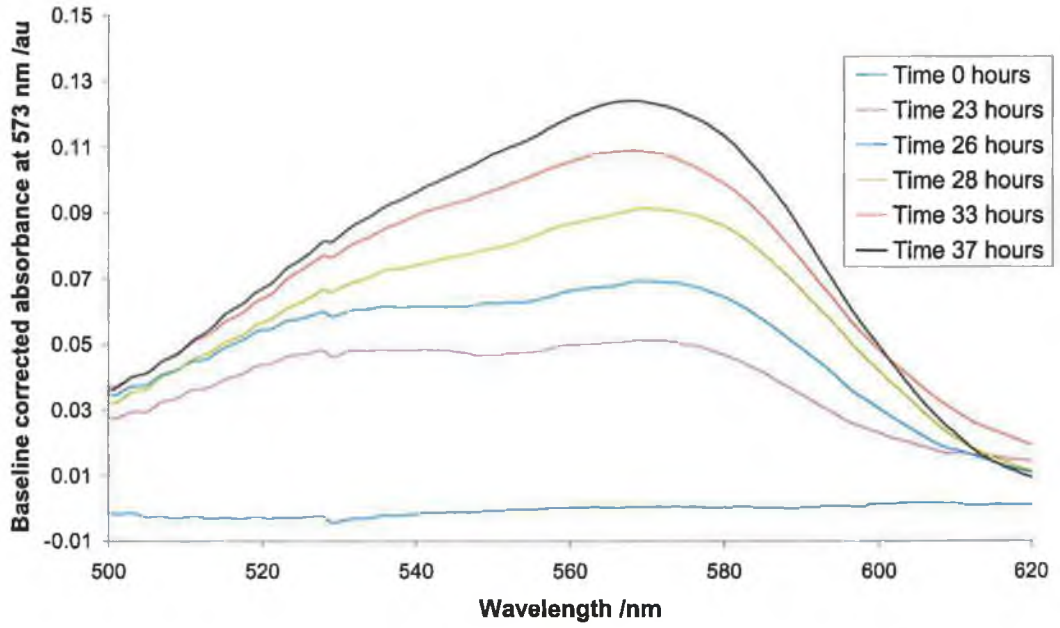

Figure 3.17: Typical absorbance spectra obtained in reflectance mode from a typical orange roughy sample (OR 1,4) from time 0-37 hours. Only some of the representative spectra are shown, for clarity. The height of the deprotonation peak (λ_{max} = 573 nm) steadily rises from approximately 23 hours.

3.3.4.1 Subtraction of reference spectra

A study was initiated to determine if reference spectral data needed to be subtracted from the sensor data obtained. There were 5 reference sensors that had no fish sample present (Figure 3.16). The average reference spectrum of all 5 reference sensors is shown in Figure 3.18. The average RSD at 451 nm (λ_{max} of the acid form) was approximately 3 %.

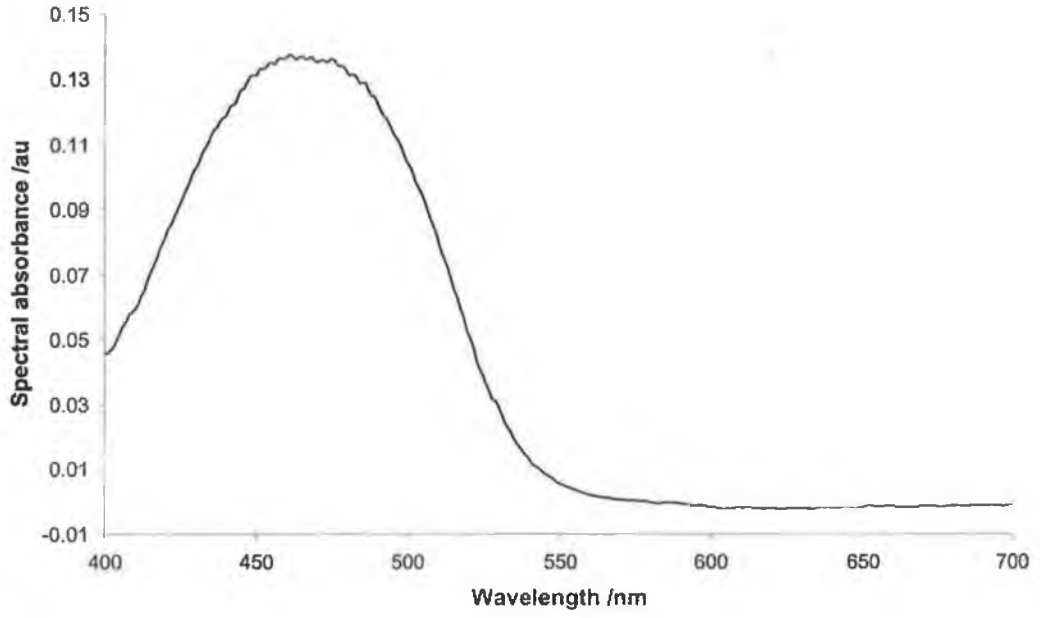

Figure 3.18: Average spectral absorbance from 5 reference sensors.

The sensor response to a typical cod sample, $C_{1,1}$, is shown in Figure 3.19. The characteristics of the sensor response are discussed in more detail in later sections.

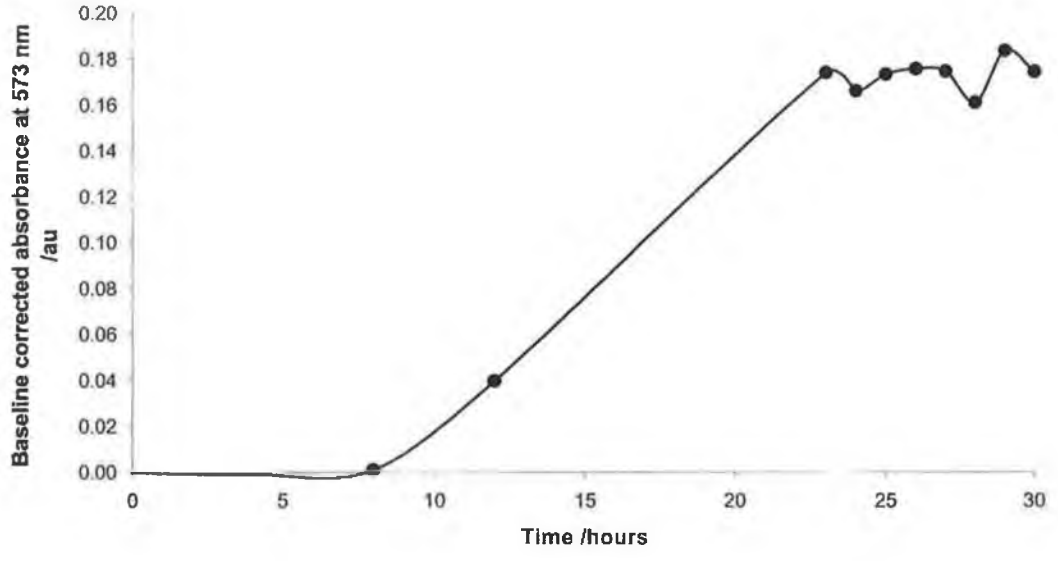

Figure 3.19: Sensor response to a typical cod sample, $C_{1,1}$. The line is drawn for visual aid only.

The average reference spectrum (Figure 3.18) was then subtracted on a wavelength-by-wavelength basis from the sensor response to cod sample $C_{1,1}$, and is shown in Figure 3.20.

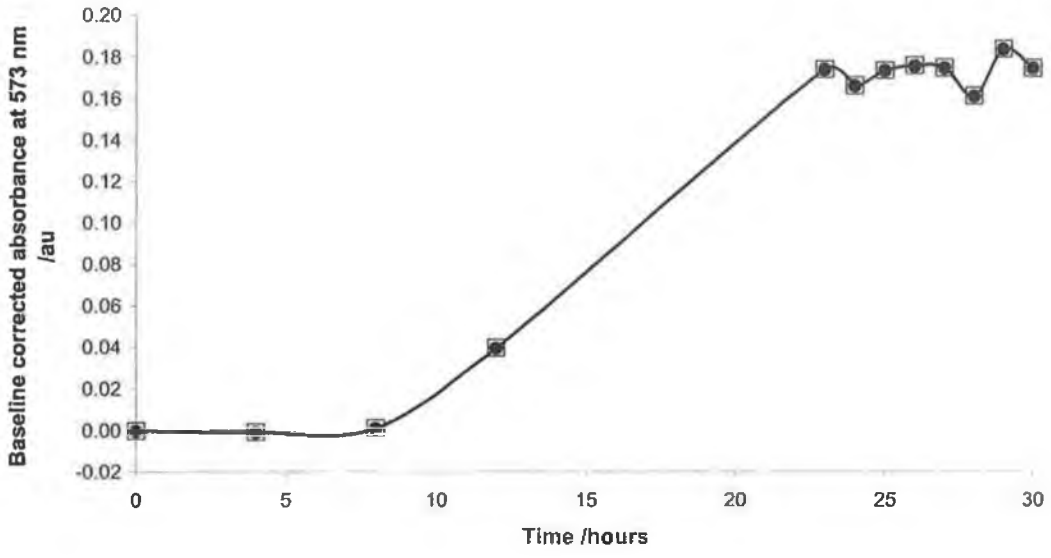

Figure 3.20: Subtraction of the reference spectra yields the same plot (o) as the unaltered spectra (?). The lines are drawn for visual aid only.

It is clear from this that subtraction of the reference spectra from the collected spectra is not required. The two sets of data (Figure 3.20) overlay exactly, indicating that the sensor response at 451 nm does not affect the sensor response at λ_{max}. Hence, there was no subtraction of reference spectra at any stage from the spectra collected using the imaging spectrograph.

3.3.4.2 Results from cod samples

The levels of TVB-N of a total of nine cod samples were monitored over a 30-hour time period. Figure 3.21, Figure 3.22 and Figure 3.23 show the absorbance vs time plots generated for the sensors monitoring the cod samples. From this experiment using a total of nine samples from three fish, there is evidence that from approximately 8-12 hours, a measurable amount of TVB-N was released. At 23 hours, there is a very large increase in the sensor response that suggests a significant increase in the TVB-N levels released by the spoiling fish. There are further increases in the sensor response during the next five hours, whereby the sensors reach a plateau from 28 hours.

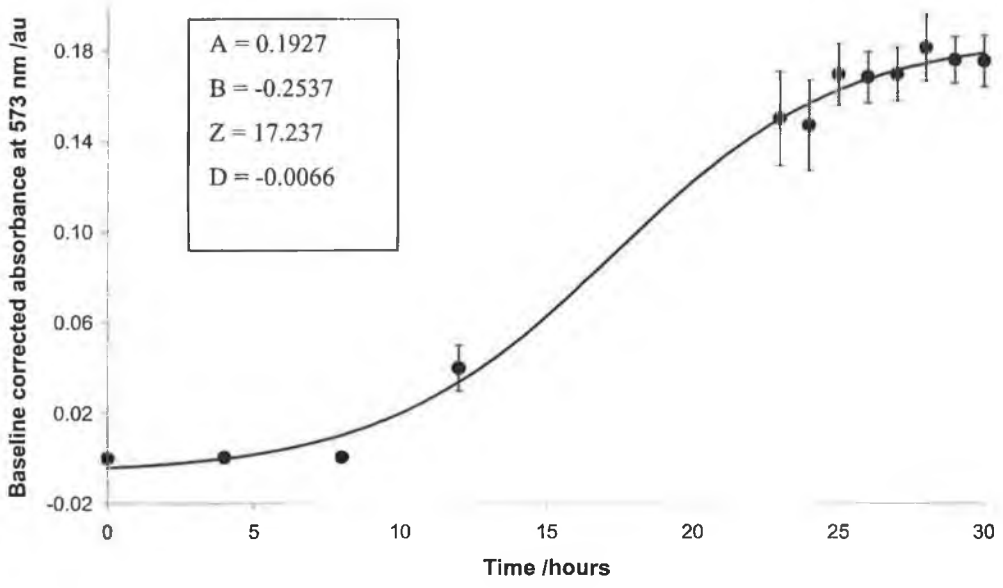

Figure 3.21: Absorbance vs time plot of the sensors monitoring the TVB-N levels of cod samples $C_{1,1}$, $C_{1,2}$ and $C_{1,3}$ (Figure 3.16). The error bars are ± standard deviation, where n=3. The sum of squared residuals for the best-fit curve is 0.0004. The best-fit parameters returned by Solver are given.

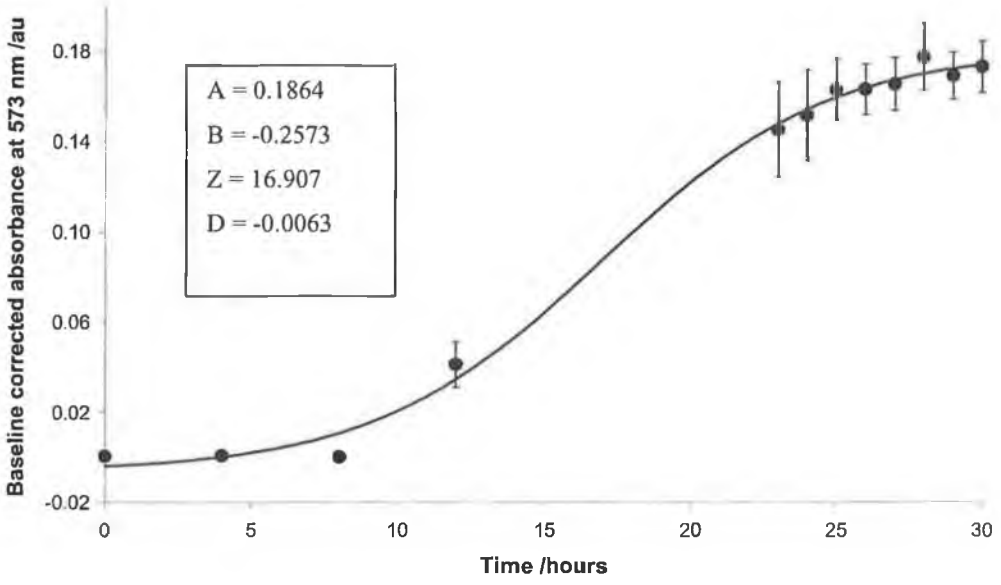

Figure 3.22: Absorbance vs time plot of the sensors monitoring the TVB-N levels of cod samples $C_{2,1}$, $C_{2,2}$ and $C_{2,3}$ (Figure 3.16). The error bars are ± standard deviation, where n=3. The sum of squared residuals for the best-fit curve is 0.0003. The best-fit parameters returned by Solver are given.

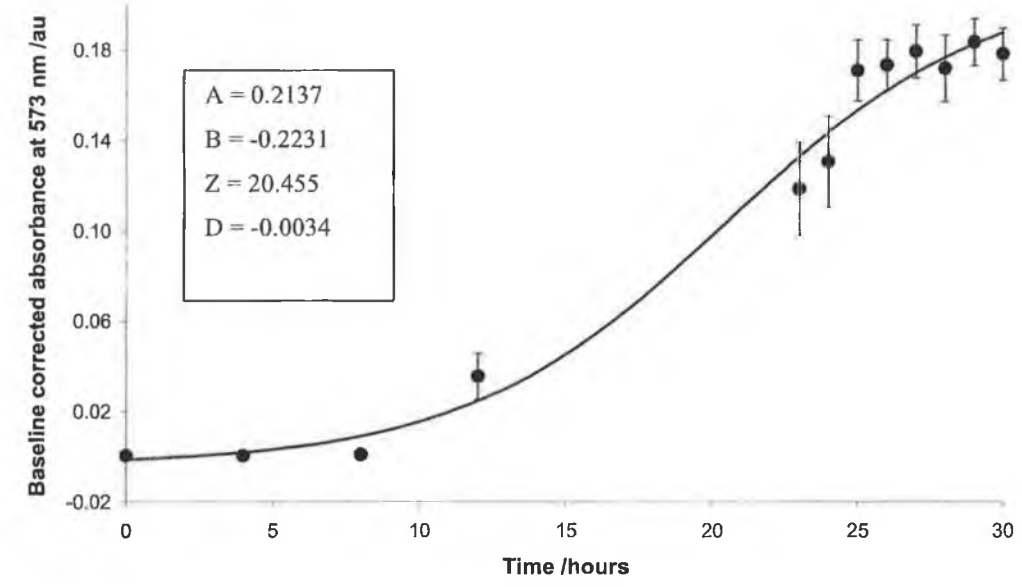

Figure 3.23: Absorbance vs time plot of the sensors monitoring the TVB-N levels of cod samples $C_{3,1}$, $C_{3,2}$ and $C_{3,3}$ (Figure 3.16). The error bars are ± standard deviation, where n=3. The sum of squared residuals for the best-fit curve is 0.0012. The best-fit parameters returned by Solver are given.

These figures show that the sensor response increases after an incubation period of approximately 8-12 hours, to form a plateau at approximately 28-30 hours. Sigmoidal response curves (solid line) were fitted to the data, using the Solver function in Microsoft Excel. The best-fit parameters are given on each chart and information was derived from these values. This is discussed in detail in Section 3.3.4.4.

3.3.4.3 Results from orange roughy samples

Similarly, the levels of TVB-N released from a total of nine orange roughy samples were monitored over a 48-hour time period. Figure 3.24, Figure 3.25 and Figure 3.26 show the absorbance vs time plots obtained for each sample tested, which illustrate that the sensors began to respond from approximately 15-20 hours. The orange roughy samples required a longer incubation period than the cod samples before a significant increase in the sensor response is seen. This allows better following of the critical time of spoilage after the overnight period, making more data available at the time where the sensor response was changing the most. The sensor response reached a steady value at approximately 40 hours.

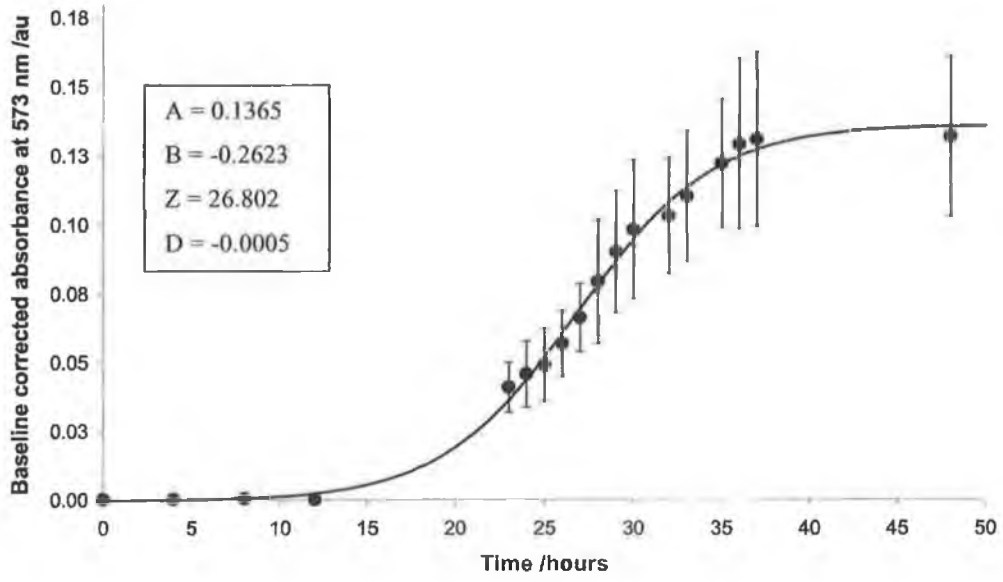

Figure 3.24: Absorbance vs time plot of the sensors monitoring the TVB-N levels of orange roughy samples $OR_{1,4}$, $OR_{1,5}$ and $OR_{1,6}$ (Figure 3.16). The error bars are ± standard deviation, where n=3. The sum of squared residuals for the best-fit curve is 0.0002. The best-fit parameters returned by Solver are given.

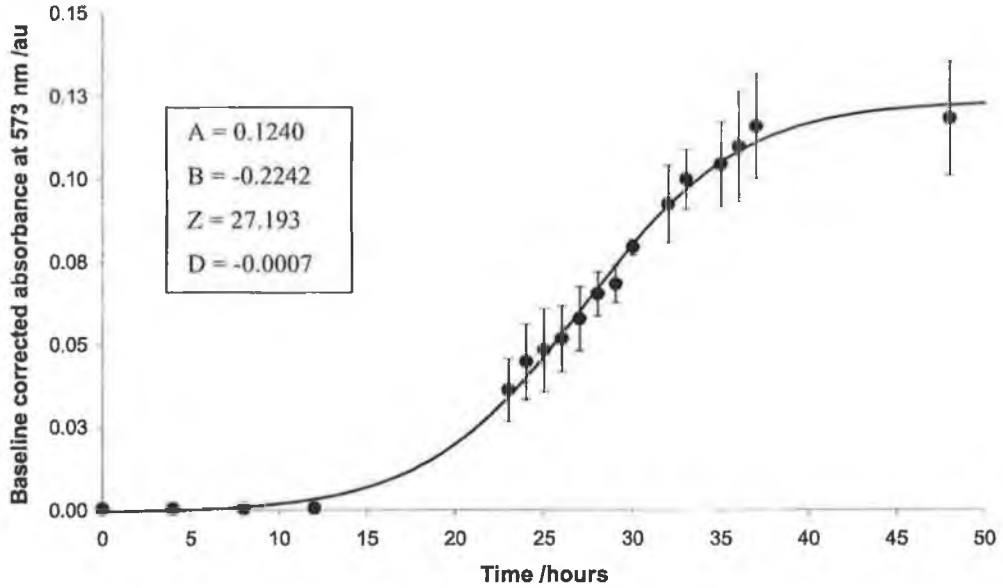

Figure 3.25: Absorbance vs time plot of the sensors monitoring the TVB-N levels of orange roughy samples $OR_{2,4}$, $OR_{2,5}$ and $OR_{2,6}$ (Figure 3.16). The error bars are ± standard deviation, where n=3. The sum of squared residuals for the best-fit curve is 0.0001. The best-fit parameters returned by Solver are given.

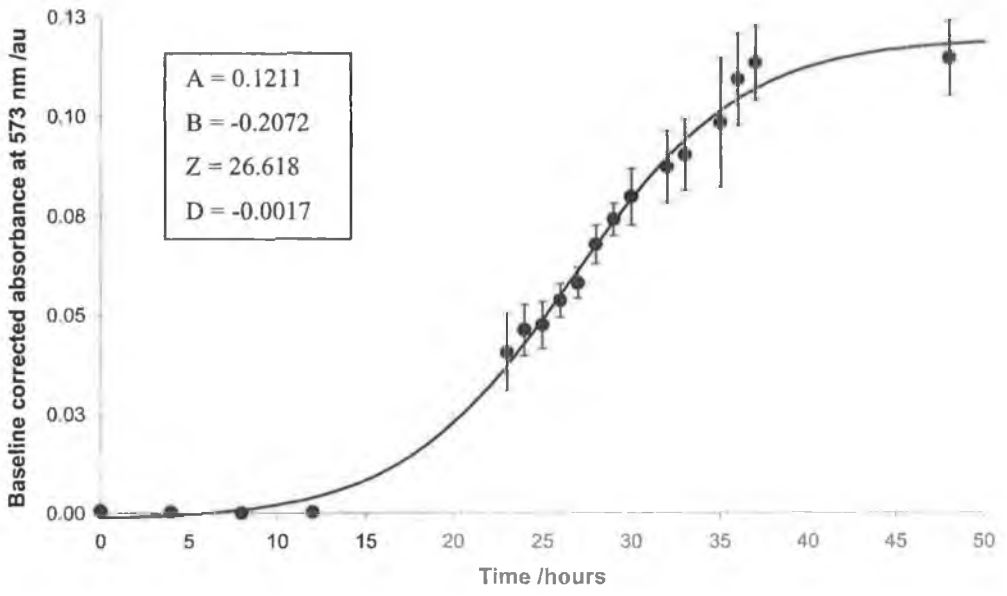

Figure 3.26: Absorbance vs time plot of the sensors monitoring the TVB-N levels of orange roughy samples $OR_{3,4}$, $OR_{3,5}$ and $OR_{3,6}$ (Figure 3.16). The error bars are ± standard deviation, where n=3. The sum of squared residuals for the best-fit curve is 0.0002. The best-fit parameters returned by Solver are given.

These figures show that the sensor response increases after an incubation period of approximately 15-20 hours, to form a plateau at approximately 40 hours. The best-fit parameters are again shown on each curve and are discussed in the following section.

3.3.4.4 History of samples

The age and condition of the samples tested were not fully known. It was believed that the orange roughy samples were approximately 1-2 days old when purchased, and that the cod samples were approximately 2-3 days old. Each type of sample may not have come from the same catch; if they did, they may not have been caught at the same time. The samples would not have been stored away from the rest of the catch, which increases the possibility of bacteria contamination. The samples were obtained filleted, thus it is highly likely that bacterial cross-contamination was introduced at this step. The key point is that there are inherent differences between samples, and these differences would cause different amounts of TVB-N to be released into the

sample headspace during gradual spoilage of the samples. Experimental error such as the mass of a sample taken for analysis is likely to contribute much less than the error from these differences between samples.

As can be seen in each of the absorbance vs time plots for orange roughy (fillets) and cod, the variations were small at the point where the sensors were only beginning to respond. At the region where the sensor response has increased significantly, the variation between sensors also increases (approximately 15 % RSD). Some useful information can be derived from the best-fit sigmoid parameters. For the cod samples, the value of "A" (the maximum absorbance that the sensor reaches) is 0.1976 au ± 0.01432 au. The value of "Z" (the time, in hours, taken for the sensor to reach the peak of its inflection on the rise) is related to the age and history of a sample. A high Z value indicates that a sample takes longer to reach the mid-point of inflection on the rise of curve, and is thus a sample that spoils more slowly than a sample with a low Z value. This indicates that the third cod fillet (Figure 3.23) is likely a fresher sample than the first (Figure 3.21) and second (Figure 3.22) cod samples, as it takes ca. 3 hours longer to reach the mid-point of the best-fit curve.

Information about the orange roughy samples was also derived. The value of A is lower than for cod, at 0.1272 au ± 0.00820 au. This suggests that the orange roughy samples may release less amines than cod, and hence the sensors reach a plateau at a lower absorbance value. The Z value is ca. 27 hours for all three fillets tested. The excellent best-fit line, which is seen in the low sum of squared residual values, strongly suggests that the 3 samples have very similar ages and histories. They were likely to be fresher than the cod samples tested, as the sensor response takes ca. 8-10 hours to reach the same point of inflection on the rise of each curve per fillet tested. This demonstrates that the sensors are able to return information about the condition of a sample. A fresher sample would, in principle, take a longer period of time to cause a significant sensor response. The time when this response happens is crucial to developing a working sensor.

3.4 Conclusion

The sensors developed in Chapter 2 were used successfully to monitor the changes in headspace TVB-N levels released from gradually spoiling fish samples. The sensors responded well, changing colour from yellow to purple during a spoilage experiment. The sensors were shown to respond to samples of whiting, orange roughy, black scabbard and cod, each being samples that were treated differently. The imaging spectrograph (PARISS) system, in combination with the simple experimental setup devised, performed very well for monitoring spectral changes in the sensor dots due to the release of amines from many samples in parallel. It was clear that the developed packaging needed to be gas-tight, to inhibit the leakage of amines into the surrounding environment.

The data obtained from the PARISS system as a function of time during a spoilage experiment is modelled on a best-fit sigmoid function. In order to obtain the best-fit function, it is essential to collect and record many data points during the spoilage timeframe. The best-fit parameters of the sigmoid function give inherent information about the quality of a sample. However, there is no data thus far that can relate the sensor response to the level of spoilage of a sample. For example, the sensor response at the critical threshold of spoilage is unknown. In order for this link to be established, it is essential that the changes in microbial populations of a spoiling sample be determined as a function of time. There should be a clear time-correlation between the data from the sensor and the microbial data, and this correlation would allow the microbial populations of a sample to be inferred from a sensor reading. This would also determine if the sensor is responding at the critical threshold of spoilage, and if so, establish the sensor response at this threshold.

The data in this chapter has a clear significance and implication for tracking food quality in individual packages. There is enormous development potential, but this requires all stakeholders and particularly consumers to be educated in how to interpret the information. A simple analysis system, such as the handheld colour scanner device developed in Chapter 5, has a clear advantage in this area.

4 Correlation of Chemical Sensor Response with Microbial Populations and Headspace Volatiles during Fish Spoilage

4.1 *Introduction*

This chapter presents results that study the time-correlations between the response of the cresol red based chemical sensors developed to monitor headspace spoilage volatiles of fish samples (Chapter 3), the headspace TVB-N concentrations and microbial populations during spoilage of fish. The sensors were used to monitor many samples in parallel, mostly from the cod species; all samples analysed had known catch histories. Headspace TVB-N levels were quantified by a titration method. A parallel study of the microbial populations was performed, for both the total viable counts (TVCs) and the pseudomonas species, one of the specific spoilage organisms (SSOs) in seafood. These results present, for the first time, a working pH-indicator based chemical sensor that can be used to infer microbial populations and headspace TVB-N levels of fish, and hence give real-time information about the onset of spoilage of seafood samples. Results from this chapter were recently accepted for publication in Sensors and Actuators B (chem.) [98].

4.2 Experimental

4.2.1 Materials and equipment

All chemicals and reagents used for sensor fabrication were as previously described (Section 2.4.2). Boric acid and methyl red were obtained from Sigma-Aldrich (Dublin, Ireland). Reagent grade hydrochloric acid was obtained from BDH (Dublin, Ireland). All equipment used for sensor spectral analysis was as previously described (Section 2.2.1). 10 ml Hamilton gastight syringe was supplied by Carl Stuart (Dublin, Ireland).

4.2.2 History of fish samples

2 whole cod (Figure 4.1, herein called "cod (a)") and 2 whole plaice (Figure 4.2) were caught approximately 20 miles northeast of Howth, Dublin, Ireland and were stored on ice on board the trawler, in separate storage from the rest of the catch. All 4 samples were caught during the same excursion to sea. The time of death of each catch was known and the samples were stored in a laboratory freezer at -20 ^{o}C, within three hours of death. When required, the samples were thawed slowly at 4 ^{o}C, before rising to room temperature of 19-21 ^{o}C. The fish were washed, bled and gutted, and aseptic techniques were used throughout to avoid any bacterial cross-contamination between samples (as described in Section 3.2.4).

Five whole cod (herein called "cod (b)") were caught approximately 15 miles northeast of Howth, Dublin, Ireland and were stored on ice on board the trawler, in separate storage from the rest of the catch. They were caught during three different excursions at sea. The time of death of each catch was known and the samples were stored identically to the cod (a) and plaice samples. When required, the fish were washed, bled and gutted, using aseptic techniques throughout. The cod (a), cod (b)

and plaice samples represent the freshest and most reproducible samples it is possible to obtain.

Figure 4.1: The cod (a) samples caught in the Irish Sea had known catch profiles. They were washed, bled and gutted within 1 hour of purchase and aseptic techniques were used throughout. The point of incision of the blade for gutting is shown.

Figure 4.2: The plaice samples that were caught in the Irish Sea also had known catch profiles. The gutting of flat fish like plaice requires the blade to be inserted carefully at the side of the fish, as shown.

4.2.3 Experimental setup

Three sub-samples were retained from the central portion of each cod (a) and plaice sample. The levels of spoilage volatiles released into the sample headspace as a function of time for each fish were monitored by the sensor dots as described in Section 3.2.4. All samples were stored whole at room temperature throughout, i.e. 19-21 °C. 25 g samples were removed from the central region of each fish in small sterile bags for TVC analysis, at time zero and at 74 hours. These times were selected since they are before and after spoilage of the samples.

Three sub-samples were retained from the central portion of each cod (b) for analysis. There were hence a total of 15 samples analysed from 5 fish. 4 of the cod samples were used for microbiological analysis and 1 sample was used for headspace TVB-N determination. 2 x 25 g samples were removed from the central region of each fish in small sterile bags for TVC and SSO analysis, at many points during the experimental timeframe, from time zero to 74 hours. All samples were stored at room temperature throughout. Figure 4.3 shows an outline of the experimental protocol used for cod (b).

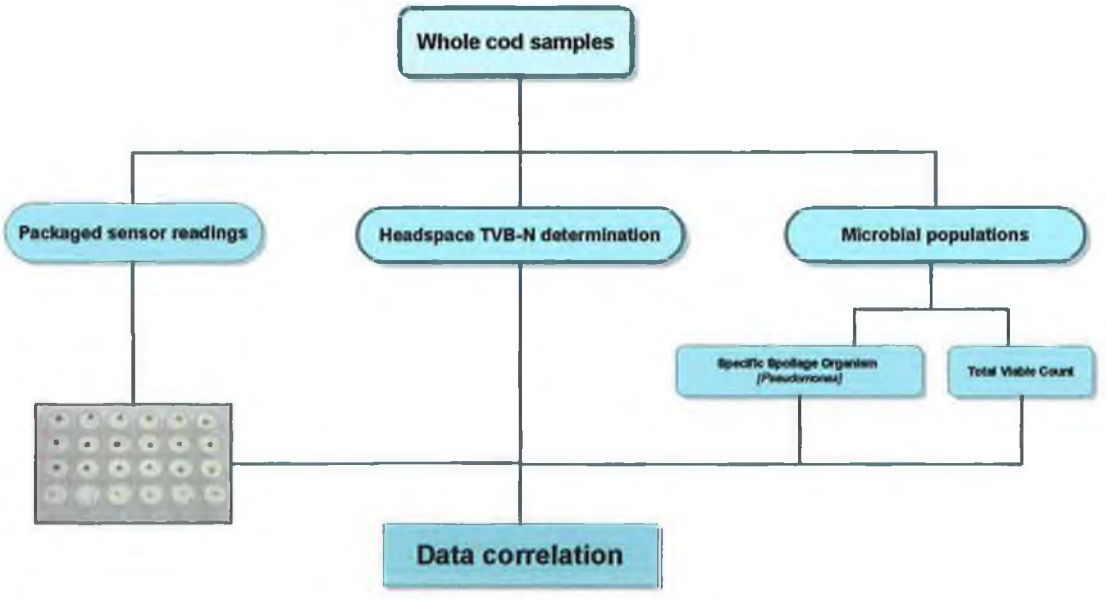

Figure 4.3: Flow chart showing experimental protocol used.

4.2.4 Determination of headspace TVB-N levels

The standard EU method for determination of TVB-N levels of tissue samples [65] was adapted to allow the quantification of *headspace* TVB-N levels at defined times. This method details that the volatile bases be extracted from a 100 g tissue sample by a 0.6 M perchloric acid solution, and then steam distilled. The volatiles are then collected by an absorbing acid receiver, 0.3 M boric acid. The volatiles neutralise some of the acidity of the boric acid, and this reduction in acidity is determined by titration against standardised 0.05 M HCl, using methyl red as visual indicator. The HCl is standardised with 0.1 M sodium carbonate. The titrant value allows an overall concentration of TVB-N, in molarity, per 100 g of fish sample tested to be calculated, equivalent to the concentration of reacted acid. To adapt this methodology, it was assumed that significantly less amines are released into the sample headspace than are present in tissue. Hence, the amount of fish sample used was increased, and the concentration of standardised HCl used was decreased, in order to be better able to detect the lower concentration of amines in the sample headspace.

Approximately 260 g of one of the cod (b) samples, taken from 3 sampling points within the sample and mixed together by grinding, was placed in a 2 litre single necked round-bottom flask, sealed with a gastight rubber septum. To ensure constant pressure in the sample headspace, a small balloon filled with nitrogen was fitted through the septum of the round-bottom flask via a syringe needle. At required times, 10 ml of sample headspace was removed using a gastight syringe and injected through a rubber septum into a 250 ml flask containing 20 ml of 0.3 M boric acid. The headspace samples were extracted for analysis in duplicate. The solutions were left stirring overnight to ensure full reaction of injected TVB-N and the receiver solution.

Each of the receiver solutions were titrated against 0.005 M standardised hydrochloric acid, using methyl red as a visual indicator. The volume of titrant used allowed the determination of the concentration of TVB-N in the sample headspace.

The data was normalised to between 0 and 100 %, by dividing the highest value into each data subset, and multiplying by 100 to convert to a % scale. The data was expressed as the concentration of TVB-N released per ml of sample headspace, per 100 g of fish sample used.

4.2.5 Enumeration of microbial populations

TVC analysis and pseudomonas counts were performed by City Biologic, Dublin City University, Ireland [99]. 2 x 25 g sections were removed from the cod (b) samples at defined points during the experimental timeframe from 0 to 74 hours and were sent for analysis. Pseudomonas counts were determined by a previously reported standardised method [100]. TVC enumeration was performed using standard ISO 4833 techniques at 30 °C.

4.3 Results and discussion

4.3.1 General trends identified

The response of the sensors monitoring the cod (a) and plaice samples fits a sigmoid function over the experimental timeframe, as expected. The best-fit parameters for each of the functions suggest that the samples were caught at similar times. The TVC analysis performed on each of these samples shows that there is a very large increase in microbial numbers during the experimental timeframe. This is the first set of results obtained that shows a relationship between the sensor response and microbial populations.

The response of the sensors monitoring the cod (b) samples was also sigmoidal and illustrates the excellent reproducibility of the sensors and the favourable catch histories. The sensor response of all 15 cod (b) samples was pooled and the RSD for a responding sensor was ca. 3 %. The correlation between the TVC values, the pseudomonas populations (both determined at many points during the experimental timeframe) and the sensor response was investigated. The headspace TVB-N levels were also shown to correlate strongly to the sensor response. This is the first set of results to show that the response of the sensors can be used to infer headspace TVB-N levels and microbial populations, and hence give information about the spoilage of a fish sample.

4.3.2 Sensors monitoring TVB-N of cod (a) and plaice

The sensors began to respond visually at ca. 24 hours, turning from yellow to a pale orange colour, which deepened to a purple colour by the end of the experimental timeframe. Regular spectral measurements were taken by the imaging spectrograph in reflectance mode of the sensors monitoring the cod samples (Figure 4.4) and the plaice samples (Figure 4.5) from time zero to 72 hours.

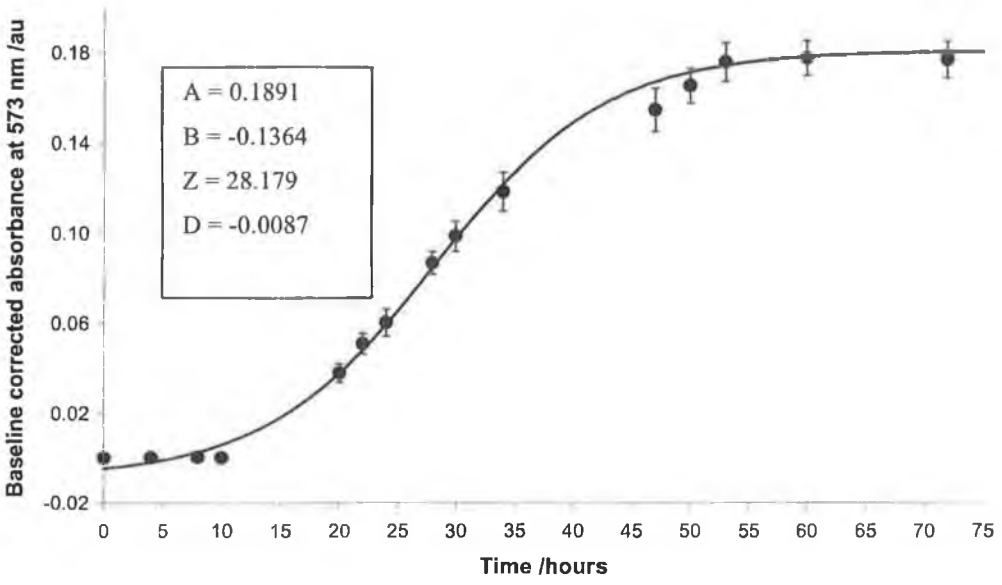

Figure 4.4: Absorbance vs time plot of the sensors monitoring the TVB-N levels of 2 cod samples. 3 sensors monitored the TVB-N levels per fish, and all 6 sensors were pooled together. The error bars are ± standard deviation, where n=6. The sum of squared residuals of the best-fit line was 0.0003. The best-fit parameters returned by Solver are given.

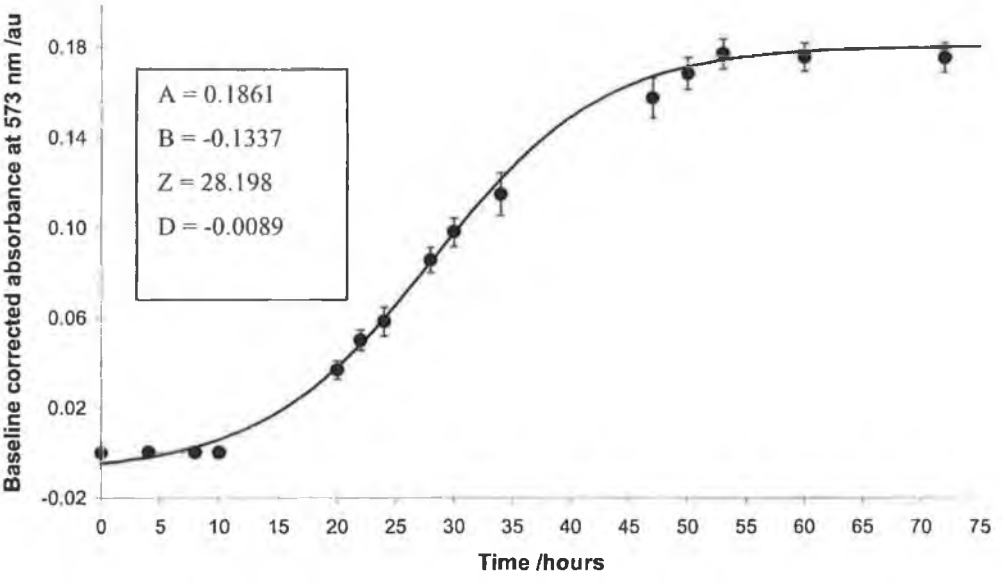

Figure 4.5: Absorbance vs time plot of the sensors monitoring the TVB-N levels of 2 plaice samples. 3 sensors monitored the TVB-N levels per fish, and all 6 sensors were pooled together. The error bars are ± standard deviation, where n=6. The sum of squared residuals of the best-fit line was 0.0002. The best-fit parameters returned by Solver are given.

The response of the sensors to these cod and plaice samples is almost identical, as confirmed by the very similar best-fit parameters returned by Solver for both sets of sigmoid curves. This suggests that both of these species release very similar levels of TVB-N during spoilage, which generates very similar sensor responses. The RSD for a responding sensor for all species tested was ca. 7 %.

4.3.3 Sensors monitoring TVB-N of cod (b)

To illustrate the changes in a fish sample over the experimental timeframe at room temperature, Figure 4.6 shows one of the cod (b) samples after storage for 60 hours. The tissue is very darkened and dried-out, and it emits a pungent, offensive odour.

Figure 4.6: After storage at room temperature for 60 hours, the cod (b) sample shown has become very darkened and dried-out.

The sensors monitoring the TVB-N levels of cod (b) show a similar response during the experimental timeframe to the results shown for those sensors monitoring cod (a) and plaice (Figure 4.7). The 5 pooled cod (b) samples were all caught and stored in very similar conditions. This is illustrated by the average RSD between readings,

which was ca. 3 %. Furthermore, the best-fit parameters are all similar to those previously obtained, as illustrated by the values shown.

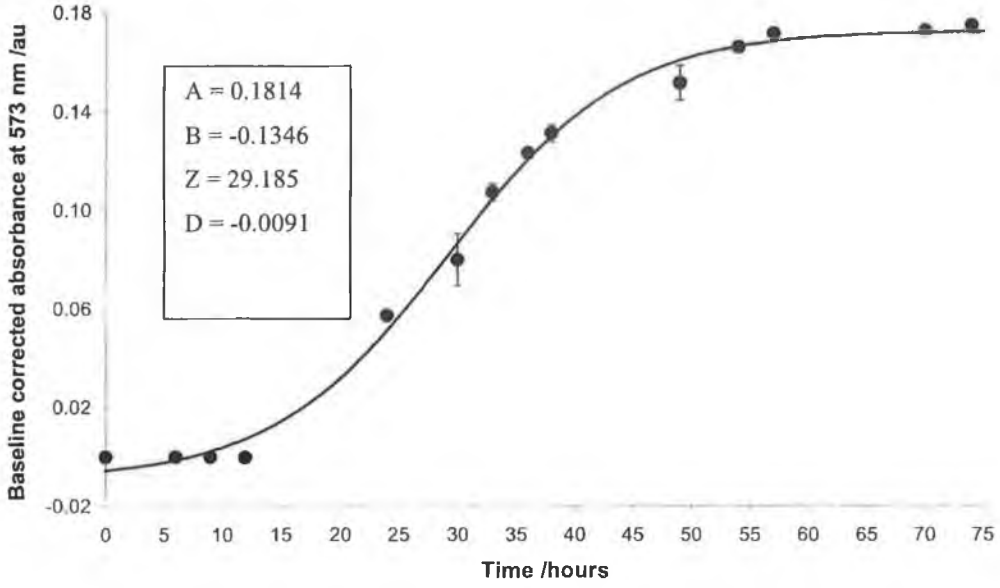

Figure 4.7: Absorbance vs time plot of the sensors monitoring the TVB-N levels of all 5 cod (b) samples. 3 sensors monitored the TVB-N levels per fish, and all 15 sensors were pooled together. The error bars are ± standard deviation, where n=15. The sum of squared residuals of the best-fit line was 0.0003. The best-fit parameters returned by Solver are given.

4.3.3.1 Reproducibility of sensor fabrication and response

There are a number of key points here:

- The 5 cod samples were caught at three different times. Two samples were caught during each of the first two times at sea, and only one sample was used from the latter catch.
- The sensors monitoring these samples were prepared *in different batches*. They were each prepared the same way, but at different times. The reproducibility of sensor fabrication is thus highly satisfactory.

- No two fish samples are the same. However, these samples, although caught at different times, were all caught from the same location, by the same trawler, stored in the same hold, on ice, separate from the rest of the catch. The samples were all treated the same way; hence they are as similar as two samples can be.

The RSD is a highly acceptable value. This is the first time that the reproducibility of the sensors monitoring real samples has been investigated, as it requires samples of this quality to be obtained. The importance of obtaining samples with a well-known and controlled history is paramount in a study such as this one.

4.3.4 Determination of headspace TVB-N levels

Quantification of the amount of amines released into the sample headspace at a particular time allowed a comparison of the sensor response and headspace TVB-N levels. HCl was used to titrate solutions of boric acid that contained injected headspace amines, and the volume of acid used to neutralise the total bases at a given time was determined.

HCl reacts with the collective volatile bases as follows:

$$\text{Base-N} + \text{HCl} \rightarrow \text{Base-N}^{+} + \text{Cl}^{-}$$

The bases are neutralised by the monoprotic acid, and it is assumed that the stoichiometry of the reaction between the acid and bases is 1:1. This is a valid assumption, as TMA, DMA and ammonia (which are the highest proportion of TVB-N) all react 1:1 with HCl.

The standard titration equation [101] was used for calculation of the number of moles of TVB-N equivalent to the number of moles of acid reacted:

$$\frac{M_1V_1}{n_1} = \frac{M_2V_2}{n_2}$$ **Equation 4-1**

where M_1, V_1 and n_1 = molarity, volume and number of moles reacted of species "1" (acid),

and M_2, V_2 and n_2 = molarity, volume and number of moles reacted of species "2" (base).

Since the volatilised bases react 1:1 with the acid titrant, the reaction is simplified:

$$M_1V_1 = M_2V_2$$ **Equation 4-2**

M_1, the concentration of the standardised HCl was calculated as 0.0066 M by titration against 0.01 M sodium carbonate (Na_2CO_3). Hence, the value of M_2 at a given time was calculated (Table 4.1). This is equal to the concentration of TVB-N released per 10 ml sample headspace volume taken, per 260 g of fish. The data were normalised, to give the concentration of TVB-N released per ml sample headspace volume, per 100 g of fish (Figure 4.8).

Time /hours	Volume HCl / ml		Average Volume HCl /ml	Average TVB-N conc. per 10ml sample per 260 g fish /10^{-3} M	Average TVB-N conc. per ml sample per 100 g fish/ 10^{-5} M
	Sample 1	Sample 2			
0	0.10	0.10	0.10 ± 0.000	0.033 ± 0.0000	0.13 ± 0.000
9	0.10	0.10	0.10 ± 0.000	0.033 ± 0.0000	0.13 ± 0.000
23	1.20	0.85	1.03 ± 0.247	0.338 ± 0.0820	1.30 ± 0.314
28	3.05	2.70	2.88 ± 0.247	0.949 ± 0.0820	3.65 ± 0.314
33	4.25	4.40	4.33 ± 0.106	1.427 ± 0.0350	5.49 ± 0.135
36	5.10	5.25	5.18 ± 0.106	1.708 ± 0.0350	6.57 ± 0.135
49	6.75	6.90	6.83 ± 0.106	2.252 ± 0.0350	8.66 ± 0.135
53	7.85	7.55	7.70 ± 0.212	2.541 ± 0.0700	9.77 ± 0.269
59	8.45	8.60	8.53 ± 0.106	2.813 ± 0.0350	10.82 ± 0.135
73	9.50	9.20	9.35 ± 0.212	3.086 ± 0.0700	11.87 ± 0.269

Table 4.1: The data shown was used to determine the TVB-N concentration released into each ml of sample headspace, per 100 g fish sample used for analysis. The data is shown graphically in Figure 4.8.

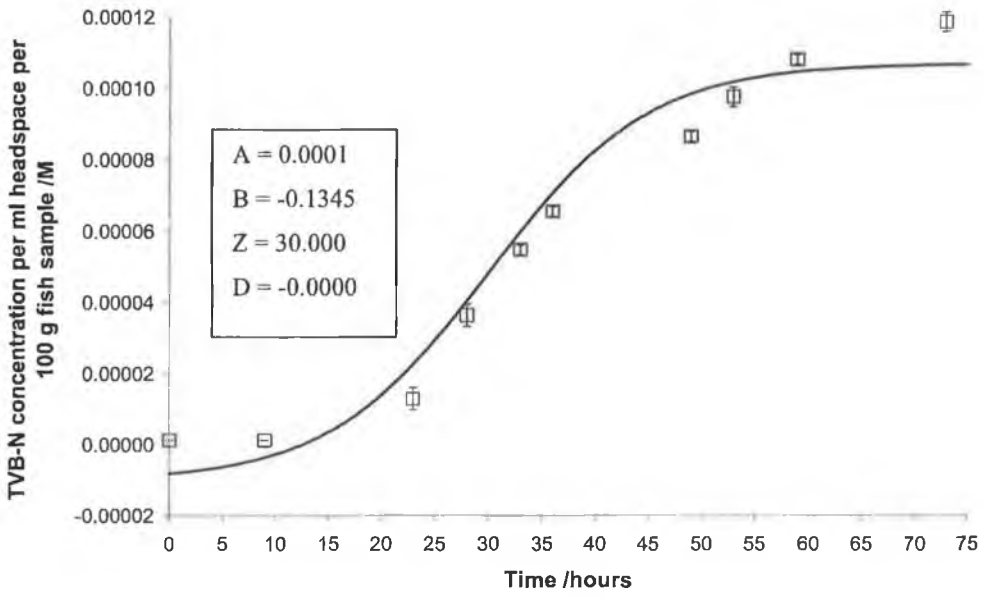

Figure 4.8: Changes in the TVB-N concentration released during spoilage with time. A best-fit sigmoid was modelled to the data. The error bars are ± standard deviation, where n=2. The sum of squared residuals of the best-fit line was 0.0030. The best-fit parameters returned by Solver are given.

The trend seen is similar to the trend identified for the sensor responses monitoring the headspace amine levels of the cod (b) samples with time. There is no significant amine output for ca. 15-20 hours, indicating that the sample has not yet begun to spoil, as TVB-N are not released until spoilage organisms have begun to grow [58]. After this time, there is a clear and measurable increase in levels of TVB-N released into the headspace. This level doesn't form a plateau, indicating that the amine levels keep rising during the experimental timeframe of 74 hours at room temperature. Hence, it may not be strictly correct to model a best-fit sigmoid equation, but nevertheless, it serves to clearly and visually demonstrate the correlation between the datasets.

4.3.4.1 Comparison of TVB-N levels and sensor response

In order to allow a direct comparison between each set of values, the data were normalised to between 0 and 100 %. This produced an overlay plot (Figure 4.9) of the sensor response and the changing TVB-N levels with time.

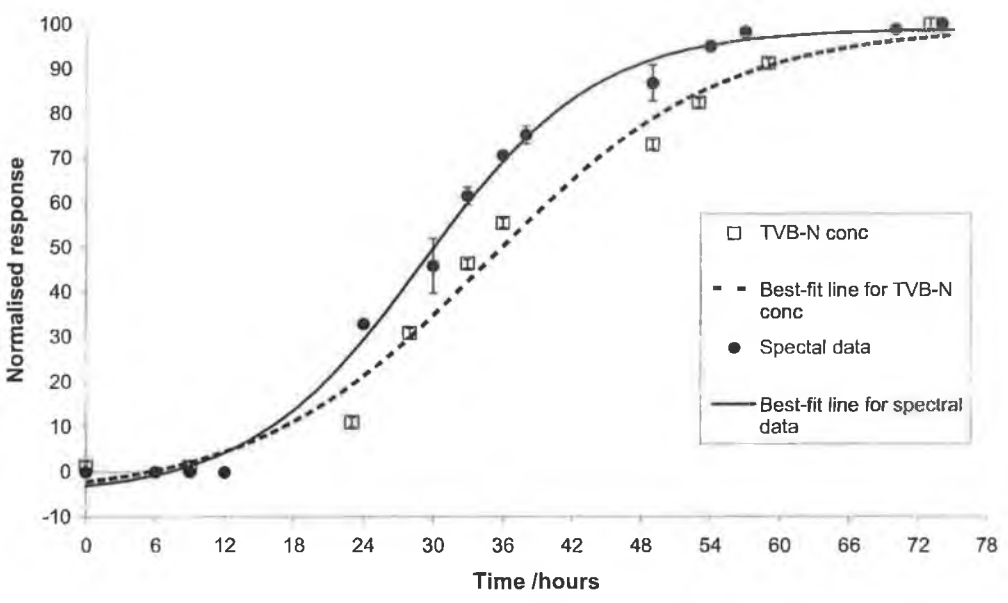

Figure 4.9: Graphical comparison of sensor response to headspace TVB-N levels. Best-fit sigmoidal curves were modelled to the data and all values have been normalised between 0 and 100 %. The sensor response was an average of 15 repeats and the changes in headspace TVB-N levels were an average of 2 repeats, and the error bars are ± the standard deviation of the replicate data.

It is clearly seen that the changing sensor response is following the dynamics of the change in headspace amine levels. The output of TVB-N does not reach a steady value during the 74 hours, which indicates that the sensor is reaching saturation at ca. 45 hours. A comparison of the best-fit model parameters also illustrates the excellent correlation between data, with very similar B and Z values, which is discussed in more detail in Section 4.3.6.

The close correlation between both datasets means that the headspace amine levels can be interpolated from a measured sensor response. This is the first set of data available that relates a chemical sensor response for monitoring spoilage levels of packaged fish to the headspace amine levels released during spoilage.

4.3.5 Microbial populations

The microbial populations were determined at defined points during the experimental timeframe. The TVC levels of cod (a) and plaice were determined at only 2 points. The TVC and pseudomonas populations of cod (b) samples were determined at many points during spoilage.

4.3.5.1 TVC of cod (a) and plaice

The response of the sensors monitoring the TVB-N of cod (a) and plaice samples was shown in Figure 4.4 and Figure 4.5 respectively. The TVC levels of each of these fish were determined at time zero and 72 hours (Table 4.2). At time zero, the samples were fresh and had little odour. At the end of the experimental timeframe, the samples (which were being stored whole) had a pungent odour, were dried out and the tissue had become hard and much darker in colour.

Sample tested	TVC (time 0 hours) CFU /g	TVC (time 72 hours) CFU /g
Cod sample 1	8.0×10^3	1.2×10^7
Cod sample 2	8.0×10^3	2.4×10^8
Plaice sample 1	2.6×10^5	1.8×10^8
Plaice sample 2	3.0×10^3	1.9×10^8

Table 4.2: Data from TVC analysis of cod (a) and plaice.

There is, on average, an increase of 4-5 orders of magnitude in microbial populations during the experimental timeframe. This increase causes more TMA and other basic volatiles to be released, which is detected through changes in the sensor response by a change in colour of the sensor dot from yellow to purple. Seafood can be considered spoiled when TVC levels are higher than 10^5 CFU /g of sample [60]. The developed sensor is clearly responding in this region. These data present the first findings that the response of a chemical sensor could be used to infer microbial populations, and hence give information about the spoilage of a seafood sample.

4.3.5.2 TVC of cod (b)

The response of the sensors monitoring the TVB-N released by the cod (b) samples was shown in Figure 4.7. The TVC levels were determined in duplicate at many points during the experimental timeframe and the results are given in Table 4.3.

Time /hours	TVC CFU/ g	
	Sample 1	Sample 2
0	2.0×10^3	2.0×10^3
9	3.0×10^3	3.0×10^3
28	3.0×10^3	1.8×10^3
33	9.0×10^6	2.7×10^5
36	1.5×10^5	1.9×10^6
49	2.0×10^6	1.4×10^7
53	3.7×10^5	1.3×10^7
59	1.6×10^6	2.3×10^7

Table 4.3: Data from TVC analysis of cod (b). Units are Colony Forming Units (CFU) / g of sample tested.

The same general trend is seen for both samples analysed. The natural flora of cod at time zero (at its freshest) is 2×10^3 CFU /g of sample tested. The TVC values stay

low for approximately 28-30 hours, where they quickly increase by ca. 3 orders of magnitude. The microbial populations stay at this approximate level until the end of the experimental timeframe. They do not decrease, which shows that the bacteria have not yet entered the death phase. The log TVC data is shown graphically in Figure 4.10.

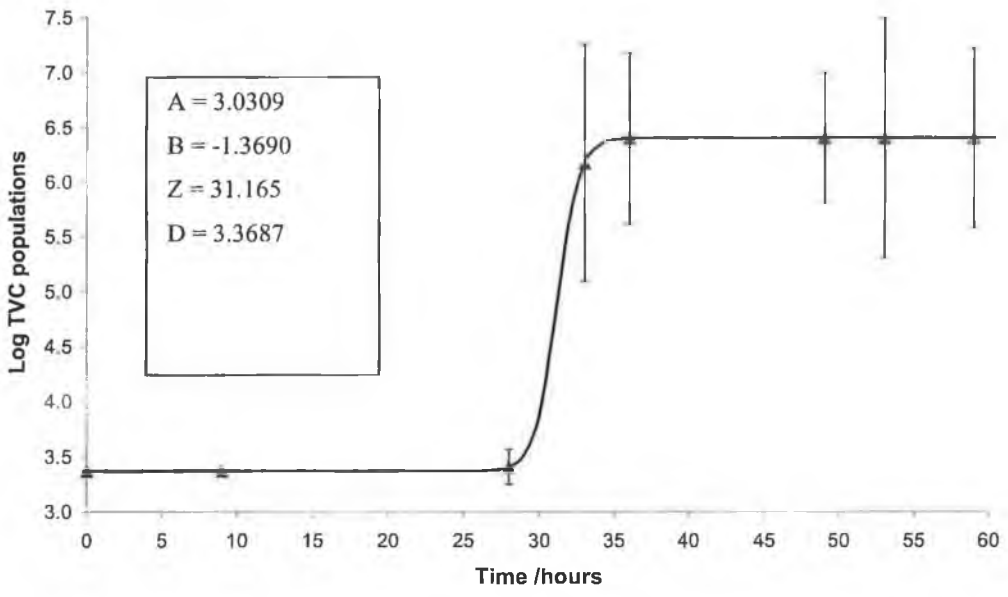

Figure 4.10: Changes in TVC populations with time for cod stored at room temperature. Duplicate samples were taken for analysis, and the error bars shown are ± the standard deviation where n=2. The sum of squared residuals for the best-fit line was 0.0021. The best-fit parameters returned by Solver are given.

The large variations seen are due to the natural differences between samples. The samples were removed aseptically, but the position from where a sample is taken is important in reproducibility of TVC enumerations. Each sample removed was taken from the same approximate place in each whole fish.

This trend closely resembles the one shown in Figure 1.11. The data was normalised between 0 and 100 % to create an overlay chart between the sensor response and the changes in TVC with time (Figure 4.11). It is shown that the sensor response is following the changing trend in microbial activity, expressed as TVC. This can also be clearly seen by the similar best-fit sigmoid parameters. Referring to Section

1.5.2.2, there should also be a close correlation between the specific spoilage organisms and the sensor response.

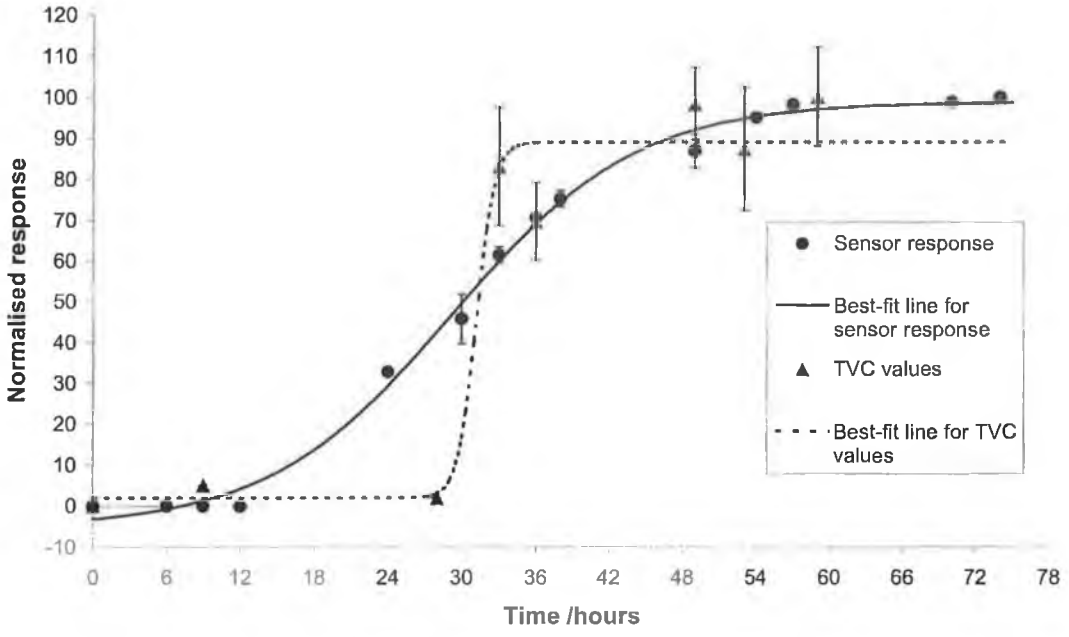

Figure 4.11: Graphical comparison of sensor response to TVC populations with time. Best-fit sigmoidal curves were modelled to the data and all values have been normalised between 0 and 100 %. The sensor response was an average of 15 repeats and the TVC levels were an average of 2 repeats. The error bars shown are ± standard deviation of the replicate data.

4.3.5.3 Pseudomonas populations of cod (b)

The pseudomonas species populations were determined in duplicate at many points during the experimental timeframe and the results are given in Table 4.4. The same trend is seen for both samples. The pseudomonas populations are very low (< 10) for the first ca. 20 hours, where they rise for the next ca. 25 hours, reaching a plateau for the end of the experimental timeframe. The data is shown graphically in Figure 4.12.

Time /hours	Pseudomonas populations CFU/ g	
	Sample 1	Sample 2
0	< 10	< 10
12	< 10	< 10
23.5	< 10	2.0×10^2
29	2.5×10^3	8.0×10^1
33	1.3×10^3	6.0×10^2
36	8.0×10^3	1.4×10^3
49	1.2×10^6	4.5×10^4
57	2.9×10^5	2.8×10^5
74	4.8×10^6	1.9×10^6

Table 4.4: Data from pseudomonas species analysis of cod (b).

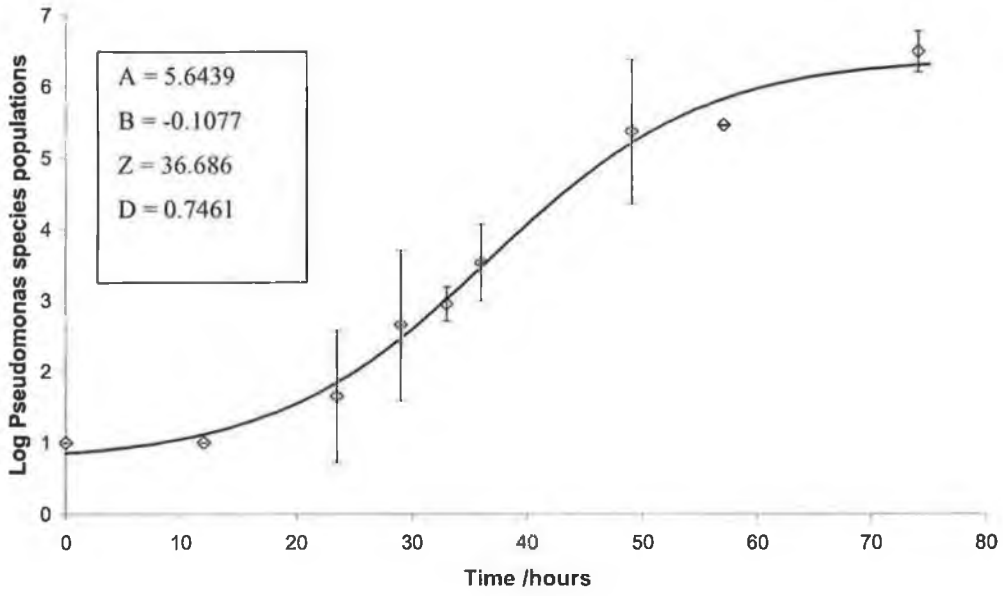

Figure 4.12: Changes in pseudomonas species populations with time for cod stored at room temperature. Duplicate samples were taken for analysis, and the error bars shown are ± the standard deviation where n=2. The sum of squared residuals for the best-fit line was 0.3122. The best-fit parameters returned by Solver are given.

Again, this trend closely resembles the one shown in Figure 1.11. The data was normalised between 0 and 100 % to create an overlay chart between the sensor response and the changes in pseudomonas species populations with time.

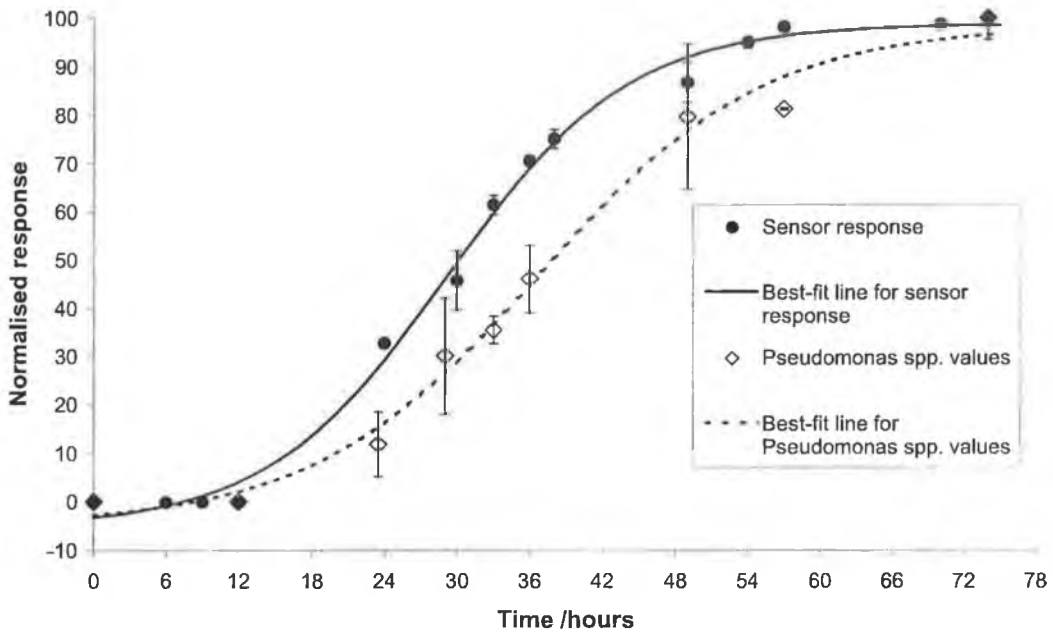

Figure 4.13: Graphical comparison of sensor response to pseudomonas species populations with time. Best-fit sigmoidal curves were modelled to the data and all values have been normalised between 0 and 100 %. The sensor response was an average of 15 repeats and the pseudomonas species levels were an average of 2 repeats. The error bars shown are ± standard deviation of the replicate data.

This overlay chart shows that when the pseudomonas species populations start to increase at ca. 20 hours, the sensor response also begins to increase. The trend follows that of the microbial growth curve, stopping at the stationary phase. It is clearly seen that the changing sensor response is following the dynamics of the change in pseudomonas species populations. A comparison of the best-fit parameters also shows the similarities between the datasets.

This presents, for the first time, data that allows the microbial populations at any time during the experimental timeframe to be inferred from a sensor reading. These

data allow the sensor response at the point of spoilage to be identified, and the headspace TVB-N levels to be determined at this point.

4.3.6 Summary of results

The population of the natural flora of the fish (TVC) at the start of the spoilage timeframe is 10^3 CFU /g (Table 4.3). The pseudomonas counts at the same point in time are <10 CFU /g (Table 4.4). The TVC levels remained almost constant for the initial 28 hours at 10^3 CFU /g, followed by a sharp increase at ca. 32-34 hours, to 10^6 CFU /g (Figure 4.10). The TVC levels remain relatively unchanged after this time. In contrast, as spoilage initially proceeds, the pseudomonas species populations rise gradually from 0 to ca. 25 hours, accelerate from 25-48 hours, and then gradually slow down for the remaining time period (Figure 4.12). There is a close correlation between the sensor response and the pseudomonas species populations (Figure 4.13), indicating that the sensor is indirectly following the levels of this specific spoilage organism. Changes in SSOs are also known to correlate well to TVB-N levels, and a summary of the correlations is shown in Figure 4.14. These trends are similar to the ones identified by a recent study of the changes in microbial populations with time (Figure 4.15).

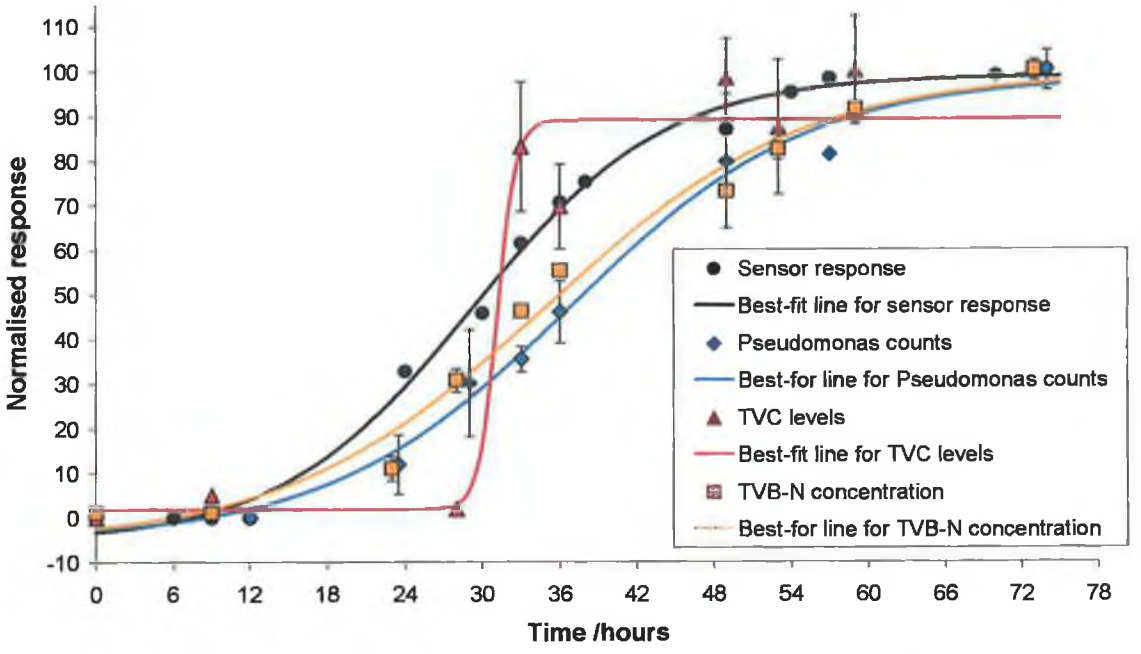

Figure 4.14: Summary of correlation between sensor response, pseudomonas species populations, TVC values and headspace TVB-N concentrations. The sensor response is clearly following the dynamics of change of the microbial populations, seen through an increase in the headspace TVB-N released. The error bars shown are all ± the standard deviation of the replicate data.

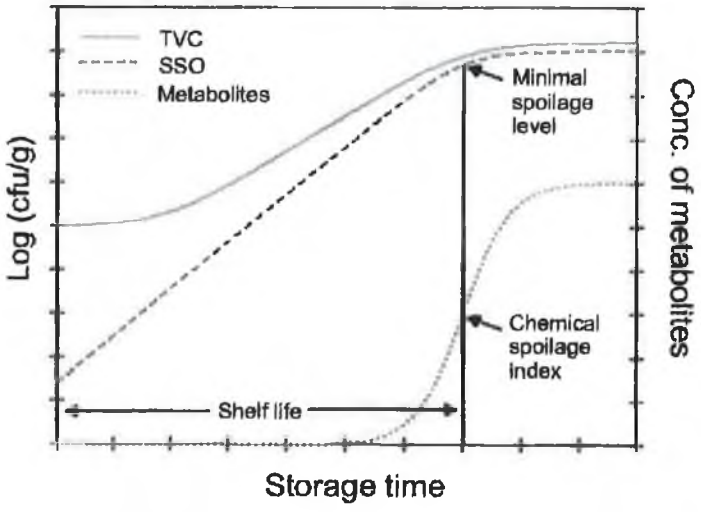

Figure 4.15: Results from a recent study show the relationship between TVCs, SSOs and the concentration of spoilage metabolites with time [50].

A summary of all the data collected is shown in Table 4.5.

Time /hours	Sensor response /absorbance units (n = 15)	Average TVB-N conc. per ml sample per 100 g fish / 10^{-5} M (n =2)	Log TVC CFU /g (n=2)	Log pseudomonas populations CFU /g (n=2)
0	-0.0001 ± 0.00010	0.13 ± 0.000	3.30 ± 0.000	1.00 ± 0.000
6	-0.0001 ± 0.00000	0.13 ± 0.000	-	-
9	-0.0001 ± 0.00000	-	3.47 ± 0.000	-
12	-0.0002 ± 0.00010	-	-	1.0000 ± 0.000
23	-	1.00 ± 0.314	-	1.65 ± 0.920
24	0.0571 ± 0.00085	-	-	-
28	-	3.65 ± 0.314	3.36 ± 0.157	-
29	-	-	-	2.65 ± 1.057
30	0.0798 ± 0.01065	-	-	-
33	0.1072 ± 0.00340	5.49 ± 0.135	6.19 ± 1.077	2.94 ± 0.237
36	0.1231 ± 0.00145	6.57 ± 0.135	5.72 ± 0.780	3.52 ± 0.535
38	0.1311 ± 0.00345	-	-	-
49	0.1514 ± 0.00715	8.66 ± 0.135	6.72 ± 0.600	5.37 ± 1.008
53	-	9.77 ± 0.269	6.34 ± 1.093	-
54	0.1657 ± 0.00190	-	-	-
57	0.1712 ± 0.00105	-	-	5.45 ± 0.011
59	-	10.82 ± 0.135	6.78 ± 0.921	-
70	0.1723 ± 0.00114	-	-	-
73	-	11.87 ± 0.269	-	-
74	0.1744 ± 0.00132	-	-	6.48 ± 0.285

Table 4.5: Comparison of sensor response at λ_{max}, the normalised headspace TVB-N concentrations, the TVC values and the pseudomonas species populations.

An additional comparison can be made by comparing the best-fit parameters from each of the datasets obtained. Table 4.6 shows a comparison of each of the best-fit model parameters obtained from each of the sigmoid functions, from all cod (b) samples analysed. The most relevant parameter for comparison is the mid-point of the inflection on the rise, in hours, parameter Z. This parameter is similar in all cases, and strengthens the case that the sensor response is following the changing dynamics of the microbial populations, and that the headspace TVB-N and microbial populations can be inferred from a simple reading of the colour of the sensor.

Best-fit parameter	Sensor response	TVB-N levels	TVC	Pseudomonas
A	0.1814	0.0001	3.0309	5.4639
B	-0.1346	-0.1345	-1.3690	-0.1077
Z	29.185	30.000	31.165	36.686
D	-0.0091	0.0000	3.3687	0.7461

Table 4.6: Comparison of the best-fit model parameters for each of the sigmoid functions obtained.

It is noted that the results should be confirmed at refrigerated temperature, since fish are not normally stored at room temperature. In order to draw successful comparisons between datasets from different experimental setups, it is essential that the samples are to be stored in the same environments. A good correlation will only be observed if the temperature of the sensors monitoring the release of TVB-N from spoilage fish samples is the same as the temperature of fish storage during the headspace TVB-N determination and the microbial population determinations. Each experimental was performed in parallel at the same storage conditions, so a good correlation was hence observed.

4.3.7 Fish spoilage prediction

There is little information available in the literature to relate pseudomonas populations to when spoilage occurs in a packaged seafood sample. However, it is likely that the pseudomonas populations would be in the region of ca. 10^2 CFU /g in order for a sample to be starting to spoil. Microbial guidelines are better defined for TVCs, and values of ca. 10^5 CFU /g are indicative of spoilage of a seafood sample [60]. The colour change of the sensor from yellow to pale orange, which was seen at ca. 23 hours, corresponds to the on-set of fish spoilage, allows a spoiling product to be identified. In our experimental work with cod at room temperature, this occurred in the region of ca. 29-36 hours, at ca. 0.07-0.08 au.

The length of time for this critical sensor reading to be established for any given seafood sample will vary on a number of key criteria, such as:

- Storage temperature.
- Species of interest.
- Age of sample.
- Sample storage regime.
- Whole versus filleted fish.
- Fish sample to headspace ratio.

The key point is that when the sensor response reaches a pre-determined value, or colour (compared to, perhaps, a set of reference colours) for a species (ca. 0.08 au for cod), this indicates that the sample has spoiled and is not fit for consumption.

It is not possible to predict freshness or remaining shelf-life from the monitoring of headspace TVB-N levels, since they essentially do not change until the spoilage organisms approach the exponential phase of growth [64], i.e. they are an index of spoilage. However, the sensor response in Figure 4.7 at ca. 0-12 hours, where the sensors remain unchanged, indicates the fish is still safe to be consumed. The linear

portion of the sensor response curve is at ca. 22-40 hours (Figure 4.16). Taking a 5 % deviation from linearity tolerance, the lower end of the linearity curve is at ca. 19.5 hours and the upper end of the linearity curve is at ca. 42.0 hours.

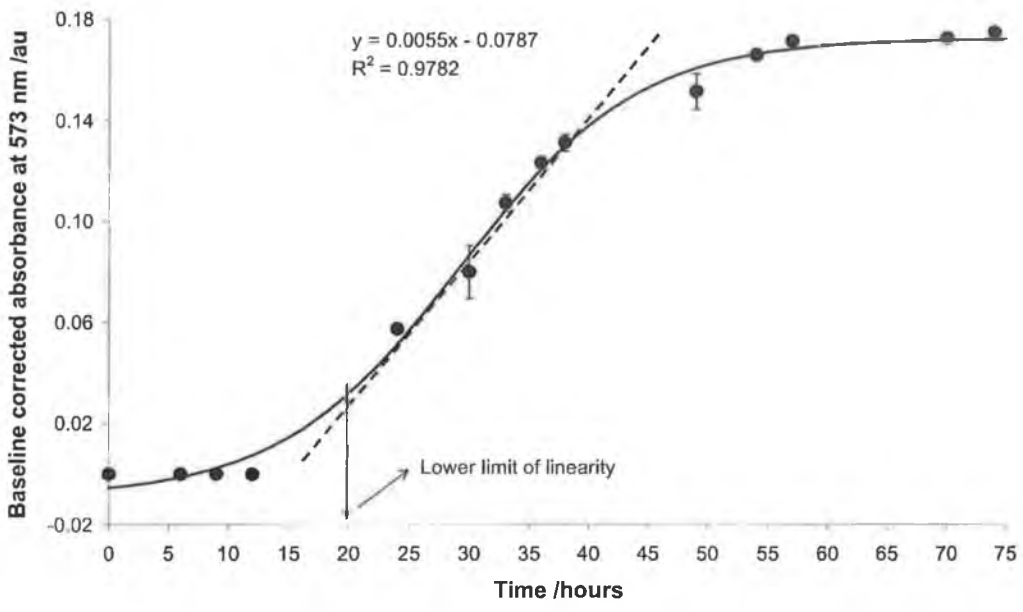

Figure 4.16: Taking a 5 % deviation from linearity, the lower limit of a reliable sensor measurement within the linear region of the curve is at ca. 19.5 hours. The error bars shown are ± the standard deviation between replicate readings, where n=15.

This indicates that a reliable sensor measurement can be taken as low as ca. 19.5 hours, where the absorbance of the best-fit curve is ca. 0.03 au. Therefore, in a closed (or packaged) environment, the sensor is capable of giving an early warning of fish spoilage. The sample is fully spoiled after ca. 29 hours, hence these set of spoilage experiments show that there exists an approximate 10-hour early warning time period of the on-set of spoilage at room temperature for cod. This time would likely be extended if the storage temperature of the fish samples was lower, since it would take longer for the spoilage organisms to multiply.

The colour of the sensors can be crudely used to indicate the on-set of spoilage. At time zero, the sensor is yellow, and remains so for a period of time as the microbial populations are increasing. At the early warning of spoilage threshold, the sensor is

pale orange, and this colour warns the user that the sample should be used or consumed quickly. At the threshold of spoilage, the sensor is dark red, and continues to react with headspace amines until a deep purple colour is reached at the point of saturation. This dark red - purple colour warns the user that the sample should no longer be consumed.

The absorbances/colours at these critical regions depend very strongly on the reproducibility of the sensors. The sensor production process needs to be very reproducible in order for the absorbances to be reproducible also. The RSD of the sensors responding to cod is ca. 3 %, where n=15. These sensors were made in different batches, yet they have excellent reproducibility. The manual production process used would never be practically considered for any commercial applications of the sensor, but is should be understood that there is a link between the printing process used, and the reproducibility of the sensor response at the thresholds of spoilage.

Figure 4.16 is essentially a calibration of the sensor, as it gives information about the response of the sensor to basic gases. It defines the upper and lower limits of linearity of response to headspace TVB-N, with a 5 % degree of tolerance of deviation of the sensor response curve from the best-fit linear curve. At these limits, the sensor response was inferred from Figure 4.7. The concentration of headspace TVB-N at these limits was inferred from Figure 4.8 and the data is summarised in Table 4.7.

Limit of linearity	Time /hours	Sensor response /absorbance units	Average TVB-N conc. per ml sample per 100 g fish / 10^{-5} M
Lower	19.5	0.0296	1.28
Upper	42.0	0.1449	8.75

Table 4.7: Summary of data at upper and lower limits of linearity. The time in hours data column refers only to cod at room temperature in these set of experiments.

Hence, the sensor can give a linear response between 1.28×10^{-5} and 8.75×10^{-5} M of TVB-N, per ml of sample, per 100 g of fish tested. Beyond these regions, it may be also be possible to obtain reliable data. The data in Table 4.7 only refers to cod stored at room temperature, and would undoubtedly vary between species and storage conditions.

This is the first set of data that successfully demonstrates an early warning of fish spoilage by monitoring headspace TVB-N. The close correlation between the data sets clearly illustrates that the sensor can be used to infer pseudomonas populations, which can, in turn, be used for shelf life determinations.

4.4 Conclusions

The data given here are the first set of results that show strong correlations between the response of a packaged headspace amine chemical sensor, the headspace TVB-N levels released and the changes in microbial populations during spoilage. The standard EU method for determination of TVB-N levels was modified to allow the determination of headspace TVB-N levels released by a sample. The sensor response at any time during a spoilage experiment can be used to infer microbial populations, and hence give information about the level of spoilage of a sample. An early warning window of spoilage was revealed at ca. 10 hours before complete spoilage occurred for cod stored at room temperature. The sensor responded from yellow (no spoilage) to pale orange (early warning of spoilage) to dark red to purple (sample fully spoiled). The length of time taken to reach these critical levels is related to the age of a sample and the storage regime used. The correlation between the datasets was shown both graphically and numerically, by comparison of the best-fit parameters of the sigmoid functions that were modelled to the data.

The outcome of these results is that a simple, easy to use sensor has been developed, that requires minimal training for use. The main drawback of the system presented lies with the instrumentation used. The imaging spectrograph (PARISS) system is a reference measurement system, essential to be used at this stage, but clearly unsuitable for use outside of the laboratory on real fish packaging. In order to keep with the general themes of sensor development, a simple colour measurement system should be used, akin to a supermarket barcode scanner, to give a rapid analysis of the sensor colour, and hence relate this in real-time to the level of spoilage of a sample.

5 Development of a Portable Handheld Colour Scanner for Analysis of Fish Spoilage Sensors

5.1 Introduction

Results from Chapters 3 and 4 demonstrate that spectroscopic measurements (taken in reflectance mode) of pH-sensitive sensors, based on cresol red entrapped in a cellulose polymer matrix, can be used to monitor the changes in headspace TVB-N levels released by gradually spoiling fish samples. The imaging spectrograph (PARISS) system used offers tremendous potential to investigate the spectral features of the sensors. However, the system is not suited to in-situ analysis, since it is an expensive, laboratory-based reference measurement system that requires trained operators for use. One of the general trends in analytical sciences is in bringing the measurement to the point-of-need, and this trend is seen in many diverse areas from medical applications to water quality monitoring. From the perspective of packaged food monitoring, there is a general trend in monitoring samples from "harvest-to-home". In principle, this allows full traceability of a package, which would allow a weak link in the distribution chain to be identified. A prerequisite in shifting the measurement from the laboratory to the point-of-need is to employ a simple measurement system that could be used by general technical staff. It was the aim of this final section of research to develop a portable, easy to use, robust, inexpensive handheld colour measurement device, henceforth termed the "scanner".

The scanner measures the scattered diffuse reflectance from a surface. The device is comprised of 2 LEDs that illuminate a small surface area and a photodiode that measures the diffuse reflected light from the surface. The device is connected to a PC via a microcontroller box, and can readily acquire and record reflected light intensity information from a surface. In principle, as the cresol red sensors react with headspace TVB-N compounds and change colour from yellow (acidic form) to purple (basic form), the reflected light intensity will decrease, since the chosen LED emission maximum is fixed close to the λ_{max} of the basic form of cresol red. Therefore, it is possible to correlate the measured light intensity (measured using the scanner) of sensors exposed to basic compounds in the headspace to the microbial populations of a sample, since this correlation was already established in chapter 4. A

reflected light intensity threshold can thus be derived to distinguish samples that are not spoiled to those that are not suitable for human consumption. Before this can be done however, it is essential to establish, through a series of control experiments, the performance of the scanner for measuring colour changes.

This chapter outlines the design and specifications of the scanner, and describes its operation in detail. The experimental approach taken was subdivided into three main areas. Firstly, the operation of the scanner was characterised. The emission spectrum of the LED in the scanner was compared to the spectral features of the cresol red sensors. The response of the scanner was characterised by measuring the reflected light intensity of a series of cresol red standards, of increasing concentration, impregnated onto filter paper discs. A study of the effect of the sensor thickness on the measured reflected light intensity was also investigated. Secondly, the response of the sensor dots to ammonia in headspace was calibrated, and the resultant colour changes were measured using the scanner. This allowed a direct comparison of data from the scanner to data from the imaging spectrograph (PARISS) system used thus far. This calibration allowed the sensor response, measured as a reflected light intensity, to be determined at the critical points of spoilage, based on microbial populations determined previously (Chapter 4). Finally, the combination of scanner and sensor was used with real fish samples purchased from a local supermarket, to test the operation of the scanner in typical storage conditions. The correlation between spoilage, as indicated by the sensor response, and the "use-by" dates printed on the package was investigated for a number of different species.

5.2 Instrumentation

As a result of a series of meetings with Whistonbrook Technologies, an electronics company specialising in analytical measurements based at Luton University in the UK [102], the scanner was designed and built to our specifications. The scanner was primarily designed for the task of measuring the reflected light intensity of the fish spoilage sensor dots, although in principle it can be used for a wide range of colour measurement applications. The generic features decided upon were to use LEDs for illumination and a photodiode for detection. All components were to be housed inside one single unit. Wide ranges of all of these components are available commercially, e.g. LED catalogues now cover practically all of the visible and part of the UV spectra. The scanner should be small, simple to use and have the potential to be used for in-field analysis, i.e. away from a PC or power source. Specifically for this application, LEDs were chosen close to the λ_{max} of the basic form of cresol red (573 nm), and the measurement aperture approximately equals the diameter of a typical sensor dot. A schematic of the scanner is shown in Figure 5.1.

The scanner was built around a hand-machined solid opaque plastic tube, 70 mm width, 20 mm length, with a 5 mm diameter hole at 90° to the end faces and two small diameter holes at 45° to the lower end face. A photodiode (reverse bias pn junction) was positioned at the top end of the vertical relative to the 90° hole, 50 mm from the measurement area. Two 3 mm diameter standard yellow LEDs with a λ_{max} of 570 nm were positioned at the top of the 45° holes. These LEDs were chosen because of their λ_{max} value, their narrow band emission, plus the small size of the LEDs ensured that a small scanner head was built to house them. The photodiode was a standard component, fitted with an IR filter, to reduce reflected light intensity above ca. 800 nm. The diode can detect most visible wavelengths; therefore it is very sensitive to environmental light effects, e.g. daylight.

The inner surface of the plastic tube was coated with a matt black finish, to reduce the amount of stray light effects as light propagates through the device, from the

LEDs to the measurement surface and reflected back to the photodiode. A hollow tube of greater diameter was slipped over the solid tube to protect the LED and photodiode connections. A printed circuit board was used to connect the leads and photodiodes to a connecting cable. A circuit to pre-amplify the signal and reduce electrical noise may be fitted to this circuit board. Light from the LEDs illuminates the measurement area (e.g. a sensor dot) at an angle of 45°. The design is such that the light from the two LEDs converges when placed in direct contact with a surface; hence this ensures maximum illumination in the 5 mm diameter measurement area. A photo of the scanner is shown in Figure 5.2.

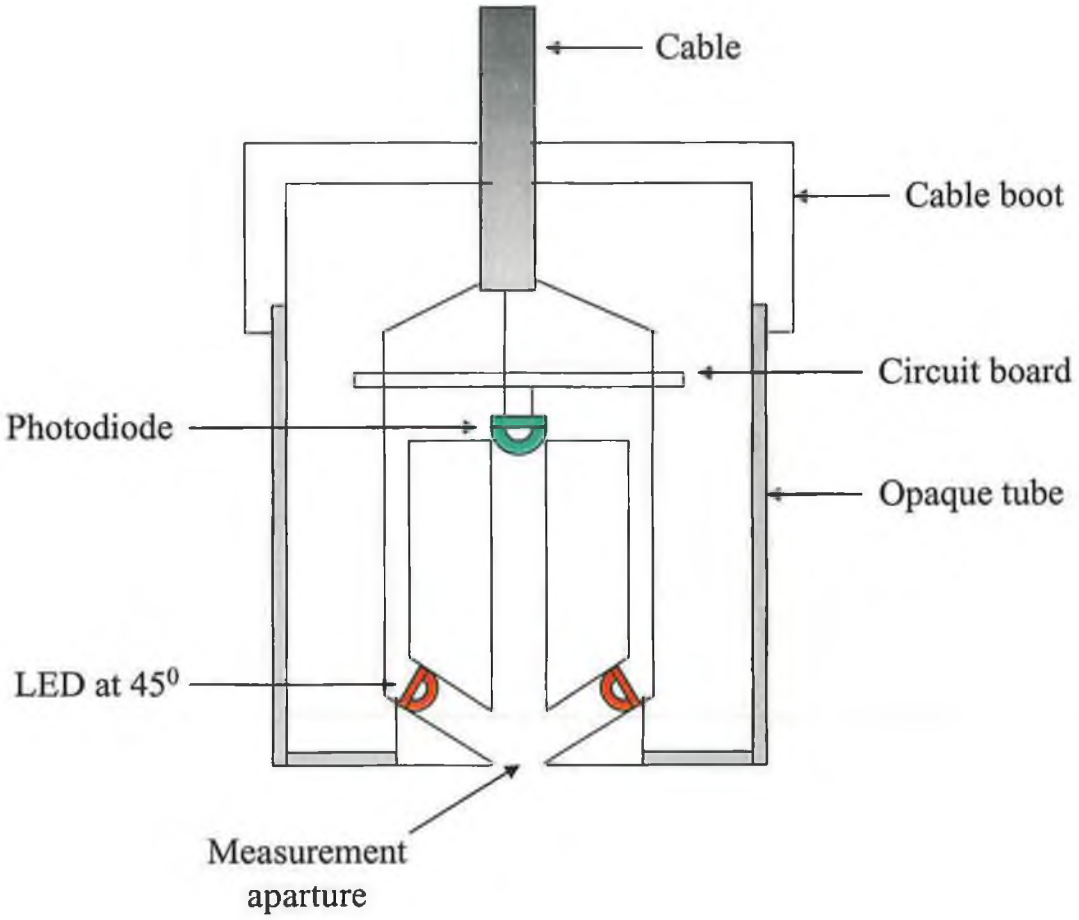

Figure 5.1: Schematic of scanner.

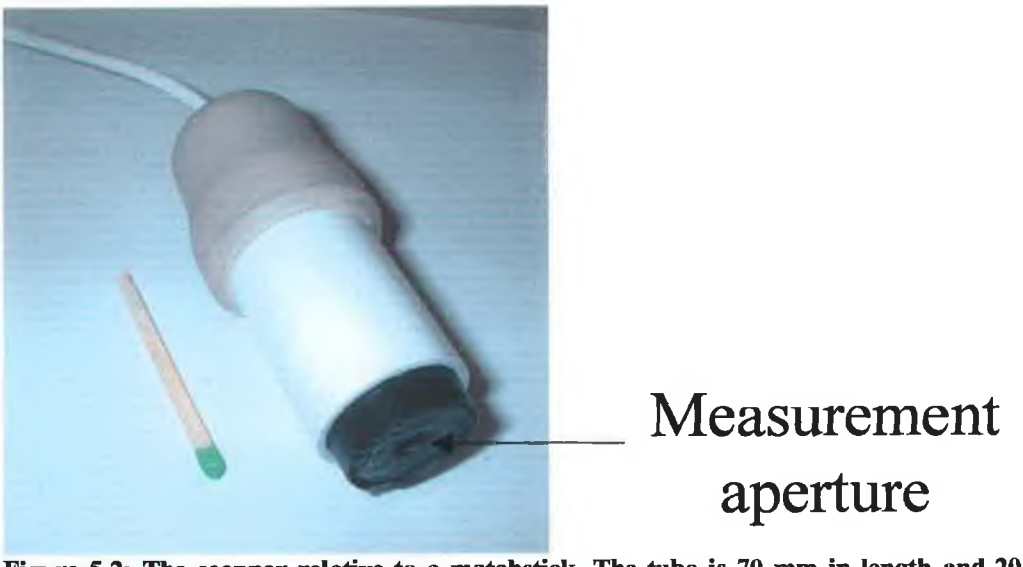

Figure 5.2: The scanner relative to a matchstick. The tube is 70 mm in length and 20 mm in width. The measurement aperture is located at the bottom of the scanner (as indicated) and is 5 mm in diameter.

Light scattered from a region of interest at 90° falls on the photodiode. Light scattered from the highly reflective surface of the sensor substrate is at 45° and is therefore not measured by the photodiode. The scanner is thus designed only to be used with a 90° angle of contact, in proximity to the measurement surface. The scanner only measures the scattered light from a surface that strikes the photodiode; some of the light intensity is lost in this process. The LED illumination is pulsed 3-4 times per second to minimise noise from environmental light sources, which can be problematic to the measured signal. The scattered light intensity incident on the photodiode is measured when the LEDs are pulsed. Several readings are taken and averaged within one pulsing sequence. This average value is converted into a digital signal by a 10-bit A-D. The circuit also contains a digital filter to remove noise at mains frequency. Hence the software displays a value of the reflected light intensity in arbitrary units. A schematic of operation of the device is shown Figure 5.3.

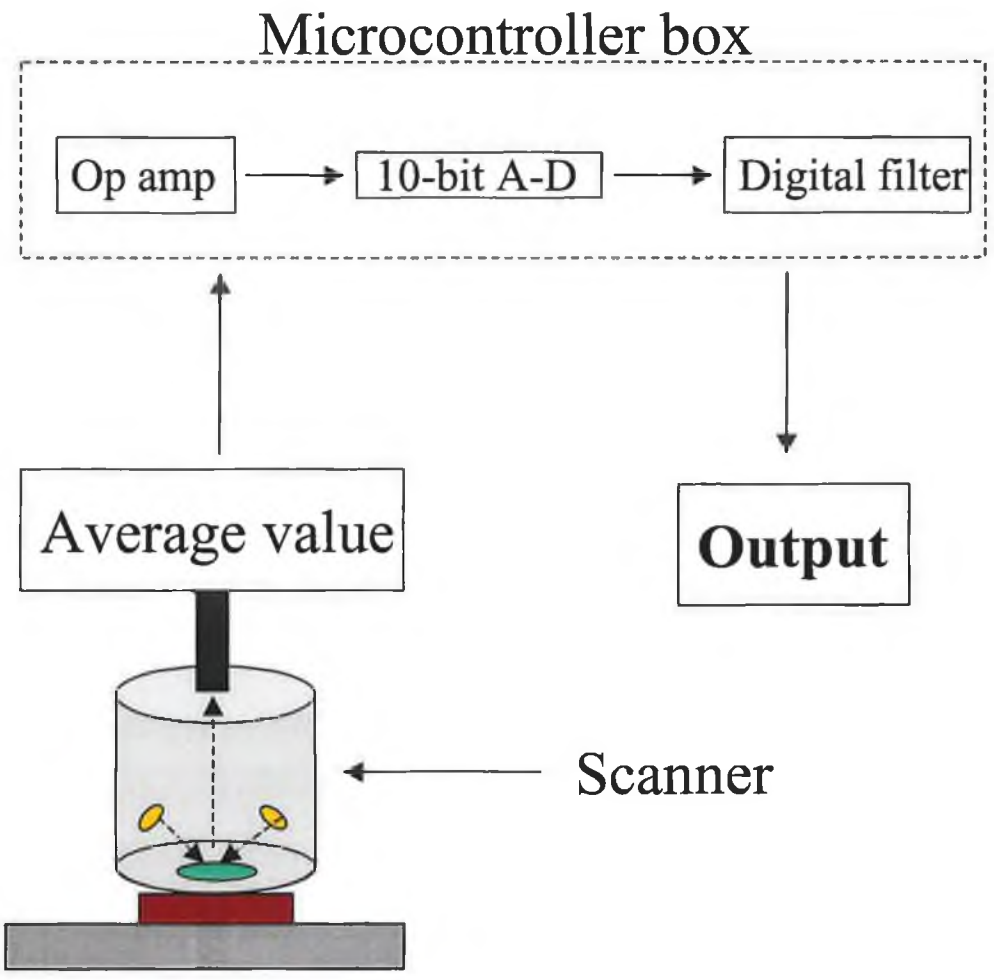

Figure 5.3: Schematic of reflected light intensity output from photodiode. The path the light takes from emission to detection is shown in dashed lines in the scanner head.

The device is connected to a PC via a microcontroller box that communicates via a standard serial port. The microcontroller box contains fully-addressable random access memory (RAM), which allows data to be stored either in the box for downloading to a PC at some future time (if not connected to a PC), or to be saved in an Excel-compatible format for post-run analysis. The electronic circuit, which includes a 5 V regulated power supply, can be mains or battery operated. All of these features and the size of the device constitute a fully portable device for in-field analysis.

Customised software written in Visual Basic displays the reflected light intensity measured by the photodiode in real-time. The value when the LEDs are not pulsed, i.e. the blank, is also captured. The software then subtracts the blank value from the measured value, to return a corrected value for the reflected light intensity. The user can collect discrete values of the light intensity at required times. Figure 5.4 shows a screen capture of the scanner software, with three key regions of interest labelled. The trace shown is a plot of reflected light intensity as a function of time.

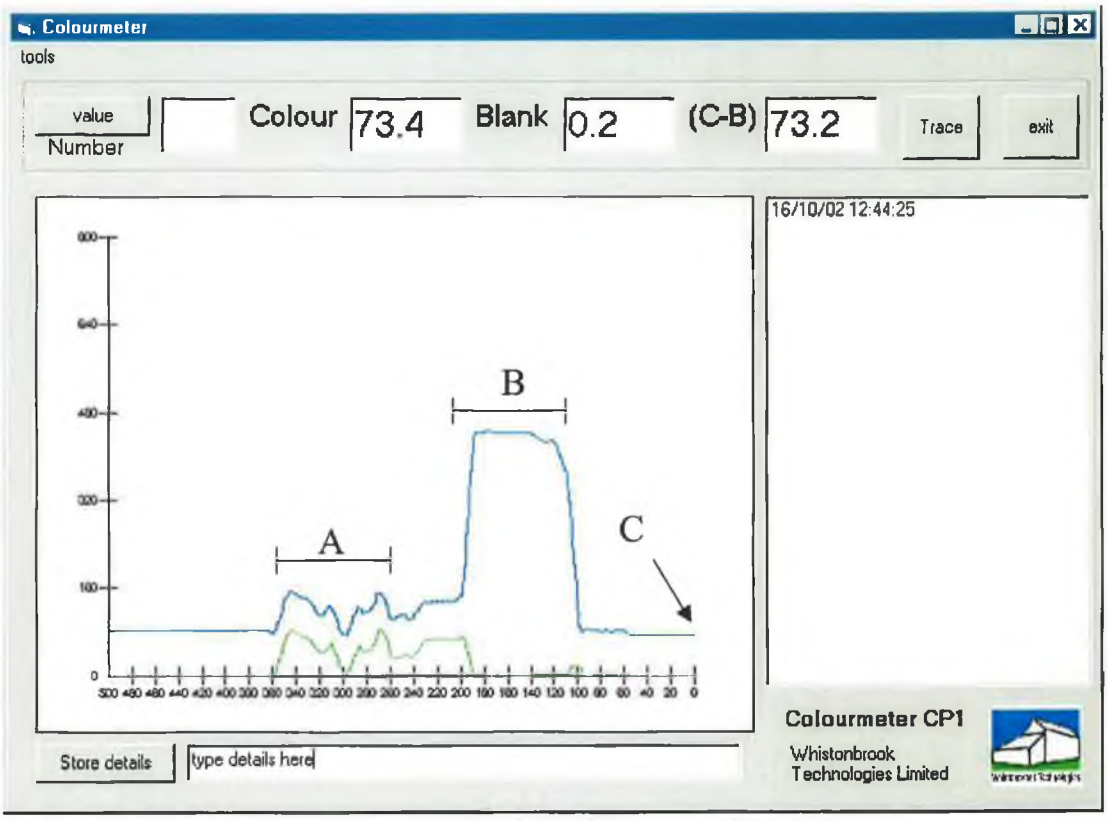

Figure 5.4: Screen capture of the supplied scanner software. The blue line is the measured reflected light intensity, and the green line is the background intensity. Three important regions have been identified in the data trace, A, B and C. Each of these regions are discussed in the text.

Each of the three labelled regions illustrate important features of the operation of the scanner and software, and are discussed in turn:

- Region A is an area where the scanner was not in direct contact with any surface. Changing the angle of contact and the distance from the surface introduces noise into the system. This noise is expressed similarly in the measured reflected light intensity and in the background intensity, and is hence known as common mode noise. This enables the user to distinguish a real measurement from noise.
- The feature at region B was observed when the scanner was placed in direct contact with a strip of dark yellow coloured paper. The common mode noise from region A was replaced by a rise in the measured reflected light intensity that was not seen in the background intensity; hence it is a real feature. The yellow card, illuminated by a yellow LED, reflected much of the light intensity back to the detector, hence the corrected reflected light intensity was a high value, ca. 460 units.
- The feature at region C was observed when the scanner was placed in direct contact with a strip of dark purple coloured paper. The paper absorbed most of the light intensity, therefore the reflected light intensity is much lower than in region B. At region C, the measured values were captured by the software, and are displayed in the boxes at the top of the screen, labelled as Colour, Blank and (C-B), i.e. Colour-Blank.

In summary, an LED and photodiode-based scanner was designed and built to our specifications to measure the diffuse scattered light intensity from a surface. This scanner was thus used in combination with the developed fish spoilage sensors to create a user-friendly and simple method of analysing the colour of a sensor exposed to spoilage volatile compounds.

5.3 Experimental

5.3.1 Materials

All chemicals and reagents used for sensor preparation were as previously described (Section 2.4.2). Sodium hydroxide and 1 cm diameter Whatman filter paper were obtained from Sigma-Aldrich (Dublin, Ireland). 10 ml Hamilton gastight syringe was supplied by Carl Stuart (Dublin, Ireland).

5.3.2 Characterisation of scanner

5.3.2.1 Characterisation of LED emission spectrum

An emission spectrum of the yellow LED in the scanner was captured using an Ocean Optics S2000 fibre-optic spectrometer (WPI Ltd., Hertfordshire, UK). A comparison of the λ_{max} of the LED and the λ_{max} of the basic form of the cresol red dye was performed.

5.3.2.2 Calibration using cresol red standards

A series of cresol red standards of increasing concentration at a fixed pH were prepared. 5 ml solutions of cresol red in 0.1 M NaOH were prepared, ranging from 0 to 0.075 mg/ml dye concentration. The NaOH was used to ensure that the dye is kept in its basic (purple-coloured) form. 100 µl of each solution was transferred to a 96-well plate and the absorbance at 573 nm was measured in a plate-well reader (Model µ-Quant, supplied by Medical Supply Company, Dublin, Ireland) to produce a Beer's plot for the dye. The calibration plot was prepared in triplicate.

25 µl of each solution was pipetted onto single units of 1 cm diameter Whatman filter paper. The excess was removed with tissue paper and the colour of each impregnated wet filter paper disc was analysed by the scanner, on a white paper background. This procedure was repeated in triplicate for each concentration of dye used, and the data obtained allowed a direct comparison of data from the scanner to the data from the benchtop plate-well reader instrument. The light intensity measured by the scanner decreases exponentially with increasing dye concentration. For comparative purposes, the intensity data from the scanner for each sample tested (I) was ratioed to the intensity data of a blank (I_o, no dye present) by the following equation:

$$S_{out} = \log_{10}\left(\frac{I_0}{I}\right) \qquad \textbf{Equation 5.1}$$

This is essentially the standard definition of absorbance [103], although it should not be confused with typical transmission readings. Instead, the difference in the ratios is a measure of the decrease in reflected light intensity due to absorbance of light by the sample. All data from the scanner was treated with Equation 5.1 to compare the output (S_{out}) to data collected using other systems.

5.3.2.3 Effect of sensor thickness on reflected light intensity

A series of cresol red sensor dots of increasing thickness were prepared, using the optimised formulation developed. This was achieved using a series of different amounts of small sticky-backed rings (reinforcement rings) on PET. 5 different thicknesses were tested, *viz.* 1, 5, 10, 15 and 20 rings, each in triplicate. The formulation was pipetted into the rings using a micropipette, and was allowed to dry overnight in a fume cupboard (Figure 5.5). The purpose of the rings ensures that the formulation can only dry in a confined area, and changing the number of rings on the PET offers a simple degree of control over the thickness of a spot produced.

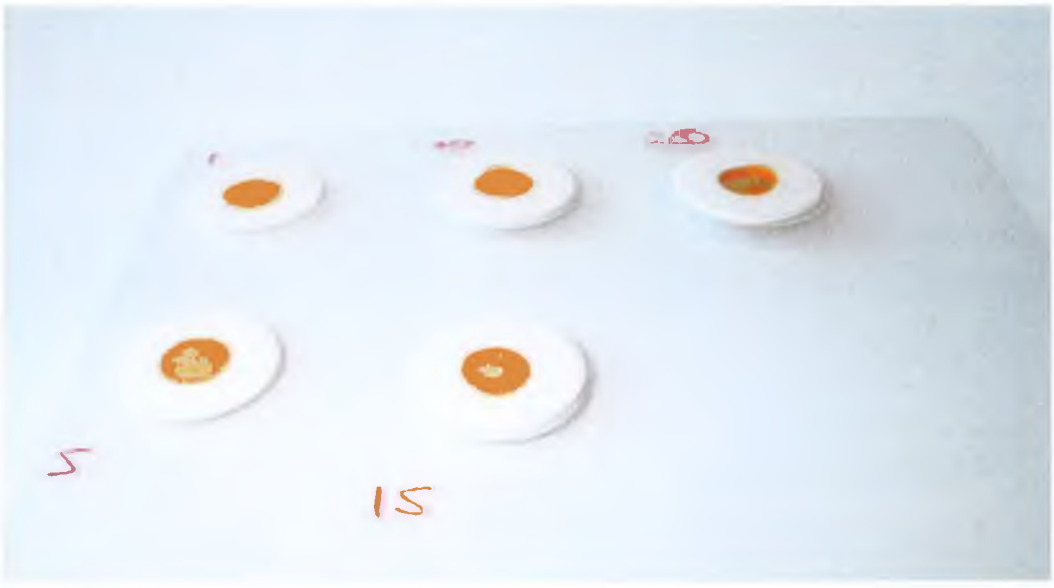

Figure 5.5: The test formulation was printed onto PET through different heights of rings, to create spots of different thicknesses.

The reflected light intensity was measured from the surface of each spot as a function of thickness using the scanner. The thickness was measured using a micrometer that can measure thickness in 10 μm steps. This was achieved by removing the rings carefully from the PET, and measuring the spot thickness on PET. The thickness of the PET was known, and was subtracted from all measurements taken.

5.3.3 Calibration of sensor dots with scanner

Cresol red based pH sensors were prepared as described in Section 2.4.2. Section 2.4.7 described how the sensors were calibrated against ammonia in headspace using a 2-necked flask with a sensor incorporated into one of the necks. The same experimental procedure was set up, and a sequential series of 0.5 ml NH_3 gas samples were injected into the flask via a rubber seal with a 10 ml gas-tight syringe. The injected gases were allowed to equilibrate with the sensor for 5 min by stirring. The scanner was attached in a fixed position to the sensor surface using sticky tape (Figure 5.6), and the reflected light intensity of the sensors as a function of headspace NH_3 concentration was measured and recorded by the scanner software.

The calibration procedure was repeated in triplicate. The data were saved in .dat format for post-run analysis in Microsoft Excel.

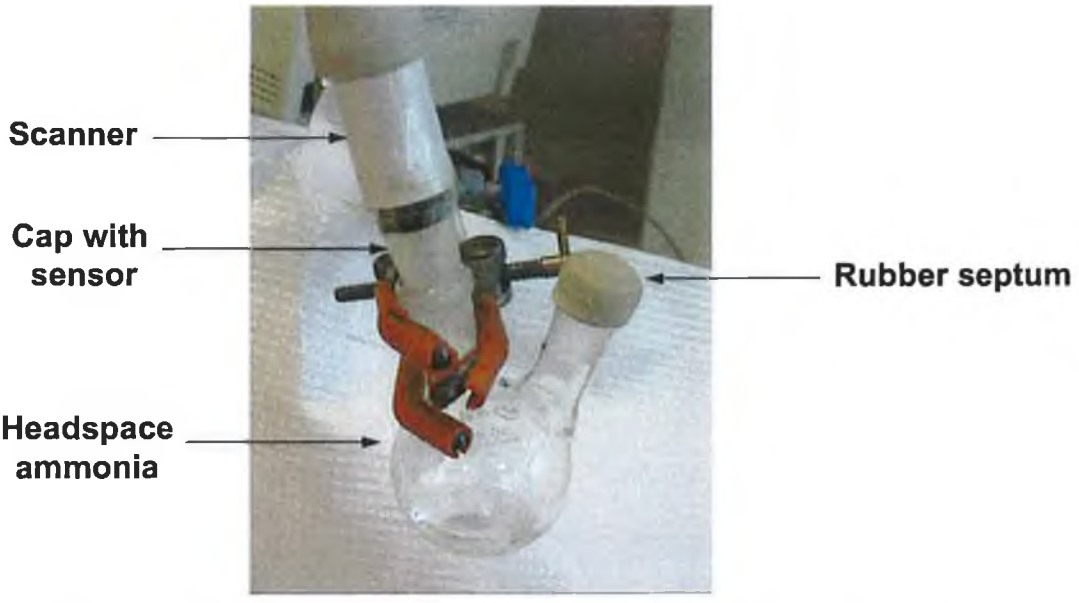

Figure 5.6: Sensor calibration setup, with scanner at fixed position above sensor. Ammonia was injected through the rubber septum using a gas-tight syringe.

5.3.4 Testing sensors and scanner with real fish samples

A series of fish samples were purchased at a local supermarket. These were all uncooked fillets that were sealed and packaged, with "sell-by" and "use-by" dates, and were stored in a supermarket fridge at the point of sale. They were packaged in very thin polyethylene (cling film), and a fresh fishy-type smell was clearly evident from the samples at the time of purchase. Two batches of samples were purchased at different times. The first batch of samples were cod, kippers, plaice, smoked coley and whiting. The kippers and smoked coley were selected to show that the sensors do not respond to fish that have been preserved by smoking. The second batch of samples were cod, haddock and whiting. The mass of all samples purchased was known.

A 5 mm diameter hole was pierced thorough the fish packaging with a sterilised blade, and a 15 mm diameter section of filter paper was placed over the hole. A single sensor on PET was placed face-down on the paper and covered with 2-3 small sections of sticky tape to inhibit amines escaping to the surrounding environment (Figure 5.7). The edges of the filter paper and hole were also covered with tape. Enough tape was used so the issue of amines leaking into the surrounding environment through the pierced hole was not significant. All samples were stored for the duration of the spoilage experiments at 4 °C in a fridge, to mimic typical storage conditions. Reflected light intensity readings were taken regularly with the scanner, by moving the sample momentarily from the fridge to the PC setup and monitoring the sensor changes. This was repeated in triplicate for the same sensor (for batch one) and for three different sensors on the same pack (for batch two). Additionally, the second batch of fish was wrapped in an extra 2 layers of cling-film, to further inhibit the amines escaping to the environment. This completely eliminated the smell of amines from the fish.

Figure 5.7: Plaice sample at time zero (i.e. just purchased) with a cresol red sensor attached. Sample was purchased on 3rd September 02.

5.4 Results and discussion

5.4.1 Characterisation of scanner

5.4.1.1 Characterisation of yellow LED

The yellow LED spectrum that was collected showed a λ_{max} at 570.88 nm (Figure 5.8).

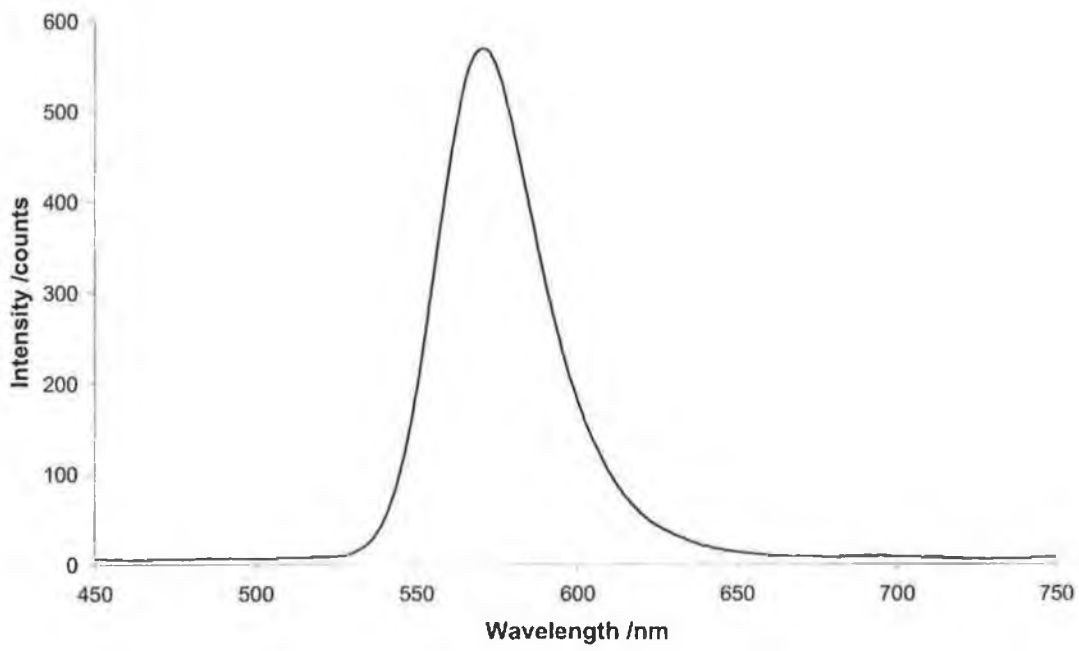

Figure 5.8: Emission spectrum of yellow LED in handheld scanner device.

The width at half maximum is 38.06 nm. This is a narrow band LED that will reduce interference effects by only exciting specific wavelengths of interest. The LED spectrum was compared to the spectral data of the cresol red dye that was obtained in Section 2.4.7 from the imaging spectrograph (PARISS) system, where the sensor dot was calibrated against NH_3 in headspace. The LED emission spectrum was normalised between the limits of the sensor response, i.e. between 0 and 0.1669 au,

by dividing by the highest value, and multiplying all values by 0.1669. An overlay chart of the normalised datasets is presented in Figure 5.9.

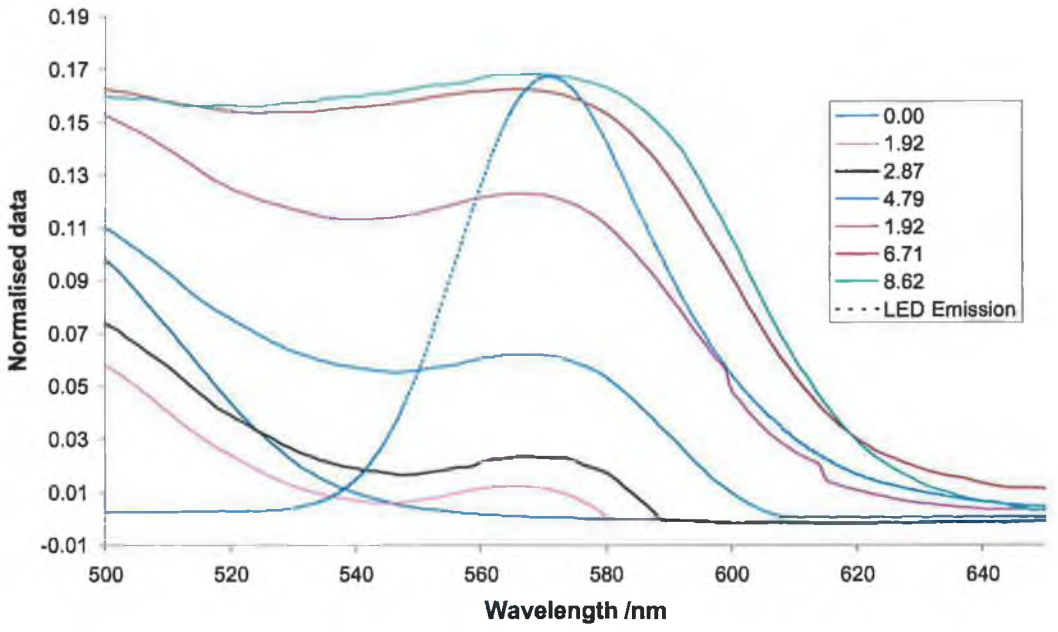

Figure 5.9: Overlay of normalised spectra from the yellow LED and the basic form of the cresol red sensor dots.

There is an excellent overlay between the spectral emission of the yellow LED and the spectral absorbance of the cresol red sensor dots. The LED will excite the λ_{max} of the basic form of the dye, to obtain reflected light intensity data from the sensor dots. This demonstrates clearly that the LED and photodiode approach used in the scanner has a strong ability to detect colour changes in the fish spoilage sensor.

5.4.1.2 Calibration using cresol red standards

The results obtained for the cresol red standard solutions in the plate-well reader clearly show that Beer's Law is obeyed (Figure 5.10). Excellent reproducibility was obtained, with an RSD of 0.28 %.

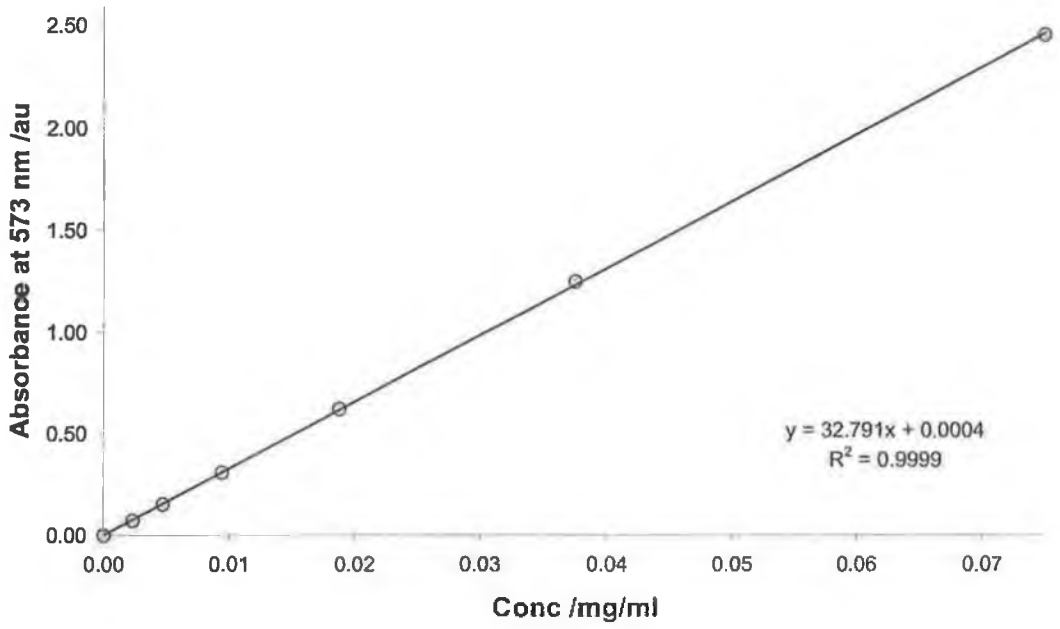

Figure 5.10: The absorbance (in transmission) of the dye at 573 nm as a function of concentration of the dye in free solution. The error bars (masked by symbols) are ± standard deviation, where n=3.

Each solution was impregnated onto a filter paper disc and the reflected light intensity was measured by the scanner device (Figure 5.11). This data shows that the working range of the scanner/sensor dot combination is between ca. 680 to ca. 150 units. When the dye is in low concentration, most of the light intensity is reflected back to the photodiode. As the concentration of dye increases, less light is reflected since more light is absorbed by the discs; hence, the intensity values decrease with increasing dye concentration.

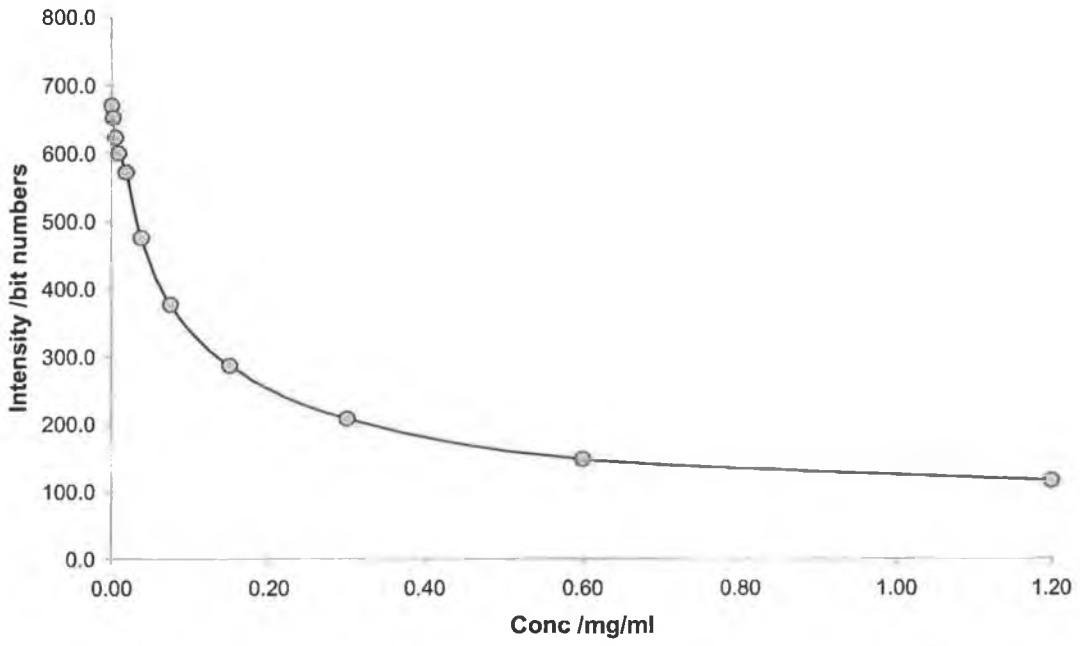

Figure 5.11: The reflected light intensity of the impregnated dye discs as a function of concentration of the dye. The error bars (masked by symbols) are ± standard deviation, where n=3.

The data in Figure 5.11 was transformed using Equation 5.1 into values analogous to regular absorbances. A straight line was obtained within the range 0 to 0.075 mg/ml (Figure 5.12), which indicates clearly that the scanner is able to distinguish each of these dye concentrations, and is obeying Beer's Law, similar to the results from the plate-well reader (Figure 5.10). Both sets of data are linear within the same concentration range. The average RSD was 2.36 %. This is higher than the value for the plate-well reader, but there are extra experimental steps involved that would introduce this error.

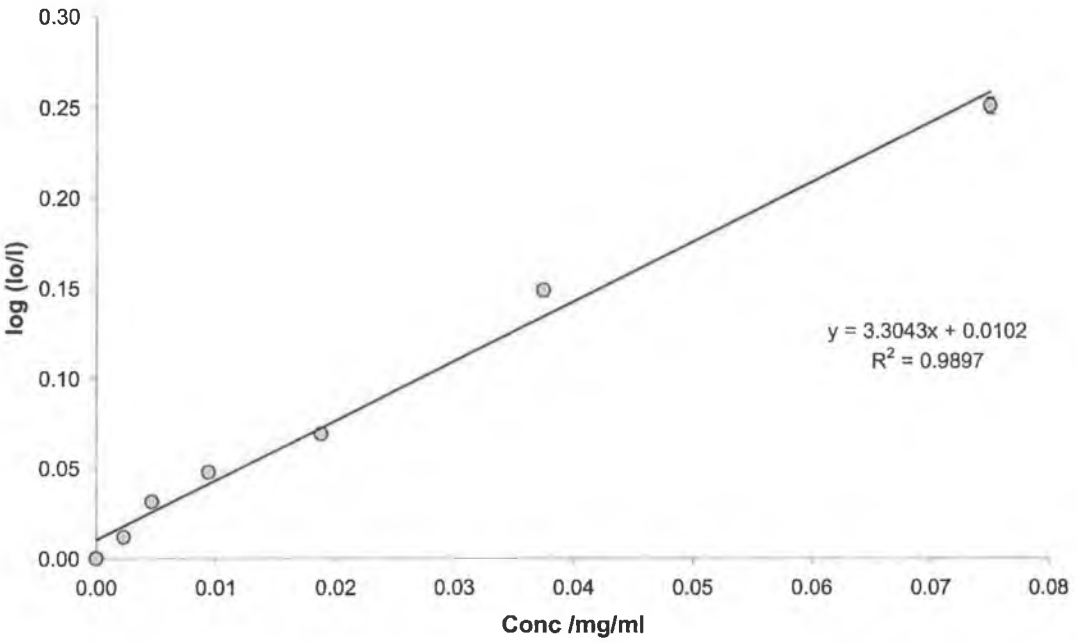

Figure 5.12: The reflected light intensity of the impregnated dye discs as a function of concentration of the dye, after data-transformation using Equation 5.1. The error bars (masked by symbols) are ± standard deviation, where n=3. I_0 was a disc impregnated with water (no dye).

The outcome of these results is that the scanner is capable of measuring spectral changes in the basic form of cresol red, and returns a Beer's plot as a function of the dye concentration. The scanner is not restricted to measuring cresol red, and would in fact work well for any dye that has a λ_{max} in the region of ca. 555 – 595 nm. This is a common wavelength range for the basic form of many pH indicator dyes, e.g. bromocresol purple, bromothymol blue and bromophenol blue (Section 1.3.2.2), the former two having been used in sensors for ammonia and amines (Section 1.5.4.1).

5.4.1.3 Effect of thickness on the reflected light intensity

3 dots were produced at each of 5 thickness tested, ranging from 100 μm to 625 μm (measured using a micrometer). The reflected light intensity at each thickness was measured using the scanner. A full trace of the reflected light intensity as a function of thickness for one of the sensors tested is shown in Figure 5.13.

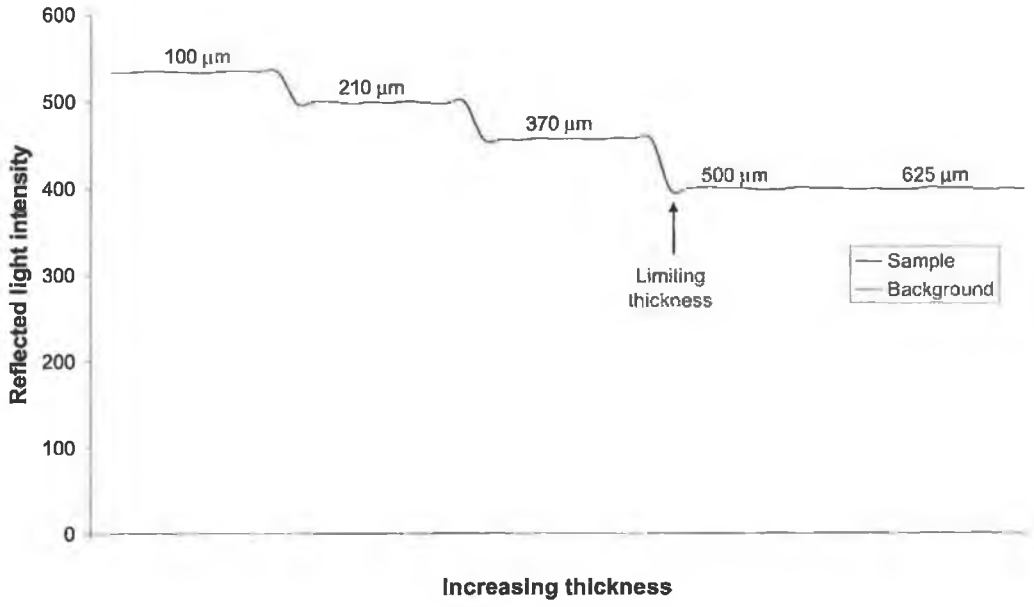

Figure 5.13: Plot of reflected light intensity, measured with the scanner, as a function of sensor thickness. The limiting thickness is clearly around 500 µm.

Each sensor was produced in triplicate, and the average reflected light intensity as a function of sensor thickness is shown in Figure 5.14.

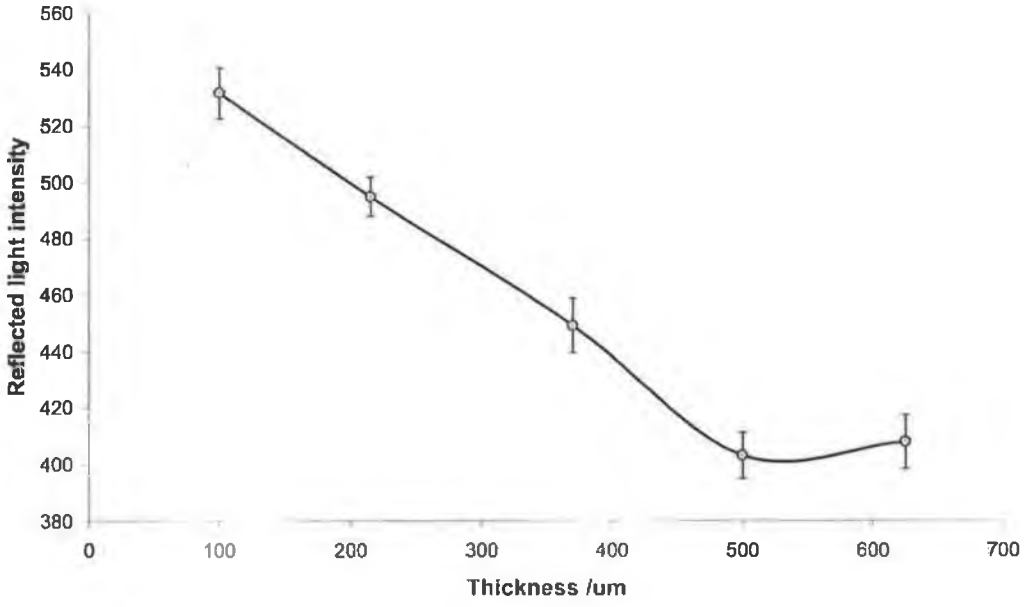

Figure 5.14: Plot of the change in reflected light intensity as a function of sensor thickness. The error bars are ± standard deviation, where n=3.

The RSD for all 5 thickness values tested was less than 3 %. The overall trend seen in Figure 5.14 can be explained in terms of the path that the light takes from the LED to the photodiode. Figure 5.15 shows the path taken by light from the LEDs, through the sensor dot, and reflected from the PET back to the photodiode.

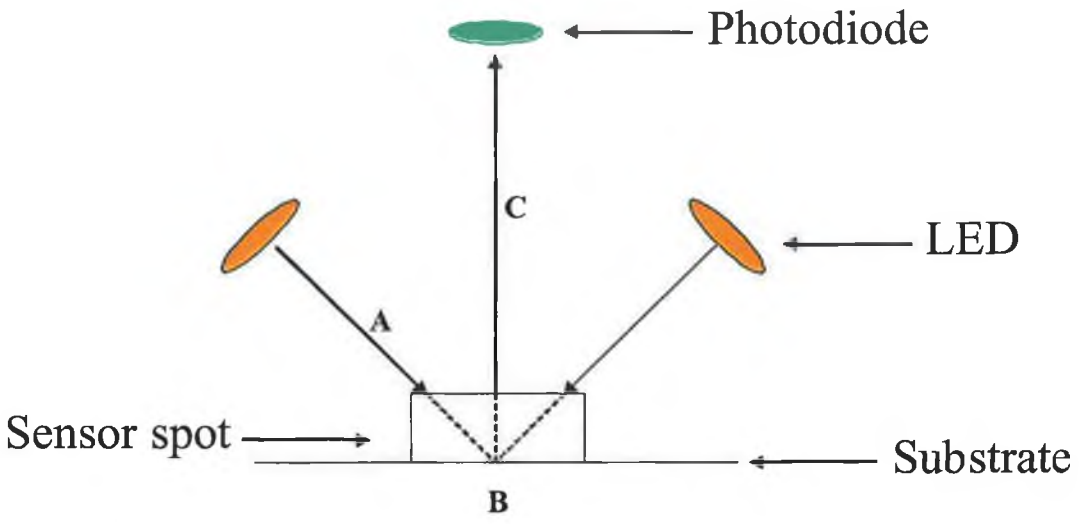

Figure 5.15: The path that light takes from the LED, through the sensor dot, reflected from the substrate onto the photodiode. The diagram is not drawn to scale.

Three key regions are labelled in Figure 5.15. At region A, the light passes from the LED to the region of interest. The black coating within the tube minimises light effects as the light propagates to the sensor dot. The LEDs should be as close to the surface as possible, to reduce any stray light lost to the environment. The device was hand-machined, so there was a limit on the distance that could be used.

At region B, the light passes through the dot and is reflected from the PET substrate. The light from the LEDs is strong enough to penetrate through the sensor, and the light is reflected from the PET along region C to the photodiode. Region B obeys Beer's Law. Changing the thickness of the dot alters the light path length, l. As the dot becomes thicker, less light is reflected back to the photodiode, since more light interacts with the sensor dot. When the dot becomes too thick, the light from the LEDs will not be able to penetrate to the PET; hence, the majority of the reflected

light comes from within the sensor dot (Figure 5.16). This is a limiting thickness, and preparing dots thicker than this has no effect on the amount of light reflected.

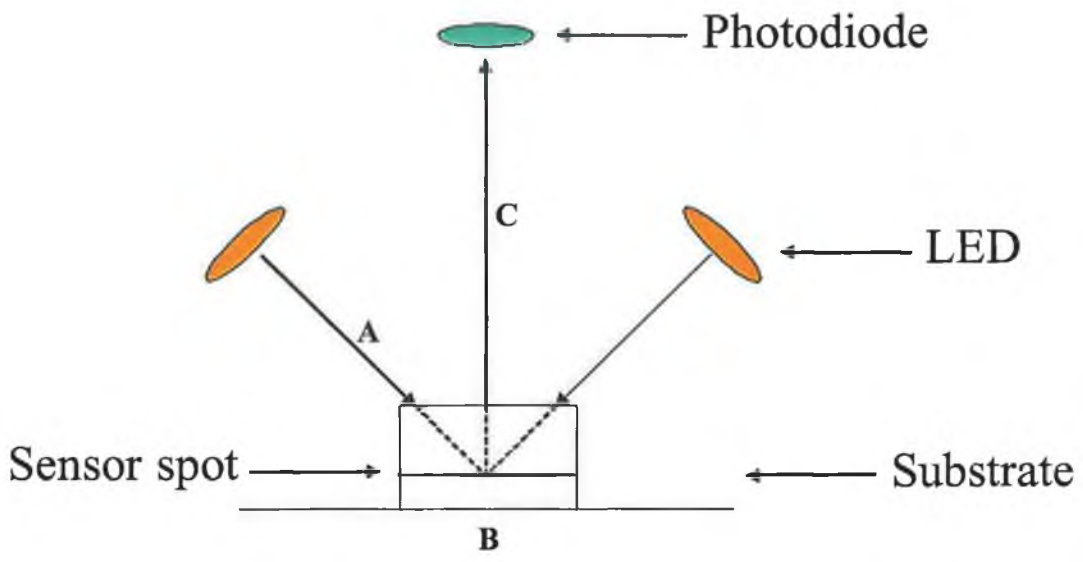

Figure 5.16: A thicker dot results in no light penetrating to the PET substrate. This defines a limiting thickness, beyond which, the reflected light intensity does not change. The diagram is not drawn to scale.

From Figure 5.14, the following effects are noticed:

- The manual sensor production process used works well for producing sensors of varying thickness, as evidenced by the low RSD value.
- As the sensor becomes thicker, the reflected light intensity decreases. This occurs since more light is interacting with the sensor (as it is thicker) and less light is being reflected from the PET substrate.
- There is an inverse linear relationship between the thickness of the sensor and the reflected light intensity.
- This relationship doesn't hold for all thickness values. The limiting thickness is ca. 500 μm. At values greater than this thickness, the vast majority of the light is reflected from within the sensor dot, and hence the thickness essentially becomes independent of the measurement of the reflected light intensity.

- The thickness of the sensor dot has a major effect on the value of the reflected light intensity. Changing the thickness from 100-500 μm causes a decrease in the reflected light intensity of ca. 140 units (> 30 % full scale operation).

It is not possible to coat sensors much thinner than ca. 100 μm using the developed hand-coating technique. In principle, however, as the sensor dots become less thick, more light will reflect from the substrate. However, a thinner film has less dye present, and it may be difficult to measure the colour changes of the sensor using the scanner. There are a number of ways around this. One simple solution is to increase the amount of dye present; this would alter the sensitivity of the sensor response however. Another solution is to modify the design of the scanner. A 16-bit photodiode could be used in place of the 10-bit photodiode, which would give higher signal resolution. The device could also be machined more carefully, with a reduction in the distance that light from the LEDs has to travel. Another approach that could be taken is to include an internal reflector in the sensor formulation. These are typically powders that can be ground finely, and may be added to the bulk solution. Barium sulphide and titanium dioxide are common examples [104]. Adding an internal reflector essentially returns all the light from the LEDs to the photodiode when the light interacts with the reflector. The reflected light intensity of the sensor dots becomes independent of thickness.

It is important from the perspective of sensor design to know the limiting thickness. If sensors are to be printed onto commercial packages, the number of false positives needs to be kept to an absolute minimum. Otherwise, batches of acceptable samples could be considered to have spoiled. Sensors should be produced at thicknesses greater than 500 μm to ensure that values returned by the sensor are not affected by sensor thickness. Another approach that is being considered is to alter the brightness of the LEDs by changing the current that powers them. A reduction in LED intensity will mean that the light will not penetrate as deeply into the sensor. The limiting thickness could thus be made greater or smaller by altering the LED intensity. In summary, the scanner should operate at a greater value than the limiting thickness, since this removes any variation in the measurement due to sensor thickness.

5.4.2 Calibration of sensors with scanner device

The reflected light intensity of the sensors as a function of headspace NH_3 concentration was measured in triplicate using the scanner. Equation 5.1 was used to ratio the reflected intensity values of a sample injection (I) to the reflected intensity value of a blank, i.e. the reflected light intensity when no NH_3 was injected (I_o). A best-fit sigmoid function was fitted to the data using Solver in Microsoft Excel (Figure 5.17), and was similar to the curve that was obtained from the imaging spectrograph.

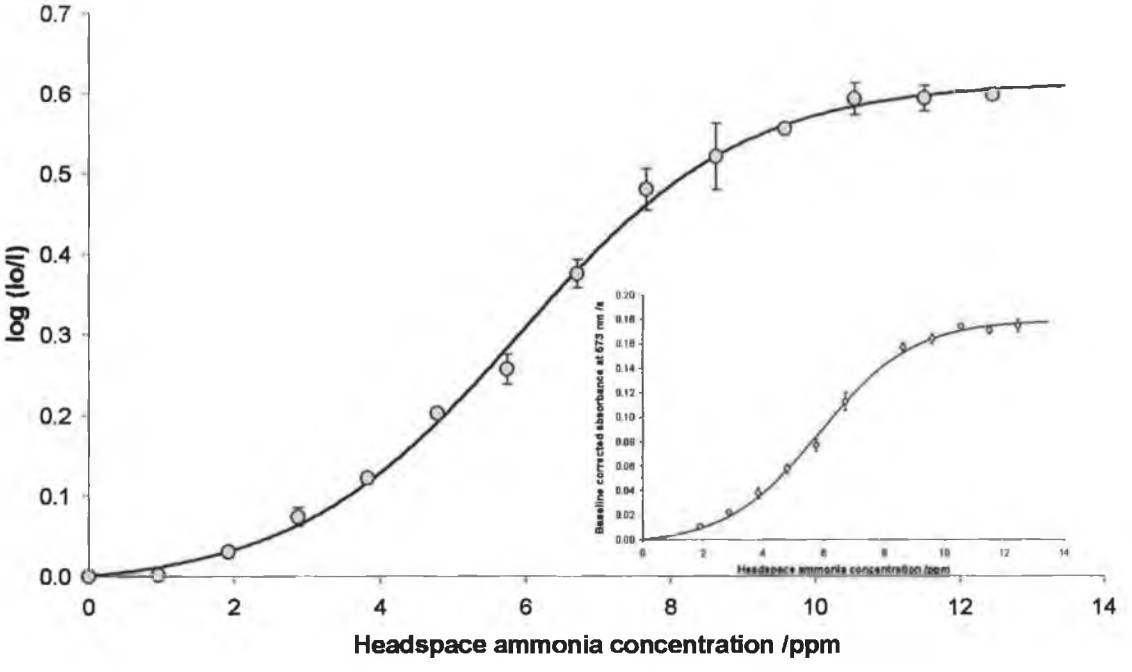

Figure 5.17: The reflected light intensity of the cresol red based pH sensors measured using the scanner as a function of the concentration of NH_3 in the headspace. The error bars are ± standard deviation, where n=3. The SSR of the best-fit curve is 0.0016. An insert of the best-fit curve obtained using the PARISS imaging spectrograph system for the same experimental setup is shown.

The clear similarities between the datasets can be further seen in Table 5.1, where a comparison of values from each best-fit curve is shown. The upper and lower limits of linearity were defined as outside a 5 % tolerance from the best-fit equation for the linear data subset (Figure 5.18). The lower limit of detection of the sensors to NH_3

was defined as three times the standard deviation of the baseline (LOD = 3σ). There is a clear comparison to be drawn between the two datasets. This demonstrates that the scanner can be used instead of the PARISS imaging spectrograph system to determine the reflected light intensity of the sensors.

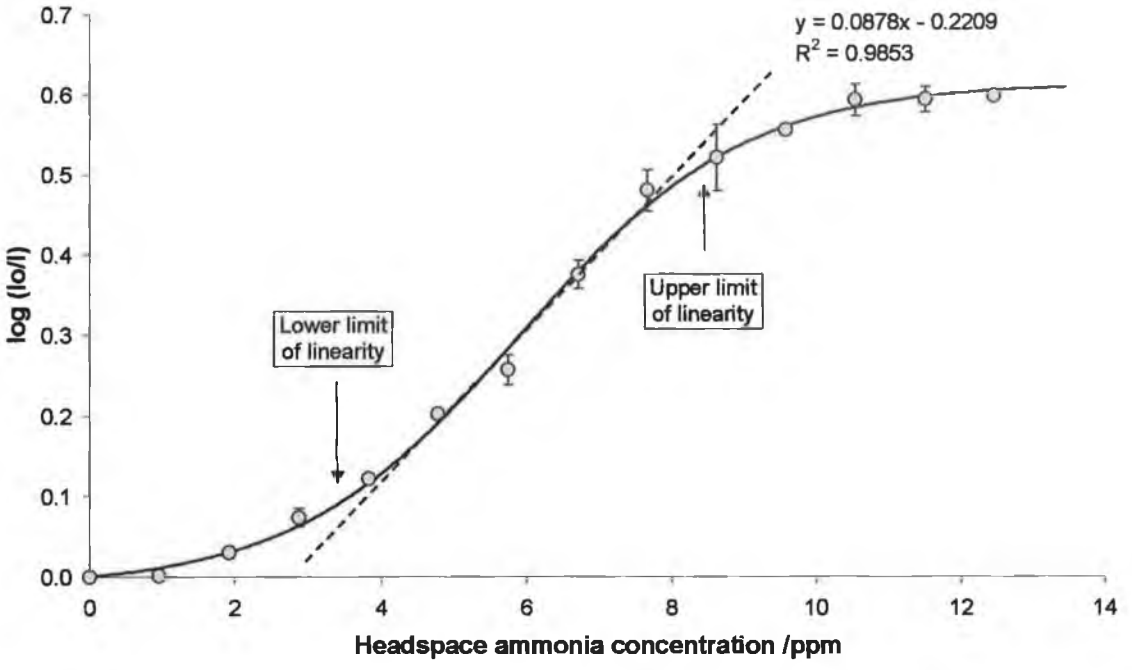

Figure 5.18: The reflected light intensity of the cresol red based pH sensors measured using the scanner as a function of the concentration of NH_3 in the headspace. The error bars are ± standard deviation, where n=3. The upper and lower limits of linearity were defined as outside the 5 % tolerance of deviation from the best-fit linear equation shown.

Parameter	PARISS	Scanner	% Difference
Mid-point of sigmoid curve /ppm	5.86	5.91	0.853
Upper limit of linearity /ppm	8.95	8.90	0.559
Lower limit of linearity /ppm	3.65	3.65	0.000
Lower LOD /ppm	0.35	0.60	71.429
Average RSD	6.45 %	4.07 %	-

Table 5.1: Comparison of best-fit values obtained from the cresol red sensors to headspace NH_3, analysed using both the PARISS system and the handheld scanner device.

The outcome of these results means that a very simple to use and inexpensive handheld portable colour scanner can be used instead of a laboratory-based reference measurement system to determine the reflected light intensity of the developed sensors. This has a clear attractiveness from both a research and commercial point of view, and aids the development of a fish spoilage sensor system immensely. It also has implications on other research that is based on colour intensity measurements, and should be incorporated into other projects that may or may not be related to the main theme of this thesis.

5.4.3 Relationship of scanner to threshold of spoilage

In Chapter 4, the link between the microbial populations of a sample and the sensor response was established. The response of the sensor at two critical regions was identified; one where the sample was beginning to spoil, i.e. an early warning of spoilage, and the second where the sample was fully spoiled and unsuitable for human consumption. Calibrating the sensor dots against NH_3 in headspace, and monitoring the resultant changes using both the PARISS imaging spectrograph system and the scanner helped determine the reflected light intensity at the thresholds of spoilage.

The threshold values measured by the PARISS system from the microbial population study of cod were 0.0296 au and 0.0835 au at the early warning of spoilage and at a fully spoiled level respectively. These values were placed into the best-fit curve fitted to the PARISS system data shown in Figure 5.17, to determine the concentrations of NH_3 in headspace that were required in order to generate an equivalent sensor response. The spectral values obtained at the point of spoilage allowed the colour of the sensors measured as reflected light intensity at these critical regions to be identified:

- The early warning of spoilage occurs where absorbance at 573 nm is 0.0296 au. The same approximate absorbance (0.0302 au) was seen in the PARISS

system calibration at 3.6 ppm headspace NH_3 exposure. The colour at this same region, measured as a reflected intensity by the scanner, is 0.1011 (log value). From Equation 5.1, the reflected light intensity at this region is 476 ± 19.4 bits, where n=3. Visually, the dye is orange at this point.

- When the sample has become fully spoiled, the absorbance at 573 nm is 0.0835 au. The same approximate absorbance (0.0826 au) is seen from the PARISS system calibration at 5.7 ppm headspace NH_3 exposure. The colour at this same region, measured as a reflected intensity by the scanner, is 0.2782 (log value). From Equation 5.1, the reflected light intensity at this region is 317 ± 12.9 bits, where n=3. Visually, the dye is light purple at this point.

This data is summarised in Table 5.2.

Analysis method	Early warning of spoilage	Sample is fully spoiled
PARISS /au	0.0296	0.0835
Scanner /bit numbers	476 ± 19.4	317 ± 12.9
Visual Inspection	Light orange	Light Orange - Purple

Table 5.2: Reflected light intensity at the thresholds of spoilage.

Hence, three regions of interest have been identified. When the scanner output is greater than ca. 476 bits, the sample has not yet begun to spoil, and is fine for consumption. When the scanner reading is between ca. 476 and ca. 317 bits, the fish sample is not yet fully spoiled, but should be flagged for quick sale or consumption. Finally, when the scanner reading is less than ca. 317 bits, the sample should no longer be consumed. This information is shown graphically in Figure 5.19.

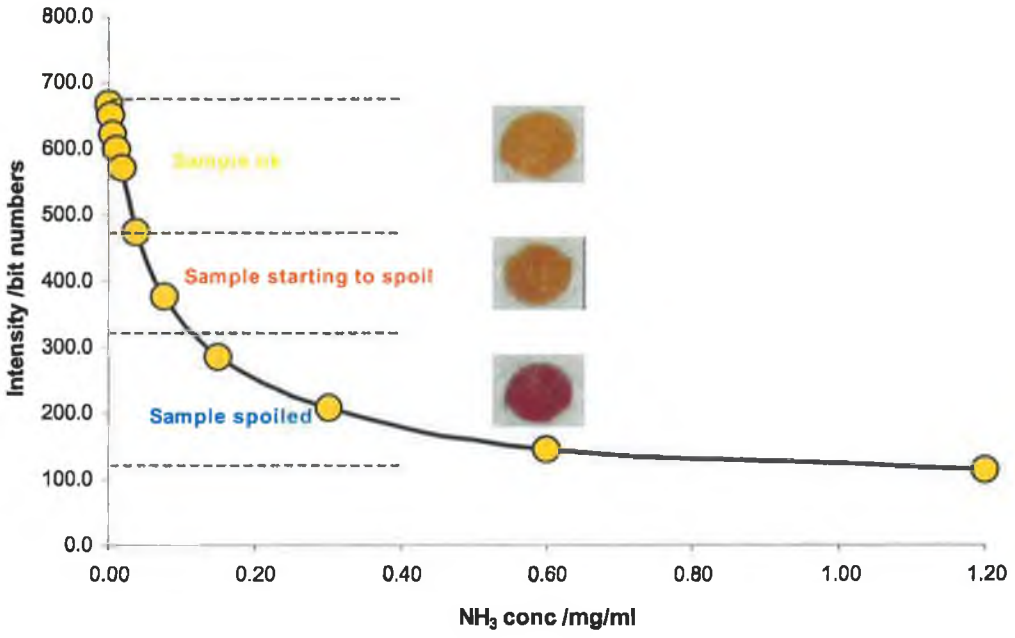

Figure 5.19: The relationship between the sensor response, measured as a reflected intensity by the scanner, and the microbial populations from Section 4.3.5. The sensor colour at each of the limits is shown approximately by the colour of the text, and by the inset photographs.

These three regions could easily be expressed as a warning system based on red, amber and green coloured lights, either in software or LEDs built into the hardware. The green light (value > 476 bits) tells the user the sample is fine, the amber light (476 bits > value > 317 bits) tells the user to quickly sell or consume the product, and the red light (value < 317 bits) tells the user to dispose of the sample, as it should not be consumed or sold. Hence, it is possible to relate the colour of a packaged sensor, the colour of which is determined by the scanner, to microbial populations and hence to the spoilage level of a sample.

5.4.4 Testing sensors and scanner with real fish samples

The results obtained in this section are split into two sub-sections for clarity, as there were some concerns with the results obtained for the first batch of samples tested that were resolved for the second batch of samples tested.

5.4.4.1 First batch of samples tested

There was a clear issue during the spoilage experiment of the first batch of samples tested that amines were leaking into the surrounding environment. Noxious odours were readily detectable, and the sensor response to the samples was poor. If the packaging is not sealed correctly and amines are escaping to the environment, then the sensors cannot give a representative picture of the degree of spoilage of a sample, since the sensor does not react with all the amines released. This is a clear issue that needs to be addressed before sensors are printed onto commercial fish packaging; the packaging needs to be gas-tight to ensure successful reaction of all amines released with the sensor. Another sensor that can be placed alongside the fish spoilage sensor that detects if a package has ruptured could be beneficial in this area.

Nevertheless, some worthwhile results were obtained from this set of experiments. Figure 5.20 shows that the sensors monitoring the smoked coley and kipper samples did not respond over the 160-hour time period of spoilage. Considering that this is ca. 90 hours after the use-by date on the package, it verifies that the sensor doesn't respond to smoked fish.

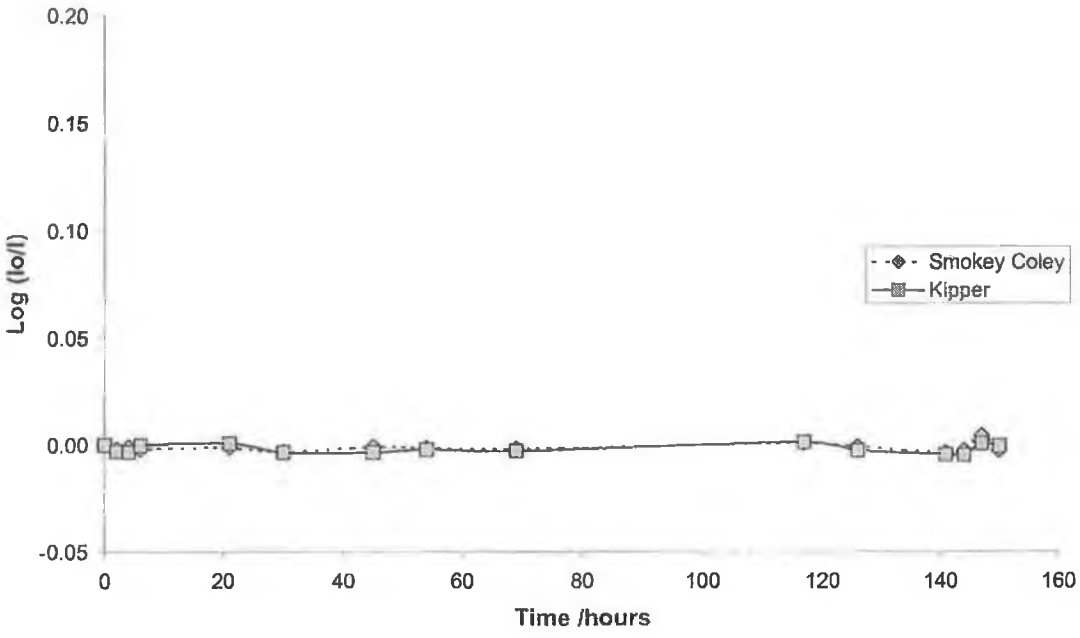

Figure 5.20: The response of the sensors monitoring two smoked fish samples measured using the scanner. The error bars are ± standard deviation, where n=3 (masked by symbols). Clearly neither fish sample causes a significant sensor response.

The sensor response for the remaining three fish samples is shown in Figure 5.21. The dashed lines, for visual aid only, show that the sensors are responding much later than expected. From the beginning of the experimental procedure, there was a clear smell of amines that became stronger over time, and this is unacceptable from an experimental point of view. Figure 5.22 shows the colour of the sensor monitoring the plaice sample after 160 hours, which further demonstrates that the amines leaked to the environment, since the sensor should by this time have changed in colour (as described in Figure 5.19).

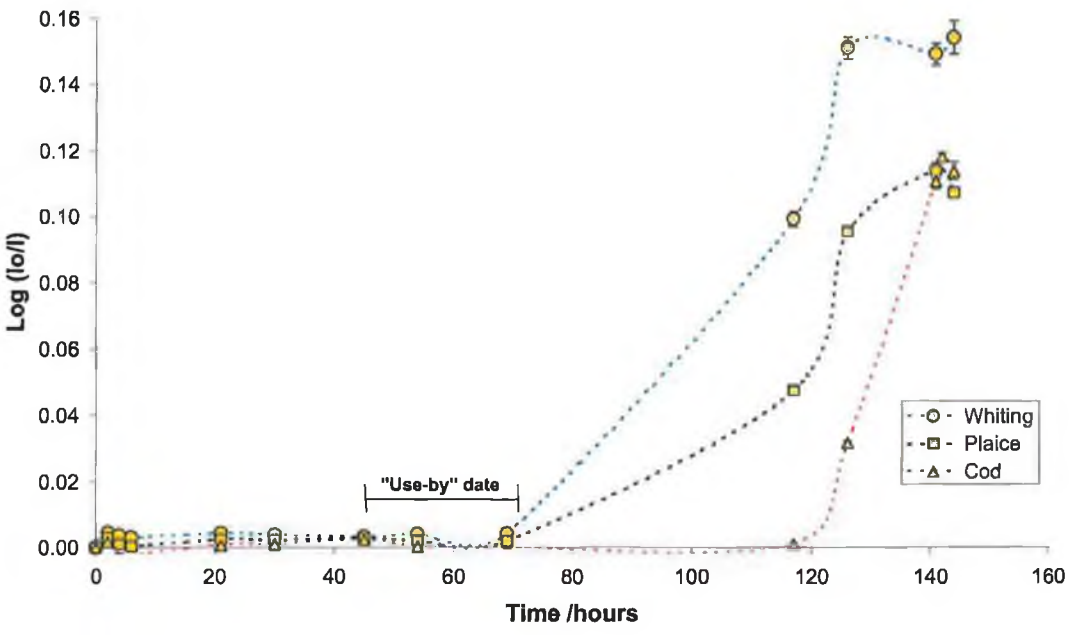

Figure 5.21: The response of the sensors monitoring three fish samples measured using the handheld scanner device. The error bars are ± standard deviation, where n=3. The dashed lines are for visual aid only.

Figure 5.22: The plaice fillet with sensor after 160 hours has clearly not reacted well with the amines released from the spoiling sample. At this stage of the experiment, there was water being released from the fish sample into the packaging environment and a noxious smell of amines, i.e. the sample has clearly spoiled. Compared to Figure 5.7, the sample is darker in colour, although the sensor dot is the same colour.

5.4.4.2 Second batch of samples tested

The issue of leaking amines was resolved here by simply covering each fish sample with extra rolls of cling film.

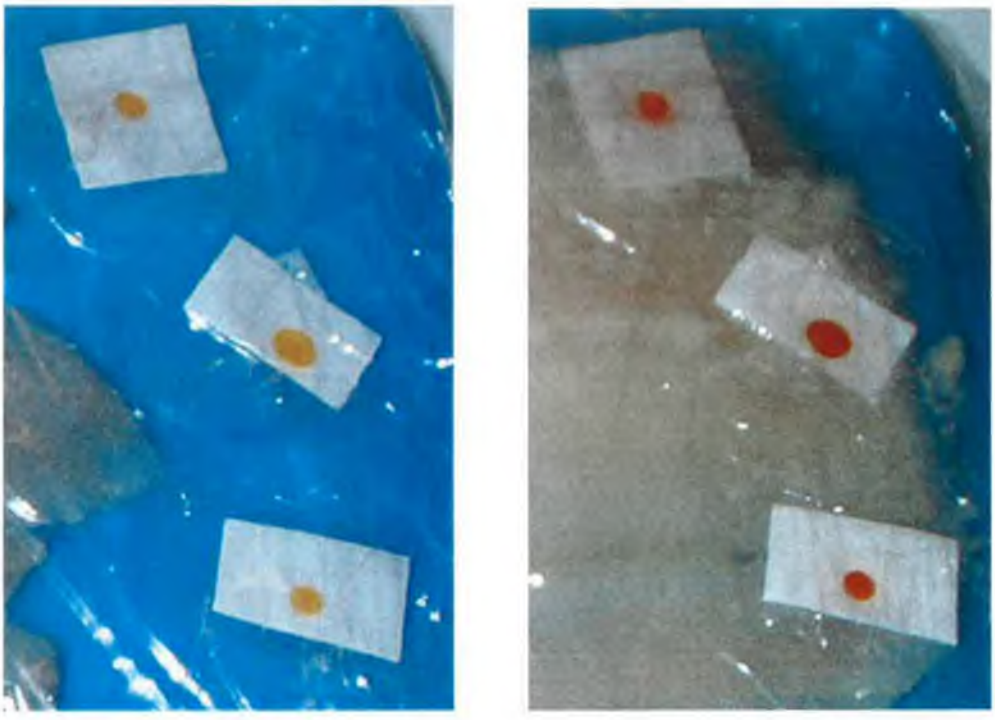

Figure 5.23: The sensors monitoring the whiting samples at time zero and time 60 hours. At time zero, the sensors are yellow, and after 60 hours at 4 °C, the sensors are dark red, indicating that the samples have spoiled.

Figure 5.23 shows the three sensors that were used on the whiting fillets at time zero and after 60 hours of refrigerated storage. There was no discernable smell of amines during the experimental timeframe, and the sensor performance is clearly much better than in the previous section.

The results from the cod samples tested are shown in Figure 5.24. The regions of early warning of spoilage (region "a") and fully spoiled (region "b") are clearly marked, and correlate to the "use-by" date printed on the packaging.

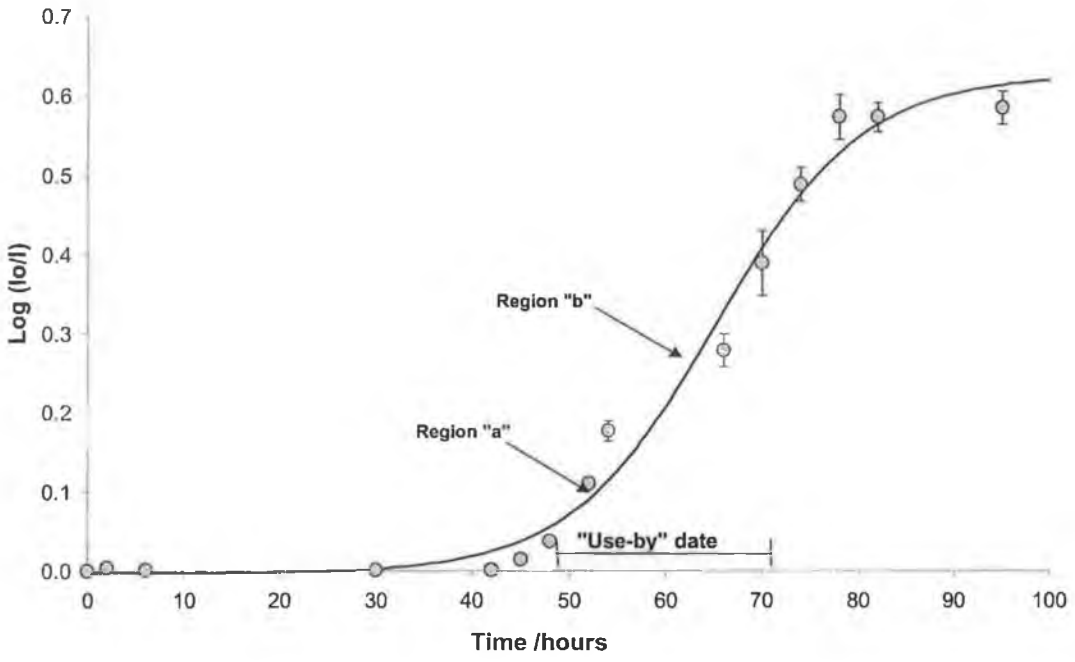

Figure 5.24: The response of the sensors monitoring three cod samples measured using the handheld scanner device. The error bars are ± standard deviation, where n=3. The SSR of the best-fit curve is 0.0188, and the mid-point of the inflection on the rise is 65.15 hours. The two regions of spoilage ("a" and "b") clearly fall into the use-by date region printed on the packaging.

These results are extremely positive. They show, for the first time, that the scanner used in combination with the cresol red based sensors can accurately determine the point of spoilage. Rather than this being a large window (i.e. 48-72 hours from the time of purchase), it is pinpointed much more precisely.

The correlation in Chapter 4 between the microbial populations of a sample and the sensor response, which allowed the link to be inferred using the scanner, was only established for the cod species. According to Section 1.5.3, the ratios of amines comprising TVB-N are species dependant and appear not to relate to the type of microorganisms that cause spoilage. Hence, the sensor response at the threshold of spoilage could change for different species. Accordingly, the sensor should in principle be recalibrated for each and every species of interest. There are advantages

and disadvantages to this. Clearly it is laborious and requires much routine work to build up a library of calibrations, however on the plus side, the user ends up with a sensor that can potentially be used for many different species of interest.

The results from the haddock samples tested are shown in Figure 5.25. No microbial analysis of haddock was performed but, as a white fish similar in appearance and physical constitution to cod [105], it was likely that the sensor would respond well to this fish. The regions of spoilage again fall inside the use-by date window. The value for the mid-point of the inflection for haddock, compared to cod, suggests that both sets of samples spoiled very similarly.

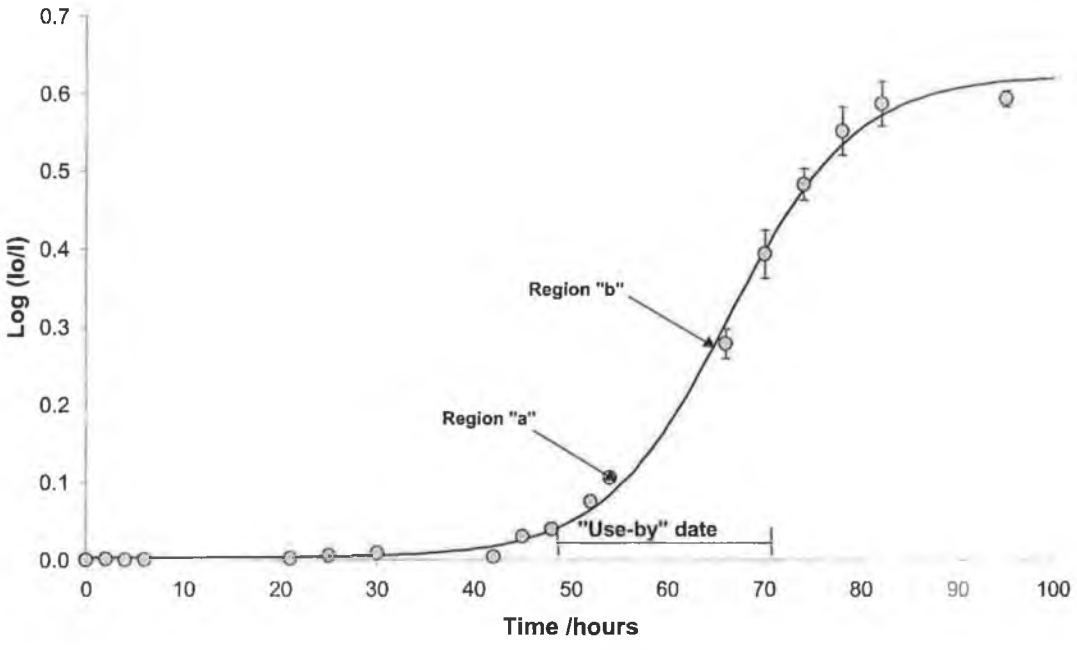

Figure 5.25: The response of the sensors monitoring three haddock samples measured using the handheld scanner device. The error bars are ± standard deviation, where n=3. The SSR of the best-fit curve is 0.0026, and the mid-point of the inflection on the rise is 66.36 hours. Once again, the two regions of spoilage ("a" and "b") clearly fall into the use-by date region printed on the packaging.

The results from the whiting samples are shown in Figure 5.26. The release of amines from whiting occurs at a faster rate than cod [82], and this explains the faster rise of the best-fit sigmoid curve. The mid-point of inflection on the rise was ca. 10

hours earlier than for the cod or haddock samples. These data highlight that the sensor needs to be re-calibrated for each species of interest, if these species release amines at a different rate than cod. However, even for a species that releases amines much faster than cod, the sensor change can still be seen clearly.

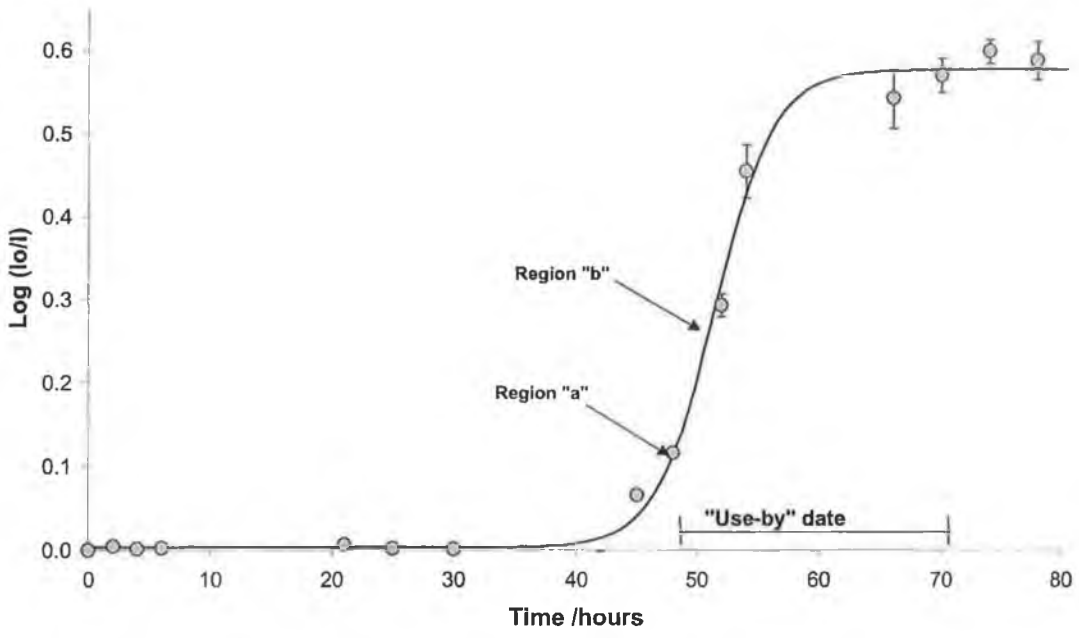

Figure 5.26: The response of the sensors monitoring three whiting samples measured using the handheld scanner device. The error bars are ± standard deviation, where n=3. The SSR of the best-fit curve is 0.0042, and the mid-point of the inflection on the rise is 51.48 hours. The release of amines from whiting is faster than cod. However, the two regions of spoilage highlighted still correlate well with the use-by date.

In summary, the results shown demonstrate that the handheld scanner is a highly useful analysis tool for colour measurements of cresol red sensors applied to the determination of spoilage in packaged fish.

5.5 Conclusions

A prototype device has been developed that can readily measure the diffuse scattered light intensity from a surface. The design of the device is neat, compact and inexpensive, and has features that ensure true portability. 2 identical yellow LEDs at 45° to the measurement aperture are located in the device, and they converge when placed in contact with a surface. The λ_{max} of the LEDs was determined to be ca. 570 nm, very close to the λ_{max} of the basic form of cresol red. Calibration of the scanner showed that it generates results that are comparable to a benchtop instrument. The sensor dot has a limiting thickness of ca. 500 μm with the current scanner setup used. Above this thickness, almost all of the light is reflected from within the sensor dot, and not from the substrate, resulting in a sensor measurement becoming independent of sensor thickness. The reflected light intensity at the thresholds of spoilage were determined, and calibration of the sensors against headspace NH_3 demonstrated that the data obtained is comparable to data from the imaging spectrograph (PARISS) system. Excellent time-correlations were established between the reflected light intensity at the thresholds of spoilage and the "use-by" date printed on a number of real fish samples that were tested.

The clear point to be made here is that the scanner is a generic colour measurement device that can easily determine the reflected light intensity from any surface, although it has been designed for monitoring the cresol red sensors. The λ_{max} of the LED suits many pH indicator dye chemistries, or indeed any colour that is orange - red - purple. One concept considered in the design phase is to create a "sensor head" that can readily be replaced, e.g. by a screw-type connection. Each sensor head would be identical in design, but would simply contain different LEDs at different required λ_{max} values. The user then simply needs to remove one head and replace it with another. This approach ensures that the design can be applied to many applications that require analysis of colour. The signal-to-noise ratio could be further improved by placing the amplifier circuit into the sensor head, sending an amplified signal straight to the microcontroller box. A reference measurement should be included in the next generation design, e.g. LEDs to measure the wavelength maxima

of both the acidic and basic forms, and to measure to isobestic point of the dye, which can be used as an internal reference, since by definition, it doesn't shift as the dye changes from one form to another.

Additionally, the circuitry may be battery-operated, and there is some RAM in the microcontroller box, along with a switch circuit. A button can simply be added to the box that is taken for in-field analysis, connected to a required sensor head. When the user presses the button, the reflected light intensity (including the subtracted blank when the LEDs are pulsed) is stored in the memory, with an address to distinguish individual values. The user can store several hundred values in the box, and then connects this to a PC or laptop, or any communications device, to download the entire data that was collected. This level of flexibility and ease of use ensures that the device has a wide-ranging applicability in the generic field of colour measurement science.

6 Overview, Trends and Future Work

An optical sensor was produced that can monitor the headspace levels of volatile amines released from gradually spoiling fish samples. The sensor is based on cresol red, which is sensitive to changes in pH of the sample headspace, physically entrapped into a cellulose polymer binder. A comprehensive review was provided in Chapter 1 of the background to the work performed in this thesis. Areas that were covered included chemical sensors, and in particular, optical sensing. The fundamentals of UV-Vis spectroscopy and pH sensing were explained, with a substantial section devoted to pH indicator dye chemistry. Various applications of pH indicators were covered, with an emphasis on methods of immobilisation of indicator dyes on solid substrates for pH measurements. The ever-expanding area of seafood spoilage monitoring was covered, with a review of well-established techniques for freshness and spoilage determinations, and up-to-date research to quantify TVB-N levels. The overall aim of this chapter was to introduce the reader to the concept of an on-package sensor that could be used for non-invasive quality control of fish samples.

Chapter 2 detailed the development of the cresol red based sensor itself. It focussed on the optimisation of the sensor formulation, and the characterisation and calibration of the sensor. A detailed description of the operation of the imaging spectrograph (PARISS system) was provided; this measurement system offered an excellent means to obtain data for all of the chapters that followed. A number of different formulations were tested, and this included varying the ratio of binder to plasticiser, the plasticiser used, the concentration of dye in the sensor, the solvent used and the drying conditions of the sensor dots after drop-coating onto PET substrate. An optimised procedure was developed that used 0.2 % w/v cresol red dye (sodium salt) in 3 % w/v cellulose acetate, with 3 % v/v dibutyl phthalate, in a mixture of 1:1 acetone:cyclohexanone. The sensors dried best in a sealed environment that was saturated with acetone vapour to control the rate of drying of the formulation. The pK_a of the dye was shown not to shift considerably when trapped in the cellulose acetate film, compared to the value obtained in free solution. The pK_a of the dye was also shown not to significantly shift at refrigerated temperature, compared to room temperature. Calibration of the sensors against

headspace NH_3 showed that the sensors have a lower LOD (at 3σ) of 0.35 ppm, with a linear response between 3.65-8.95 ppm headspace concentration. On the basis of these results, the sensor was proposed for monitoring of volatile amines released from real fish samples.

Chapter 3 demonstrated the first set of results that used the sensor developed in Chapter 2 for monitoring the release of volatile amines from real fish samples. A number of different species were tested, each with different catch profiles and histories. A system that can monitor up to 24 samples in parallel was developed. It was clear that the sensor incorporated into a package needs to be gas-tight in order to obtain satisfactory data and prevent amines leaking into the surrounding environment. Nevertheless, the data from this chapter clearly shows that the sensor responds to the changing levels of headspace amines. The sensor packaging was further refined to eliminate the issue of leaking amines, and was tested against different deepwater fish species. The results suggest that the response of the sensor gives information pertaining to the history and condition of the samples.

Chapter 4 took this data several steps forward, by successfully establishing, for the first time, a time-correlation between the sensor response, the headspace TVB-N levels and the microbial populations of a spoiling sample. The sensor response was shown to be very reproducible, with an RSD of ca. 3 % (n=15). An excellent source of fresh cod and plaice samples was traced, and this aided the project development immensely. The EU method for determination of TVB-N levels of a seafood sample was modified to allow the headspace TVB-N levels to be determined. These were shown to follow the changing dynamics of the sensor response as a function of time. The pseudomonas species and the TVC levels were also shown to correlate over time with the sensor response, and this allowed the sensor response at the thresholds of spoilage to be identified. Interestingly, it appears that the sensor is capable of indicating an early warning of spoilage, in this case, ca. 10 hours before complete spoilage at room temperature for the cod species. The sensor responded from yellow (no response) to pale orange (early warning of spoilage) to dark red to purple (sample fully spoiled).

Chapter 5 combined data from the previous chapters to develop a handheld portable scanner that gives a measurement of the diffuse scattered light intensity from a surface. It is based on 2 yellow LEDs and a photodiode at 90° to the measurement area, and a full explanation of the operation of the device was given. Through a series of calibrations of the scanner, it was shown to offer intensity data that was comparable to reflectance data from the PARISS system. A study of the effect of sensor thickness on the reflected light intensity showed that the sensor has a limiting thickness of ca. 500 μm. The response measured by the scanner at the thresholds of spoilage was determined. Some supermarket-purchased samples were tested using the sensor/scanner combination. An excellent correlation between the "use-by" dates printed on the packaging and the sensor response at the spoilage thresholds was established. To conclude overall, the sensor is performed excellently for the task at hand, and the project has been seen through from conception to producing a working sensor that correlates to the level of spoilage of a packaged seafood sample.

There are a number of areas to be targeted for future works in this project. The sensor may be incorporated directly onto the packaging. If so, packaging technologies need to be investigated to consider the best way forward. For example, the sensor could be printed by the manufacturers onto the packaging, or it could be placed on the outside of the package and exposed to headspace volatiles through a small gas-sampling port. There is much scope in this area for further research. There are issues about placing a chemical sensor in close proximity with foodstuffs, e.g. the leaching of the sensor material onto the food sample, which could occur in the event of large amounts of condensation building up on the packaging during storage. Toxicity data needs to be collected and validated before any commercial applications of the sensor can be considered. Furthermore, a number of different scanner devices should be built and tested, in order to determine any statistical differences between different scanners.

One additional area that we are fully aware of relates to how much information should be provided to the consumer. This is an on-going discussion that has many interesting viewpoints, and has extreme relevance for potential commercial partners. In a sense, this is outside the remit of this thesis, but nevertheless is an important

point to note. The sensor response also needs to be recalibrated for different species of interest, since different species release different levels of volatile amines during spoilage. One particular area that is recommended for further study is the early-warning spoilage window. The dye chemistry could be tweaked, for example, to make the sensor more sensitive to this region, and potentially could detect spoilage much earlier than is presently possible. Additionally, adding small amounts of a substance that reacts with amines, e.g. a weak acid, could extend the working range. This would react with the TVB-N released during the early stages of spoilage; thus the sensor would only respond at higher concentrations. This may not be necessary for fish spoilage monitoring, but it may be of interest as future work development of an ammonia gas sensor. All in all, these are just some of the areas of further research that are recommended to be performed.

These are exciting times for research in the sciences. Many of the points raised in this thesis are hinting at some of the areas that the sciences are achieving. By way of example, the following are the areas of Sixth Framework EU funding that were recently announced for all EU member states, covering 2002-2006:

- Life sciences
- Nanotechnologies
- Aeronautics and space
- Citizens & governance in a knowledge-based society
- Sustainable development
- Information society technologies
- Food quality and safety

There is a proposed budget of € 17.5 billion to be distributed across each of these seven areas, in order of differing priorities. Food quality and safety, for example, is expected to receive € 685 million during the four year period. This is to cover seven key areas, which include traceability processes all along the distribution chain (given the term "from the farm to the fork") and methods of analysis, detection and control of food safety and quality. These are relevant to the work performed in this thesis.

The EU white paper (2000) on food safety emphasises the international dimension of food quality, and describes how the EU is the world's largest importer and exporter of food. The areas of food safety and control are global issues that are rightly being addressed. The EU has recognised the debate about the availability of information under food quality and safety, and has invited proposals under the area of "communication: a challenge and a duty". This addresses the clear points that are relevant to anybody working in the field of food safety.

€ 3,625 million is expected to be budgeted for the area of information society technologies, which includes "the all-communicating world" and "the age of ambient intelligence". Many of these aspects are being reflected in current trends in sensor developments. Various projects are striving to produce sensing technologies that are capable of autonomous communication that can integrate as seamlessly as possible with current technologies, e.g. wearable sensors, to mention but one example. The future for chemical sensing is clear. Low-cost sensors that can generate large volumes of data are increasingly of interest across many research groups worldwide. Devices are becoming smaller, to a point where they can be hidden in the background of our daily lives. Research into chemical sensing is at present stimulating and exciting, and will continue to be a main player in the sciences over the coming years.

References

1 Diamond, D., *Principles of Chemical and Biological Sensors,* Wiley Inter-Science, New York, USA, 1998, p. 2.

2 Diamond, D., *Principles of Chemical and Biological Sensors,* Wiley Inter-Science, New York, USA, 1998, p. 235.

3 Janata, J., *Principles of Chemical Sensors*, Plenum Press, London, UK, 1989, p.3.

4 Janata, J., *Principles of Chemical Sensors*, Plenum Press, London, UK, 1989, p.39

5 Janata, J., *Principles of Chemical Sensors*, Plenum Press, London, UK, 1989, p.55.

6 Janata, J., *Principles of Chemical Sensors*, Plenum Press, London, UK, 1989, p.81.

7 Diamond, D., *Principles of Chemical and Biological Sensors,* Wiley Inter-Science, New York, USA, 1998, p. 19.

8 Wolfbeis, O. S., *Fibre-Optic Chemical Sensors and Biosensors* (Volume 1), CRC Press, London, UK, 1991, p. 2-4.

9 Wolfbeis, O. S., *Fibre-Optic Chemical Sensors and Biosensors* (Volume 1), CRC Press, London, UK, 1991, p. 10-13.

10 Janata, J., *Principles of Chemical Sensors*, Plenum Press, London, UK, 1989, p.241-250.

11 http://micro.magnet.fsu.edu/primer/java/electromagnetic/ [last accessed 25-10-2002].

12 Willard, H.H., Merritt, L.L., Dean, J.A. and Settle, F.A., *Instrumental Methods of Analysis* (7th Edition), Wadsworth Publishing Company, California, USA, 1988, p. 98.

13 Diamond, D., *Principles of Chemical and Biological Sensors,* Wiley Inter-Science, New York, USA, 1998, p. 204-206.

14 Skoog, D.A and West, D.M., *Fundamentals of Analytical Chemistry* (7th Edition), Saunders College Publishing, Philadelphia, USA, 1996, p. 392.

15 Bates, R.G., *Determination of pH: Theory & Practice* (2nd Edition), Wiley & Sons, New York, USA, 1973, p. 171.

16 Bates, R.G., *Determination of pH: Theory & Practice* (2nd Edition), Wiley & Sons, New York, USA, 1973, p. 17.

17 Bishop, E., *Indicators*, Pergamon Press, Oxford, UK, 1972, p. 65-75.

18 Bates, R.G., *Determination of pH: Theory & Practice* (2nd Edition), Wiley & Sons, New York, USA, 1973, p. 341.

19 Tilley, R., *Colour and the Properties of Materials*, Wiley & Sons, New York, USA, 2000, p. 180-194.

20 Green, F.J., *The Sigma-Aldrich Handbook of Stains, Dyes and Indicators*, Sigma-Aldrich Corporation, Wisconsin, USA, 1991.

21 Cotton, F.A., Wilkinson, G., Gaus, P.L., *Basic Inorganic Chemistry* (3rd Edition), Wiley & Sons, New York, USA, 1995, p. 74.

22 Wolfbeis, O. S., *Fibre-Optic Chemical Sensors and Biosensors* (Volume 1), CRC Press, London, UK, 1991, p. 306-308.

23 Leiner, M.J.P. and Hartmann, P., *Sensors and Actuators B*, 1993, **11**, 281-289.

24 Diamond, D., *Principles of Chemical and Biological Sensors,* Wiley Inter-Science, New York, USA, 1998, p. 220.

25 Lin, J., *Trends in Analytical Chemistry*, 2000, **9**, 541-552.

26 Diamond, D., *Principles of Chemical and Biological Sensors,* Wiley Inter-Science, New York, USA, 1998, p. 195.

27 Wolfbeis, O. S., *Analytical Chemistry*, 2002, **74**, 2663-2678.

28 Serra, G., Schirone, A. and Boniforti, R., *Analytica Chimica Acta*, 1990, **232**, 337-344.

29 Koronczi, I., Reichert, J., Ache, H-J., Krause, C., Werner, T. and Wolfbeis, O.S., *Sensors and Actuators B*, 2001, **74**, 47-53.

30 Barnard, S.M. and Walt, D.R., *Nature*, 1991, **353**, 338-340.

31 Dickinson, T.A., White, J., Kauer, J.S. and Walt, D.R., *Nature*, 1996, **382**, 697-700.

32 White, J., Kauer, J.S., Dickinson, T.A. and Walt, D.R., *Analytical Chemistry*, 1996, **68**, 2191-2202.

33 Albert, K.J., Walt, D.R., Gill, D.S. and Pearce, T.C., *Analytical Chemistry*, 2001, **73**, 2501-2508.

34 Diamond, D., *Principles of Chemical and Biological Sensors,* Wiley Inter-Science, New York, USA, 1998, p. 223-226.

35 Lin, J. and Liu, D., *Analytica Chimica Acta*, 2000, **408**, 49-55.

36 Cho, E.J. and Bright, F.V., *Analytical Chemistry*, 2002, **74**, 1462-1466.

37 Lobnik, A., Majcen, N., Niederreiter, K. and Uray, G., *Sensors and Actuators B,* 2001, **74**, 200-206.

38 Makote, R. and Collinson, M.M., *Analytica Chimica Acta*, 1999, **394**, 195-200.

39 Nicholson, J.W., *The Chemistry of Polymers*, Royal Society of Chemistry, Cambridge, UK, 1991, p. 21.

40 Dybko, A., Wróblewski, W., Maciejewski, J., Romaniuk, R. and Brzózka, Z., *Sensors and Actuators B*, 1997, **38-39**, 207-211.

41 Nicholson, J.W., *The Chemistry of Polymers*, Royal Society of Chemistry, Cambridge, UK, 1991, p. 51-56.

42 Jones, T.P. and Porter, M.D., *Analytical Chemistry*, 1988, **60**, 404-406.

43 Kostov, Y., Tzonkov, S., Yotova, L. and Krysteva, M., *Analytica Chimica Acta*, 1993, **280**, 15-19.

44 Mohr, G.J. and Wolfbeis, O.S., *Analytica Chimica Acta*, 1994, **292**, 41-48.

45 Safavi, A. and Abdollahi, H., *Analytica Chimica Acta*, 1998, **367**, 167-173.

46 Wróblewski, W., Roznіecka, E., Dybko, A. and Brzózka, Z., *Sensors and Actuators B*, 1998, **48**, 471-475.

47 Cardwell, T.J., Cattrall, R.W., Deady, L.W., Dorkos, M. and O'Connell, G.R., *Australian Journal of Chemistry*, 1995, **48**, 1081-1087.

48 Cardwell, T.J., Cattrall, R.W., Deady, L.W., Dorkos, M. and O'Connell, G.R., *Talanta*, 1993, **40**, 765-768.

49 EU directive 79/112/EEC, available from:
http://biosafety.ihe.be/GB/Dir.Eur.GB/FF/79_112/79_112.html [last accessed 12-06-2002].

50 Dalgaard P., *Freshness, Quality and Safety in Seafood*, Flair Flow Europe, F-FE 380A/00, 2000.

51 Bolta, J.R., *Evaluation of Seafood Freshness Quality*, VCH, 1995, p.180.

52 EU directive 91/493/EEC, available from:
http://europa.eu.int/comm/fisheries/doc_et_publ/factsheets/legal_texts/sani_en.htm
[last accessed 12-06-2002]

53 Larsen, P., Heldbo, J., Jespersen, M. and Liston, J., *Quality Assurance in the Fish Industry*, Elsevier, Amsterdam, The Netherlands, 1992, p. 351.

54 http://www.qim-eurofish.com [last accessed 26-11-2002]

55 Olafsdóttir, G., Martinsdóttir, E., Oehlenschlager, J., Dalgaard, P., Jensen, B., Undeland, I., Mackie, I.M., Henehan, G. and Nielsen, J., *Trends in Food Science and Technology,* 1997, **8**, 258-265.

56 Austin, B. and Austin, D.A., *Methods for the Microbiological Examination of Fish and Shellfish*, John Wiley & Sons, New York, USA, 1989, p. 23.

57 Jay, J.M., *Modern Food Microbiology*, Chapman & Hall, UK, 1992, p. 201.

58 Jay, J.M., *Modern Food Microbiology*, Chapman & Hall, UK, 1992, p. 221-224.

59 Prescott, L.M., Harley, J.P. and Klein, D.A., *Microbiology* (2nd Edition), W.C. Brown, Iowa, USA, 1993, p. 113-114.

60 Department of Health, *Microbiological Guidelines for Meat and Meat Products, Milk, Cream, Ice Cream, Eggs and Fish*, Dublin, Ireland, 1992.

61 Seaver, M., *Microbiological Standards and Guidelines for Fish and Fishery Products*, WEFTA, The Netherlands, 1999.

62 Air Products, *Principle Food Spoilage and Food Poisoning Microorganisms,* available from:
http://www3.airproducts.com/freshline/principle_food_organisms.html [last accessed 30-07-2002].

63 Jørgensen, B.R., Gibson, D.M. and Huss, H.H., *International Food Microbiology*, 1998, **6**, 295-307.

64 Food and agriculture organisation, available from:
http://www.fao.org/docrep/v7180e/V7180E0h.htm [last accessed 30-07-2002].

65 EU directive 95/149/EEC, available from:
http://europa.eu.int/comm/fisheries/doc_et_publ/factsheets/legal_texts/sani_en.htm [last accessed 12-06-2002].

66 Béné, A., Fornage, A., Luisier, J.L., Pichler, P. and Villettaz, J.C., *Sensors and Actuators B*, 2001, **72**, 184-187.

67 Béné, A., Hayman, A., Reynard, E., Luisier, J.L. and Villettaz, J.C., *Sensors and Actuators B*, 2001, **72**, 204-207.

68 O'Connell, M., Valdora, G., Peltzer, G. and Martín Negri, R., *Sensors and Actuators B*, 2001, **80**, 149-154.

69 Zhao, C., Pan, Y., Ma, L., Tang, Z., Zhao, G. and Wang, L., *Sensors and Actuators B*, 2002, **81**, 218-222.

70 Gupta, S. and Misra, T.N., *Sensors and Actuators B*, 1997, **41**, 199-202.

71 Werner, T., Klimant, I., and Wolfbeis, O.S., *Analyst*, 1995, **120**, 1627-1631.

72 Trinkel, M., Trettnak, W., Reininger, F., Benes, R., O'Leary, P. and Wolfbeis, O.S., *Analytica Chimica Acta*, 1996, **320**, 235-243.

73 Caglar, P. and Narayanaswamy, R., *Analyst*, 1987, **112**, 1285-1288.

74 Malins, C., Butler, T.M. and MacCraith, B.D., *Thin Solid Films*, 2000, **368**, 105-110.

75 Zhou, Q., Bonnell, L., Kritz, D. and Sigel, G.H., *Applied Optics*, 1989, **28**, 2022-2025.

76 Potyrailo, R.A., Golubkov, S.P., Borsuk, P.S., Talanchuk, P.M. and Novosselov, E.F., *Analyst*, 1994, **119**, 443-448.

77 Potyrailo, R.A., Mikheenko, L.A., Borsuk, P.S., Golubkov, S.P. and Talanchuk, P.M., *Sensors and Actuators B*, 1994, **21**, 65-70.

78 Sadok, S., Uglow, R.F. and Haswell, S.J., *Analytica Chimica Acta*, 1996, **321**, 69-74.

79 McCarrick, M., Harris, S. J. and Diamond, D., *Analyst*, 1993, **118**, 1127-1130.

80 Diamond, D. and Nolan, K., *Analytical Chemistry*, 2001, **73**, 22A-29A.

81 Grady, T., Butler, T., MacCraith, B. D., Diamond, D. and McKervey, M.A., *Analyst*, 1997, **122**, 803-806.

82 Loughran, M. and Diamond, D., *Food Chemistry*, 2000, **69**, 97-103.

83 D.W. Miller, J.G. Wilkes and E.D. Conte, Food Quality Indicator Device, Patent number WO9904256, 1999.

84 Cox Technologies, available from: http://www.coxtec.com/cox.htm [last accessed 01-12-2002].

85 T.J. Horan, Method for determining bacteria contamination in food package, Patent number US5753285, 1998.

86 Byrne, L., Lau, K.T. and Diamond, D. *The Irish Journal of Agricultural and Food Research*, 2002, accepted for publication.

87 http://www.lightforminc.com/FAQ/faq.html [last accessed 08-10-2001].

88 http://www.lightforminc.com/Technology/BIOSPECTRAL/spectrosbiospectral.html [last accessed 08-10-2001].

89 http://www.lightforminc.com/Image_Gallery/image_gallery.html [last accessed 08-10-2001].

90 http://www.chemfinder.com [last accessed 28-08-2002].

91 Hislip, S., Pennarun-Thomas, G., Manning, B., O'Kennedy, R., Edwards, S. and Diamond, D., *Proceedings of SPIE,* **38**, 1999, 56.

92 Bates, R.G. *Determination of pH: Theory & Practice* (2nd edition), Wiley & Sons, New York, USA, 1973, p. 107.

93 Diamond, D. and Hanratty, V.C.A., Spreadsheet Applications in Chemistry using Microsoft Excel, John Wiley & Sons, New York, USA, 1997, p. 197-200.

94 Woody, T.W., *Photonics Spectra*, **16**, 1991, 167.

95 Byrne, L., Lau, K.T. and Diamond, D. *The Analyst*, 2002, **127**, 1338-1341.

96 Common Fisheries Policy (2001), http://europa.eu.int/comm/fisheries/policy_en.htm [last accessed 13-03-2002].

97 http://europa.eu.int/comm/fisheries/doc_et_publ/factsheets/legal_texts/docscom/en/com_01_764_en.pdf [last accessed 13-12-2002].

98 Byrne, L., Lau, K.T. and Diamond, D. *Sensors and Actuators B (chem.)*, 2002, Accepted for publication.

99 City Biologic, School of Biotechnology, Dublin City University, available from: http://www.dcu.ie/~biotech/Pages/cbiol/page1.htm [last accessed 19-07-2002].

100 Roberts, D., Hooper, W and Greenwood, M., *Practical Food Microbiology*, PHLS, USA, 1995.

101 Skoog, D.A and West, D.M., *Fundamentals of Analytical Chemistry* (7th Edition), Saunders College Publishing, Philadelphia, USA, 1996, Ch. 6.

102 http://www.whistonbrook.com [last accessed 16-08-2002].

103 Skoog, D.A., West, D.M and Holler, F.J., *Fundamentals of Analytical Chemistry* (7th Edition), Saunders College Publishing, London, UK, 1996, p. 503.

104 Leach, R.H. and Pierce, R.J. *The Printing Ink Manual*, Kluwer Academic Publishers, London, UK, 1999, pp. 189-195.

105 Bord Iascaigh Mhara and the Department of the Marine and Natural Resources, *Whitefish Quality Guide*, BIM, Ireland.

Appendix A: pH buffers

Buffers are defined as "substances, which by their presence in solution, increase the amount of acid or alkali that must be added to cause unit change in pH" [1]. From Equation 1.10:

$$[H_3O^+] \propto \frac{[HA]}{[A^-]} \qquad \textbf{Equation A.1}$$

Buffers are typically an acid and its conjugate base, or vice versa. In a buffer solution, both [HA] and $[A^-]$ are kept relatively high; the proton concentration can be tweaked, but is optimum when $[HA] = [A^-]$. Addition of acid or base will then cause the following interactions:

$$H_3O^+ + A^- \rightleftharpoons HA$$

$$HA + OH^- \rightleftharpoons A^- + H_2O$$

Thus the concentration of protons in solution remains constant. The buffer capacity, β, is a unit used to numerically express buffer effects and is defined as a differential ratio [1]:

$$\beta = \frac{db}{dpH} \qquad \textbf{Equation A.2}$$

where db= increment of strong base added,
dpH= change in pH.

Buffers can be made up at practically any pH value required, and tables of buffer preparations are commonly available [1].

Composition of pH buffers used

pH	x	Buffer Capacity
1.0	67.0	0.310
1.1	52.8	0.240
1.2	42.5	0.190
1.3	33.6	0.160
1.4	26.6	0.130
1.5	20.7	0.100
1.6	16.2	0.077
1.7	13.0	0.060
1.8	10.2	0.049
1.9	8.1	0.037
2.0	6.5	0.030
2.1	5.1	0.026
2.2	3.9	0.022

25 ml 0.2M KCl, x ml 0.2M HCl, diluted to 100 ml.

Table A1: Buffers between pH 1.0 and pH 2.2.

pH	x	Buffer Capacity	pH	x	Buffer Capacity
2.2	49.5	0.036	4.1	1.3	0.016
2.3	45.8	0.035	4.2	3.0	0.017
2.4	42.2	0.034	4.3	4.7	0.018
2.5	38.8	0.033	4.4	6.6	0.020
2.6	35.4	0.032	4.5	8.7	0.022
2.7	32.1	0.032	4.6	11.1	0.025
2.8	28.9	0.032	4.7	13.6	0.027
2.9	25.7	0.033	4.8	16.5	0.029
3.0	22.3	0.034	4.9	19.4	0.030
3.1	18.8	0.033	5.0	22.6	0.031
3.2	15.7	0.030	5.1	25.5	0.031
3.3	12.9	0.026	5.2	28.8	0.030
3.4	10.4	0.023	5.3	31.6	0.026
3.5	8.2	0.020	5.4	34.1	0.025
3.6	6.3	0.018	5.5	36.6	0.023
3.7	4.5	0.017	5.6	38.8	0.020
3.8	2.9	0.015	5.7	40.6	0.017
3.9	1.4	0.014	5.8	42.3	0.015
4.0	0.1	0.014	5.9	43.7	0.013

50 ml 0.1M KH Phthalate, x ml 0.1M HCl, diluted to 100 ml.

Table A2: Buffers between pH 2.2 and pH 5.9.

pH	x	Buffer Capacity
5.8	3.6	-
5.9	4.6	0.010
6.0	5.6	0.011
6.1	6.8	0.012
6.2	8.1	0.015
6.3	9.7	0.017
6.4	11.6	0.021
6.5	13.9	0.024
6.6	16.4	0.027
6.7	19.3	0.030
6.8	22.4	0.033
6.9	25.9	0.033
7.0	29.1	0.031
7.1	32.1	0.028
7.2	34.7	0.025
7.3	37	0.022
7.4	39.1	0.020
7.5	41.1	0.018
7.6	42.8	0.015
7.7	44.2	0.012
7.8	45.3	0.010
7.9	46.1	0.007
8.0	46.7	-

50 ml 0.1M KH_3PO_4 Phthalate,

x ml 0.1M NaOH, diluted to 100 ml.

Table A3: Buffers between pH 5.8 and 8.

pH	x	Buffer Capacity
8.0	3.9	-
8.1	4.9	0.010
8.2	6.0	0.011
8.3	7.2	0.013
8.4	8.6	0.015
8.5	10.1	0.016
8.6	11.8	0.018
8.7	13.7	0.020
8.8	15.8	0.022
8.9	18.1	0.025
9.0	20.8	0.027
9.1	23.6	0.028
9.2	26.4	0.029
9.3	29.3	0.028
9.4	32.1	0.027
9.5	34.6	0.024
9.6	36.9	0.022
9.7	38.9	0.019
9.8	40.6	0.016
9.9	42.2	0.015
10.0	43.7	0.014
10.1	45.0	0.013
10.2	46.2	-

50 ml of a mixture with respect to both KCl and H_3BO_3, x ml 0.1M NaOH,
diluted to 100 ml

Table A4: Buffers between pH 8 and 10.2.

---

1 Bates, R.G., *Determination of pH: Theory & Practice* (2nd Edition), Wiley & Sons, New York, USA, 1973, p. 107.